Spectral characterisation of devices: at high frequencies and measurement methods

Hassan, Yahya Mat

SPECTRAL CHARACTERISATION OF DEVICES AT HIGH FREQUENCIES AND MEASUREMENT METHODS

By

YAHYA MAT HASSAN, B.Sc(Malaya)
M.Sc.(CNAA), Graduate Society.

A Thesis submitted to the Faculty of Science,
University of Durham for the degree of
Doctor of Philosophy

Department of Applied Physics and Electronics,
University of Durham, U.K.

June, 1984.

ABSTRACT

The properties of nonlinear devices, semiconductor diodes, were determined at high frequencies using the method of spectral characterisation. Such characterisation was carried out employing a specially developed technique where the components of the harmonic spectrum generated within these diodes at radio and microwave frequencies were measured.

The theory of spectral analysis, based on Fourier principles, was reviewed. It was applied to the periodic gate function, which plays a fundamental role in signal analysis, in order to lay the foundation for the theoretical investigation carried out between pulses of known shapes and their corresponding spectra. Some useful relationships were established and applied in the evaluation of devices. Based on the fundamental properties of the periodic gate function, two new sampling procedures were introduced.

The harmonic generating properties of practical diodes, where the nonlinearity in the element is an inherent condition, were examined. It was established that the spectrum generated within the device, at a particular drive level, gives the "fingerprint" of the diode, i.e. represents fully its nonlinearity. Measurement methods, both at low and high frequencies, were also discussed.

The new technique, called the Multiple Reflections Resonant Line (MRRL) method was developed and described in the thesis to measure a complete spectrum. The method employed a coaxial slotted line system terminated by the device under test. The basic transmission line theory was extended to include the phenomena of multiple reflections along and resonance of, the line. The properties of the standing waves were then related to the device parameters. The twelve microwave diodes were successfully modelled which included parasitics using the new spectral technique. An attempt was made to evaluate these devices for particular applications.

ACKNOWLEDGEMENTS

I would like to express my gratitude to Dr.B.L.J. Kulesza and Dr. J.S. Thorp for their guidance, enthusiasm and continued interest throughout the entire period of research. I am indebted to Dr. Kulesza for introducing me to the fascinating subject of nonlinearity. It is gratefully acknowledged that without the facilities afforded by Professor G.G. Roberts, Head of the Department of Applied Physics and Electronics, University of Durham, the project could not have been undertaken.

My appreciation is also due to other colleagues of the High Frequency Measurements and Applications Group, the technical staff of the department for their generous co-operation, Mrs. S. Mellanby and Mr. N. Thompson.

I am grateful to the Universiti Pertanian Malaysia (University of Agriculture, Malaysia), for granting the study leave, and the Government of Malaysia for the sponsorship.

Finally, I would like to record my thanks to my wife, Zaimi, for her patience and constant encouragement throughout the course of study.

CONTENTS

LIST OF ILLUSTRATIONS

Following page

LIST OF SYMBOLS

a_n = Fourier coefficient of the cos component, at nth harmonic

b_n = Fourier coefficient of the sin component, at nth harmonic

c_n = The amplitude of the Fourier coefficients at nth harmonic

ϕ_n = Phase angle at the nth harmonic

Z = Complex impedance,

subscript g for generator

subscript L for load

subscript n for the generator (harmonic) at nth harmonic

subscript o for the line

$Z_i(x, \ell)$ = Complex impedance (input) at a point, distance 'x' from the load, for the slotted line of length 'ℓ' at nth harmonic

R = Resistive component of the complex impedance,

subscript L for the load

subscript o for the line

subscript n at the nth harmonic

X = Reactive component of the complex impedance,

subscript L for the load

subscript n at the nth harmonic

C_n = Capacitance with subscript n for the value measured at the nth harmonic

ρ = Complex reflection coefficient,

subscript L for the load

subscript g for the generator

subscript n for the generator (harmonic) at nth harmonic

ψ = Phase angle for the complex reflection coefficient,

subscript L for the load

subscript g for the generator

subscript n for the generator (harmonic) at nth harmonic

k = Integral value in the expression for phase angle (complex reflection coefficient) at resonant and anti-resonant conditions

m = Integral value in the expression for phase angle (complex reflection coefficeint) at the conditions corresponding to standing wave maximum and minimum

V = Voltage in general,

subscript i for the initial

subscript n for the generated harmonic voltage at the nth harmonic

subscript a for the applied voltage

subscript B for the barrier potential

V_{gn} = Voltage at the generator end after nth reflection

V_{Ln} = Voltage at the load end after nth reflection

$V(x,\ell)$ = Voltage at the point, distance 'x' from the load, and for the slotted line of length 'ℓ'

x = Distance from a point, on the slotted line, to the load,

subscript max for the point at the standing wave maximum

subscript min for the point at the standing wave minimum

ℓ = Length of the slotted line,

subscript max for the resonant condition

subscript min for the anti-resonant condition

i,I = Current in general,

subscript S for reverse saturation

subscript f for forward

subscript 1 for the fundamental frequency

$I(x,\ell)$ = Current at a point, distance 'x' from the load, and for the slotted line of length 'l'

γ = Complex propagation constant

α = Attenuation constant

β = Phase constant,

subscript n for the nth harmonic

f_{co} = Cut-off frequency under zero-bias

r_{so} = Dynamic resistance at zero-bias

C_{jo} = Junction capacitance at zero-bias

A^{*} = Richardson constant

CHAPTER 1

1. INTRODUCTION

Nonlinearity, a subject of great mathematical and physical interest is on the whole multidisciplinary, i.e. it includes electronics, optics and astronomy. Nonlinearity of devices, especially forms an extensive topic within this branch of technology. Many high frequency components and systems use nonlinear solid state devices as passive or active elements. The design of such components requires a knowledge of the behaviour of the semiconductor devices under varying d.c. bias and microwave operating conditions. Many modern applications in electrical technology are based in a fundamental way on this nonlinear phenomenon. It is particularly important in the field of communication where the essential circuits like harmonic generators and frequency converters operate only if a nonlinear element is present. It is therefore advantageous to know the full extent of their harmonic generating capabilities for the efficient performance.

At the present time, the extent and the method of characterisation of these devices, especially at high frequencies is grossly inadequate. The data sheets provided by most manufacturers are generally incomplete. Normally, the device parameters available are the static characteristics and those obtained from low frequency measurements. If the dynamic characteristics are given, they are generally at one particular test frequency and drive level. It is important to note that the behaviour of a nonlinear device is critically dependent on the drive level. For most high frequency applications, it is not adequate to rely on the low frequency measurement of the device, because some of its parameters, even parasitics, inherent and due to encapsulation, may be frequency dependent. Besides, measurement of the series resistance at low frequencies is difficult

and inaccurate. High frequency measurements are therefore necessary for the complete device characterisation.

The efficiency of frequency conversion depends on the amplitudes of the harmonic voltages and currents generated within the nonlinear element. In order to describe fully a device by means of its harmonic spectrum, there is a need to know the amplitude of each component as well as its relative phase. At present there are no single instruments available that can measure the complete spectrum of amplitudes and phases. Existing spectrum analysers cover a wide range of frequencies right up to about 40 GHz but can only measure the amplitudes of the input frequencies. If the phase spectrum is not known, a great deal of information is lost especially about the imaginary, usually frequent-dependent, terms of the physical or electrical parameters. However, if the response waveform of the element is known then the complete spectrum may be found by the usual Fourier analysis methods. There are however, three main constraints with such an approach. Firstly, it is difficult to derive a precise law for the practical device. Secondly, the analysis which is normally lengthy requires a lot of approximation and consequently further assumptions. Thirdly, the method is restricted to lower frequencies because of the sampling rate difficulties.

In order to determine the properties of a nonlinear device at high frequencies, there is a need to measure the spectral content generated within it. It is further justified by the fact that such spectra are the unique representations of the device nonlinearity which provides the constants (harmonic coefficients) inherently associated with a particular behaviour. The complete spectrum thus gives the "fingerprint" of the device at a specific drive level. On achieving this, there is no need to rely on the inaccurate I-V or C-V laws.

The main objective of this work was to characterise a family of devices at high frequencies by means of the spectral components generated within their nonlinearities. This resulted in the development of the technique called the Multiple Reflections Resonant Line (MRRL) method.

In Chapter 2, the thoery of spectral analysis based on the Fourier principles are reviewed. A periodic gate function, which often plays a fundamental role in signal analysis is Fourier analysed and its properties reviewed. This will form a basis in the theoretical investigation, where relations are established, of the spectral behaviour of pulses of different shapes.

Chapter 3 outlines the harmonic generating properties of nonlinear devices. It begins with the classification of high frequency practical diodes which are solid state and nonlinear in behaviour. The phenomenon of nonlinearity and the historical development of its analysis are described. The proposed device characterisation and evaluation by the method of spectral representation are considered and the display of the unique dynamic characteristics constitutes the "fingerprint" of the device. Measurement methods at high and low frequencies are also indicated. Finally, general applications of nonlinear devices are given.

The theory of the new technique of spectrum measurements called the Multiple Reflections Resonant Line method is described in Chapter 4. The method employs the coaxial slotted line system. The operating principles consist of the setting up of multiple reflections, the creation of harmonic standing waves and establishing the conditions of resonance under known conditions. The nonlinear device, terminating the line acts as the harmonic generator, is driven by a single frequency source. The expressions for the generated harmonic voltage and the complex impedance at harmonics, are also derived.

In Chapter 5, measurement and experimental procedures are covered. The equipments and experimental arrangements are first described followed by the calibration procedures. The setting of the resistive multiple termination which forms an important component in the experimental set-up is discussed. The spectrum analyser, which is a selective voltmeter, plays a key role in the measurements for it is used to measure the standing waves at harmonics and the fundamental drive current. Other discussion includes the d.c. measurements and some detailed aspects related to the technique described. Finally, the experimental procedures are listed to avoid ambiguity.

The results of both the d.c. and the harmonic measurements are presented in Chapter 6. The static characteristics of the twelve diodes chosen for the project are tabulated and their properties examined. The results of harmonic measurements are presented in the form of graphs for the following spectral quantities,the generated voltage, relative phase, impedance magnitude and the parasitic capacitance plotted against the fundamental drive current. Discussion on the harmonic generating properties of each diode will then be made in terms of these new spectral representations. This includes the examination of the behaviour of one spectral quantity, for example the harmonic amplitude, in relation to other quantities like relative phases and impedance, within the given drive level range.

Finally, in Chapter 7, an assessment of the method covering the accuracy and errors, significance and possible improvements are given. Evaluations of devices will be made on the basis of the experimental results of the spectral characterisation presented in Chapter 6. This includes the explanation and interpretation of the results which will ultimately provide the basis for device classification. Suggestions for future work arising from this research are also offered.

CHAPTER 2

THEORY OF SPECTRAL ANALYSIS

2.1 INTRODUCTION

The ultimate aim of employing any analytical method in the experimental investigation of device behaviour is generally to obtain, if possible, a closed form expression for its response. The devices used are the non-linear microwave diodes. However, in normal experimental work only the method of piecewise analysis may be possible. As the energising function will normally be periodic, i.e. of sinusoidal or periodic waveform, the resulting response will be a harmonic frequency spectrum. Consequently, the procedure adopted in the determination of the components in the frequency spectrum may be referred to as spectral analysis. The resultant Fourier series may be obtained, at low frequencies, from a time function display on the oscilloscope using numerical methods and computer facilities. In a few lucky cases it may be possible to obtain a formula for such a time function. The direct numerical method from a time display is restricted however by the bandwidth limitation of the oscilloscope, with the upper cut-off of about 70 MHz. The frequency spectrum of the response can be measured directly using a wave or spectrum analyser. Normally wave analysers can be used up to 500 MHz and spectrum analysers up to 220 GHz.

The fundamentals of Fourier analysis for periodic signals and the required mathematical constraints in its applications are first reviewed. This is followed by a brief treatment of the concept of the Fourier integral as used in the analysis of aperiodic signals. A detailed illustration of Fourier analysis using the well-known periodic gate function is also presented in this Chapter. In addition, applications of a periodic gate function in the analyses of arbitrary waveforms are given. Generated spectra of both

periodic and aperiodic waveforms are theoretically determined and examined.

2.2 FUNDAMENTAL RELATIONS IN FOURIER ANALYSIS

A general trigonometric Fourier series[1] for a periodic function may be written as,

$$f(t) = a_o + \sum_{n=1}^{\infty} a_n \cos(n\omega_o t) + \sum_{n=1}^{\infty} b_n \sin(n\omega_o t) \qquad (2.2.1)$$

or simplified to,

$$f(t) = \sum_{n=o}^{\infty} C_n \cos(n\omega_o t + \phi_n) \qquad (2.2.2)$$

where

$$C_n = (a_n^2 + b_n^2)^{\frac{1}{2}} \qquad (2.2.3)$$

$$\phi_n = \tan^{-1}\left(-\frac{b_n}{a_n}\right) \qquad (2.2.4)$$

The coefficient C_n represents the amplitude while ϕ_n is the phase shift for the n^{th} harmonic and ω_o is the fundamental frequency.

The Fourier coefficients are given by:

$$a_o = \frac{1}{T} \int_{-\frac{T}{2}}^{\frac{T}{2}} f(t)dt \qquad (2.2.5)$$

$$a_n = \frac{2}{T} \int_{-\frac{T}{2}}^{\frac{T}{2}} f(t)\cos(n\omega_o t)dt \qquad (2.2.6)$$

$$b_n = \frac{2}{T} \int_{-\frac{T}{2}}^{\frac{T}{2}} f(t)\sin(n\omega_o t)dt \qquad (2.2.7)$$

The function can also be represented by an exponential form,

$$f(t) = \sum_{n=-\infty}^{\infty} F_n e^{jn\omega_o t}, \quad t_1 < t < t_2 \qquad (2.2.8)$$

$$\text{where } F_n = \frac{1}{t_2 - t_1} \int_{t_1}^{t_2} f(t)e^{-jn\omega_o t} dt \qquad (2.2.9)$$

All the above equations are valid subject to certain requirements. These are summarised by the well known weak or strong Dirichlet conditions [2]

which involve singularities, uniqueness, orthogonality and convergence criteria (outlined in the Appendix A) and are based on the finite energy concept.

The Fourier series as represented by eqn. 2.2.8 is applicable to a periodic signal. The transition to an aperiodic signal representation is obtained by making the period approach infinity. This can be achieved by considering initially the exponential form of the Fourier series of a periodic function. The derivation (given in Appendix B) leads eventually to the final expression for Fourier transforms, i.e.

$$F(\omega) = \mathcal{F}\left[f(t)\right] = \int_{-\infty}^{+\infty} f(t)e^{-j\omega t}\,dt \qquad (2.2.10)$$

and where

$$f(t) = \mathcal{F}^{-1}\left[F(\omega)\right] = \frac{1}{2\pi}\int_{-\infty}^{+\infty} F(\omega)e^{j\omega t}\,d\omega \qquad (2.2.11)$$

There are two types of spectra, discrete and continuous, which are obtained from periodic and aperiodic signals respectively. In the discrete or line spectrum the components are harmonically-related. With successive increase in the period the signal tends to become aperiodic, resulting in an increase in the density of harmonic components. In the limit, as the period T tends to infinity, the spectrum no longer remains discrete but becomes continuous. Hence an aperiodic signal represents the limiting behaviour of the Fourier series. However, pulses of similar waveform whether periodic or aperiodic will produce similar envelopes of their amplitude spectra.

2.3 PROPERTIES OF THE PERIODIC GATE FUNCTION

One of the most important functions, (which plays a fundamental role in signal analysis), is the train of pulses[3] shown in Fig.2.1. Its importance lies in the fact that it is often utilised as a gating waveform in the analysis of various functions. This periodic gate function is a single polarity rectangular wave whose height and markspace ratio can be varied according to the needs. Its Fourier coefficients may be obtained using eqn. 2.2.9, i.e.

$$F_n = \frac{1}{T} \int_{-\frac{T}{2}}^{\frac{T}{2}} f(t) e^{-jn\omega_o t} \, dt$$

$$= \frac{\tau_m}{T} \cdot \frac{\sin x}{x} \qquad (2.3.1)$$

$$f(t) = 0 \quad \left\{ \frac{\tau_m}{2} < |t| < \frac{T}{2} \right.$$

$$= 1 \quad \left\{ |t| < \frac{\tau_m}{2} \right.$$

$$x = n\omega_o \, \tau_m/2$$

The ratio $\frac{\sin x}{x}$ is called the Fourier kernel[4] and is sometimes symbolised (or denoted) as sinc(x). Its spectrum is identical to that of the familiar optical diffraction pattern, illustrated in Fig.2.2. As this important function occurs very often in communication theory, a brief review of its properties may be useful. The main features are that the peak value of the main lobe is unity occurring at the origin, i.e. x 0, the zeros are at the nonzero multiples of π and the sidelobes are relatively slowly decaying.

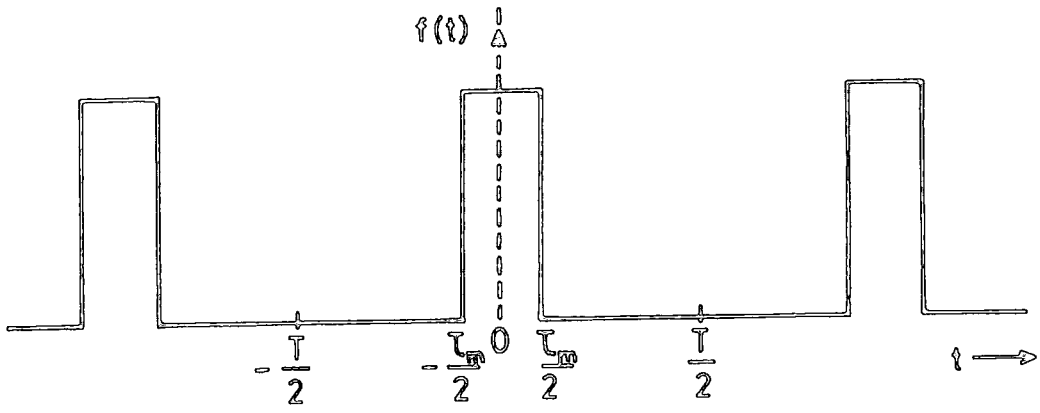

FIG. 2·1 A PERIODIC TRAIN OF PULSES

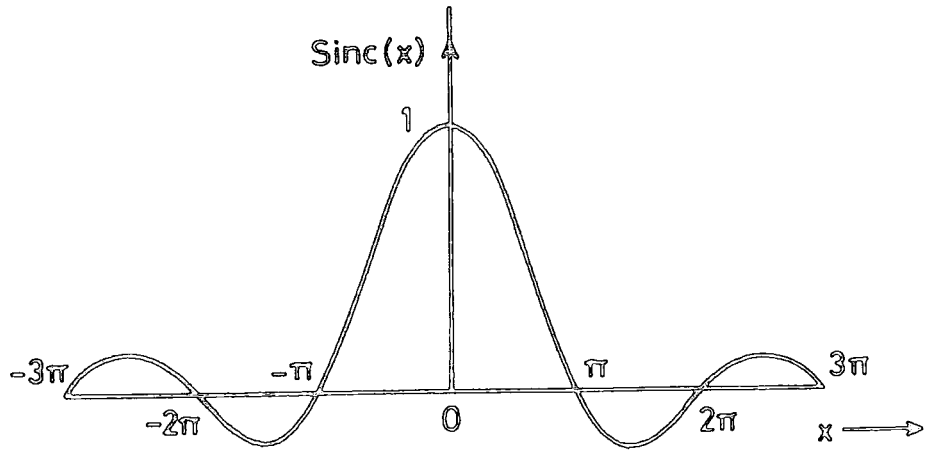

FIG. 2·2 A SINC (x) SPECTRUM

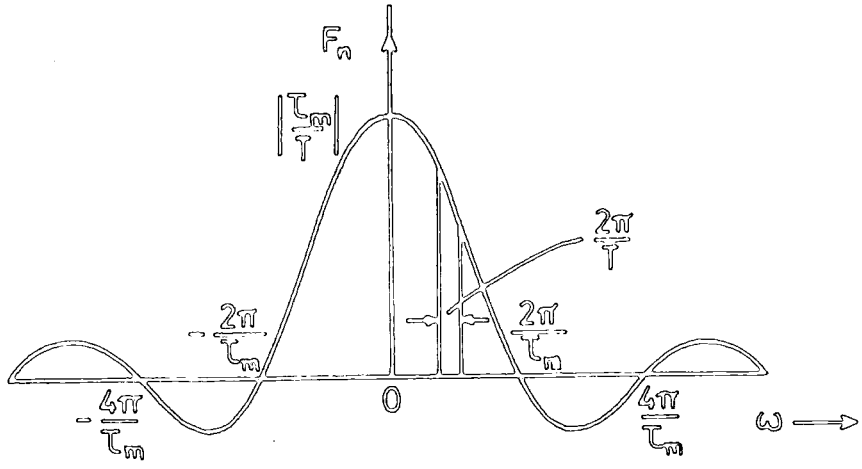

FIG. 2·3 AMPLITUDE SPECTRUM

The frequency spectrum which may be deduced from eqn. 2.3.1 is a line or discrete spectrum with components located at the multiples of the fundamental frequency ω_o, which is given by $\frac{2\pi}{T}$, as shown in Fig.2.3. As the period T becomes larger and larger, the fundamental frequency $\frac{2\pi}{T}$ becomes smaller and smaller and hence there are more and more frequency components in a given range of frequency. On simplifying equation 2.3.1 the Fourier coefficient F_n is given by :

$$F_n = \frac{\sin\left[n\pi \frac{\tau_m}{T}\right]}{n\pi} \qquad (2.3.2)$$

Thus, on increasing the period T, the amplitude of the frequency components will decrease as $\frac{1}{n\pi} \sin\left[(n\pi\tau_m)\frac{1}{T}\right]$ for particular values of n and τ_m. Rewriting eqn. 2.3.1 in terms of fundamental frequency, the Fourier coefficient F_n is given by :

$$F_n = \frac{\sin\left(n\omega_o \frac{\tau_m}{2}\right)}{n\pi} \qquad (2.3.3)$$

Thus the zeros will occur at integral multiples of π and the sine term will correspond to

$$n\omega_o \frac{\tau_m}{2} = k\pi \quad , \quad n,k = 1,2,..... \qquad (2.3.4)$$

Hence the frequencies corresponding to zero amplitude are:

$$\omega = \frac{2\pi}{\tau_m} , \frac{4\pi}{\tau_m} , ... \frac{2k\pi}{\tau_m} \qquad (2.3.5)$$

Therefore the envelope of the spectrum depends upon the pulse shape, given by τ_m. When, on the other hand, T is kept constant and τ_m is

increased ($\tau_m < T$), the amplitude of the frequency components will will increase according to eqn. 2.3.1.

$$\frac{1}{n\pi} \sin \left[\left(\frac{n\pi}{T}\right) \tau_m \right],$$

and the frequencies corresponding to zeros will fall. However, the frequency spacings between adjacent harmonics remain the same. The pulse width τ_m determines the frequency of the first zero of the amplitude function, as given by eqn. 2.3.5. This helps as a first approximation to establish the range of frequencies required to reconstruct the pulse from Fourier components.

The Fourier series for a train of pulses of unit height which are symmetrical may now be written as,

$$S(t) = \frac{\tau_m}{T} + \frac{2\tau_m}{T} \sum_{n=1}^{\infty} \frac{\sin x}{x} \cos(n\omega_o t) \qquad (2.3.6)$$

$$x = \left(\frac{n\omega_o \tau_m}{2} \right)$$

It is called the switching or the periodic gate function. It may be written as :

$$f(t) = A \cdot S(t)$$

where A is the amplitude. By varying different parameters involved in this kind of periodic train of pulses, the extreme conditions may be deduced. As T tends to infinity[3], the function f(t) consists only of non-repetitive pulse, and the spectrum then represents a non-periodic function over the whole interval $(-\infty, \infty)$. The term $\frac{\tau_m}{T}$ in eqn. 2.3.6 is defined as d.c. level for a

unit pulse height. Other periodic trains of pulses of different shapes and symmetries may also be considered and their corresponding periodic gate functions found. In general, the function S(t) can be multiplied by an arbitrary waveform f(t) to give a sampled function $f_s(t)$ i.e.

$$f_s(t) = f(t) \circ S(t)$$

whose properties may be easier to examine.

2.4 ANALYSIS AND SPECTRA OF PERIODIC WAVEFORMS

2.4.1 Introduction

The relationship between pulse shapes and their frequency spectra[5,6] will be examined next. A detailed analysis was carried out for the periodic waveforms which then were categorised as (a) symmetrical and (b) asymmetrical types. Next, within each group the geometrical shapes were chosen to be representative of the types normally met in practice. In every case the behaviour of such pulses was also chosen to be mathematically definable.

In the symmetrical case, the pulse is defined as the shape that has a vertical line of symmetry. The analysis was carried out by considering two positions of the origin, i.e. the one that lies on the vertical axis of symmetry and the other at the leading edge. In the former case the waveform may be considered to be in even-function symmetry while in the latter in odd-function symmetry. The selected shapes were rectangular, trapezoidal, sinusoidal, sinusoidal squared, and triangular as shown in Tables 2.1 and 2.2. The asymmetrical pulses however are defined as the shapes that do not have a vertical line of symmetry. The choice made was as shown in Table 2.3. The start of the pulse was taken as the origin in the analysis of each

TABLE 2·1 - SYMMETRICAL PULSES
(EVEN FUNCTION SYMMETRY)

PULSE	f(t)	FOURIER COEFFICIENT EXPRESSIONS		SPECTRA
		a_o	a_n	
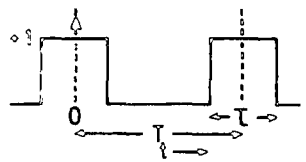 1 - RECTANGULAR	$f(t) = 1 \quad \lvert t\rvert \leq \tau/2$ $= 0 \quad \lvert t\rvert > \tau/2$	τ/T	$\frac{2\tau}{T}\,\frac{\sin(n\omega_o\tau/2)}{(n\omega_o\tau/2)}$	as in FIG.2·4(b)
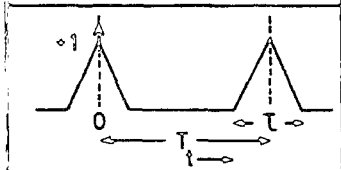 2 - TRIANGULAR	$f(t) = (1+\frac{2t}{\tau}),\ -\frac{\tau}{2} \leq t \leq 0$ $= (1-\frac{2t}{\tau}),\ 0 \leq t \leq \frac{\tau}{2}$	$\tau/2T$	$\frac{\tau}{T}\left(\frac{\sin(n\omega_o\tau/4)}{(n\omega_o\tau/4)}\right)^2$	"
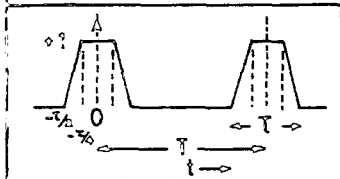 3 - TRAPEZOIDAL	$f(t) = 2(1+\frac{2t}{\tau}),\ -\frac{\tau}{2} \leq t \leq -\frac{\tau}{4}$ $= 1 \qquad \lvert t\rvert \leq \frac{\tau}{4}$ $= 2(1-\frac{2t}{\tau}),\ \frac{\tau}{4} \leq t \leq \frac{\tau}{2}$	$\frac{3}{4}\cdot\frac{\tau}{T}$	$\frac{3}{2}\,\frac{\tau}{T}\left\{\frac{\sin(n\omega_o\tau/8)}{(n\omega_o\tau/8)}\cdot\frac{\sin(3n\omega_o\tau/8)}{(3n\omega_o\tau/8)}\right\}$	"
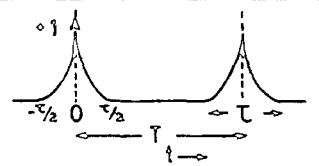 4 - EXPONENTIAL	$f(t) = \frac{(\exp(-k\omega_o t)-m)}{(1-m)} \quad 0 \leq t \leq \frac{\tau}{2}$ $= \frac{(\exp(k\omega_o t)-m)}{(1-m)} \quad -\frac{\tau}{2} \leq t \leq 0$ $m = e^{-k\omega_o\tau/2}$	$\frac{1}{\pi k}(1-m+m\ln m)$	$\frac{2}{\pi(n^2+k^2)}\left[k - mk\cos(n\omega_o\tau/2) - \frac{mk^2}{n}\sin(n\omega_o\tau/2)\right]$	"

------ Cont.

TABLE 2·1 – Continued.

PULSE	f(t)	FOURIER COEFFICIENT EXPRESSIONS		SPECTRA
		a_o	a_n	
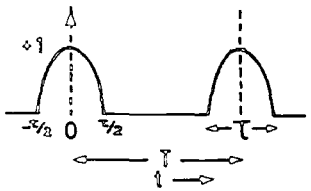 5 – COSINUSOIDAL	$f(t)=\left(\frac{\cos(\omega_o t)-\cos(\omega_o \tau/2)}{1-\cos(\omega_o \tau/2)}\right)$ $\lvert t\rvert \leq \tau/2$	$\frac{1}{\pi(1-\cos(\omega_o\tau/2))}\pi$ $\left[\sin(\omega_o\tau/2)-\frac{\omega_o\tau}{2}\cos(\omega_o\tau/2)\right]$	$a_1=\frac{1}{n}\cdot\frac{\left((\omega_o\tau/2)-\frac{\sin(\omega_o\tau)}{2}\right)}{(1-\cos(\omega_o\tau/2))}$ $a_n=\frac{2}{\pi n(n^2-1)(1-\cos(\omega_o\tau/2)}\pi$ $\left[\sin(\omega_o\tau/2)\cos(n\omega_o\tau/2)-\cos(n\omega_o\tau/2)\sin(n\omega_o\tau/2)\right]$	as in FIG. 2·4 (b)
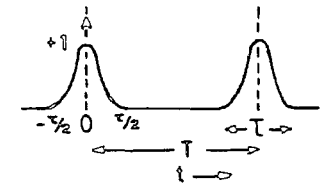 6 – COSINUSOIDAL SQUARED	$f(t)=\left(\frac{\cos(\omega_o t)-\cos(\omega_o\tau/2)}{1-\cos(\omega_o\tau/2)}\right)^2$ $\lvert t\rvert \leq \tau/2$	$\frac{1}{4\pi(1-\cos(\omega_o\tau/2))^2}\pi$ $\left[\omega_o\tau(2\cdot\cos(\omega_o\tau))-3\sin\omega_o\tau\right]$	$a_1=\frac{1}{6\pi(1-\cos(\omega_o\tau/2))^2}\left\{9\sin(\omega_o\tau/2)\cdot\sin(\frac{3}{2}\omega_o\tau)-6\omega_o\tau\cos(\omega_o\tau/2)\right\}$ $a_2=\frac{1}{24\pi(1-\cos(\omega_o t/2))^2}\left\{3\left[4\sin(\omega_o\tau)\cdot\sin 2\omega_o\tau\cdot 2\omega_o\tau\right]-16\cos(\omega_o\tau/2)\left[\sin(\frac{3}{2}\omega_o\tau)\cdot 3\sin(\omega_o\tau/2)\right]\cdot 24\cos^2(\omega_o\tau/2)\sin\omega_o\tau\right\}$ $a_n=\frac{2}{\pi(1-\cos(\omega_o\tau/2))^2}\left\{\frac{\sin(n\omega_o\tau/2)}{2n}\left[2\cdot\cos\omega_o\tau\right]\cdot\frac{1}{2(n^2-4)}\left[n\sin(n\omega_o\tau/2)\cos n\omega_o\tau-2\cos(n\omega_o\tau/2\sin\omega_o\tau\right]-\frac{2\cos(n\omega_o\tau/2)}{(n^2-1)}\left[n\sin(n\omega_o\tau/2)\times\cos(n\omega_o\tau/2)-\cos(n\omega_o\tau/2)\sin(\omega_o\tau/2)\right]\right\}$	

TABLE 2·2 - SYMMETRICAL PULSES
(ODD FUNCTION SYMMETRY)

PULSE	$f(t)$	FOURIER COEFFICIENT EXPRESSIONS			SPECTRA
		a_0	a_n	b_n	
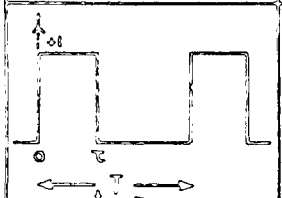 1 - RECTANGULAR	$f(t)=0,\ t<0$ $t>\tau$ $=1,\ 0\le t\le\tau$	τ/T	$\frac{1}{n\pi}\sin n\omega_0\tau$	$\frac{1}{n\pi}(1-\cos n\omega_0\tau)$	as in FIG.2·5(c)
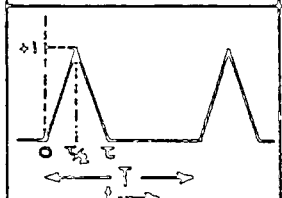 2 - TRIANGULAR	$f(t)=2t/\tau,$ $0<t<\tau/2$ $=(2-2t/\tau)$ $\tau/2<t<\tau$	$\tau/2T$	$\frac{4}{\pi n^2(\omega_0\tau)}\cos(n\omega_0\tau)(1-\cos(n\omega_0\frac{\tau}{2}))$	$\frac{4}{\pi n^2(\omega_0\tau)}\sin(n\omega_0\tau)(1-\cos(n\omega_0\frac{\tau}{2}))$	as in FIG.2·5(d)
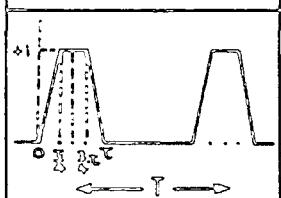 3 - TRAPEZOIDAL	$f(t)=4t/\tau, 0\le t\le\tau/4$ $=1,\ \tau/4\le t\le 3\tau/4$ $=4(1-t/\tau),$ $3\tau/4\le t\le\tau$	$\frac{3}{4}\cdot\frac{\tau}{T}$	$\frac{4}{\pi n^2(\omega_0\tau)}\left[\cos(n\omega_0\frac{\tau}{4})\cdot\right.$ $\left.\cos(\frac{3}{4}n\omega_0\tau)-\cos(n\omega_0\tau)-1\right]$	$\frac{4}{\pi n^2(\omega_0\tau)}\left[\sin(\frac{n\omega_0\tau}{4})\cdot\right.$ $\left.\sin(\frac{3}{4}n\omega_0\tau)-\sin(n\omega_0\tau)\right]$	as in FIG.2·5(e)

TABLE 2·2 - continued

PULSE	f(t)	FOURIER COEFFICIENT EXPRESSIONS			SPECTRA
		a_0	a_n	b_n	
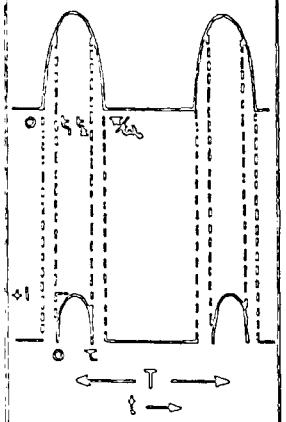 4 - SINUSOIDAL	$f(t) = \frac{\sin\omega_0(t_1 \circ t)}{(1-\sin(\omega_0 t_1))} - \frac{\sin(\omega_0 t_1)}{(1-\sin(\omega_0 t_1))}$ $0 < t < \tau$ $\tau = (t_2 - t_1)$	$-\frac{1}{2\pi(1-\sin(\omega_0 t_1))}\left\{\cos(\omega_0(\tau \circ t_1)) - \cos(\omega_0\tau) \circ \omega_0\tau\sin(\omega_0 t_1)\right\}$	$a_1 = -\frac{1}{4\pi(1-\sin(\omega_0 t_1))}\left\{\left[\cos(\omega_0(2\tau \circ t_1)) - \cos(\omega_0 t_1) - 2\omega_0\tau\sin(\omega_0 t_1)\right] \circ 4\sin(\omega_0 t_1)\sin(\omega_0\tau)\right\}$ $a_n = \frac{1}{\pi(1-\sin(\omega_0 t_1))}\left\{-\frac{1}{2(1-n)}\left[\cos(\omega_0(t_1 \circ (1-n)\tau)) - \cos(\omega_0 t_1)\right] - \frac{1}{2(n \circ 1)}\left[\cos(\omega_0(t_1 \circ (n \circ 1)\tau)) - \cos(\omega_0 t_1)\right] - \frac{\sin(\omega_0 t_1)}{n}\sin(n\omega_0\tau)\right\}$	$b_1 = \frac{1}{4\pi(1-\sin(\omega_0 t_1))}\left\{2\omega_0\tau\cos(\omega_0 t_1) - \left[\sin(\omega_0(2\tau \circ t_1)) - \sin(\omega_0 t_1)\right] \circ 4\sin(\omega_0 t_1)\left[\cos(\omega_0\tau) - 1\right]\right\}$ $b_n = \frac{1}{\pi(1-\sin(\omega_0 t_1))}\left\{\frac{1}{2(1-n)}\left[\sin(\omega_0(t_1 \circ (1-n)\tau)) - \sin(\omega_0 t_1)\right] - \frac{1}{2(n \circ 1)}\left[\sin(\omega_0(t_1 \circ (1 \circ n)\tau)) - \sin(\omega_0 t_1)\right] \circ \frac{\sin(\omega_0 t_1)}{n}\left[\cos(n\omega_0\tau) - 1\right]\right\}$	as in FIG. 2·5(f)

TABLE 2.2 - continued

PULSE	f(t)	FOURIER COEFFICIENT EXPRESSIONS			SPEC-TRA
		a_0	a_n	b_n	
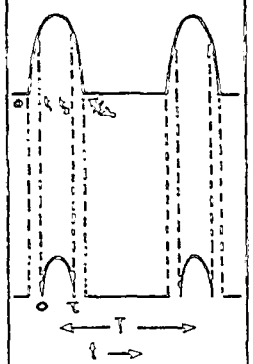 5 - SINUSOIDAL SQUARED	$f(t) = \left\{ \frac{\sin\omega_0(t_1+t)}{(1-\sin(\omega_0 t_1))} - \frac{\sin(\omega_0 t_1)}{(1-\sin(\omega_0 t_1))} \right\}^2$	$\frac{1}{2\pi(1-\sin(\omega_0 t_1))^2}\left\{\frac{1}{2}\omega_0\tau - \frac{1}{4}\left[\sin 2\omega_0(t_1+\tau) - \sin 2\omega_0 t_1\right] + 2\sin\omega_0 t_1\left[\cos(\omega_0(\tau+t_1)) - \cos\omega_0 t_1\right] + \omega_0\tau\sin(\omega_0 t_1)\right\}$	$a_1 = \frac{1}{\pi(1-\sin\omega_0 t_1)^2}\left\{\frac{1}{2}\sin\omega_0\tau - \frac{1}{2}\left[\sin(\omega_0(3\tau+2t_1)) - \sin 2\omega_0 t_1\right] - \frac{1}{4}\left[\sin(\omega_0(\tau+2t_1)) - \sin 2\omega_0 t_1\right] + \frac{\sin\omega_0 t_1}{2}\left[\cos(\omega_0(2\tau+t_1)) - \cos(\omega_0 t_1)\right] - \sin^2(\omega_0 t_1)\left[\omega_0\tau\right] + \sin^2(\omega_0 t_1)\left[\sin\omega_0\tau\right]\right\}$	$b_1 = \frac{1}{\pi(1-\sin(\omega_0 t_1))^2}\left\{\frac{1}{2}(1-\cos(\omega_0 t_1)) + \frac{1}{2}\left[\cos(\omega_0(3\tau+2t_1)) - \cos 2\omega_0 t_1\right] - \frac{1}{4}\left[\cos(\omega_0(\tau+2t_1)) - \cos(2\omega_0 t_1)\right] - \omega_0\tau\sin(\omega_0 t_1)\pi\cos(\omega_0 t_1) + \frac{\sin(\omega_0 t_1)}{2}\left[\sin(\omega_0(2\tau+t_1) - \sin(\omega_0 t_1) - \sin^2(\omega_0 t_1)\left[\cos(\omega_0\tau) - 1\right]\right]\right\}$	as in FIG. 2.5(g)
			$a_2 = \frac{1}{\pi(1-\sin(\omega_0 t_1))^2}\left\{\frac{1}{4}\sin 2\omega_0\tau - \frac{1}{16}\left[\sin(\omega_0(4\tau+2t_1)) - \sin(2\omega_0 t_1) - \frac{1}{4}\cos(2\omega_0 t_1)\pi(\omega_0\tau) + \frac{\sin(\omega_0 t_1)}{3}\left[\cos(\omega_0(3\tau+t_1)) - \cos(\omega_0 t_1)\right] - \sin(\omega_0 t_1)\left[\cos\omega_0(t_1-\tau) - \cos(\omega_0 t_1)\right] + \frac{\sin^2(\omega_0 t_1)}{2}\left[\sin 2\omega_0\tau\right]\right\}$	$b_2 = \frac{1}{\pi(1-\sin(\omega_0 t_1))^2}\left\{-\frac{1}{4}\left[\cos(2\omega_0\tau) - 1\right] + \frac{1}{16}\left[\cos(\omega_0(4\tau+2t_1)) - \cos(2\omega_0 t_1) + \frac{1}{4}\sin(\omega_0 t_1)\pi(\omega_0\tau) + \sin(\omega_0 t_1)\left[\sin\omega_0(t_1-\tau) - \sin(\omega_0 t_1)\right] + \frac{\sin(\omega_0 t_1)}{3}\left[\sin(\omega_0(3\tau+t_1)) - \sin(\omega_0 t_1)\right] + \frac{\sin^2(\omega_0 t_1)}{2}\left[\cos(2\omega_0\tau) - 1\right]\right\}$	
			$a_n = \frac{1}{\pi(1-\sin(\omega_0 t_1))^2}\left\{\frac{\sin(n\omega_0\tau)}{2n} - \frac{1}{4(n+2)}\left[\sin\left[\omega_0((n+2)\tau+2t_1)\right] - \sin(2\omega_0 t_1)\right] - \frac{1}{4(n-2)}\left[\sin\left[\omega_0((n-2)\tau-2t_1)\right] + \sin(2\omega_0 t_1)\right] + \frac{\sin(\omega_0 t_1)}{(n+1)}\left[\cos\left[\omega_0((n+1)\tau+t_1)\right] - \cos(\omega_0 t_1)\right] - \frac{\sin(\omega_0 t_1)}{(n-1)}\left[\cos\left[\omega_0((n-1)\tau-t_1)\right] - \cos(\omega_0 t_1)\right] + \frac{\sin^2(\omega_0 t_1)}{n}\sin(n\omega_0\tau)\right\}$	$b_n = \frac{1}{\pi(1-\sin(\omega_0 t_1))^2}\left\{\frac{1}{2n}(1-\cos(n\omega_0\tau) + \frac{1}{4(n+2)}\left[\cos\left[\omega_0((n+2)\tau+2t_1)\right] - \cos(2\omega_0 t_1)\right] + \frac{1}{4(n-2)}\left[\cos\left[\omega_0((n-2)\tau-2t_1)\right] - \cos(2\omega_0 t_1)\right] - \frac{\sin(\omega_0 t_1)}{(n-1)}\left[\sin\left[\omega_0((n-1)\tau-t_1)\right] + \sin(\omega_0 t_1)\right] + \frac{\sin(\omega_0 t_1)}{(n+1)}\left[\sin\left[\omega_0((n+1)\tau+t_1)\right] - \sin(\omega_0 t_1)\right] + \frac{\sin^2(\omega_0 t_1)}{n}\left[1-\cos(n\omega_0\tau)\right]\right\}$	

TABLE 2·3 ASYMMETRICAL PULSES

PULSE	f(t)	FOURIER COEFFICIENT EXPRESSIONS			SPECTRA
		a_0	a_n	b_n	
1 - TRIANGULAR WITH VARYING SHAPES 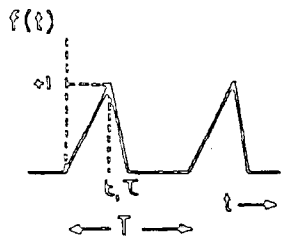	$f(t)=\frac{t}{t_1}, 0\le t\le t_1$ $=\left(\frac{\tau-t}{\tau-t_1}\right), t_1\le t\le\tau$	$\frac{\omega_0\tau}{4\pi}$	$\frac{1}{\pi n^2\omega_0 t_1(\tau-t_1)}\left[\omega_0\tau\cos(n\omega_0 t_1) - \omega_0(\tau-t_1) - \omega_0 t_1\cos(n\omega_0\tau)\right]$	$\frac{1}{\pi n^2\omega_0 t_1(\tau-t_1)}\left[\omega_0\tau\sin(n\omega_0 t_1) - \omega_0 t_1\sin(n\omega_0\tau)\right]$	
	A $t_1=0$	$\frac{\omega_0\tau}{4\pi}$	$\frac{1}{\pi n^2\omega_0\tau}\left[1-\cos(n\omega_0\tau)\right]$	$\frac{1}{\pi n^2\omega_0\tau}\left[n\omega_0\tau-\sin(n\omega_0\tau)\right]$	as in Fig 2·6(c)
	B $t_1=\tau$	$\frac{\omega_0\tau}{4\pi}$	$\frac{1}{\pi n^2\omega_0\tau}\left[n\omega_0\tau\sin(n\omega_0\tau) + \cos(n\omega_0\tau) - 1\right]$	$\frac{1}{\pi n^2\omega_0\tau}\left[\sin(n\omega_0\tau) - n\omega_0\tau\cos(n\omega_0\tau)\right]$	as in Fig 2·6(d)
	C $t_1=2(\tau-t_1)$ ie. $t_1=\frac{2}{3}\tau$	$\frac{\omega_0\tau}{4\pi}$	$\frac{9}{2\pi n^2\omega_0\tau}\left[\cos(\frac{2}{3}n\omega_0\tau) - \frac{1}{3} - \frac{2}{3}\cos(n\omega_0\tau)\right]$	$\frac{9}{2\pi n^2\omega_0\tau}\left[\sin(\frac{2}{3}n\omega_0\tau) - \frac{2}{3}\sin(n\omega_0\tau)\right]$	as in Fig 2·6(e)
	D $t_1=\left(\frac{\tau-t_1}{2}\right)$ ie. $t_1=\frac{1}{3}\tau$	$\frac{\omega_0\tau}{4\pi}$	$\frac{9}{2\pi n^2\omega_0\tau}\left[\cos(\frac{n\omega_0\tau}{3}) - \frac{2}{3} - \frac{1}{3}\cos(n\omega_0\tau)\right]$	$\frac{9}{2\pi n^2\omega_0\tau}\left[\sin(\frac{n\omega_0\tau}{3}) - \frac{1}{3}\sin(n\omega_0\tau)\right]$	as in Fig 2·6(f)

TABLE 2·3 Cont.

PULSE	f(t)	FOURIER COEFFICIENT EXPRESSIONS			SPECTRA
		a_0	a_n	b_n	
2 – TRAPEZOIDAL WITH VARYING SHAPES 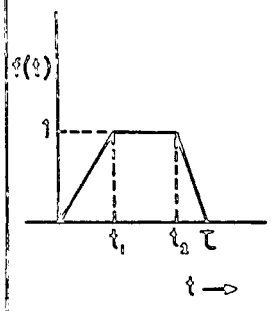	$f(t)=\frac{t}{t_1}$, $0<t<t_1$ $=1$, $t_1<t<t_2$ $=\left(\frac{t-\tau}{t_2-\tau}\right)$, $t_2<t<\tau$	$\frac{1}{T}\left[\frac{1}{2}(\tau+t_2-t_1)\right]$	$\frac{1}{\pi n^2\omega_0 t_1(\tau-t_2)}\{(\tau-t_2)\cos(n\omega_0 t_1)+t_1\cos(n\omega_0 t_2)-t_1\cos(n\omega_0\tau)-(\tau-t_2)\}$	$\frac{1}{\pi n^2\omega_0 t_1(\tau-t_2)}\{(\tau-t_2)\sin(n\omega_0 t_1)+t_1\sin(n\omega_0 t_2)-t_1\sin(n\omega_0\tau)\}$	
	A $t_1=\frac{\tau}{10}$ $t_2=\frac{5\tau}{10}$	$\frac{7}{20}\frac{\omega_0\tau}{\pi}$	$\frac{2}{\pi n^2\omega_0\tau}\{5\cos(\frac{n\omega_0\tau}{10})+\cos(\frac{n\omega_0\tau}{2})-\cos(n\omega_0\tau)-5\}$	$\frac{2}{\pi n^2\omega_0\tau}\{5\sin(\frac{n\omega_0\tau}{10})+\sin(\frac{n\omega_0\tau}{2})-\sin(\frac{n\omega_0\tau}{2})\}$	as in Fig 2·6(g)
	B $t_1=\frac{2\tau}{10}$ $t_2=\frac{6\tau}{10}$	$\frac{7}{20}\frac{\omega_0\tau}{\pi}$	$\frac{5}{2}\frac{1}{\pi n^2\omega_0\tau}\{2\cos(\frac{n\omega_0\tau}{5})+\cos(\frac{2}{5}n\omega_0\tau)-\cos(n\omega_0\tau)-2\}$	$\frac{5}{2}\frac{1}{\pi n^2\omega_0\tau}\{2\sin(\frac{n\omega_0\tau}{5})+\sin(\frac{2}{5}n\omega_0\tau)-\sin(n\omega_0\tau)\}$	as in Fig 2·6(h)
	C $t_1=\frac{3\tau}{10}$ $t_2=\frac{7\tau}{10}$	$\frac{7}{20}\frac{\omega_0\tau}{\pi}$	$\frac{10}{3}\frac{1}{\pi n^2\omega_0\tau}\{\cos(\frac{3}{10}n\omega_0\tau)+\cos(\frac{7}{10}n\omega_0\tau)-\cos(n\omega_0\tau)-1\}$	$\frac{10}{3}\frac{1}{\pi n^2\omega_0\tau}\{\sin(\frac{3}{10}n\omega_0\tau)+\sin(\frac{7}{10}n\omega_0\tau)-\sin(n\omega_0\tau)\}$	as in Fig 2·6(i)

TABLE 2·3 Cont.

PULSE	f(t)	FOURIER COEFFICIENT EXPRESSIONS			SPECTRA
		a_0	a_n	b_n	
2 - continued TRAPEZOIDAL WITH VARYING SHAPES	D $t_1=\frac{4}{10}\tau$ $t_2=\frac{8}{10}\tau$	$\frac{7}{20}\left(\frac{\omega_0\tau}{\pi}\right)$	$\frac{5}{2}\cdot\frac{1}{\pi n^2\omega_0\tau}\left\{\cos\left(\frac{2}{5}n\omega_0\tau\right)\circ 2\cos\left(\frac{4}{5}n\omega_0\tau\right)-2\cos(n\omega_0\tau)-1\right\}$	$\frac{5}{2}\cdot\frac{1}{\pi n^2\omega_0\tau}\left\{\sin\left(\frac{2}{5}n\omega_0\tau\right)\circ 2\sin\left(\frac{4}{5}n\omega_0\tau\right)-2\sin(n\omega_0\tau)\right\}$	as in Fig 2·6(j)
	E $t_1=\frac{5}{10}\tau$ $t_2=\frac{9}{10}\tau$	$\frac{7}{20}\left(\frac{\omega_0\tau}{\pi}\right)$	$\frac{2}{\pi n^2\omega_0\tau}\left\{\cos\left(\frac{n\omega_0\tau}{2}\right)\circ 5\cos\left(\frac{9}{10}n\omega_0\tau\right)-5\cos(n\omega_0\tau)-1\right\}$	$\frac{2}{\pi n^2\omega_0\tau}\left\{\sin\left(\frac{1}{2}n\omega_0\tau\right)\circ 5\sin\left(\frac{9}{5}n\omega_0\tau\right)-5\sin(n\omega_0\tau)\right\}$	as in Fig 2·6(k)
3 - EXPONENTIAL 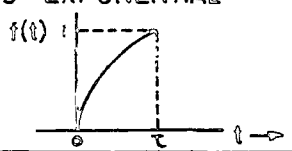	$f(t)=\frac{(1-e^{-k\omega_0 t})}{(1-m)}$ $m=e^{-k\omega_0\tau}$	$\frac{1}{2\pi k(1-m)}\times\left[m-1-\ln m\right]$	$\frac{1}{\pi(n^2\circ k^2)(1-m)}\left\{k\left[m\cos(n\omega_0\tau)-1\right]\circ\left[n-mn\circ\frac{k^2}{n}\right]\sin(n\omega_0\tau)\right\}$	$\frac{1}{\pi(n^2\circ k^2)(1-m)}\left\{k^2\circ\left[mn-n-\frac{k^2}{n}\right]\cos(n\omega\tau)\circ mk\sin(n\omega_0\tau)\right\}$	as in Fig 2·6(l)
4 - EXPONENTIAL 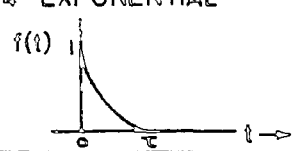	$f(t)=\frac{(e^{-k\omega_0 t}-m)}{(1-m)}$ $m=e^{-k\omega_0 t}$	$\frac{1}{2\pi k(1-m)}\times\left[1-m\circ m\ln m\right]$	$\frac{1}{\pi(n^2\circ k^2)(1-m)}\left\{k-mk\cos(n\omega_0\tau)-\frac{mk^2}{n}\sin(n\omega_0\tau)\right\}$	$\frac{1}{\pi(n^2\circ k^2)(1-m)}\left\{\left[n-mn-\frac{mk^2}{n}\right]\circ\frac{mk^2}{n}\cos(n\omega_0\tau)-mk\sin(n\omega_0\tau)\right\}$	as in Fig 2·6(m)

TABLE 2·3 Cont.

PULSE	f(t)	FOURIER COEFFICIENT EXPRESSIONS			SPECTRA
		a_0	a_n	b_n	
5 - EXPONENTIAL 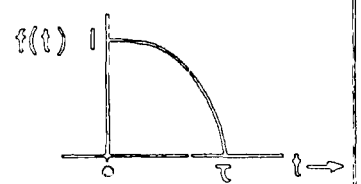	$f(t)=\frac{(m-e^{k\omega_0 t})}{(m-1)}$ $m=e^{k\omega_0 t}$	$\frac{1}{2\pi k(m-1)}\times[m\ln m-m+1]$	$\frac{1}{\pi(k^2+n^2)(m-1)}\left\{\frac{mk^2}{n}\sin(n\omega_0\tau)+k\left[1-m\cos(n\omega_0\tau)\right]\right\}$	$\frac{1}{\pi(m-1)(k^2+n^2)}\left\{\left[\frac{mk^2}{n}+mn-n\right]-mk\sin(n\omega_0\tau)-\frac{mk^2}{n}\cos(n\omega_0\tau)\right\}$	as in Fig 2·6(n)
6 - SINUSOIDAL 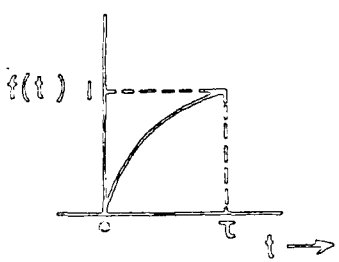	$f(t)=\left\{\sin\left[\omega_0(bt+\tau)\right]-\sin(\omega_0\tau)\right\}\times\frac{1}{a\sin(\omega_0\tau)}$	$\frac{1}{2\pi a}\left\{\frac{1}{b\sin(\omega_0\tau)}\left[\cos(\omega_0\tau)-\cos\omega_0\tau(1+b)\right]-\omega_0\tau\right\}$	$\frac{1}{2\pi a(b^2-n^2)}\left\{2b\cot(\omega_0\tau)-\frac{(b-n)\cos\left[\omega_0\tau(b+n)+\omega_0\tau\right]}{\sin(\omega_0\tau)}-\frac{(b+n)\cos\left[\omega_0\tau(b-n)+\omega_0\tau\right]}{\sin(\omega_0\tau)}-\frac{2(b^2-n^2)}{n}\sin(n\omega_0\tau)\right.$	$\frac{1}{2\pi a(b^2-n^2)}\left\{\frac{1}{\sin(\omega_0\tau)}\left[(b+n)\sin(\omega_0(b-n)\tau+\omega_0\tau)-(b-n)\sin(\omega_0(b+n)\tau+\omega_0\tau)\right]-\frac{2(b^2-n^2)}{n}\left[1-\cos(n\omega_0\tau)\right]-2n\right\}$	as in Fig 2·6(o)

TABLE 2·3 Cont.

PULSE	f(t)	FOURIER COEFFICIENT EXPRESSIONS			SPECTRA
		a_0	a_n	b_n	
7 - SINUSOIDAL 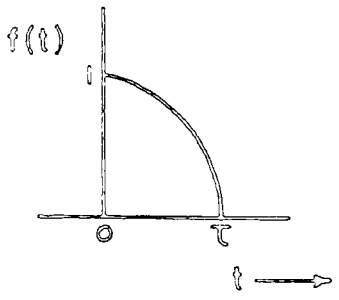	$f(t) = \left[\frac{1}{1-\cos(\omega_0\tau)}\right] \times \left[\cos(\omega_0 t) - \cos(\omega_0\tau)\right]$	$\frac{1}{2\pi\left[1-\cos(\omega_0\tau)\right]} \times \left[\sin(\omega_0\tau) - \omega_0\tau\cos(\omega_0\tau)\right]$	$\frac{1}{4\pi\left[1-\cos(\omega_0\tau)\right]}\left[2\omega_0\tau - \sin(2\omega_0\tau)\right]$ for $n=1$ $\frac{1}{\pi n(n^2-1)\left[1-\cos(\omega_0\tau)\right]}\{\sin(n\omega_0\tau)\cos(\omega_0\tau) - n\cos(n\omega_0\tau)\sin(n\omega_0\tau)\}$ for $n\geq 2$	$\frac{1}{4\pi\left[1-\cos(\omega_0\tau)\right]}\left[\cos(2\omega_0\tau) + 3 - 4\cos(\omega_0\tau)\right]$ for $n=1$ $\frac{1}{\pi n(n^2-1)\left[1-\cos(\omega_0\tau)\right]}\{n^2 - \cos(n\omega_0\tau)\cos(\omega_0\tau) - n\sin(n\omega_0\tau)\sin(\omega_0\tau) - (n^2-1)\cos(\omega_0\tau)\}$ for $n\geq 2$	as in Fig 2·6(p)

asymmetrical waveform. Every pulse was first Fourier analysed to obtain the expressions for its coefficients ; from these the relative amplitudes and phases of the harmonics were determined and examined. Finally, the amplitude and phase spectra were plotted for each pulse waveform under consideration. The knowledge of symmetry of the function f(t) is important because this very often helps to simplify the analysis and hence reduce the computing time.

2.4.2 The Methods of Analysis and Computation

A rectangular, single polarity train of pulses, repeated periodically, was chosen as the reference waveform within which other pulse configurations were introduced. This provided an easy comparison between different pulse shapes. It also reduced the choice of the shapes needed to cover as wide a range of variations as possible. The reference pulse was made to have its origin at the leading edge or the central line of symmetry, be of unity height and have the ratio of its duration (τ) to the pulse repetition period (T) equal to 0.1, i.e. $\frac{\tau}{T} = 0.1$. The well-known spectrum of this type of pulse, often called the periodic gate function, has a $\frac{\sin x}{x}$ distribution of amplitudes and its envelope consists of a number of lobes. For this particular case, i.e. $\frac{T}{\tau} = 10$, each lobe will contain nine harmonic components, whilst every tenth harmonic will be zero.

If a periodic waveform is completely described by a known time function, then its Fourier coefficients can be obtained using eqns. 2.2.5, 2.2.6 and 2.2.7. However, for the case where this is not possible separate expressions must be derived. Thus, it is obvious that the Fourier coefficients can be determined provided that the pulse waveform can be completely described and the integral equations solvable. A summary of all expressions for the Fourier coefficients of the pulses considered is presented in Tables 2.1, 2.2 and 2.3.

2.4.3 Symmetrical Pulses

In the case of even-function symmetrical waveforms (types chosen are shown in Table 2.1) only cosine terms are present and the amplitude spectrum is given by the coefficient a_n, where 'n' is an integer. Since the coefficient b_n is equal to zero for all 'n', the phase within each lobe remains constant at 0^o or 180^o. Waveforms with odd-function symmetry do have both cosine and sine terms, resulting in the existence of phase in addition to amplitude spectra. However, for the square pulse with odd-function symmetry, the series comprised only the sine terms. For convenience, the amplitude spectra may be represented by 'spectrum envelope'. Attempts were made to establish any relationships between the areas of different pulse waveforms and other parameters. It was found from the spectrum envelopes, that the fundamental amplitudes are approximately proportional to the areas of the pulses (shown in Table 2.4).

From the expressions for the Fourier coefficients (Table 2.1), it can be seen that they are either positive or negative, depending on the harmonic number 'n'. As the Fourier coefficient expression for the rectangular pulse is a sine function, the Fourier coefficients do have both positive and negative values. However, in the case of triangular pulses whose Fourier coefficient expression is given by the square of the sine function, all the coefficients will have positive values. If the area of the pulse under consideration is greater than one half that of the reference pulse, the amplitude spectra have both positive and negative values. On the other hand if this area is less than one half that for the reference pulse, the amplitude spectra are always positive.

Theoretically, pulses of identical shapes produce the same amplitude spectrum envelope, irrespective of where the origin lies. This can be verified for even function symmetry by considering Table 2.1 and the corresponding

TABLE 2.4: The Values of Pulse Area and their Corresponding Phase Variation and the Amplitude at the Fundamental

PULSE		PHASE VARIATION IN			
Waveform	Area (square units)	Major Lobe	First Minor Lobe	Second Minor Lobe	$C_1 \times 10^{-2}$
Rectangular	200	0^{o}-180^{c}	0^{o}-180^{o}	0^{o}-180^{o}	19.8
Trapezoidal	150	0^{o}-234^{o}	54^{o}-306^{o}	126^{o}-306^{o}	14.8
Sinusoidal	133	0^{o}-270^{o}	90^{o}-270^{o}	90^{o}-270^{o}	13.3
Sinusoidal Squared	106	0^{o}-342^{o}	162^{o}-340^{o}	162^{o}-340^{o}	10.6
Triangular	100	0^{o}-360^{o}	0^{o}-360^{o}	-	9.9

Figs 2.4(a) and 2.4(b). Data for odd function symmetry is given in Table 2.2 and Figs 2.5 ; here Fig.2.5(a) shows symmetrical pulses of different shapes while Fig 2.5(b) gives their respective amplitude spectra ; Fig 2.5(c) to 2.5(g) gives amplitude and phase spectra for the pulses listed in Table 2.2. Phases are computed from the Fourier coefficients a_n and b_n, and the phase angles fall to the quadrant corresponding to the signs of these coefficients. The observations on the phase variations between harmonics up to the thirty sixth harmonic for different pulse waveforms are summarised in Table 2.4. The upper limiting values of the phases in the major lobes appear to have some relationship with the areas of the pulse waveform. This is illustrated in Fig 2.7 plotted from data obtained in Table 2.4. Another significant observation here is that the phase variations are linear within each lobe ; furthermore the range of variation depends on pulse shapes.

2.4.4 Asymmetrical Pulses

The pulses considered here are those of triangular and trapezoidal of varying shapes,exponential and sinusoidal. However, those of symmetrical shapes are the special cases of the general pulses. The origin is chosen to be at the leading edge. All appropriate expressions are summarised in Table 2.3. Figs 2.6(a) and 2.6(b) refer to pulses of triangular and trapezoidal shapes. Figs. 2.6(c) to 2.6(f) detail the amplitude and phase spectra for different triangular pulses. Figs.2.6(g) to 2.6(k) refer to trapezoidal pulses and Figs 2.6(l) to 2.6(p) refer to exponential and sinusoidal pulses. As each of the pulses considered had to be fitted into the reference pulse, the basic equations for some pulses require modification. In general phase variations for asymmetrical pulses are nonlinear.

A lobe in an amplitude spectral envelope is said to exist if the curve crosses a zero-point. In all cases except for those of triangular cases of

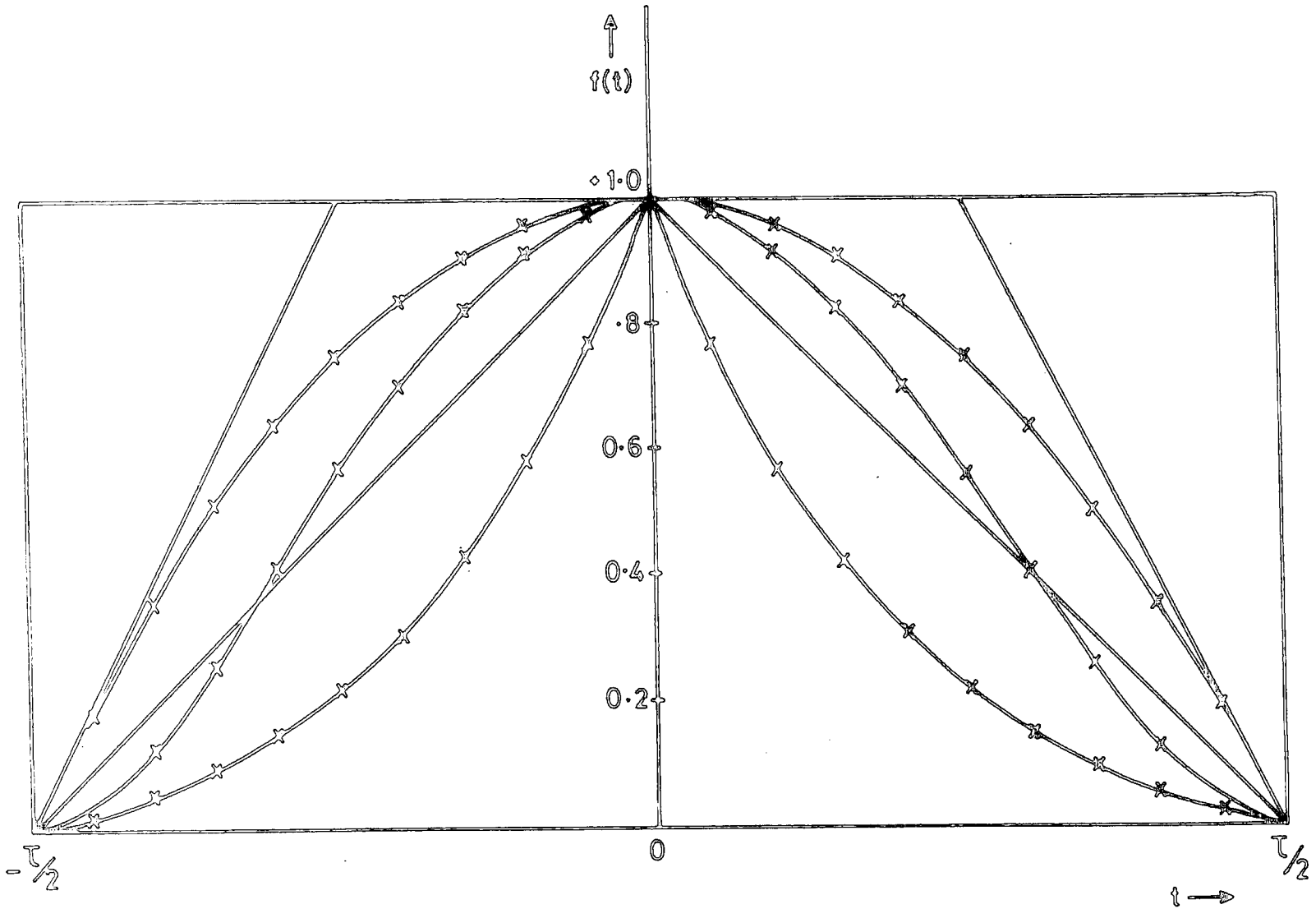

FIG. 2·4 (a) PULSES – SYMMETRICAL CASES
(EVEN FUNCTION SYMMETRY)

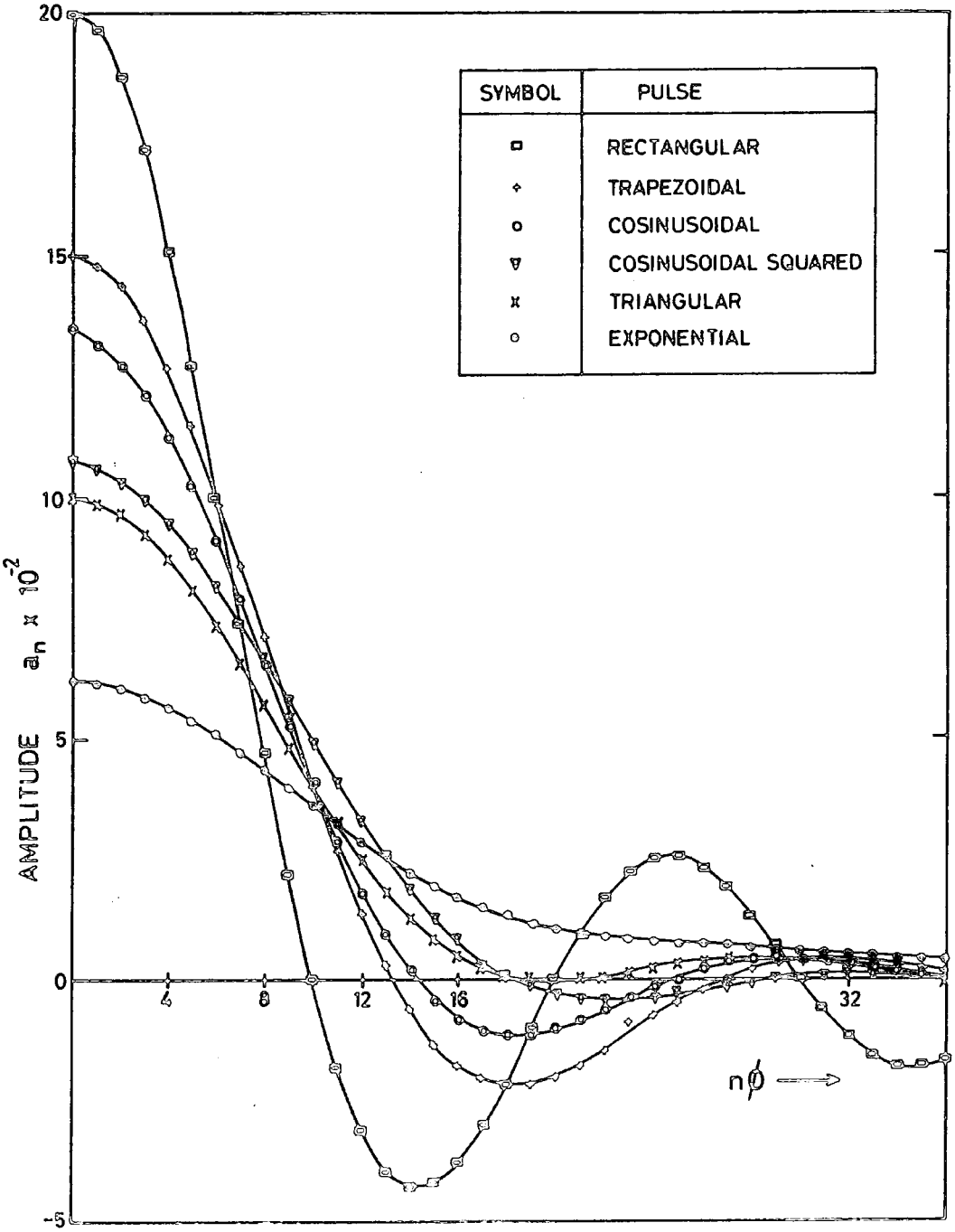

AND PHASE

FIG. 2·4(b) AMPLITUDE/SPECTRA (symmetrical case)

EVEN FUNCTION SYMMETRY

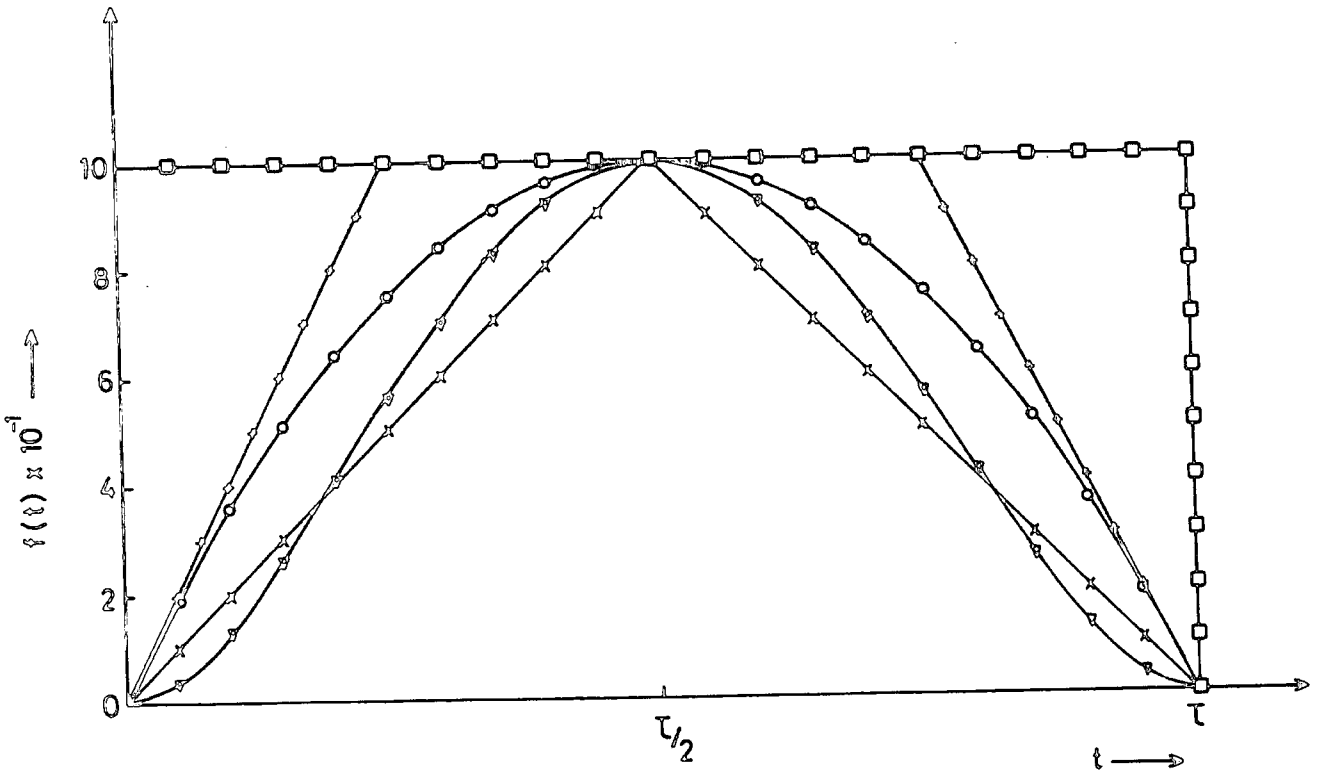

FIG. 2·5(a) PULSES - SYMMETRICAL CASES
(ODD FUNCTION SYMMETRY)

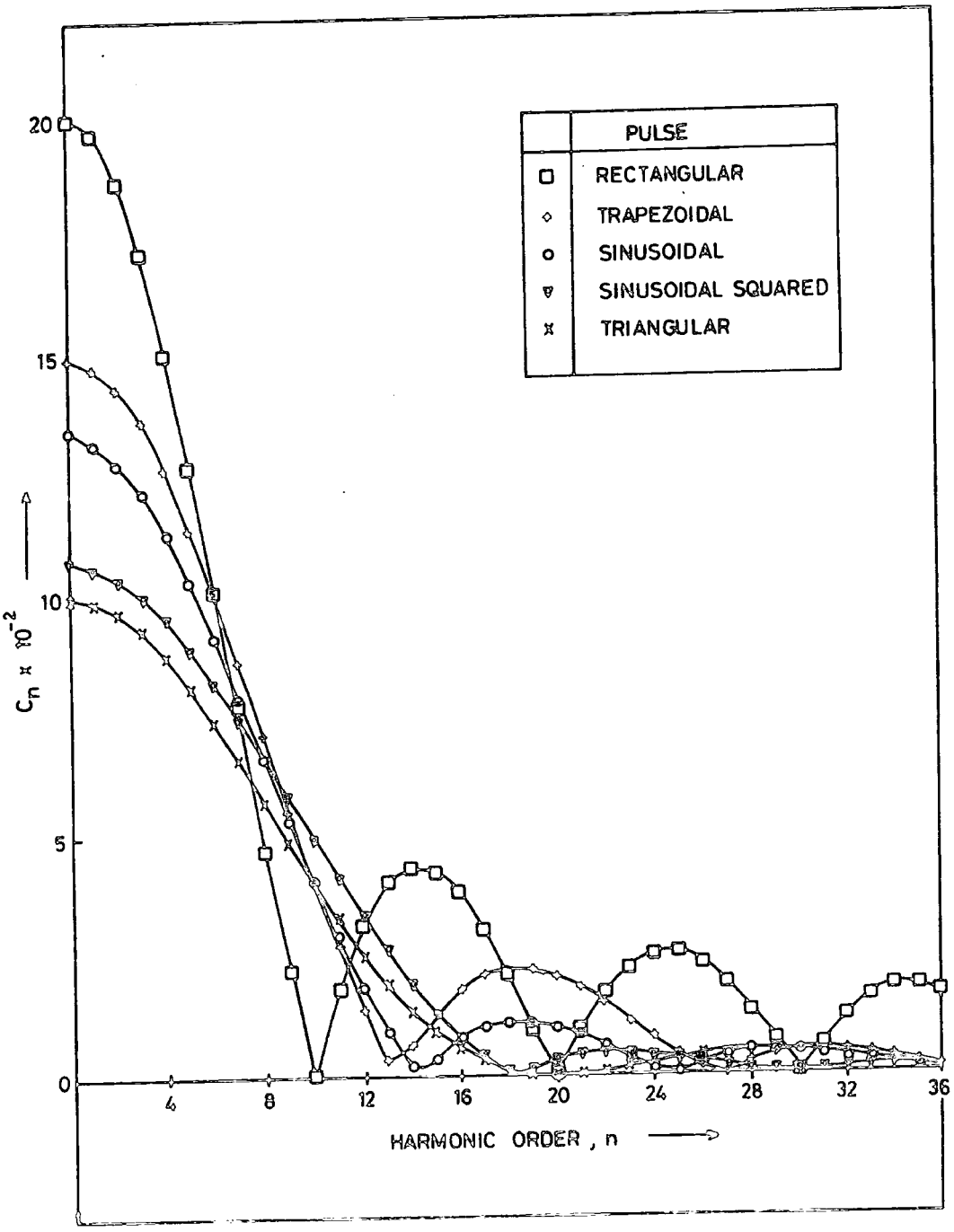

FIG. 2·5(b) AMPLITUDE SPECTRA - SYMMETRICAL CASES (ODD FUNCTION SYMMETRY)

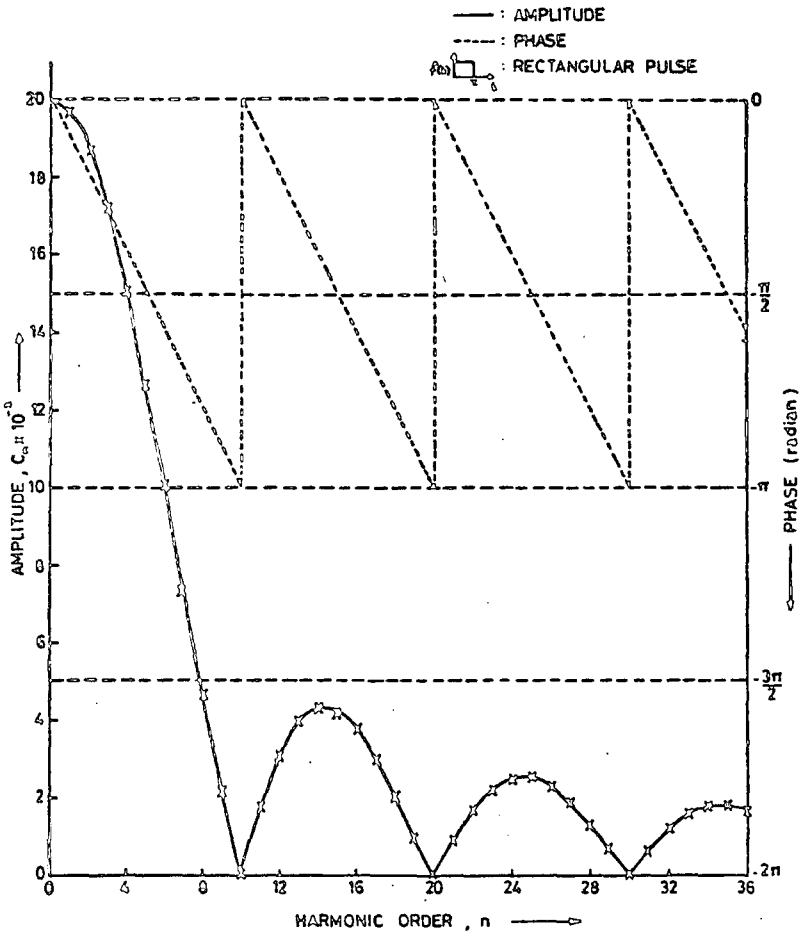

FIG. 2·5(c) AMPLITUDE AND PHASE SPECTRA

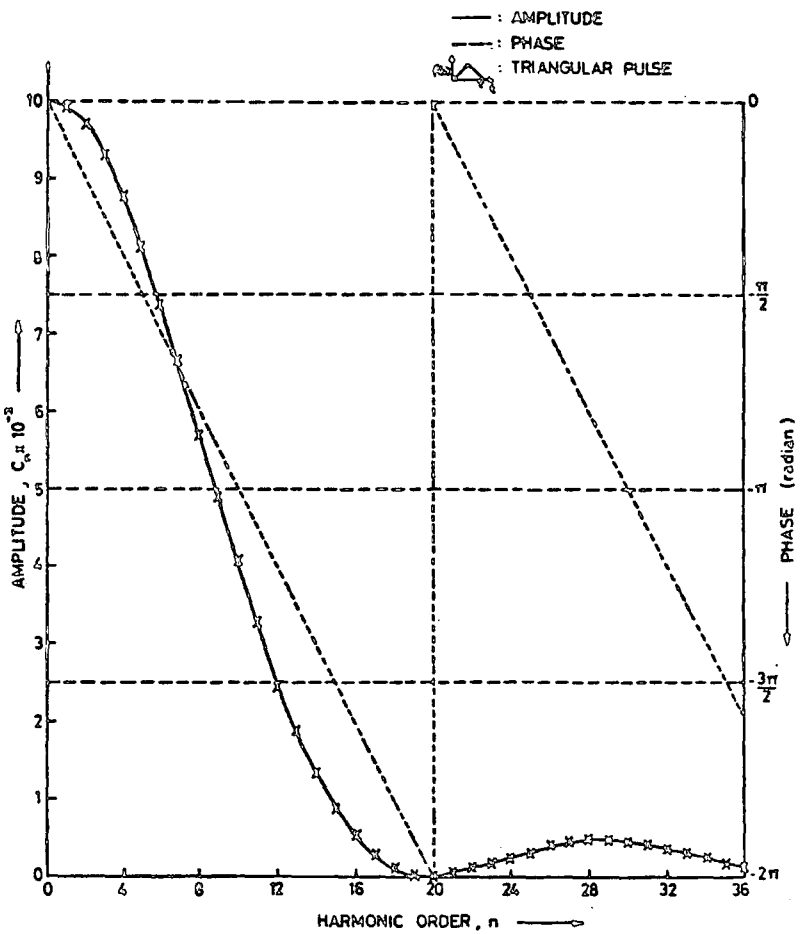

FIG. 2·5 (d) AMPLITUDE AND PHASE SPECTRA

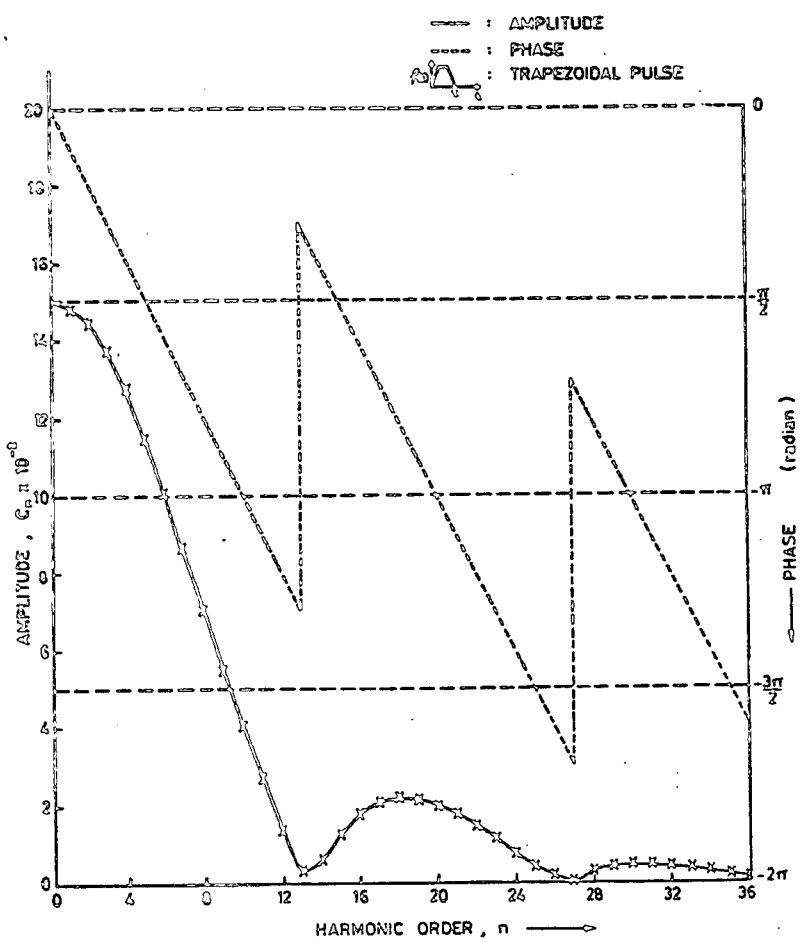

FIG. 2·5(e) AMPLITUDE AND PHASE SPECTRA

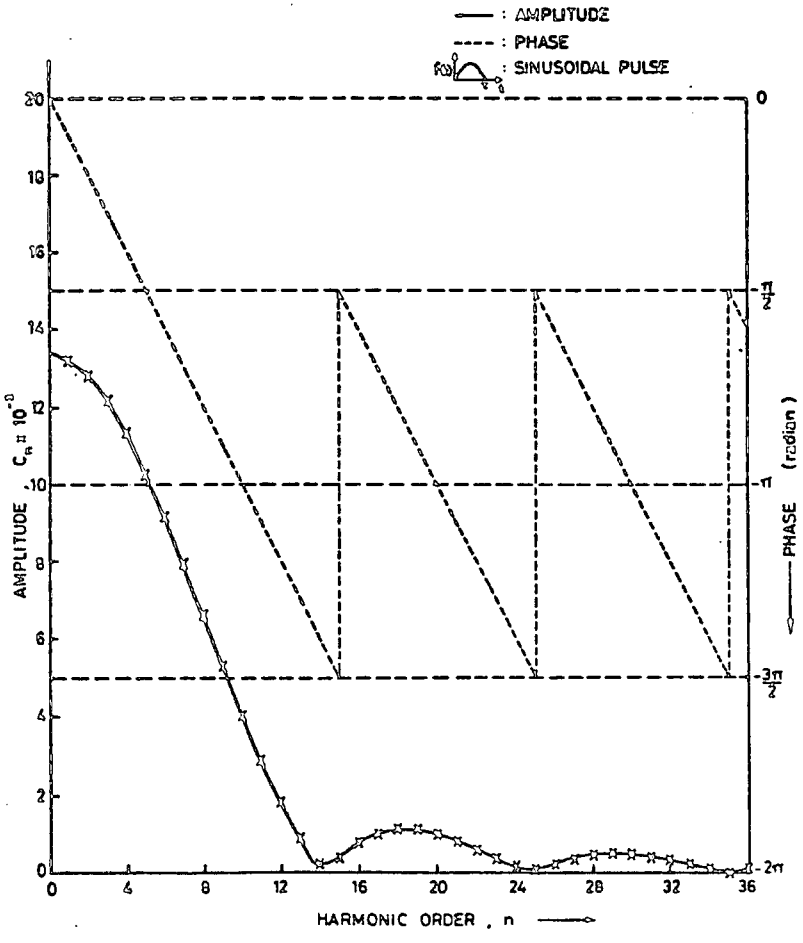

FIG. 2·5(f) AMPLITUDE AND PHASE SPECTRA

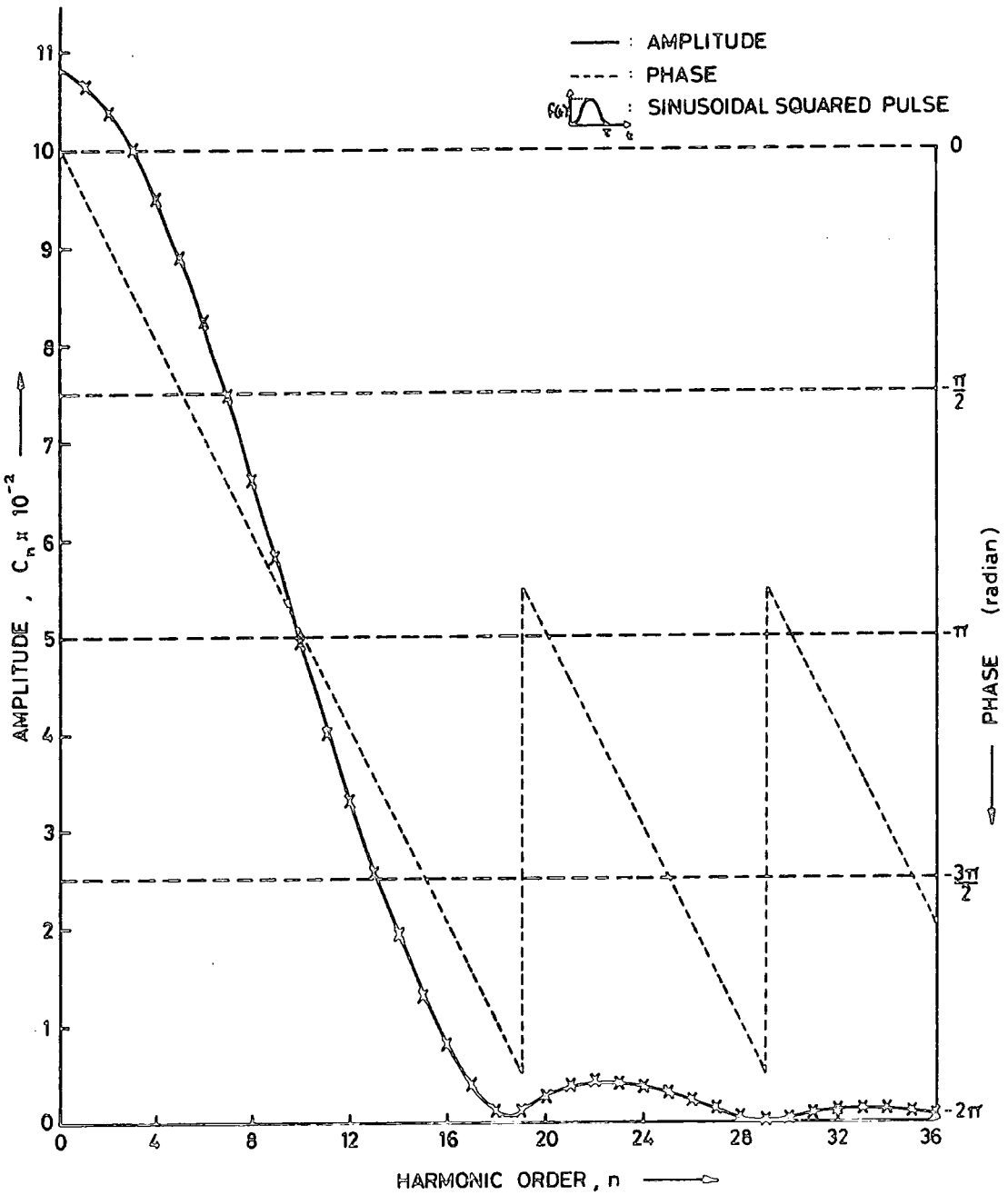

FIG. 2·5 (g) AMPLITUDE AND PHASE SPECTRA

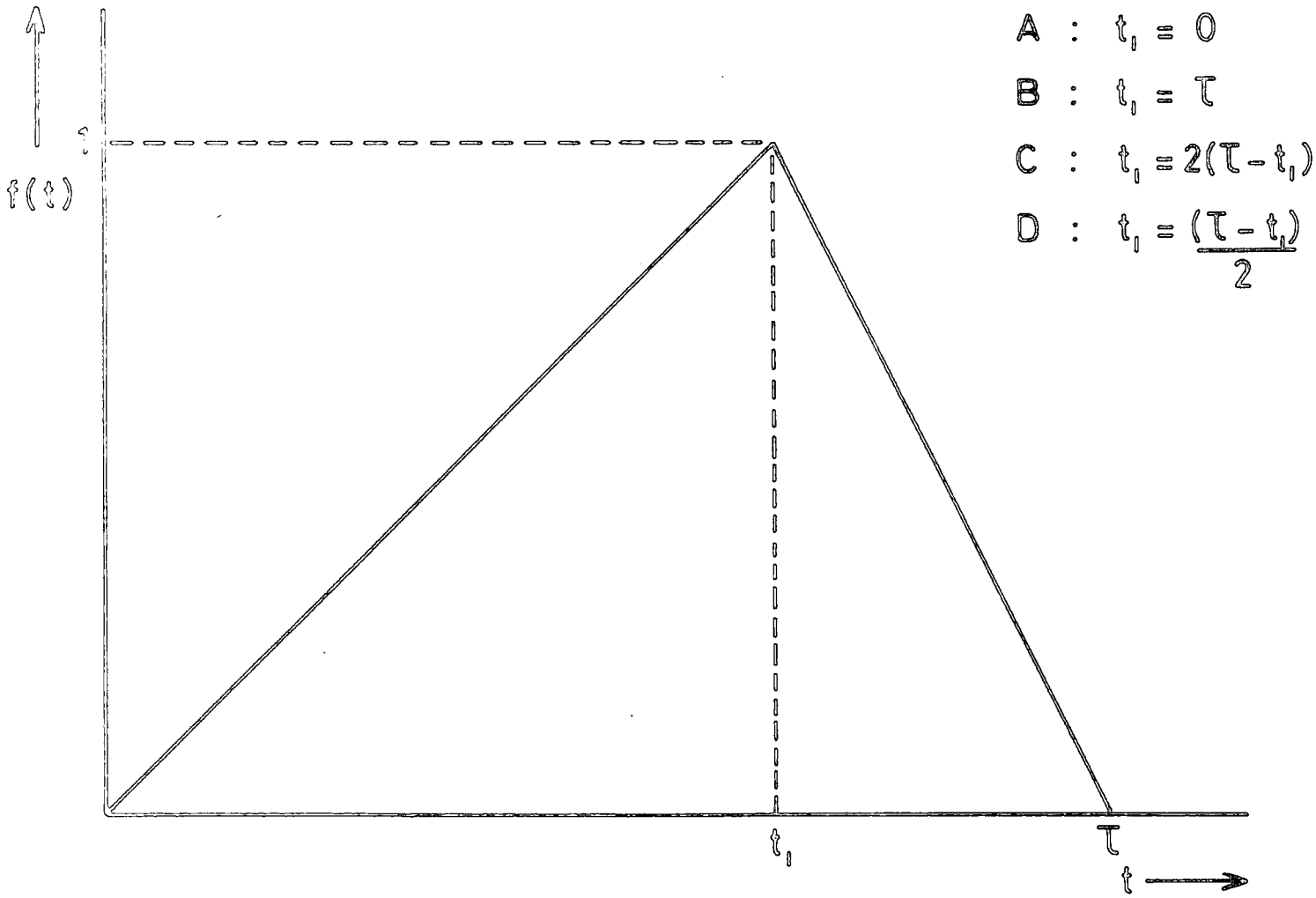

FIG. 2·6(a) PULSES - TRIANGULAR CASES

FIG.2·6(b) PULSES - TRAPEZOIDAL CASES

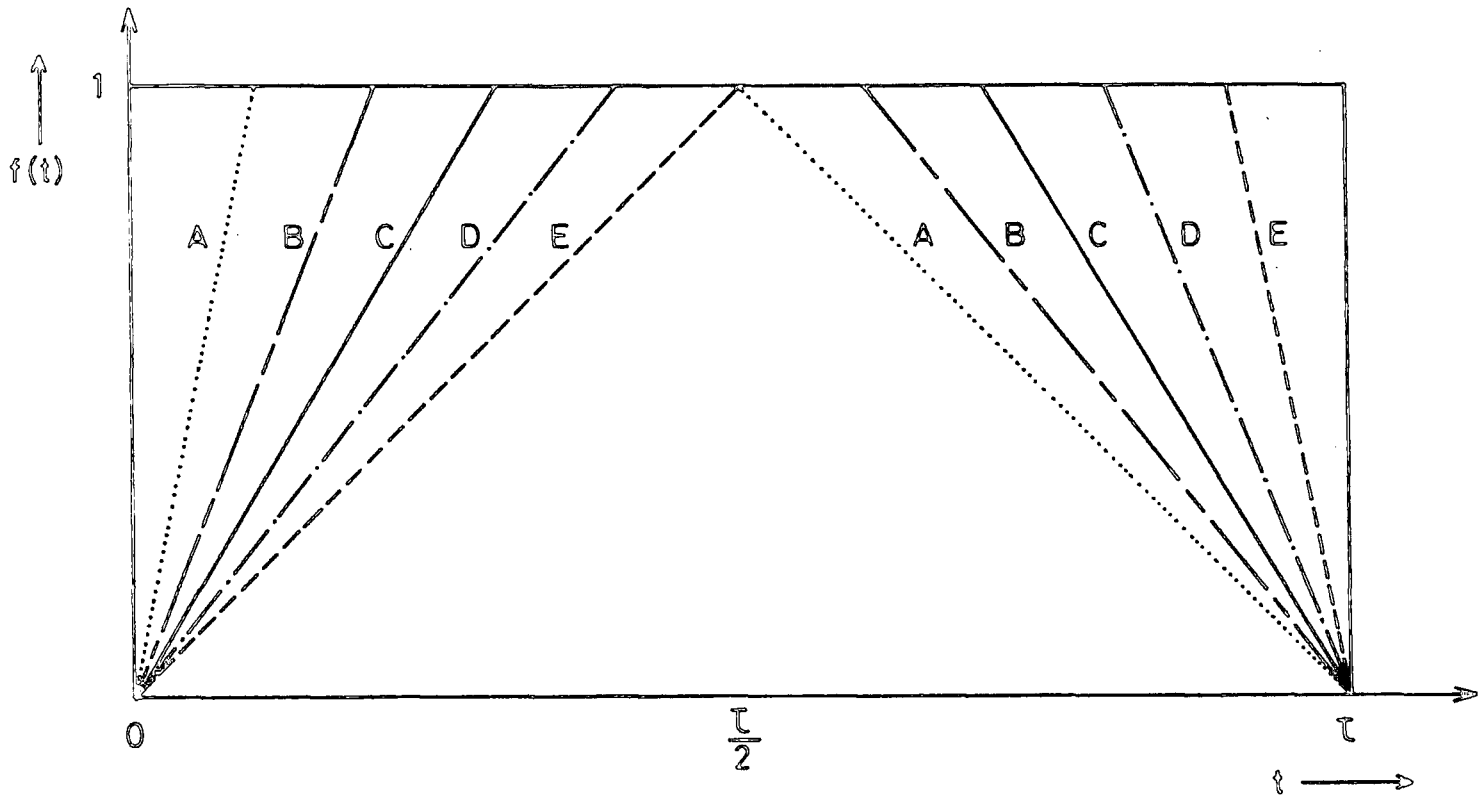

Cases : A : $t_1 = \frac{\tau}{10}$, $t_2 = \frac{5}{10}\tau$

B : $t_1 = \frac{2}{10}\tau$, $t_2 = \frac{6}{10}\tau$

C : $t_1 = \frac{3}{10}\tau$, $t_2 = \frac{7}{10}\tau$

D : $t_1 = \frac{4}{10}\tau$, $t_2 = \frac{8}{10}\tau$

E : $t_1 = \frac{5}{10}\tau$, $t_2 = \frac{9}{10}\tau$

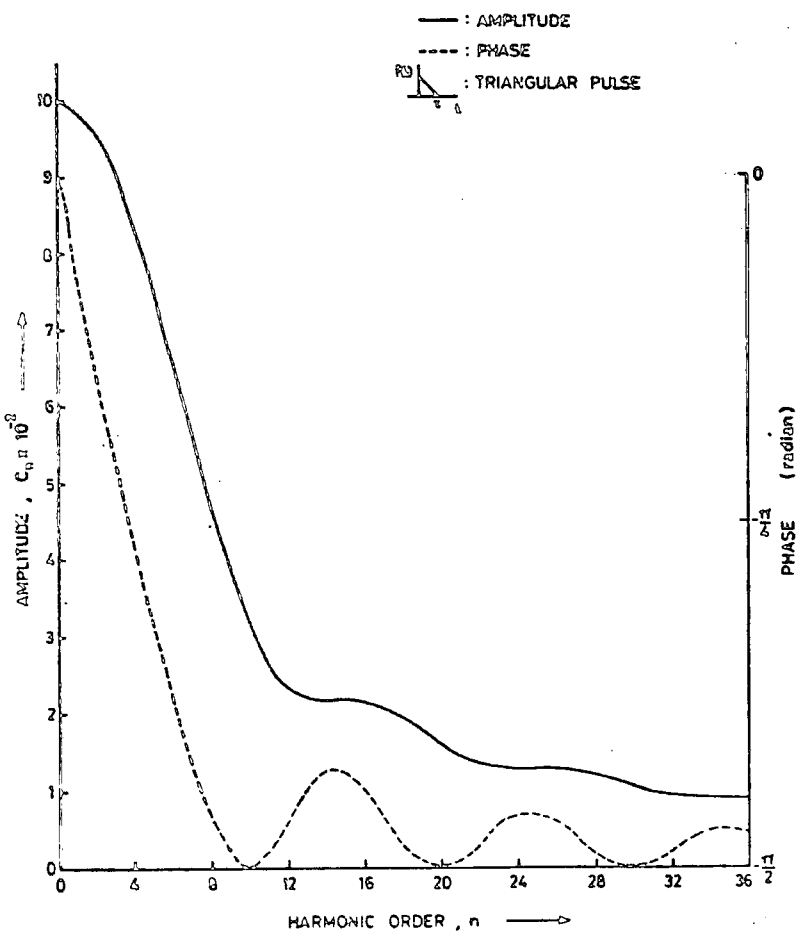

FIG. 2·6 (c) AMPLITUDE AND PHASE SPECTRA

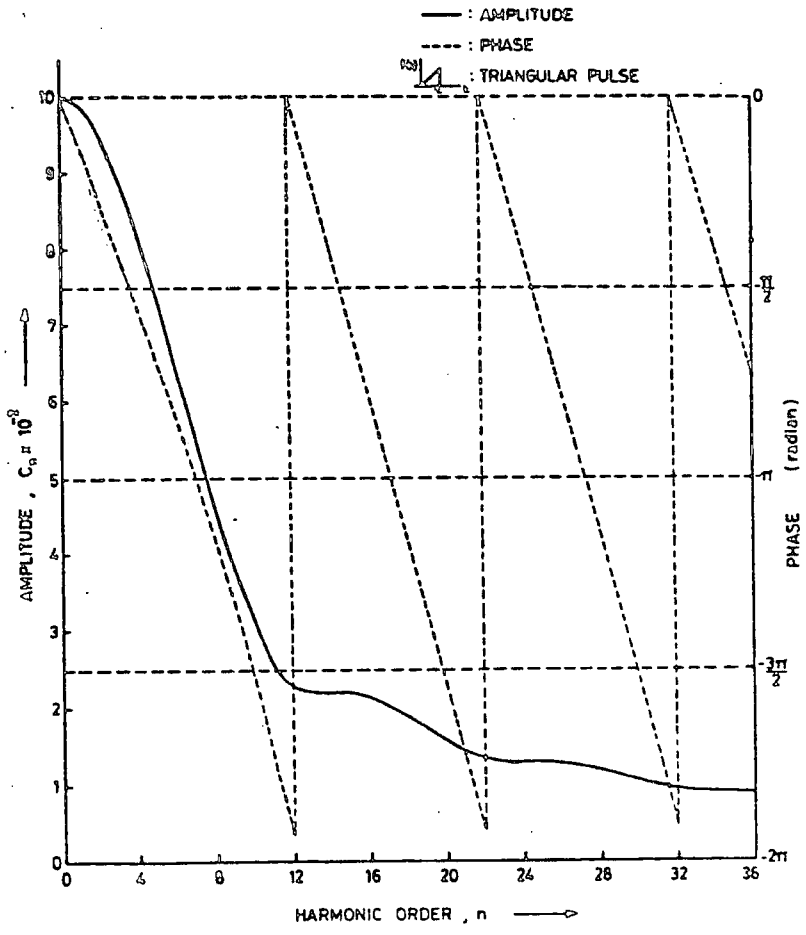

FIG. 2·6 (d) AMPLITUDE AND PHASE SPECTRA

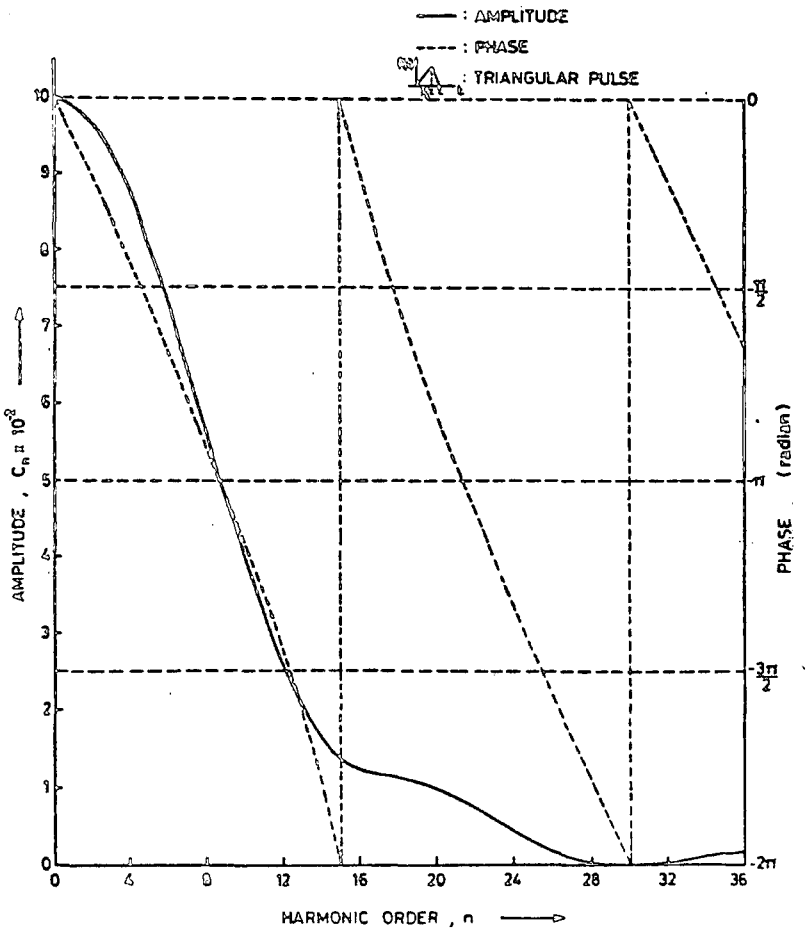

FIG. 2·6 (e) AMPLITUDE AND PHASE SPECTRA

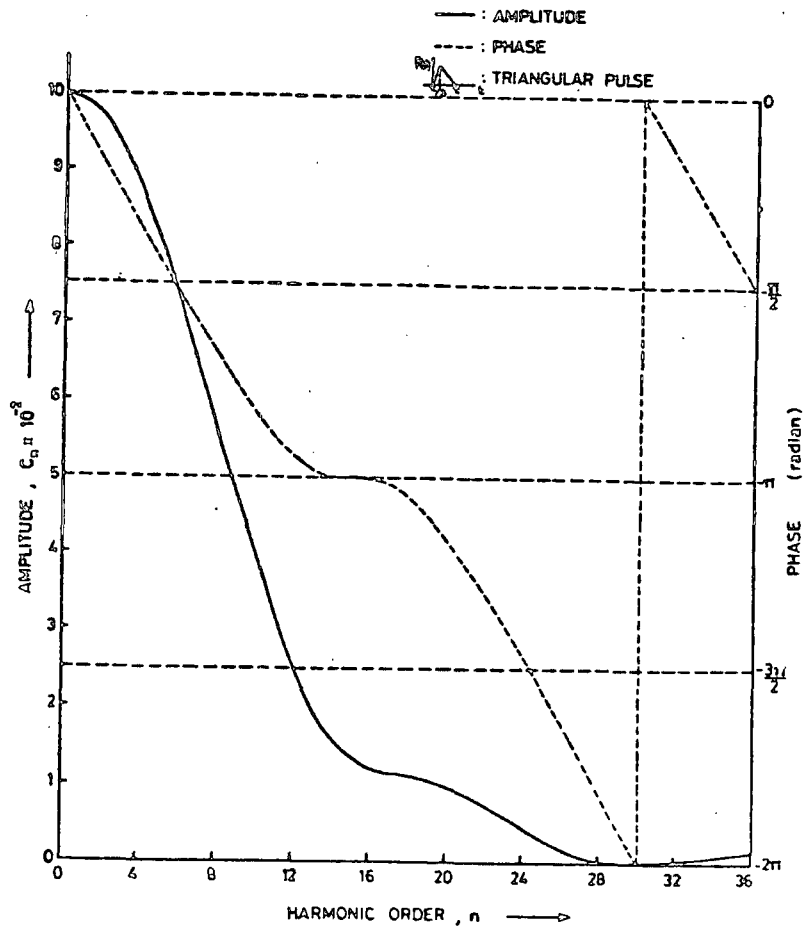

FIG. 2·6 (f) AMPLITUDE AND PHASE SPECTRA

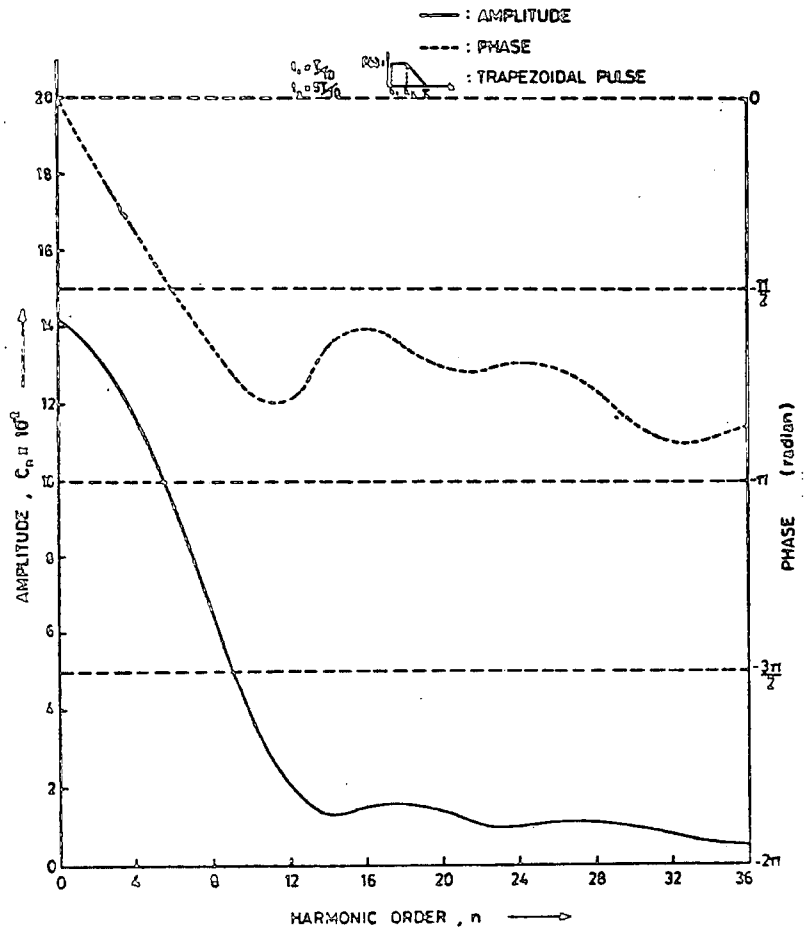

FIG. 2·6(g) AMPLITUDE AND PHASE SPECTRA

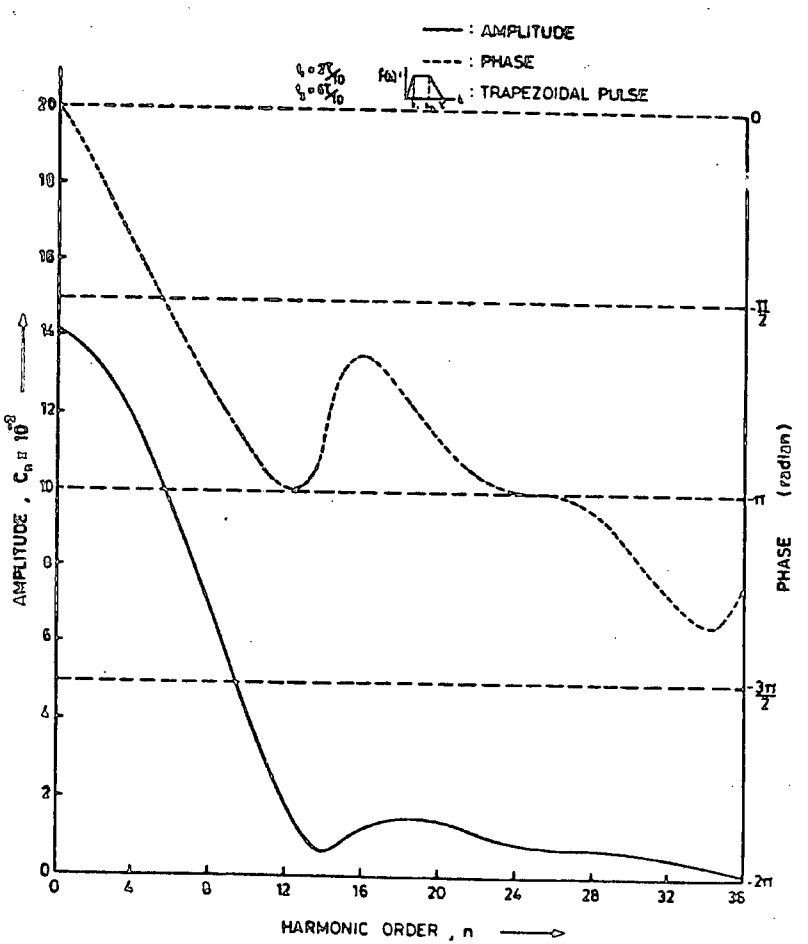

FIG. 2·6(h) AMPLITUDE AND PHASE SPECTRA

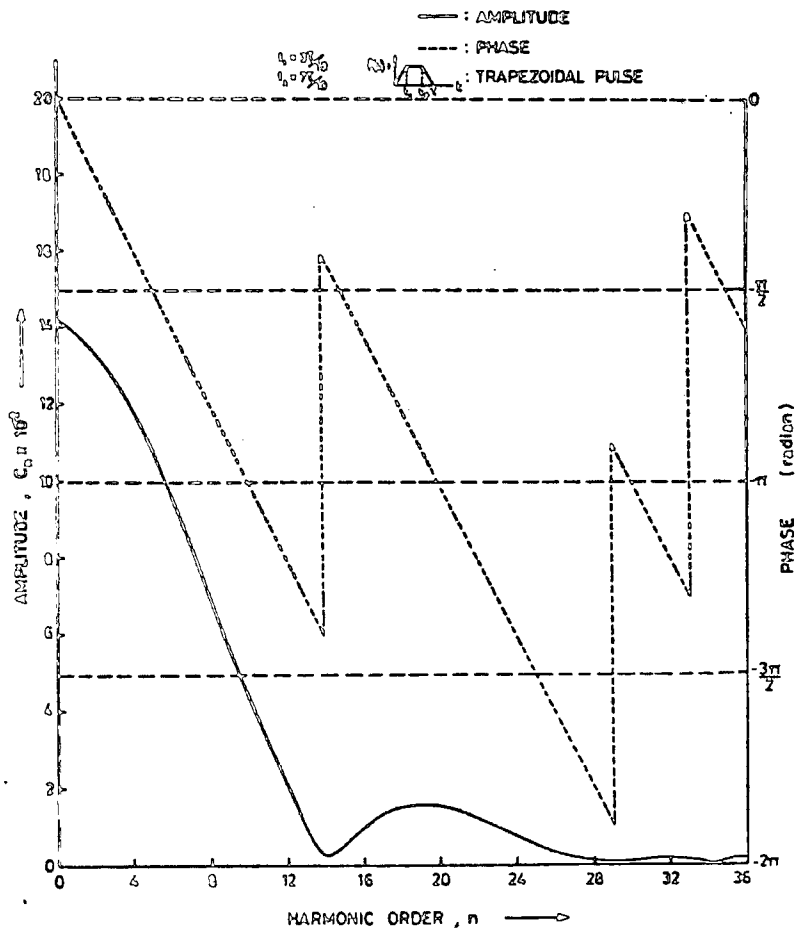

FIG.2·5(i) AMPLITUDE AND PHASE SPECTRA

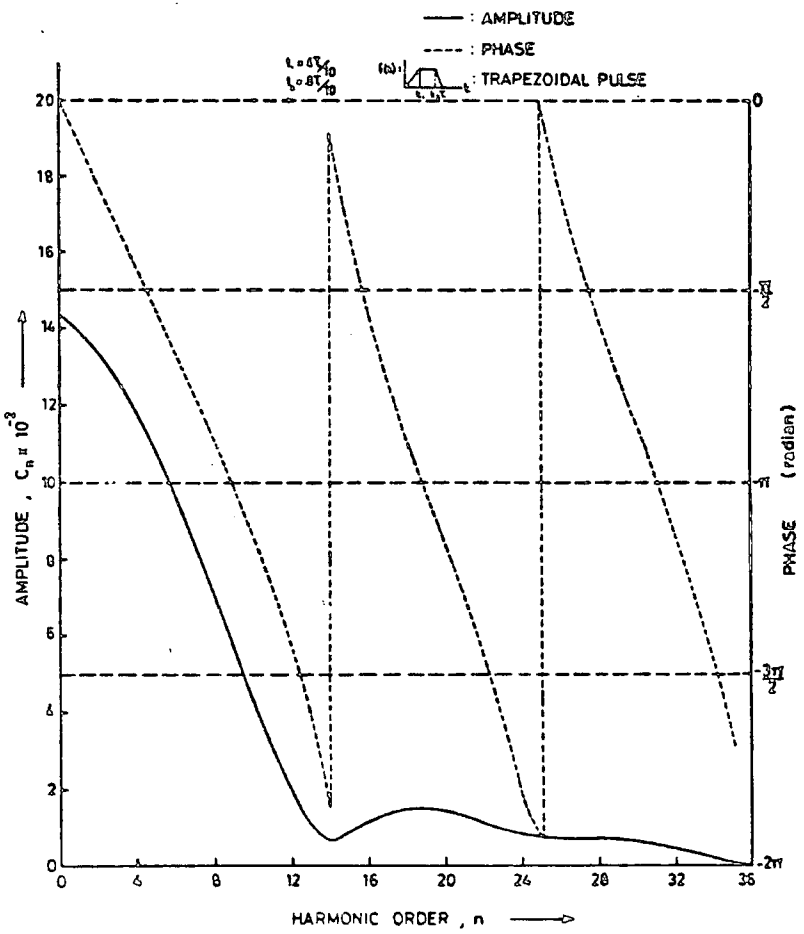

FIG.2·6(j) AMPLITUDE AND PHASE SPECTRA

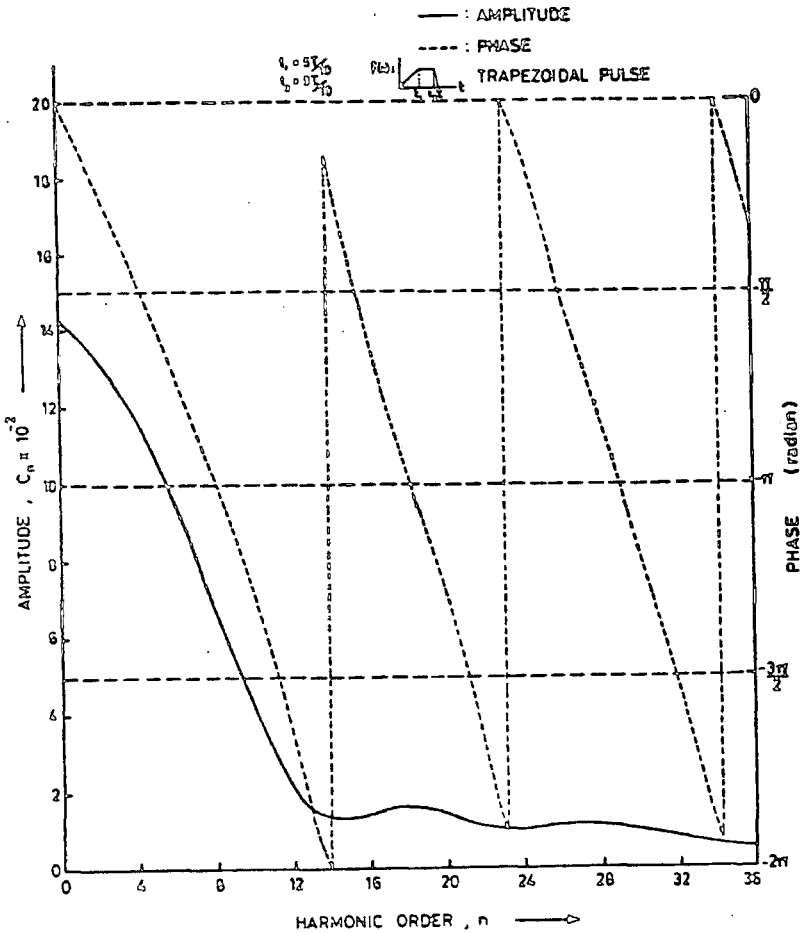

FIG. 2·6 (k) AMPLITUDE AND PHASE SPECTRA

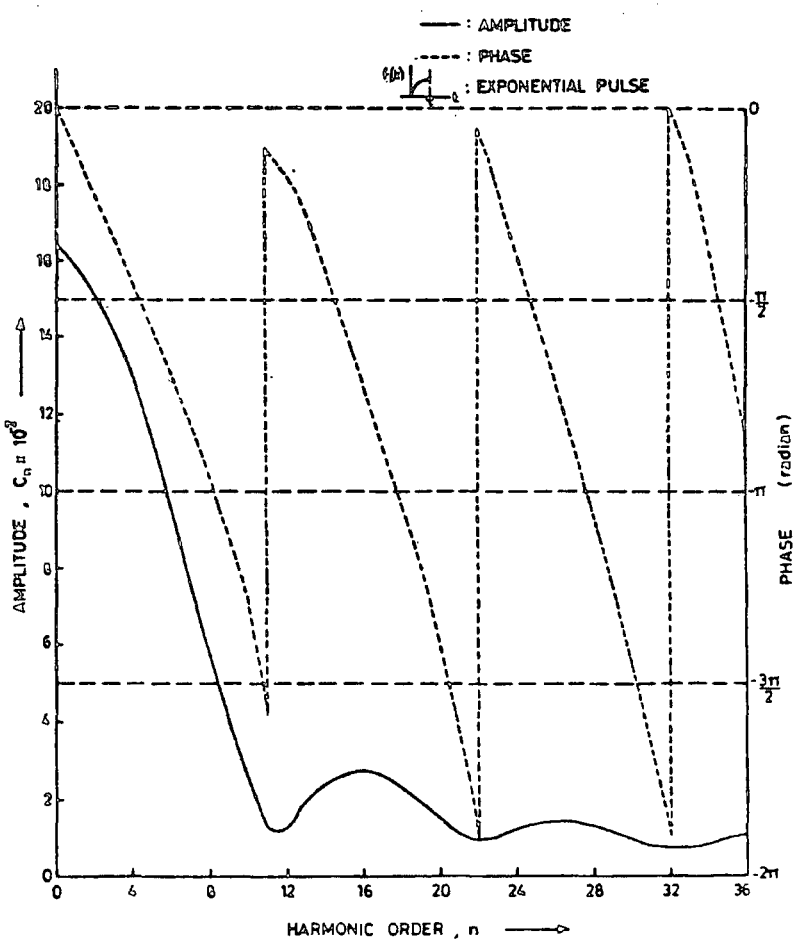

FIG. 2·6 (l) AMPLITUDE AND PHASE SPECTRA

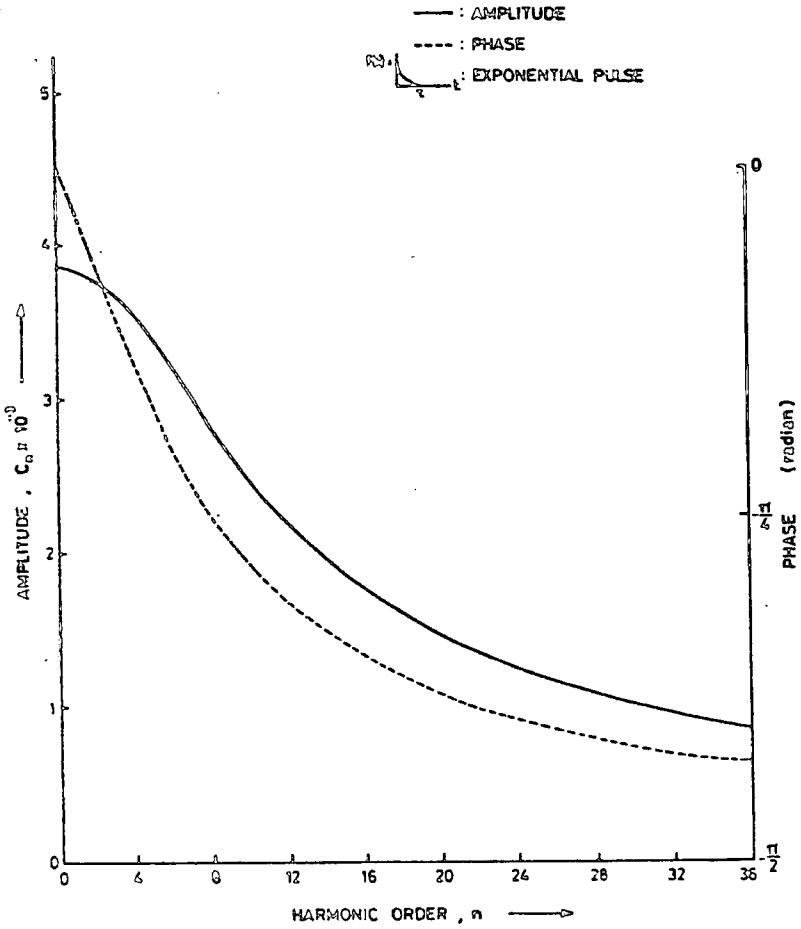

FIG. 2·6(m) AMPLITUDE AND PHASE SPECTRA

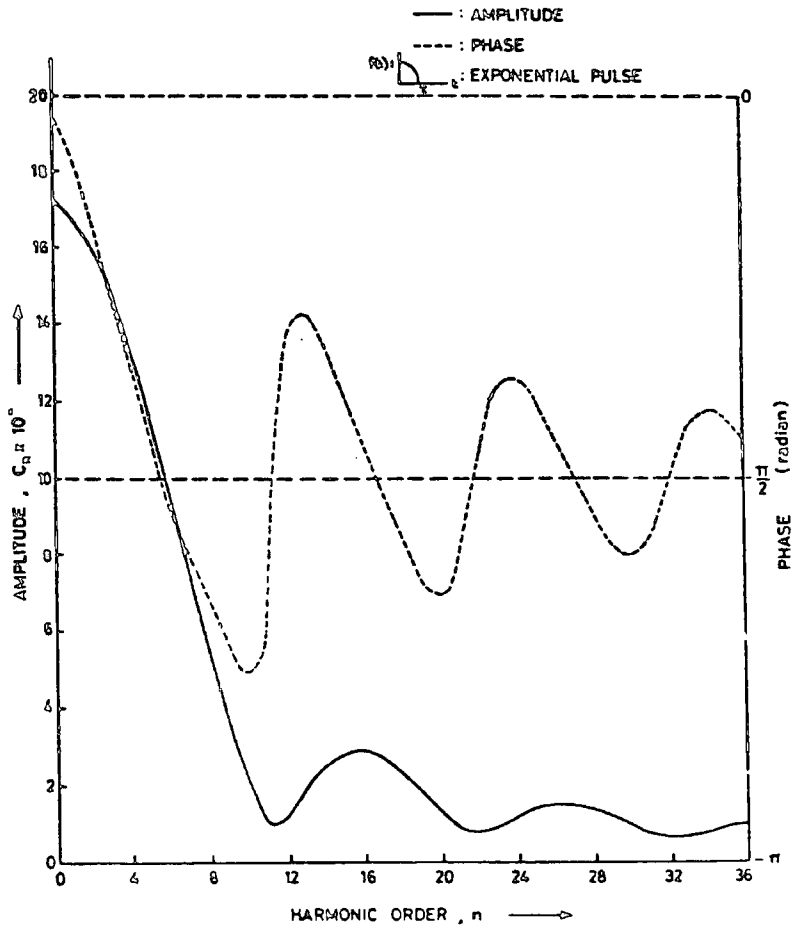

FIG. 2·6(n) AMPLITUDE AND PHASE SPECTRA

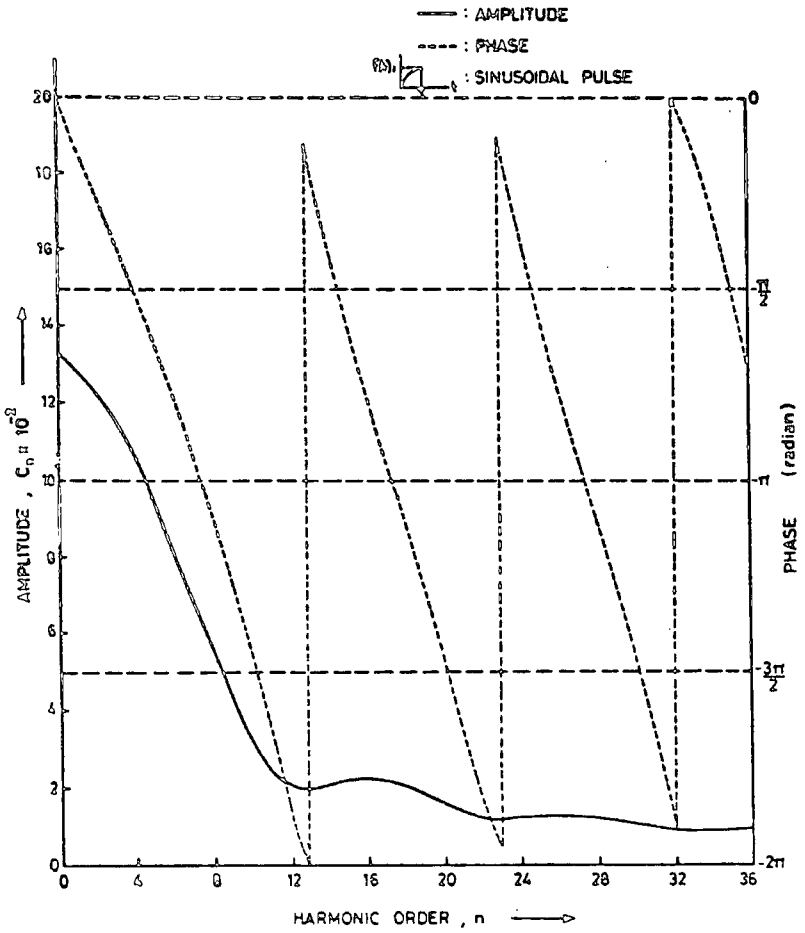

FIG.2-6(o) AMPLITUDE AND PHASE SPECTRA

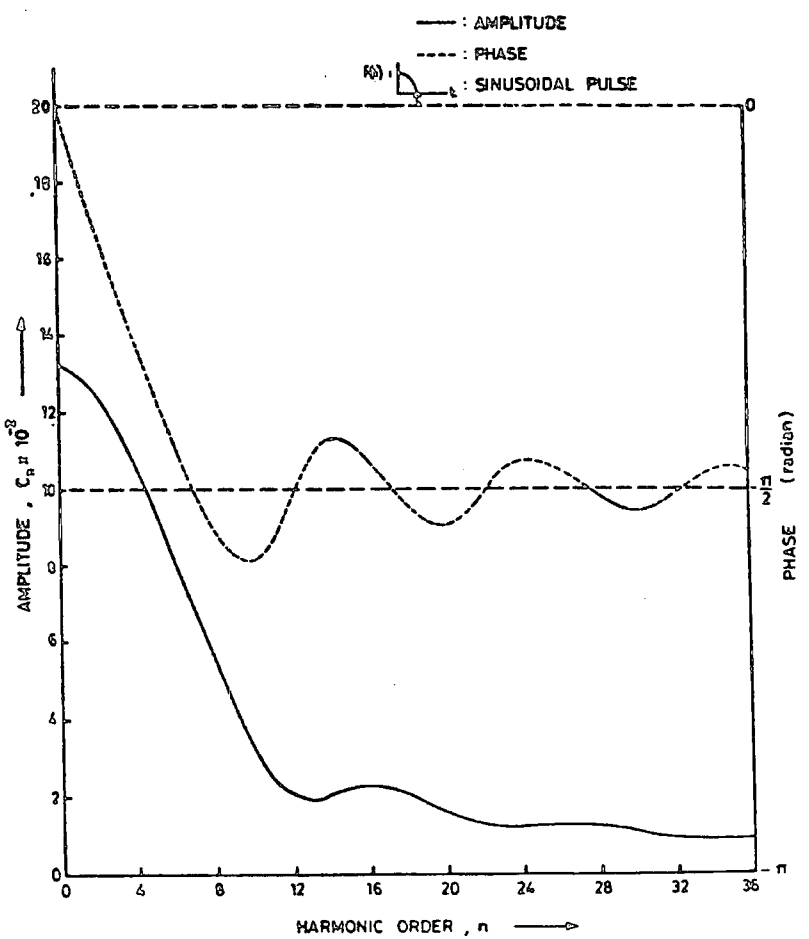

FIG.2-6(p) AMPLITUDE AND PHASE SPECTRA

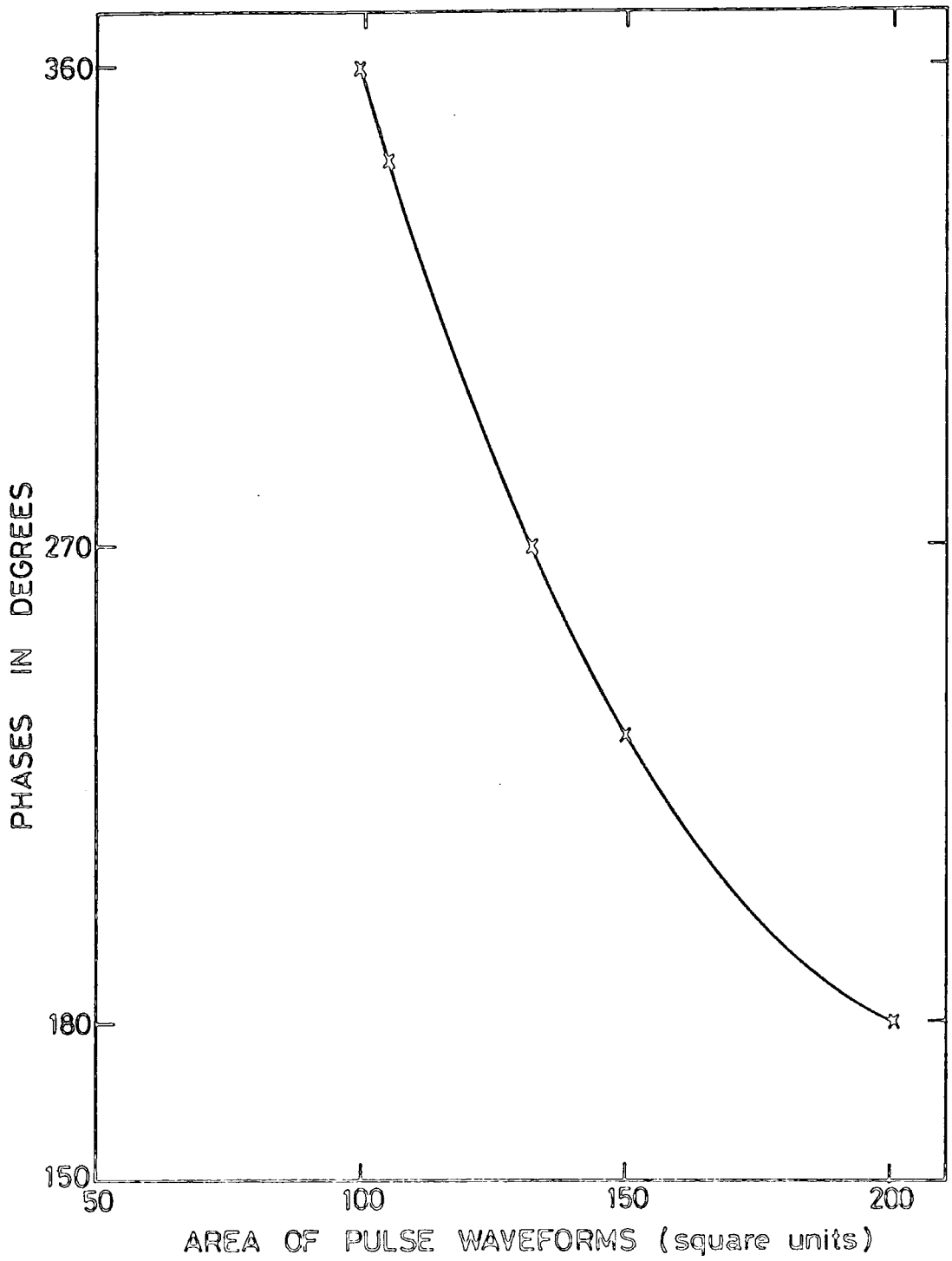

FIG. 2·7 PHASES (UPPER LIMIT OF MAJOR LOBES) AGAINST AREA (PULSE WAVEFORMS)

C and D, all asymmetrical waveforms considered do not have any lobe. However, these amplitude spectral envelopes do have crests and troughs.

2.5 ANALYSIS AND SPECTRA OF APERIODIC WAVEFORMS

An aperiodic waveform may be defined as that where the period of its oscillation is undefined. The period can either be infinite or varying randomly. Generally aperiodic signals are generated by a cluster of non-harmonically related sinusoidal frequencies around some centre frequency which is closely associated with some characteristic peculiar to device producing the signal. In this analysis it is more instructive to consider cases where the period is infinite.

The Fourier analysis of aperiodic signals will lead to the existence of Fourier transform, as given in the Appendix B. The Fourier coefficient of a rectangular train of periodic pulses is given by, (as in eqn. 2.2.9).

$$F_n = \frac{1}{T} \int_{-\frac{T}{2}}^{\frac{T}{2}} f(t) e^{-jn\omega_o t} \, dt$$

$$= \frac{\tau_m}{T} \cdot \frac{\sin x}{x} \quad \text{where} \quad x = \frac{n\omega_o \tau_m}{2} \tag{2.5.1}$$

F_n is discrete dependent upon the integral values of n. The Fourier transform for the corresponding same aperiodic pulse is given by (in the Appendix)

$$F(\omega) = \int_{-\infty}^{\infty} f(t) e^{-j\omega t} \, dt \tag{2.5.2}$$

As the pulse repetition period tends to infinity, hence correspondingly the fundamental frequency will tend to zero. So the harmonic spectrum will comprise components of 'zero fundamental frequency' and hence become infinitely close together. Thus ω and $F(\omega)$ become continuous. Comparing eqns. 2.5.1 and 2.5.2, it will be seen that a single 'universal' envelope curve may be plotted for a given pulse shape independent of its repetition period.

2.6 APPLICATION OF PERIODIC GATE FUNCTION

In applying the periodic gate function two new methods of sampling are presented. Both are involved with the analysis of an arbitrary waveform. In the analysis of an arbitrary periodic waveform, sampling is normally done and often carried out horizontally. This is because the waveform is sampled into time intervals over the entire period. The first method, to be known as the pulse width method, involves with the vertical sampling. In the second method the waveform under consideration is divided into pulses of standard shapes with known spectra. Each of the pulses then constitutes a periodic gate function.

The Pulse Width Method

A periodic pulse of arbitrary shape is first considered. Sampling is carried out by breaking the waveform into pulses. The pulses are of equal height but of varying widths, as shown in Fig 2.8(a). Effectively, the vertical axis of the waveform is divided into intervals of equal height. This type of apprpach leads finally to a summation of trains of pulses of various widths and hence the method may be referred to as the pulse width method. The resulting waveform after sampling will be a step approximation as shown in Fig 2.8(b).

The phase shift may be considered by making the lowest pulse the reference whose midpoint is chosen to be zero. A vertical axis may then

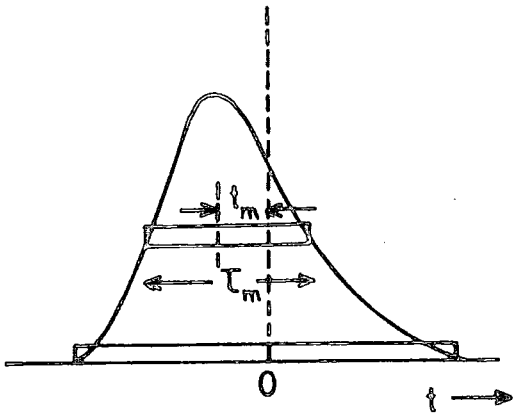

FIG. 2·8(a) SAMPLING OF A WAVEFORM BY THE PULSE WIDTH METHOD

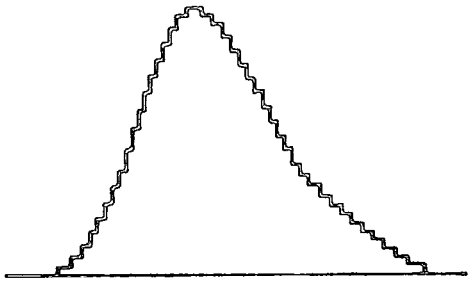

FIG. 2·8(b) A STEP APPROXIMATION

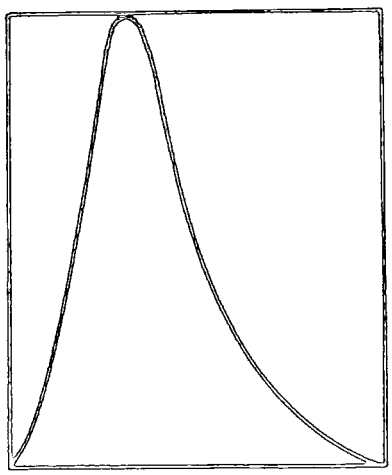

FIG. 2·9(a) AN ARBITRARY PERIODIC WAVEFORM

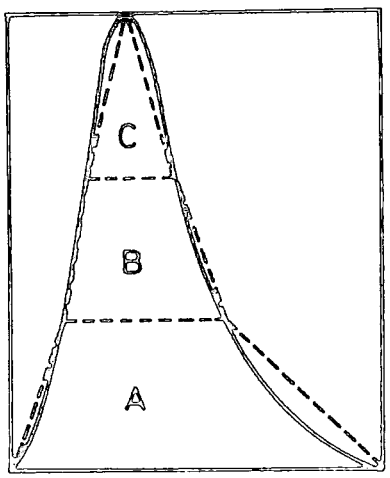

FIG. 2·9(b) SAMPLING OF AN ARBITRARY WAVEFORM INTO STANDARD PULSES

be drawn through the point. The centre points for other pulses are now found and the differences between these and the chosen point give the relative phase shifts. Rewriting eqn. 2.3.2 to include the phase shift term, the Fourier series may now be written as,

$$f(t) = A \sum_{m=1}^{M} \left[\frac{\tau_m}{T} + \frac{2\tau_m}{T} \sum_{n=1}^{\infty} \left(\frac{\sin x}{x} \right) \cos n\omega_o (t \pm t_m) \right] \qquad (2.6.1)$$

where M is the number of sampling pulses,

$$x = \frac{n\omega_o \tau_m}{2}$$

and the Fourier coefficients are given by

$$a_o = A \sum_{m=1}^{M} \tau'_m \qquad (2.6.2)$$

$$a_n = 2A \sum_{m=1}^{M} \tau'_m \frac{\sin(n\pi\tau'_m)}{(n\pi\tau'_m)} \cdot \cos(n\omega_o t_m) \qquad (2.6.3)$$

$$b_n = \pm 2A \sum_{m=1}^{M} \tau'_m \frac{\sin(n\pi\tau'_m)}{(n\pi\tau'_m)} \cdot \sin(n\omega_o t_m) \qquad (2.6.4)$$

where $\tau'_m = \frac{\tau_m}{T}$ is the duty cycle.

Standard Pulse Sampling Method

The second method of sampling concerns with the division of an arbitrary periodic waveform into pulses of identifiable shapes. The common shapes are trapezoidal, rectangular and triangular. Pulses of

these standard shapes have their own spectra. As an example, the waveform as shown in Fig 2.9(a) may be approximated to comprise pulses of trapezoidal (pulses A and B) and triangular (pulse C) shapes, as in Fig 2.9(b). The behaviour of the whole waveform may then be approximated to the sum of the behaviour of the sampled pulses. This is justified because the concern is essentially in the area under the curve. Hence, the Fourier coefficients for the whole waveform become the sum of Fourier coefficients of individual pulses. The general behaviour of the spectra due to pulses of these standard shapes can be easily obtained, as discussed in section 2.4.

2.7 SUMMARY

As the concepts of amplitude and phase spectra are derived from Fourier analysis, the basic ideas of Fourier analysis were reviewed and the conditions governing the validity of its application were discussed. Fourier series and transforms are the mathematical representation of the periodic and aperiodic phenomena, respectively. It is well-known that the analytical relationship between time and frequency domains may be established by using Fourier series and integrals. Representation of Fourier series may be made in terms of trigonometric or complex functions. It is widely applied in studies related to electrical circuits and mechanical vibrating systems which involve periodic potentials and forces, respectively. The Fourier transform pair is in fact one of the integral transforms that are commonly used in operational analysis. The frequency distribution of harmonics in Fourier series is a line spectrum whereas that in a Fourier integral is a continuous spectrum. For convenience the line spectra are represented by the spectrum envelopes. It is significant to note that a given pulse whether periodic or aperiodic gives identical spectrum envelope, hence amplitude spectra.

The response of the element may be examined for the steady state or transient behaviour. Depending which behaviour is of interest it may be

advantageous to use different types of excitation signals. From the harmonic components computed, the physical properties of the element may be determined and if possible expressed in terms of electrical analogues. It will be very important initially to establish whether the element is linear or nonlinear. From the inductive and capacitative analogues and the behaviour of the response, the characteristics of the element may be derived.

The behaviour of spectra due to periodic gate function under different conditions was discussed. The periodic gate (switching) function as represented by the Fourier series can be applied in the analysis of an arbitrary waveform. In this application two new sampling procedures are introduced whereby a waveform under consideration is sampled into pulses vertically or divided into pulses of standard shapes. This is in contrast to the conventional mode of sampling where sampling is carried out horizontally.

Spectra of mathematically defined waveforms of different shapes, fixed height and duty cycle were theoretically examined. Each of the waveforms was Fourier analysed and the Fourier coefficient expressions are summarised in Tables 2.1, 2.2 and 2.3. The relationship between the pulse shapes and the frequency spectra investigated are presented in Figs 2.4(b), 2.5(b) to 2.5(g) and 2.6(c) to 2.6(p). Such information based on the analysis of pulse shapes and hence spectra generated within, can help in the characterisation of devices. Apart from obvious "fingerprinting", the approach may help in obtaining the equivalent circuits, i.e. physical modelling of devices. The properties of such equivalent circuits may then be examined using the spectra over a wider range of frequencies. The effects of parasitic components may be deduced from the shapes of the spectrum envelopes and the relative amplitude and phases of the harmonic components.

CHAPTER 3

HARMONIC GENERATING PROPERTIES OF NONLINEAR DEVICES

3.1 CLASSIFICATION OF PRACTICAL DEVICES

The practical devices to be considered here are solid-state diodes which are nonlinear in behaviour and which operate at high frequencies. The amount of work concerned with high frequency applications now constitutes a significant area of the electronics industry. It is comparatively recent in origin and its growth has been as phenomenal as that of semiconductor technologies. The growth of the latter has been due to the ever increasing demand for specific devices. This demand has led to the creation of more varieties and families of semiconductor devices, which in turn have resulted from improved fabrication techniques and advances in technical knowledge. Systematic studies on these devices require that suitable criteria be established for their classification.

According to Watson[7] these devices may be divided into two groups based, with some overlapping, on the device behaviour and the device structure. Their behaviour may further classify them as (a) variable resistances (varistors), (b) variable reactances (varactors), (c) controllable impedance diodes and (d) negative resistance elements. All these devices display nonlinear behaviour. The varistor is predominantly a nonlinear resistive element with a small reactive component whereas the varactor behaves as a nonlinear reactive element with a small resistive component ; the reactance in the former case and resistance in the latter are normally described as parasitics. The varactors may have planar p-n junction structures or point-contact structures which can operate as metal-semiconductor Schottky barriers. The controllable impedance diodes are wide-spaced p-i-n diodes where the conductance is very nearly proportional to the minority carrier population stored within them. As the carrier mobility

is low within the space-charge layer at microwave frequencies, such diodes have a quasi-linear impedance, whose value depends upon the direct current or low frequency bias. Negative resistance diodes form an important separate class. They exhibit a terminal impedance which has a negative real part over a finite bandwidth and dynamic range. This property is often exploited in circuits where low power oscillations are involved.

Devices may also be classified on the basis of their structural features, as is evident by considering the structures of planar p-n junctions, metal-semiconductor (Schottky barrier) diodes, microwave bipolar transistors, field effect transistors (FETs), metal-insulator-semiconductor (MIS) and metal-oxide-semiconductor (MOS) devices and point contact diodes. Planar p-n junction diodes are extensively used in electronic circuitry. When heavily doped to give a very thin depletion layer these can be used as tunnel or backward diodes. Gunn and IMPATT diodes are also examples of devices having a planar p-n structure ; here however the space-charge region is sufficiently large to give a finite transit time, resulting in the negative resistance effect which in turn allows oscillation to take place. Schottky barrier diodes consist of metal-semiconductor contacts, with rectifying properties based on majority carrier conduction ; in normal operation they exhibit virtually no storage of minority carriers, a problem in early p-n junctions. Microwave transistors behave in a similar way to normal transistors but require that the transit-time is reduced. Field effect transistors (FETs) are unipolar devices. They are constructed from either p or n type material with the field existing between the source and the drain ; the flow of current is controlled by the bias at the gates. They have the following characteristic features : (a) voltage in addition to current gain (b) efficiency higher than that of bipolar (c) low noise figure (d) operating frequency of up to X-band and (e) high input impedance. Point contact diodes are made by

placing a sharp pointed wire in contact with the surface of a suitable semiconductor ; the main feature is the low parasitic capacitance. There are other classifications, based on different criteria which however do not contribute towards any further simplification in the studies of devices.

The devices chosen for the project were of different semiconductor material, structure and mechanism of operation. They comprised silicon point contact diodes, Schottky barrier diodes made from silicon and gallium arsenide and germanium backward diodes.

3.2 THE PHENOMENON OF NONLINEARITY

When a device is excited by a signal and the output is proportional to the input the device is referred to as linear. If this is not so the device is nonlinear. The nonlinearity in a device may be examined by considering the basic elements whithin it, the resistance R, the inductance L and the capacitance C, which may contribute to the storage and dissipative effects. In an electrical network the circuit element capable of storing electromagnetic energy is defined as reactance, whereas that which dissipates it is resistance. If the stored energy is predominantly in the electric field, the reactance is said to be capacitive and if the stored energy is predominantly in the magnetic field, the reactance is said to be inductive. However, it is more convenient to deal in terms of currents and voltages rather than electromagnetic fields. Hence in general, nonlinearity in devices may be due to any or all of these elements where each may exist with varying degree. In many device applications the nonlinearity of one of these elements is utilised, while the others (which are considered as parasitics) are suppressed.

When a nonlinear element is energised by a sinusoid of single frequency generation of new frequencies will result in addition to the

direct current. These new frequencies are inter-related and are integral multiples of the fundamental frequency. However, if two or more sinusoidal inputs are used to drive the nonlinear element, intermodulation will be produced ; this comprises the sum and difference frequencies of the individual inputs.

However, for the purpose of this work nonlinearity in electrical networks and systems will be highlighted. The significance of the need for a deeper understanding of nonlinear electrical system is obvious. It is remarkable to note that almost the entire modern electrical technology is essentially based on nonlinear phenomena, for example, data processing and work related to microprocessors involve non-linear networks. Communication systems employ non-linear devices for processes such as modulation, frequency conversion, detection, signal processing, decision processes and even linear amplification. The operation of control systems where optimisation is essential also involves non-linear elements.

The development[8] of the work related to non-linear analysis occurred during the eighteenth century. The effort included acquiring the solution in closed and in an approximate form. Eminent workers during the period from 1880 to 1920 included Poincare, Linstedt, Liaupounoff and Bendixsen. The general development during this period tended towards covering specialised cases of nonlinear mechanics. During the period between 1920 to 1940 the theory and methods of analysis received the greatest attention. This was due to the interest concentrated upon the rapid development of nonlinear electric-circuit behaviour. Van der Pol[9] (1920) started the work on the analysis of triode oscillation and this was followed by a number of other papers on electron-tube devices. With growing interest in military applications, intense development on this topic took place. After this period the major efforts were directed towards the develop-

ment of non-linear control systems. Since then contemporary interests, related to modern applications like communication systems, have received wide support.

Higgins[8] listed twenty four general methods of solving non-linear problems. As the methods are wide ranging, depending upon various applications and constraints, it is not necessary to describe them. One of the central themes of this thesis is spectral measurements and analysis is involved in the manipulation of spectra. The spectral measurements give the impedance of the device under particular operational conditions. From the amplitude and phase spectra, the general behaviour of the system may be predicted. In addition, equivalent circuits may also be proposed.

It is interesting to note that the development of classical and modern theory of non-linear differential equations is closely linked to the development of non-linear mechanics and electrical circuits[10,11] As the non-linear analysis methods[11] employed often have serious limitations in terms of accuracy, length of calculation and area of application, there seems to be always a need to improve existing methods in addition to employing methods used in other fields. With the approximate approach[12] to procedures and the analysis of results, it becomes essential to monitor continually the physical significance and the precise mathematics involved. A precise and complete insight[13] of the behaviour of non-linear systems can be achieved through an intensive investigation and analysis of the actual system together with the associated solution of the corresponding differential equations of performance. Approximating to linear systems may be useful only within limited conditions of operation. Studying a particular branch of non-linear analysis is quite a challenge because of the few references available. It becomes complex because of the absence of a unified theory and the imperfections in the results. In addition[14], the theory has been developed by people with differing interests and background such as,

astronomers, pure and applied mathematicians, mechanical, electronic, control and acoustical engineers, etc. and they use different approaches.

3.3 PROPERTIES OF GENERATED HARMONIC SPECTRA

One way of representing the responses of devices or circuits excited by sources of different frequencies is by their spectra. The spectral representation is a plot showing the relative output of harmonic components as a function of frequency for the non-linear device, circuit or system. Two types of spectra amplitude and phase are normally distinguished. They are given by equations 2.2.3 and 2.2.4 respectively. The frequency content of the response of a non-linear device is given in terms of harmonic frequencies ; for a linear device, of course no harmonics are generated.

The frequency spectrum is a unique representation of the device behaviour, dependent upon the drive level and the device parameters. The impedance is the most important electrical parameter which is dependent upon the drive level. So, anything that causes variation in complex impedance will correspondingly cause variation in both the amplitude and phase spectra. These spectra provide a graphical method of representing the device or its impedance. From the behaviour of these spectra at different levels, the behaviour at the intervening or extrapolated levels may be easily predicted provided that the device law does not change. From the device behaviour as represented by the frequency spectrum, it may be possible to propose and hence verify an a.c. equivalent circuit for the device.

In the design, fabrication, operation and application of any device or circuit, it is essential to know both its static and dynamic characteristics and parameters. The device or circuit behaviour is normally found under different operational conditions for the purposes of assessing its suitability

for various functions and performance requirements. As an example, under certain optimum conditions, a varactor can be used as an amplifier and because of its low loss property may satisfy one of the important performance requirements for amplifiers.

In low frequency work the two spectra, amplitude and phase, are usually obtained from Fourier analysis carried out on the distorted wave-form (generated by the non-linear device) which can easily be displayed. At high frequencies this technique is not suitable because of the limited bandwidth of the oscilloscope used to display the output and only the amplitude spectra are obtainable, generally through the use of spectrum analysers. Consequently, a technique which is central to this thesis called the Multiple Reflections Resonance Line method was developed with which both amplitude and phase can be obtained at different harmonics.

3.4 MODELLING AND 'FINGERPRINTING' OF DEVICES

In solving nonlinear problems[15] any attempt to generalise the formulation of their solutions often leads to unwieldy results. Hence, non-linear analysis depends on different types of characterisation procedures where there are preferred methods for a particular set of problems. Many nonlinear problems can naturally be solved through the use of nonlinear differential equations. However, as their solutions cannot often be written in a closed form, development of other methods becomes necessary. A new technique central to the thesis is presented in the next Chapter. It involves the harmonic spectrum of a nonlinear device leading towards the 'fingerprinting'.

Modelling is a procedure where the behaviour of a physical system is approximated. In recent years the concept of physical modelling has been widely developed and proved successful. It is one of the most basic principles[16] in scientific analysis because a physical system is seldom

analysed in its original form. The main reason for the need for modelling is that the actual physical system is too complex to have a simple analysis. The complexity may arise from nonessential factors. However, the basic principle in modelling is to extract the essentials. The main aim is to establish a relationship between physical device parameters and the device characteristics. The device is normally characterised in its simplest form and with an acceptable accuracy so that the performance of a particular circuit using this device, operating within specific conditions can be predicted. A given device is first properly formulated in terms of certain physical variables and explicit expressions derived meeting all the requirements of the device designs and circuits. This abstracted problem can then be solved by a suitable technique and the results of the analysis can be expressed in terms of appropriate parameters. As these parameters represent the device characteristics they can be related to and interpreted in terms of the original problem. This general approach facilitates access to the fundamental problems and highlights the special cases from a wide variety of problems using the same general ideas.

In dealing with physical modelling[17] it is essential initially to know the objective of the work in order to have an overall picture. The ranges of variables involved ought to be known so as to ensure that the extent and limitation of the operation and the applications are known. The choice of mathematical technique must be known too because this will determine how complex the analysis will be. It is important to know the physical mechanism of operation of the device or system as modelling is the realisation of such a device or system.

'Fingerprinting' of a device is a modelling process where the device behaviour can be uniquely described. The harmonic frequency spectrum generated by a nonlinear device is a unique representation of the actual device behaviour.

Therefore 'fingerpriting' of a device can be made using the harmonic frequency spectrum. At present there is no satisfactory way of 'fingerprinting' a nonlinear device. The dynamic characteristics are not presented over defined ranges of frequency and drive level. Hence, for simple, reliable and accurate 'fingerprinting' of a device certain criteria must be established and conditions defined. One of the most important criteria is that the device must remain stable throughout the measurement and this represents non-destructive testing. A single frequency source is another criterion, for this ensures the production of a unique harmonic frequency spectrum. Other criteria include (a) drive level, this is because the frequency spectrum is level dependent and (b) stability of conditions, they are the physical system and environment.

The basic difference between 'fingerprinting' and modelling is that the former gives the true representation of the device under the actual working conditions. The quantities chosen or adopted in the 'fingerprinting' may then be related to the real behaviour of the devices. In this work the spectral representation of the device constitutes the mode of 'fingerprinting'. The behaviour of the amplitude and phase spectra may be used in the assessment. At present, in most manufacturers' data sheets for devices, only static characteristics are supplied ; if dynamic characteristics are given they are generally incomplete. As an example, quantities like noise figure, conversion loss and r.f. impedance are given at a particular test frequency without any specification of the operating level. Taking the mixer application as an example of device assessment a matched pair of particular devices is required ; on carrying out the spectral characterisation for both the devices the device behaviour at harmonics may be compared or matched.

3.5 NUMERICAL FOURIER ANALYSIS[1,2] AT LOW FREQUENCIES

This method involves the examination of a distorted waveform due to a response from a nonlinear device. Suppose this waveform is as shown in Fig.3.1. It is subdivided equally into M sections over a period T along the time-axis. If each section be Δt, then $T = M\Delta t$. Let t_m be the time at the end of the m^{th} time interval. It may be written as, $t_m = m\Delta t$, for $1 \leq m \leq M$. So at t_m, there exists a corresponding ordinate $f(t_m)$. Therefore, the approximate Fourier coefficients for a periodic case may be written as,

$$a_o \simeq \frac{1}{M} \sum_{m=1}^{M} (m\Delta t) \tag{3.5.1}$$

$$a_n \simeq \frac{2}{M} \sum_{m=1}^{M} (m\Delta t) \cos(nm\Delta t) \tag{3.5.2}$$

$$b_n \simeq \frac{2}{M} \sum_{m=1}^{M} (m\Delta t) \sin(nm\Delta t) \tag{3.5.3}$$

So from the above equations it can be seen that the variables involved are: M, m, Δt, n and $f(t_m)$. Hence, for a certain fixed value of M and at particular values of harmonic n and $f(t_m)$ obtained for all values of m from one to M, the Fourier coefficients can be numerically determined. Thus, the amplitude and phase spectra can be obtained.

It is obvious that the higher the value of M, the closer is the approximation to the actual value of the coefficients. In the limit as Δt tends to zero, the Fourier coefficient equations 3.5.1, 3.5.2 and 3.5.3 tend to integrals as given by equations 2.2.5, 2.2.6 and 2.2.7 respectively. The numerical evaluation of the Fourier coefficients may be easily carried

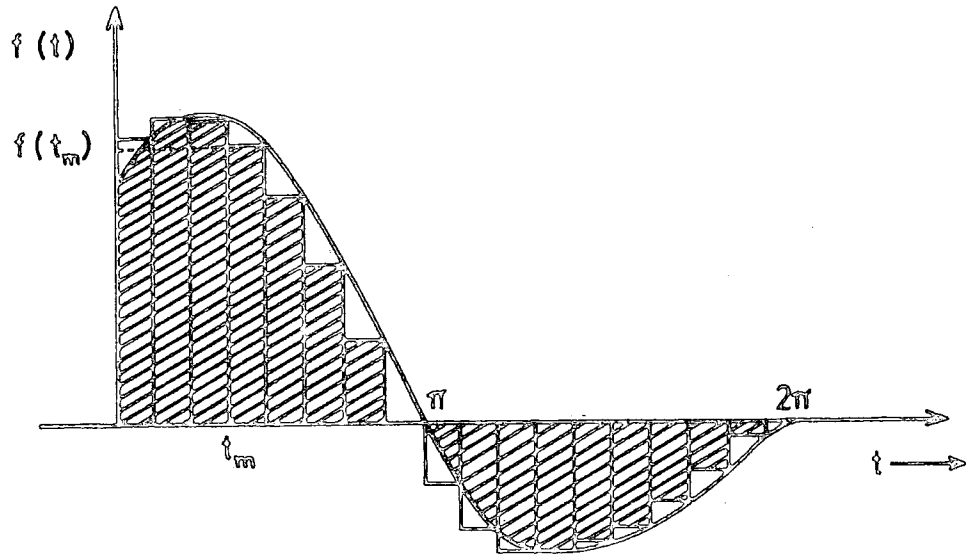

FIG. 3·1 ARBITRARY WAVEFORM TO BE ANALYSED

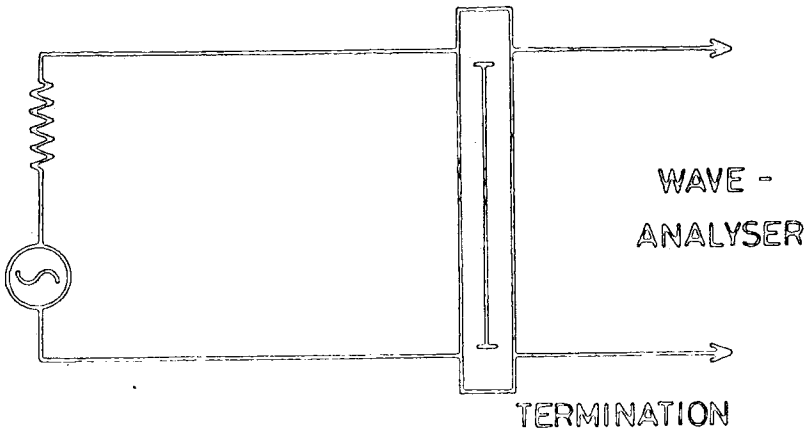

FIG. 3·2 CIRCUIT DIAGRAM – MEASUREMENT OF I_1

out using a computer or a programmable calculator, where the subroutines are available. As the number of sections M and the harmonic order n to be considered will be relatively small, it may not be necessary to use the fast Fourier transform method. The accuracy of the result depends greatly upon the technique by which the ordinates are obtained. They are obtained either by direct measurement from the time function displayed on the oscilloscope or from the manual or photographic reproduction.

Next, an experiment is described where the method of numerical Fourier analysis is applied. The circuit diagrams are shown in Figs 3.2 and 3.3. Throughout the experiment, the open-circuit voltage of the oscillator is taken as a reference and this is calibrated using a high impedance valve voltmeter. At any particular reference voltage, the fundamental current is first noted using the wave analyser as illustrated in Fig 3.2. Next, with the device connected in the circuit shown in Fig 3.3, the source oscillator level is adjusted to give the same fundamental current as before, using the wave analyser. Then the distorted waveform generated by the device is displayed on the oscilloscope. The harmonic content of the distorted waveform is analysed by numerical Fourier analysis, and the amplitude and phase spectra are obtained. This method is suitable for low frequency work because there is sufficient bandwidth in available oscilloscopes. However, the bandwidth may be increased with the use of accessories like sampling adaptors connected to the oscilloscope to extend measurements up to 1GHz. The amplitude spectra at this particular reference voltage may also be found using the wave analyser. This is done by tuning the wave analyser to any desired harmonic frequency and the current obtained.

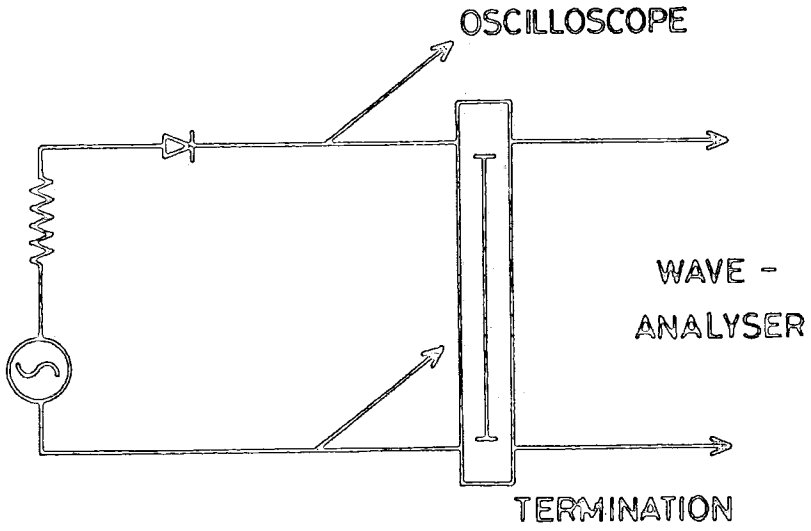

FIG. 3·3 CIRCUIT DIAGRAM - MEASUREMENT OF HARMONIC CONTENT OF A DIODE

3.6 APPLICATION OF NONLINEAR DEVICES

The nonlinear devices form basic units in a variety of systems applications. Traditionally, they are often referred to in terms of crystal rectifiers, used as detectors, frequency converters, noise and harmonic generators. In early works on radio communication[18], the crystal rectifiers were almost universally used as low level detectors in radio receivers. The point contact diode for example was used because of its low impedance rectification. In the past[19] nonlinear devices were found to be useful in certain applications, after which particular methods of characterisation and analysis were developed. In modern applications, variable impedance devices became significant[20]. Their development was stimulated by the advent of microwave radar during the Second World War. In modern terms, these devices are referred to as mixer diodes used for frequency conversion in heterodyne receivers and detector diodes used in video receivers.

These nonlinear devices[21,22] have wide ranging applications from communication systems, radio astronomy, space navigation, radar systems to missile electronic systems. A communication system is involved with transmitting and receiving speech, data or TV pictures. The transmitter and the receiver may be separated by a large distance. A radar system will be concerned with the transmission and detection of high frequency signals. The subsystems like transmitters and receivers will be involved with processes like mixing, detecting and amplification of signals. Each process must satisfy certain specific requirements within the overall performance of the subsystems and systems. Thus, there is a need to know the characteristics not only of the subsystems and systems but also of the devices to be used.

So, the choice of a nonlinear device in any application will normally depend upon (a) its behaviour and (b) the performance requirement with some overlap between them. Taking as an example of device behaviour[7] its nonlinear reactive properties can be seen that the varactor can be applied in frequency converters, frequency multipliers, dividers, mixers, modulators, parametric amplifiers ; high frequency power sources ; power conversion from one frequency to another. The useful frequency range is limited by parasitic series resistance and in some cases parasitic lead inductance.

The performance requirements of the device are dictated by the system in which it is to be used. In the case of a receiver for example, the overall performance requirements are: sensitivity, bandwidth and powerhandling capability. If, for instance, a high gain amplifier is required one might consider using a negative resistance device where the narrow band width and high gain characteristics are advantageous.

3.7 MEASUREMENT METHODS AT HIGH FREQUENCIES

Progress in high frequency applications[23,24] goes hand in hand with the development of the measurement techniques at these frequencies. Whatever measurement method is developed, it has to be adapted for use either in the laboratory, factory or field, keeping in view its precision and convenience. At low frequencies where the physical dimensions of the circuits are very much smaller than those of the associated wavelengths, the circuit elements can be characterised by four dimensions, viz ; mass, length, time and charge. Consequently, the technique of lumped circuit analysis works very well. However, as the operating frequencies get higher, the dimensions of the circuits required get smaller to the extent that they become comparable to the associated wavelengths. Thus, the passive elements in a microwave frequency system may take the form of hollow-pipe waveguide transmission lines or striplines.

In these the waves are characterised by their power, and frequency ; their analysis requires the adoption of a distributed circuit approach. The measurements are made on the basis of the effects of disturbances of the electromagnetic field due to discontinuities in the propagation of guided waves[21,25]. As there are no simple methods of measuring these fields, circuit and device parameters are indirectly measured.

Prior to 1965, almost all high frequency measurement systems[22] employed coaxial, waveguide or stripline circuits. With the improvement in integrated circuit technology microstrip lines have recently been widely used. As the demand for operation at ever higher frequencies is increasing, there is a continuing effort towards working with smaller circuits[23].

3.8 CONCLUSION AND COMMENTS

The Chapter started with the classification of solid-state nonlinear devices as applied in high frequency work. A systematic approach becomes essential because of the rapid rate of growth of the types of devices. The proliferation of devices is due to advancement in device technology initiated by their applications each of which carried varying sets of performance requirements. It is interesting to note that modelling has become an essential part of the characterisation and analysis of different types of devices.

In the discussion of the phenomenon of nonlinearity, it is indicated how the phenomenon and its associated problems originated. A brief historical perspective is also given, emphasising the period together with the workers and their contributions. The application and significance of nonlinear devices are also given. Initially nonlinearity is discussed in a broad sense and is followed by more specific examples. The analytical methods developed tend to be related to particular problems rather than covering the general cases. It can also be seen that the subject of nonlinearity is multidisciplinary within the confines of physical sciences.

The idea of spectral representation is introduced because finger-printing of devices may be made using these spectra. This represents a new approach towards device assessment and characterisation. This is because the spectra give the dynamic characteristics of the device and hence the operational conditions may be specified. The spectra obtained may be related to the established device parameters. Thus the spectra provide a way of characterising a device whereby an equivalent circuit may be proposed and assessed. Spectral representations give a new high frequency technique where both amplitude and phase spectra may be obtained.

Numerical Fourier analysis suitable for low frequency work is presented in some detail. The idea of spectral representation at high frequency is in fact developed from this low frequency work. Various applications of nonlinear devices are discussed because their wide range of application has significant scientific interests which revolutionise systems like communication and computers where there are vital commercial and military implications. The development of measurement methods plays a key role in device application, since the device can then be specially adapted for any desired application. In the upper range of high frequency applications, the sizes of circuits and systems become very small thereby increasing the difficulties of precision fabrication of every component.

CHAPTER 4

THE MULTIPLE REFLECTIONS RESONANT LINE (M.R.R.L.) METHOD FOR SPECTRUM MEASUREMENTS

4.1 INTRODUCTION

A novel high frequency spectrum measurement technique has been developed called the Multiple Reflections Resonant Line Method. This method offers a means of measuring a complete spectrum generated within a nonlinear device. A complete spectrum refers to both the amplitude and phase spectra. The method employs a slotted line system with accessories such as a probe and carriage assembly, adjustable transmission line, precision attenuators and instruments like a power-meter and an r.f. valve voltmeter. In addition a spectrum analyser, a key component in the measurement, is used to measure standing waves at the harmonics and the fundamental.

A number of important transmission line properties [26,27,28] are employed in the mathematical formulation of the method. The effects of the multiple reflections [29,30] along the line and the line resonance [21] form the foundations in the theory of the method. This accounts for the behaviour of the standing waves at the harmonics and the fundamental when a nonlinear device is used to terminate the line. The creation of resonance conditions is made possible with the incorporation of an adjustable length of line. However, the idea of matching or mismatching at the ends of the line still forms the operational basis in the measurement technique. The most important aspect of the method is the creation of standing waves at the harmonics and the fundamental under standard conditions when the mismatched termination is known. The standing waves at different harmonics are measured using a spectrum analyser which acts as a selective detector.

The nonlinear device terminating the line is energised by the fundamental frequency incident wave. This causes generation of harmonics which are then transmitted towards the excitation source end. A deliberate mismatch of the generator impedance is made so that standing waves at the harmonics can be obtained. This is because the standing waves will only be created if there is a mismatched load. The behaviour of the standing waves is dependent upon that termination. As both ends of the line are mismatched, multiple reflections occur. By varying the length of the line, the amplitude of the standing waves peaks and the line then is at a resonant condition. From the standing wave measurements the device impedance Z_n, phase ϕ_n and open circuit voltage V_n at the n^{th} harmonic may be obtained.

At the present time only the magnitude of the harmonic voltages or currents produced by the nonlinear devices at high frequencies can be measured using the existing instruments. No single instrument is available for the direct measurement of relative phases of the harmonics. The Multiple Reflections Resonant Line Method discussed here represents a way of measuring a complete spectrum. It also provides a means of collecting the necessary data for spectral characterisation and evaluation and hence device fingerprinting.

4.2 THE THEORY OF MULTIPLE REFLECTIONS

Whenever there is a matched termination at the load end of a transmission line system, all the incident waves will be absorbed and none will be reflected. If however there is a mismatch, then standing waves will be created. In general, whatever the value of the source impedance, the behaviour of the waves will only be affected by the terminating impedance of the line. Further, there will be multiple reflections of waves when the excitation and the load ends of the line

are mismatched. The incident wave at the fundamental frequency is first reflected at the load end and then reflected at the excitation end. These continued reflections back and forth will create standing waves when equilibrium is achieved. The stationary wave pattern is governed solely by the reflection coefficient at the receiving end. The effect of multiple reflections is merely to alter all values by a constant factor. The importance of the standing wave measurements lies in the fact that properties like voltage standing wave ratio (VSWR), phase shift and wavelength can be related to the device impedance.

Fig. 4.1 is an equivalent circuit for a slotted line with its ends connected to a generator and load respectively. The right-hand side of LL' refers to the load end and that of the left of EE' refers to the excitation source end. The subscripts 'g', 'L' and '0' of the impedance Z represent signal generator, load and the line, respectively. The length 'ℓ' is the total length of the line and 'x' is a point measured from the load end. The phasor voltage, $V(x,\ell)$, at a point 'x' and for the line of length 'ℓ' will now be derived when Z_g and Z_L are not equal to the characteristic impedance Z_o of the line.

When the excitation source is connected to the line, the initial steady state wave will see the apparent impedance of the line as Z_o. Therefore, the initial voltage at the generator end of the line is

$$V_i = V_g \frac{Z_o}{Z_g + Z_o} \qquad (4.2.1)$$

This term represents a voltage divider at the excitation end. On traversing a distance 'ℓ' to reach the load, the voltage may be written as $V_i e^{-\gamma \ell}$.

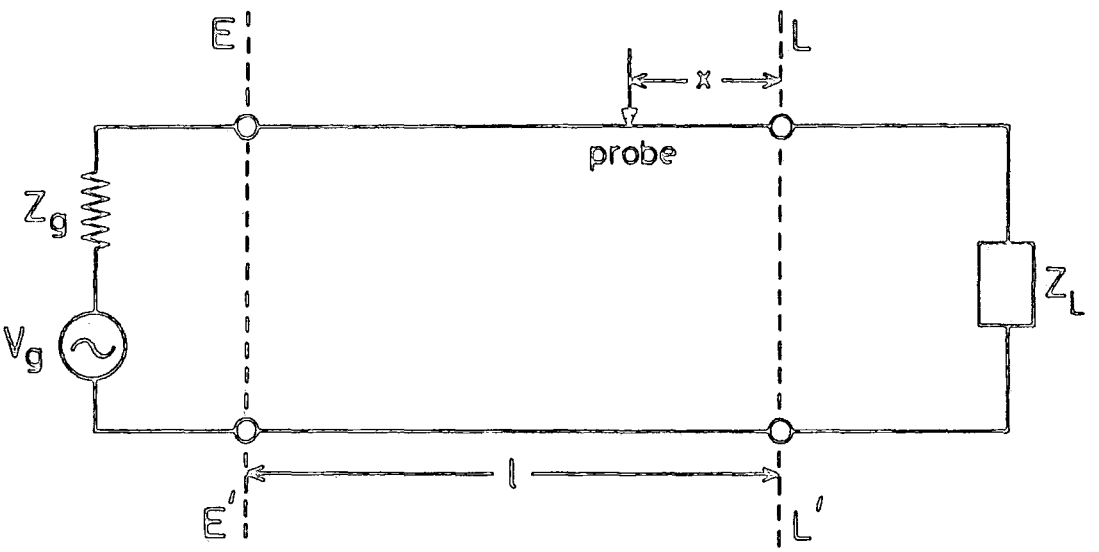

FIG.4·1 A GENERAL CIRCUIT DIAGRAM FOR A COAXIAL SLOTTED LINE

As the load impedance is mismatched, the incident wave on reaching the load produces a reflected voltage,

$$V_{L1} = \rho_L V_i e^{-\gamma \ell}$$

where ρ is the coefficient of reflection defined as

$$\rho = \frac{Z - Z_o}{Z + Z_o} \qquad (4.2.2)$$

The complex wave propagation constant γ is given by

$$\gamma = \alpha + j\beta \qquad (4.2.3)$$

where α and β are the attenuation and phase constants respectively. The voltage V_{L1} signifies the first reflection at the load end. This reflected wave will undergo further reflection on reaching the signal generator and because of introduced mismatch. The magnitude of the reflected voltage now is

$$\rho_g V_{L1} e^{-\gamma \ell}$$

which may be designated as V_{g1} implying the first reflection at the signal generator end. This may now be written on substitution for V_{L1} as

$$V_{g1} = \rho_g \rho_L V_i e^{-2\gamma \ell} \qquad (4.2.3\ a)$$

Similarly, it can be shown that for second reflections

$$V_{L2} = \rho_g \rho_L^2 V_i e^{-3\gamma\ell} \tag{4.2.4}$$

$$V_{g2} = \rho_g^2 \rho_L^2 V_i e^{-4\gamma\ell} \tag{4.2.5}$$

or in general for the n^{th} reflections,

$$V_{Ln} = \rho_g^{(n-1)} \rho_L^n V_i e^{-(2n-1)\gamma\ell} \tag{4.2.6}$$

$$V_{gn} = (\rho_g \rho_L)^n V_i e^{-2n\gamma\ell} \tag{4.2.7}$$

In conclusion, the voltage at any point x from the load end and for the line of length 'ℓ' $V(x,\ell)$ is the sum of all the voltages due to the initial incident wave at x and the multiple reflections that follow. Hence,

$$V(x,\ell) = V_i e^{-\gamma(\ell-x)} + \sum_{n=1}^{\infty} V_{Ln} e^{-\gamma x} + \sum_{n=1}^{\infty} V_{gn} e^{-\gamma(\ell-x)} \tag{4.2.8}$$

Rewriting gives,

$$V(x,\ell) = e^{-\gamma(\ell-x)} \left[V_i + \sum_{n=1}^{\infty} V_{gn} \right] + e^{-\gamma x} \left[\sum_{n=1}^{\infty} V_{Ln} \right]$$

which, on substitutiuon for V_{Ln} and V_{gn}, results in

$$V(x,\ell) = V_i e^{-\gamma(\ell-x)} \left\{ 1 + \rho_g\rho_L e^{-2\gamma\ell} + \rho_g^2\rho_L^2 e^{-4\gamma\ell} + \ldots \right\}$$

$$+ V_i e^{-\gamma x} \left\{ \rho_L e^{-\gamma\ell} + \rho_g\rho_L^2 e^{-3\gamma\ell} + \ldots \right\} \quad (4.2.9)$$

Now, by extracting a common factor in the second term of eqn. 4.2.9 and rearranging the expression, we get

$$V(x,\ell) = \left[V_i e^{-\gamma(\ell-x)} + \rho_L V_i e^{-\gamma(\ell+x)} \right] \left[1 + \rho_g\rho_L e^{-2\gamma\ell} + \rho_g^2\rho_L^2 e^{-4\gamma\ell} + \ldots \right]$$

leading finally to,

$$V(x,\ell) = V_i e^{-\gamma\ell} \left[e^{\gamma x} + \rho_L e^{-\gamma x} \right] \left[\frac{1}{1 - \rho_g\rho_L e^{-2\gamma\ell}} \right]$$

since the infinite series in the second factor may be written in a closed form. The expression for the voltage can further be written as,

$$V(x,\ell) = V_g \left(\frac{Z_o}{Z_g + Z_o} \right) \left[\frac{1 + \rho_L e^{-2\gamma x}}{1 - \rho_g\rho_L e^{-2\gamma\ell}} \right] e^{-\gamma(\ell-x)} \quad (4.2.10)$$

which finally represents a general equation for the phasor voltage $V(x,\ell)$.

If the load impedance Z_L is equal to the characteristic impedance

Z_o, then the reflection coefficient of the load ρ_L becomes zero, and eqn. 4.2.10 reduces to

$$V(x,\ell) = V_g\left(\frac{Z_o}{Z_g + Z_o}\right) e^{-\gamma(\ell-x)} \qquad (4.2.11)$$

where there is only the incident wave. On the other hand, if the generator impedance Z_g is made equal to Z_o, ρ_g will be equal to zero, and eqn. 4.2.10 is simplified to

$$V(x) = \frac{V_g}{2}\left[e^{\gamma x} + \rho_L e^{-\gamma x}\right] \qquad (4.2.12)$$

The above equation for the phasor voltage is valid in conventional applications of the slotted line (with no multiple reflections) and is independent of the line length 'ℓ'. This kind of equation[31] is generally written as

$$V(x) = A\, e^{\gamma x} + Be^{-\gamma x} \qquad (4.2.13)$$

where $Ae^{\gamma x}$ and $Be^{-\gamma x}$ represent the waves travelling towards and away from the load, respectively.

Normally, the slotted line used is lossless, i.e. $\alpha = 0$ giving $\gamma = j\beta$ and eqn. 4.2.10 may then be written as

$$V(x,\ell) = V_g\left(\frac{Z_o}{Z_g + Z_o}\right) \frac{\left(1 + \rho_L e^{-j2\beta x}\right)}{\left(1 - \rho_L \rho_g e^{-j2\beta\ell}\right)} e^{-j\beta(\ell-x)} \qquad (4.2.14)$$

resulting in the magnitude

$$\left| V(x,\ell) \right| = \left| V_g \left(\frac{1 - \rho_g}{2} \right) \right| \frac{|1 + \rho_L e^{-j2\beta x}|}{|1 - \rho_L \rho_g e^{-j2\beta \ell}|} \qquad (4.2.15)$$

where $\left| V_g \left(\frac{Z_o}{Z_g + Z_o} \right) \right| = \left| V_g \left(\frac{1 - \rho_g}{2} \right) \right|$

Eqn. 4.2.15 is one of the key equations in the theory of this measurement method.

4.3 RESONANCE ALONG THE LINE

Standing waves can be created along a transmission line of any particular length. However, with multiple reflections, variation of the line length will change the magnitude of the standing waves, though the pattern remains the same. The typical standing wave pattern is as shown in Fig.4.2a. If the length of the slotted line is continuously increased, the magnitude of the standing wave will undergo a series of alternating maxima and minima. This is illustrated in Fig.4.2b where at a point x, the magnitudes vary between points A and B. The incidence of maxima and minima of the waves suggests the resonance and anti-resonance behaviour of the line. Thus the length of the line that corresponds to the magnitude at its maximum may be referred to as ℓ_{max} and that for the minimum as ℓ_{min}. This is as shown in Fig.4.2c. As the resonance or extreme value of the magnitude occurs at a particular length of the slotted line, the behaviour may be referred to as the line resonance.

This resonance behaviour may also be seen mathematically in eqn.4.2.15 by examining the denominator more closely. The definition of reflection

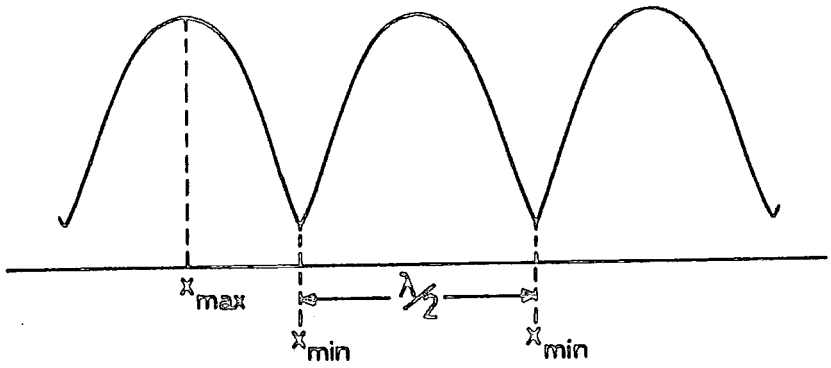

FIG. 4·2 a STANDING WAVE PATTERN ALONG THE SLOTTED LINE OF A PARTICULAR LENGTH

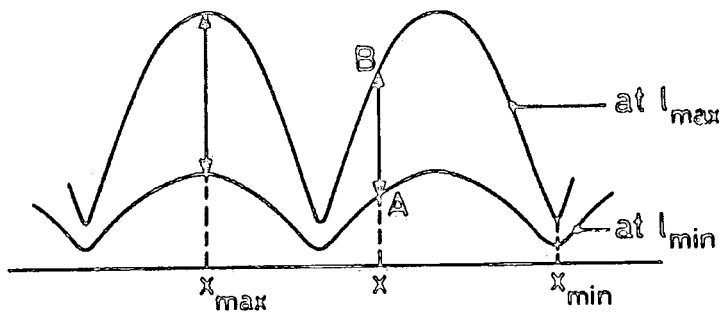

FIG. 4·2 b VARIATION OF THE STANDING WAVE MAGNITUDES AT A POINT x WITH THAT OF THE SLOTTED LINE LENGTH

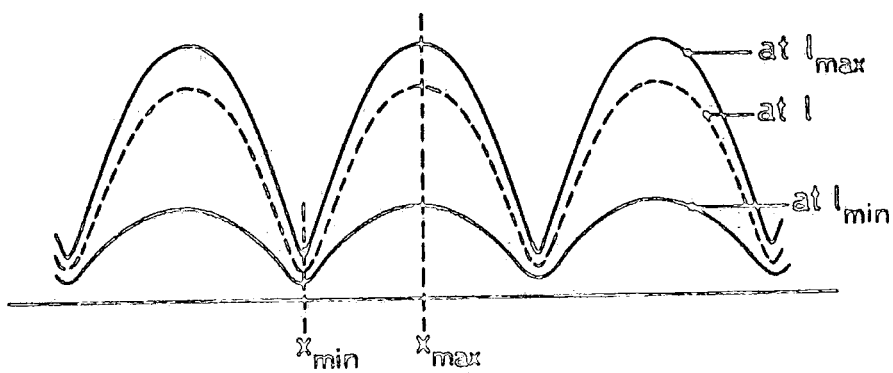

FIG. 4·2 c VARIATION OF STANDING WAVE MAGNITUDES WITH THAT OF THE SLOTTED LINE LENGTH

coefficient shows that if the generator impedance Z_g is real and less than Z_o, Z_g will be negative. If the load impedance is complex, then the load reflection coefficient may be written as

$$\rho_L = |\rho_L| e^{j\psi_L} \tag{4.3.1}$$

Consequently, eqn. 4.2.15 may be modified to

$$|V(x,\ell)| = \left|V_g'\right| \frac{\left|\left[1 + |\rho_L| e^{-j(2\beta x - \psi_L)}\right]\right|}{\left|\left[1 + |\rho_L||\rho_g| e^{-j(2\beta\ell - \psi_L)}\right]\right|} \tag{4.3.2}$$

where

$$|V_g'| = \left|V_g \left(\frac{1 - \rho_g}{2}\right)\right|$$

and further simplified to

$$|V(x,\ell)| = |V_g'| \frac{\left\{1 + 2|\rho_L| \cos(2\beta x - \psi_L) + |\rho_L|^2\right\}^{1/2}}{\left\{1 + 2|\rho_L||\rho_g|\cos(2\beta\ell - \psi_L) + |\rho_L|^2|\rho_g|^2\right\}^{1/2}} \tag{4.3.3}$$

The only variable in the denominator of eqn. 4.3.3 is the line length 'ℓ', which in turn contributes towards the variation of $|V(x,\ell)|$. The value of $V(x,\ell)$ as the line length 'ℓ' is varied reaches a maximum when

$$\cos(2\beta\ell_{max} - \psi_L) = -1 \tag{4.3.4}$$

and a minimum when

$$\cos(2\beta\ell_{min} - \psi_L) = 1 \tag{4.3.5}$$

So $|V(x,\ell)|$ now designated as $\left|V\left(x, \ell_{\substack{\max \\ \min}}\right)\right|$ may be written on substitution of the above conditions as

$$\left|V\left(x,\ell_{\substack{\max \\ \min}}\right)\right| = \left|V_g'\right| \frac{\left\{1 + 2|\rho_L| \cos(2\beta x - \psi_L) + |\rho_L|^2\right\}^{\frac{1}{2}}}{\left[1 \mp |\rho_L||\rho_g|\right]} \qquad (4.3.6)$$

The conditions under which $|V(x,\ell)|$ reaches maximum i.e. $|V(x,\ell_{max})|$ may be aptly referred to as that of resonance and when $|V(x,\ell_{min})|$ is minimum as anti-resonance.

Using these resonant conditions, the phase ψ_L of the complex reflection coefficient of the load may be determined either from eqn.4.3.4, giving

$$2\beta\ell_{max} - \psi_L = (2k + 1)\pi \qquad (4.3.7)$$

or eqn. 4.3.5, giving

$$2\beta\ell_{min} - \psi_L = (2k\pi) \qquad (4.3.8)$$

where

$$\beta = \frac{\omega}{v_{ph}} = \frac{2\pi}{\lambda}, \quad k = 0, 1, 2.....$$

and

$$\psi_L = 2\beta\ell_{max} - (2k + 1)\pi = 2\beta\ell_{min} - 2k\pi \qquad (4.3.9)$$

It is to be noted that k is zero or an integral value in the expression for phase ψ_L under resonant or anti-resonant condition.

In conclusion it should be emphasised that the extreme values of the magnitudes of the standing wave $|V(x,\ell)|$ are dependent upon the resonant conditions of the line at any point x ; the existence of resonance depends critically on multiple reflections and the key variable is the line length.

4.4 STANDING WAVE PROPERTIES

4.4.1 Complex Reflection Coefficient

Whenever two identical waves of the same frequency travel in opposite directions along a slotted line system standing waves will be created. This fundamental phenomenon of interference in an electrical network is caused by a discontinuity, for example a mismatched termination. Under normal measurement techniques standing waves are obtained for only one frequency. The circuit for this kind of measurement was shown in Fig.4.1. In most cases, the generator or the source impedance, Z_g, is equal to the characteristic impedance Z_o of the line. Thus standing waves created will be solely due to the reflection at the load end. If however, in addition to the mismatch at the load end, there is one at the generator end, multiple reflections will result.

Whenever there are multiple reflections standing wave properties may be deduced from the stationary wave measurements based on eqn. 4.3.3. It will be seen that the numerator depends upon the value of x, i.e. the distance from the load end. As discussed in the last section, the denominator depends upon the line length 'ℓ'. At a particular length 'ℓ' of this transmission line, the extreme value of $|V(x,\ell)|$ can either be maximum or minimum, with the corresponding values of x as x_{max} or x_{min},

respectively. The magnitude of the standing wave is maximum, i.e. $|V(x_{max}, \ell)|$ when

$$\cos (2\beta x_{max} - \psi_L) = 1 \tag{4.4.1}$$

and minimum, i.e. $|V(x_{min}, \ell)|$ when

$$\cos (2\beta x_{min} - \psi_L) = -1 \tag{4.4.2}$$

This implies that

$$2\beta x_{max} - \psi_L = 2m\pi \tag{4.4.3}$$

and $$2\beta x_{min} - \psi_L = (2m + 1)\pi \tag{4.4.4}$$

where

$$m = 0, 1, 2.....$$

giving

$$\psi_L = (2\beta x_{max} - 2m\pi) = 2\beta x_{min} - (2m + 1)\pi \tag{4.4.5}$$

It is again to be noted that m is zero or an integral value in the expression for phase ψ_L at x_{max} or x_{min}.

Therefore, in summary, the magnitude of the standing waves at maximum and minimum for a particular length of the line is given by

$$|V(x_{max}, \ell)| = |V_g'| \frac{\left[1 \pm |\rho_L|\right]}{\left\{1 + 2|\rho_L||\rho_g|\cos(2\beta\ell \mp \psi_L) + |\rho_L|^2 |\rho_g|^2\right\}^{1/2}} \tag{4.4.6}$$

The extreme values for the standing wave magnitude under the conditions as given by eqns. 4.3.6 and 4.4.6 may be summarised as,

$$\left|V(x_{max}, \ell_{max})\right| = \left|V_g'\right| \left[\frac{1 \pm |\rho_L|}{1 \mp |\rho_L||\rho_g|}\right] \qquad (4.4.7)$$

The phase of the complex reflection coefficient of the load ψ_L may be computed from eqn. 4.4.5. It is to be emphasised that this is applicable for the case of the complex load impedance, at a particular frequency. The eqn. 4.4.7 sugests that under two extreme conditions of x, i.e. x_{max} and x_{min} and those for 'ℓ' , i.e. ℓ_{max} and ℓ_{min}, there are four combinations $|V(x,\ell)|$ that can be measured, they are :

$$\left|V(x_{max}, \ell_{max})\right| = \left|V_g'\right| \left[\frac{1 + |\rho_L|}{1 - |\rho_L||\rho_g|}\right] \qquad (4.4.8)$$

$$\left|V(x_{max}, \ell_{min})\right| = \left|V_g'\right| \left[\frac{1 + |\rho_L|}{1 + |\rho_L||\rho_g|}\right] \qquad (4.4.9)$$

$$\left|V(x_{min}, \ell_{max})\right| = \left|V_g'\right| \left[\frac{1 - |\rho_L|}{1 - |\rho_L||\rho_g|}\right] \qquad (4.4.10)$$

$$\left|V(x_{min}, \ell_{min})\right| = \left|V_g'\right| \left[\frac{1 - |\rho_L|}{1 + |\rho_L||\rho_g|}\right] \qquad (4.4.11)$$

These equations may be manipulated to give an expression for $|\rho_L|$ as,

$$|\rho_L| = \frac{1}{|\rho_g|} \cdot \frac{|V(x_{max}, \ell_{max})| - |V(x_{max}, \ell_{min})|}{|V(x_{max}, \ell_{max})| + |V(x_{max}, \ell_{min})|} \qquad (4.4.12)$$

This is an important equation derived in order to compute the value for the magnitude of the complex reflection coefficient of the load, $|\rho_L|$. Basically two measurements under conditions of resonance (at ℓ_{max}) and anti-resonance (at ℓ_{min}) are required to obtain $|\rho_L|$ and they are,

$$|V(x_{max}, \ell_{max})| \qquad \text{and} \qquad |V(x_{max}, \ell_{min})|$$

The quantity $|\rho_g|$ is known, because it is fixed. The most interesting points demonstrated by eqn. 4.4.12 are that it is simple, the quantities involved are easily measurable and only relative measurements are required. The phase angle ψ_L may be computed using either eqn. 4.3.9 or 4.4.5. Hence the complex reflection coefficient for the load ρ_L may be computed.

The eqn. 4.4.12 may also be written as,

$$|\rho_L| = \frac{1}{|\rho_g|} \cdot \frac{\left[|V(x_{max}, \ell_{max})| \,/\, |V(x_{max}, \ell_{min})|\right] - 1}{\left[|V(x_{max}, \ell_{max})| \,/\, |V(x_{max}, \ell_{min})|\right] + 1} \qquad (4.4.13)$$

where the ratio

$$|V(x_{max}, \ell_{max})| \,/\, |V(x_{max}, \ell_{min})|$$

is an important quantity. This ratio may be examined by referring back to the expression for $|V(x,\ell)|$ as given by eqn. 4.3.3. It can be shown that,

$$\frac{|V(x, \ell_{max})|}{|V(x, \ell_{min})|} = \frac{|V_g|}{|V_g|} \cdot \frac{1 + |\rho_L|\,|\rho_g|}{1 - |\rho_L|\,|\rho_g|} \qquad (4.4.14)$$

This means that the ratio has a constant value, at every point x along the line provided that the load impedance does not change. However, for purposes of measurements, the point x_{max} is chosen in order to work with bigger voltages.

4.4.2 Input Impedance of the Line

The expression for the current $|I(x,\ell)|$ at a point x along a transmission line of length 'ℓ' may be obtained based on the same ideas as that for the voltage $|V(x,\ell)|$. It can be shown that,

$$\left|I(x,\ell)\right| = \left|\frac{V_g}{Z_g + Z_o}\right| \frac{\left|1 - \rho_L e^{-j2\beta x}\right|}{\left|1 - \rho_L \rho_g e^{-j2\beta\ell}\right|} \qquad (4.4.15)$$

On substituting the complex reflection coefficient ρ_L for the load into eqn. 4.4.13 gives, on simplification

$$\left|I(x,\ell)\right| = \left|\frac{V_g}{Z_g + Z_o}\right| \frac{\left\{1 - 2|\rho_L|\cos(2\beta x - \psi_L) + |\rho_L|^2\right\}^{1/2}}{\left\{1 + 2|\rho_g||\rho_L|\cos(2\beta\ell - \psi_L) + |\rho_g|^2|\rho_L|^2\right\}^{1/2}} \qquad (4.4.16)$$

From eqns. 4.3.3 and 4.4.16 for $|V(x,\ell)|$ and $|I(x,\ell)|$, respectively, an expression for the input impedance $|Z(x,\ell)|$ may be found, i.e.

$$\left|Z(x,\ell)\right| = \frac{|V(x,\ell)|}{|I(x,\ell)|}$$

$$\left|Z(x,\ell)\right| = \left|Z_o\right| \frac{\left\{1 + 2|\rho_L|\cos(2\beta x - \psi_L) + |\rho_L|^2\right\}^{1/2}}{\left\{1 - 2|\rho_L|\cos(2\beta x - \psi_L) + |\rho_L|^2\right\}^{1/2}} \qquad (4.4.17)$$

4.4.3 Load Impedance - General Relationships

Suppose a load terminating the line has a complex impedance Z_L which may be written in the usual way as

$$Z_L = R_L + j X_L \tag{4.4.18}$$

On normalising with the characteristic impedance, it becomes,

$$\frac{Z_L}{Z_o} = \frac{R_L}{Z_o} + j \frac{X_L}{Z_o} \tag{4.4.19}$$

But, from the definition of the complex reflection coefficient, it can be shown that,

$$\frac{Z_L}{Z_o} = \frac{(1 + \rho_L)}{(1 - \rho_L)} \tag{4.4.20}$$

Substituting ρ_L from eqn. 4.3.1 into that of 4.4.20 leads to the expression[30] for the normalised real and imaginary parts of the impedance, which are ;

$$\frac{R_L}{R_o} = \frac{(1 - |\rho_L|^2)}{\left\{1 - 2|\rho_L| \cos\psi_L + |\rho_L|^2\right\}} \tag{4.4.21}$$

$$\frac{X_L}{R_o} = \frac{2|\rho_L| \sin \psi_L}{\left\{1 - 2|\rho_L| \cos \psi_L + |\rho_L|^2\right\}} \tag{4.4.22}$$

Thus the magnitude of the complex load impedance is given by,

$$|Z_L| = \left| (R_L^2 + X_L^2)^{\frac{1}{2}} \right| \qquad (4.4.23)$$

and that for the phase :

$$\phi_L = \tan^{-1} \left(\frac{X_L}{R_L} \right) \qquad (4.4.24)$$

4.5 THE NON-LINEAR DEVICE AS THE LOAD

4.5.1 Equivalent Circuit of the Device

The behaviour of a nonlinear device is level dependent. In most cases current through the device may be expressed as a power series of the voltage applied, i.e.

$$i(t) = \sum_{o}^{\infty} a_n \left[v(t) \right]^n \qquad (4.5.1)$$

and for a sinusoidal drive,

$$v(t) = V_o \cos(\omega_o t)$$

the current i(t) may be written as,

$$i(t) = \sum_{o}^{\infty} V_n \cos(n\omega_o t + \phi_n) \qquad (4.5.2)$$

which is the summation of components of the harmonic spectrum. This leads to the idea of the equivalent circuit for the non-linear device terminating the line.

At the fundamental frequency, reflection of the excitation signal occurs at the device end and there will be reflections at the energising source end if Z_g is not equal to Z_o. So far in the case where there are multiple reflections, the circuit may be represented as shown in Fig 4.3. However, the approximate equivalent circuit for the nonlinear device at the fundamental may be represented as shown in Fig 4.4.

At the n^{th} harmonic, the nonlinear device might be looked upon as a generator comprising its own harmonic impedance Z_n' and an open-circuit voltage V_n, as shown in Fig.4.5. Therefore to the nonlinear device the excitation end becomes the load of Z_g impedance where x is the distance of that load to the probe, as shown in Fig.4.6. Retaining the equivalent circuit for the nonlinear device which includes all harmonics it may be drawn as in Fig.4.7. The measurements will lead towards the computations of the complex reflection coefficient, ρ_n, the complex impedance, Z_n, and the amplitude and relative phases of the nonlinear device at the n^{th} harmonic.

4.5.2 Standing Waves at Harmonics

When a load terminating the slotted line is a nonlinear device, then on excitation harmonics will be generated. This nonlinear device becomes the harmonic generator. The harmonics generated will be transmitted towards the excitation end. In order, however, for the standing waves to be created at harmonics, there must be a mismatch at the energising source. Thus it is essential that a deliberate mismatch be devised. This mismatch of the slotted line at both ends will create multiple reflections at the harmonic frequencies. Next, by varying the length of the line a resonant condition is obtained which will be indicated by achieving a maximum amplitude of the standing wave pattern.

Comparing the circuits of Figs 4.1 and 4.6, it is clear that they are similar in form. Fig.4.1 shows the circuit working at the fundamental while that of Fig.4.6 indicates that the circuit is valid at the n^{th} harmonic.

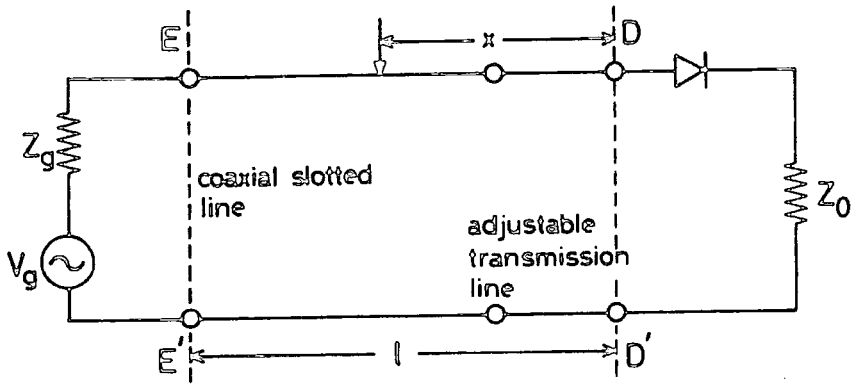

FIG.4·3 THE SLOTTED LINE CIRCUIT AT THE FUNDAMENTAL

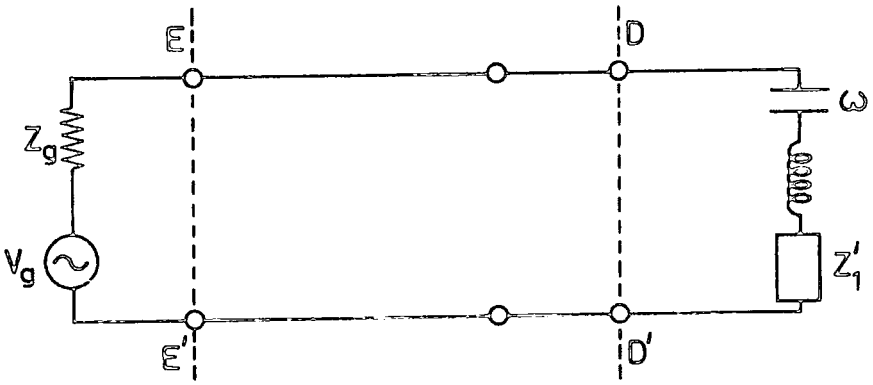

FIG.4·4 APPROXIMATE EQUIVALENT CIRCUIT FOR THE DEVICE AT THE FUNDAMENTAL

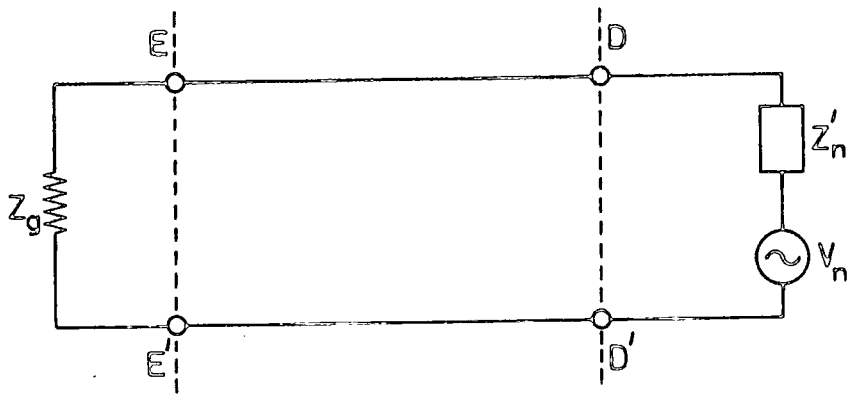

FIG.4·5 CIRCUIT DIAGRAM WHEN THE DEVICE AND THE SLOTTED LINE ARE WORKING AT THE HARMONICS

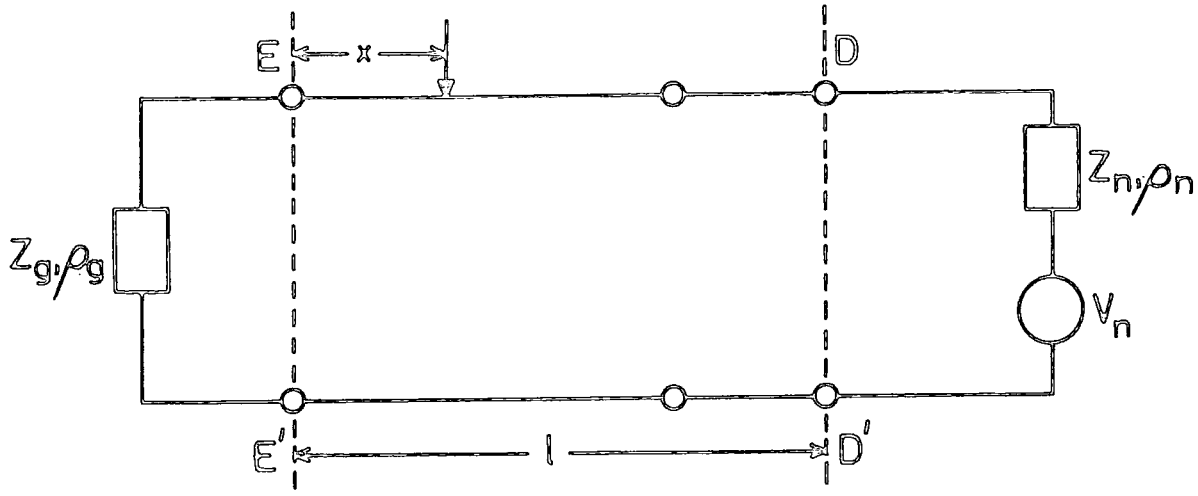

FIG.4·6 CIRCUIT DIAGRAM FOR THE SLOTTED LINE AT n^{th} HARMONICS

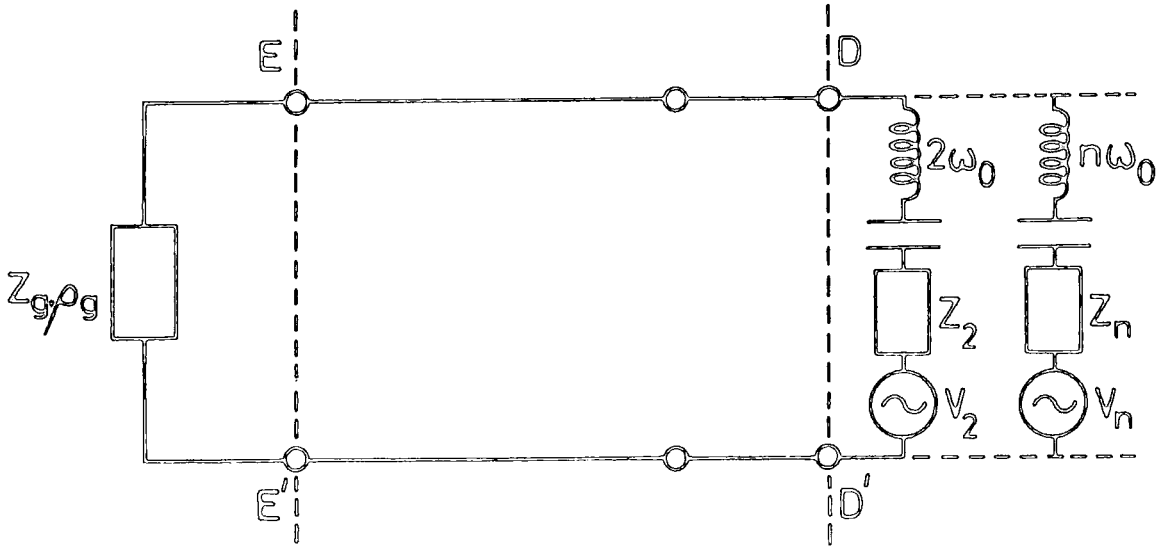

FIG.4·7 APPROXIMATE EQUIVALENT CIRCUIT FOR THE DEVICE AT HARMONICS

Therefore, the equation for the magnitude of voltage $|V(x,\ell)|$ at the n^{th} harmonic will also be similar in form to that at the fundamental. The standing wave magnitude at the fundamental frequency is given by eqn.4.2.15, i.e.

$$|V(x,\ell)| = \left| V_g \left(\frac{1 - \rho_g}{2}\right) \right| \left| \frac{|1 + \rho_L e^{-j2\beta x}|}{|1 - \rho_L \rho_g e^{-j2\beta\ell}|} \right|$$

Hence, at a particular n^{th} harmonic, the voltage $|V(x,\ell)|$, now denoted as $|V_n(x,\ell)|$, may be written as,

$$|V_n(x,\ell)| = \left| V_n \left(\frac{1 - \rho_n}{2}\right) \right| \left| \frac{|1 + \rho_g e^{-j2\beta_n x}|}{|1 - \rho_n \rho_g e^{-j2\beta_n \ell}|} \right| \qquad (4.5.3)$$

The generator voltage V_g and its reflection coefficient ρ_g are replaced by the open circuit voltage V_n and the reflection coefficient ρ_n of the harmonic generator, respectively. Similarly, the reflection coefficient of the load ρ_L is replaced by that of the generator, i.e. ρ_g. This is so because the generator impedance now becomes the load. As ρ_n is complex, it may be written as

$$\rho_n = |\rho_n| e^{j\psi_n} \qquad (4.5.4)$$

The generator impedance Z_g can be made resistive and fixed at a definite value in terms of a fraction of the characteristic impedance Z_0.

This will make the reflection coefficient ρ_g real and negative. The equation 4.5.3. may now be written as,

$$\left|V_n(x,\ell)\right| = \left|V_n'\right| \frac{\left|\left(1 - |\rho_g| e^{-j2\beta_n x}\right)\right|}{\left|\left(1 + |\rho_n||\rho_g| e^{-j(2\beta_n \ell - \psi_n)}\right)\right|}$$

which may be simplified to

$$\left|V_n(x,\ell)\right| = \left|V_n'\right| \frac{\left\{1 - 2|\rho_g|\cos(2\beta_n x) + |\rho_g|^2\right\}^{1/2}}{\left\{1 + 2|\rho_n||\rho_g \cos(2\beta_n \ell - \psi_n) + |\rho_g|^2 |\rho_n|^2\right\}^{1/2}} \quad (4.5.5)$$

where,

$$\left|V_n'\right| = \left|V_n \frac{(1 - \rho_n)}{2}\right| \quad (4.5.6)$$

or $$\left|V_n'\right| = \left|\frac{V_n}{2}\right| \left\{1 - 2|\rho_n|\cos\psi_n + |\rho_n|^2\right\}^{1/2} \quad (4.5.7)$$

and $$\beta_n = \frac{\omega_n}{v_{ph}} = \frac{2\pi}{\lambda_n}$$

4.5.3 Complex Reflection Coefficients at the Harmonics

The complex reflection coefficient at the n^{th} harmonic, ρ_n, may be derived by methods similar to those used in the case of the fundamental frequency. Initially (by considering the standing waves at the n^{th} harmonic the expression for the voltage at a point x for the line length 'ℓ') $|V_n(x,\ell)|$ is as given by eqn. 4.5.5. The extreme conditions (maxima and minima for the line lengths ℓ_{max} and ℓ_{min} and distances x_{max}, and x_{min} respectively) in eqn. 4.5.5. for the harmonic cases can be examined in a similar way as

for the fundamental (eqn. 4.3.3.). Consequently, the expression for $|V_n(x, \ell)|$ under the conditons of maxima and minima can be obtained and this is

$$\left| V_n(x_{\substack{max \\ min}}, \ell_{\substack{max \\ min}}) \right| = \left| V_n' \right| \frac{\left[1 \pm |\rho_g| \right]}{\left[1 \mp |\rho_n||\rho_g| \right]} \qquad (4.5.8)$$

It is important to note that $|V(x,\ell)|$ as given by eqn.4.3.3. is derived for the case of fundamental frequency when the load impedance is complex. As a result the phase angle term ψ_L for the complex reflection coefficient of the load appears in both the numerator and the denominator of that equation. This results in two expressions for the phase angle ψ_L and they are given by eqns. 4.3.9 and 4.4.5. However, the voltage $|V_n(x, \ell)|$ for the n^{th} harmonic, as given by eqn. 4.5.5, contains the load impedance which is real. This results in the phase angle, ψ_n, for the complex reflection coefficient, ρ_n, of the device at the n^{th} harmonic appearing only in the denominator. By considering the maximum and minimum values of $|V_n(x, \ell)|$, it can be shown that,

$$\psi_n = 2\beta_n \ell_{max} - (2k + 1)\pi = 2\beta_n \ell_{min} - 2k\pi \qquad (4.5.9)$$

where

$$k = 0, 1, 2.....$$

The variable k as defined above appears in the expression for the phase angle ψ_n at the conditions of resonance and anti-resonance. The eqn.4.5.8 allows four combinations of extreme voltage values of $|V_n(x,\ell)|$. With

the quantity $|\rho_g|$ known and the term $|V_n'|$ eliminated, the magnitude of reflection coefficient of the nonlinear device at the n^{th} harmonic can then be written as,

$$|\rho_n| = \frac{1}{|\rho_g|} \cdot \frac{|V_n(x_{max},\ell_{max})| - |V_n(x_{max},\ell_{min})|}{|V_n(x_{max},\ell_{max})| + |V_n(x_{max},\ell_{min})|} \qquad (4.5.10)$$

or

$$|\rho_n| = \frac{1}{|\rho_g|} \cdot \frac{|V_n(x_{min},\ell_{max})| - |V_n(x_{min},\ell_{min})|}{|V_n(x_{min},\ell_{max})| + |V_n(x_{min},\ell_{min})|} \qquad (4.5.11)$$

4.5.4 Input Impedance of the Line at Harmonics

The expression for the input impedance of the line at the harmonics may be obtained using the general eqn. 4.4.17. This equation is applicable for any frequency for which the load is complex whose reflection coefficient is ρ_L. The circuit diagram is the same as that already shown in Fig.4.1. However at the harmonics, the load is made deliberately resistive, hence its reflection coefficient is real and may be written as $|\rho_g|$. The circuit is shown in Fig.4.6. The expression for the input impedance at the n^{th} harmonic may finally be written as

$$|Z_n(x,\ell)| = |Z_o| \cdot \frac{\left\{1 - 2|\rho_g|\cos(2\beta_n x) + |\rho_g|^2\right\}^{1/2}}{\left\{1 + 2|\rho_g|\cos(2\beta_n x) + |\rho_g|^2\right\}^{1/2}} \qquad (4.5.12)$$

The relationship between the input impedance of the line and the conditions of resonance and anti-resonance will now be established.

From eqn. 4.5.9 it can be shown that,

$$\ell_{max} = (2k + 1)\frac{\lambda_n}{4} + \frac{\psi_n}{2\beta_n} \qquad (4.5.13)$$

and

$$\ell_{min} = \frac{k\lambda}{2} + \frac{\psi_n}{2\beta_n} \qquad (4.5.14)$$

where ℓ_{max} and ℓ_{min} are the resonant and anti-resonant line lengths, respectively. This is illustrated in Figs.4.8a and b. At the point along the line (Fig.4.8a) where $x = \ell_{max} - \frac{\psi_n}{2\beta_n}$, the voltage is maximum. The term $\cos(2\beta_n x)$ in eqn. 4.5.12 then becomes

$$\cos(2\beta_n x) = \cos(2\beta_n \ell_{max} - \psi_n)$$

$$= -1$$

under resonant conditions, giving

$$|Z_n\left((\ell_{max} - \frac{\psi_n}{2\beta_n}), \ell_{max}\right)| = |Z_o|\left[\frac{1 + |\rho_g|}{1 - |\rho_g|}\right]$$

By definition, the voltage standing wave ratio (VSWR) is

$$|VSWR| = \frac{1 + |\rho_g|}{1 - |\rho_g|}$$

giving in conclusion

$$|Z_n\left((\ell_{max} - \frac{\psi_n}{2\beta_n}), \ell_{max}\right)| = |Z_o| \times |VSWR| \qquad (4.5.15)$$

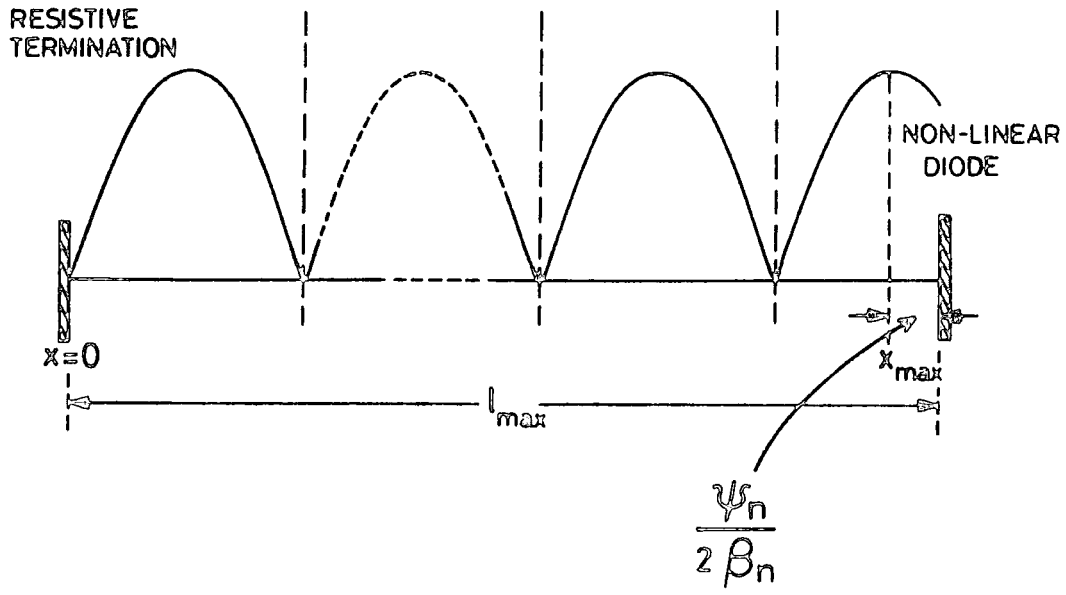

FIG. 4·8a THE BEHAVIOUR OF STANDING WAVES UNDER RESONANT CONDITION

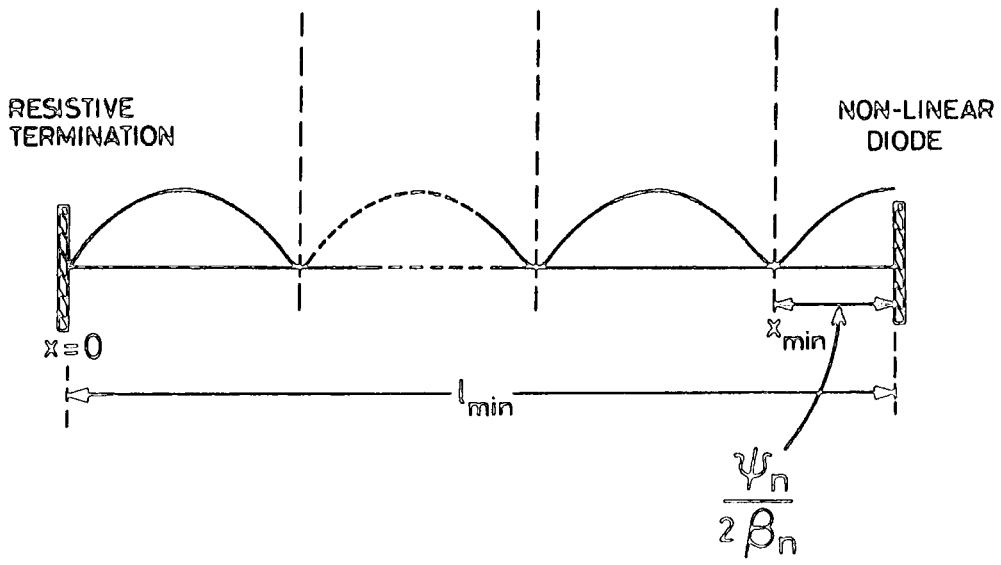

FIG. 4·8b THE BEHAVIOUR OF STANDING WAVES UNDER ANTI - RESONANT CONDITION

This shows that at resonance, the point at which the voltage is maximum corresponds to that of the maximum input impedance. This then represents the parallel resonance circuit of the line at x_{max}, where it now becomes $(\ell_{max} - \frac{\psi_n}{2\beta_n})$.

On the other hand, at a point (Fig. 4.8b) where $x = (\ell_{min} - \psi_n/2\beta_n)$, the term $\cos(2\beta_n x)$ in eqn. 4.5.12 becomes

$$\cos(2\beta_n x) = \cos(2\beta_n \ell_{min} - \psi_n)$$

$$= 1$$

under the anti-resonant condition, giving

$$\left| Z_n\left((\ell_{min} - \frac{\psi_n}{2\beta_n}), \ell_{min}\right)\right| = \left|Z_o\right| \left[\frac{1 - |\rho_g|}{1 + |\rho_g|}\right]$$

$$\left| Z_n\left((\ell_{min} - \frac{\psi_n}{2\beta_n}), \ell_{min}\right)\right| = \frac{|Z_o|}{|VSWR|} \qquad (4.5.16)$$

Thus, it is seen that, under anti-resonant conditions of the line, the voltage minimum occurs at a point where the input impedance of the line is minimum. This implies that at this particular point, the equivalent circuit of the line is of a series resonance type.

4.5.5 Device Impedance

In considering the impedance of a diode, its equivalent circuit must first be examined. The approximate equivalent circuits for the non-linear device at the fundamental and the harmonic frequencies are shown in Figs. 4.4 and 4.7, respectively. Let the apparent value of the complex

impedance of the diode at the n^{th} harmonic be Z_n' . For a series equivalent circuit, Z_n' may be written in the normal complex form as

$$Z_n' = Z_n + R_o \tag{4.5.17}$$

where

$$Z_n = R_n + jX_n$$

The resistive component of the diode impedance is R_n and that of the reactive part is X_n. The reactance is basically capacitive. The apparent impedance comes about because the device is terminated with the characteristic impedance R_o. On normalising with the characteristic impedance, eqn. 4.5.17 becomes

$$\frac{Z_n'}{R_o} = \frac{R_n'}{R_o} + j\frac{X_n}{R_o} \tag{4.5.18}$$

But, from the definition of the coefficient of reflection for the device at a particular harmonic n, it can be shown that,

$$\frac{Z_n'}{R_o} = \frac{(1 + \rho_n)}{(1 - \rho_n)} \tag{4.5.19}$$

Substituting ρ_n from eqn. 4.5.4 into eqn. 4.5.19 leads to the expression for the normalised real and imaginary parts of the complex impedance of the device which are, respectively

$$\frac{R_n'}{R_o} = \frac{\left[1 - |\rho_n|^2\right]}{\left[1 - 2|\rho_n|\cos\psi_n + |\rho_n|^2\right]} \tag{4.5.20}$$

and

$$\frac{X_n}{R_o} = \frac{2|\rho_n|\sin\psi_n}{\left[1 - 2|\rho_n|\cos\psi_n + |\rho_n|^2\right]} \qquad (4.5.21)$$

These quantities can be calculated from the complex value of the reflection coefficient ρ_n.

From the value of the apparent resistive component R_n' of the diode impedance, the true value of the component R_n may be deduced. In the same way from the value of the reactance X_n, the capacitance C_n at the n^{th} harmonic can be obtained. Finally, the magnitude of the impedance i.e.

$$Z_n = \left|(R_n^2 + X_n^2)^{\frac{1}{2}}\right| \qquad (4.5.22)$$

and that of its phase ϕ_n, i.e.

$$\phi_n = \tan^{-1}\left(\frac{X_n}{R_n}\right) \qquad (4.5.23)$$

may be found.

4.5.6 Amplitude and Relative Phases

Basically, the whole aim of the measurements is to produce the amplitude and relative phase spectra. The amplitude spectrum is the variation of the magnitude of the open-circuit voltage $|V_n|$ of the device with harmonic frequency. The relative phase spectrum is a plot of $(\phi_n - \phi_1)$ versus harmonic frequency where ϕ is the phase of the complex impedance of the device. The subscript of ϕ refers to the harmonic number. The relative phases are represented with respect to that of the fundamental. An expression for $|V_n|$ may be derived by first considering any of the combinations of $|V_n(x_{\substack{max\\min}}, \ell_{\substack{max\\min}})|$ as given by eqn. 4.5.18. Suppose

$V_n(x_{max}, \ell_{max})$ is considered, i.e.

$$|V_n(x_{max}, \ell_{max})| = |V_n'| \frac{(1 + |\rho_g|)}{(1 - |\rho_g||\rho_n|)} \tag{4.5.24}$$

hence,

$$|V_n'| = \frac{|V_n(x_{max}, \ell_{max})|}{\left(\frac{1 + |\rho_g|}{1 - |\rho_g||\rho_n|}\right)} \tag{4.5.25}$$

But from Equation 4.5.7, $|V_n'|$ is given by:

$$|V_n'| = \left\{ \frac{|V_n|}{2} \left[1 - 2|\rho_n|\cos \psi_n + |\rho_n|^2 \right] \right\}^{1/2} \tag{4.5.26}$$

Equating $|V_n'|$ from Equations 4.5.25 and 4.5.26, an expression for $|V_n|$ can be derived, i.e.

$$|V_n| = \frac{2\,|V_n(x_{max}, \ell_{max})|}{\left(\frac{1 + |\rho_g|}{1 - |\rho_g||\rho_n|}\right)\left\{ 1 - 2|\rho_n|\cos \psi_n + |\rho_n|^2 \right\}^{1/2}} \tag{4.5.27}$$

All the quantities in the denominator can be found and the absolute value of $V_n(x_{max}, \ell_{max})$ may be computed by considering the coupling coefficient between the probe and the slotted line at the respective harmonics. Hence the magnitude of open circuit voltage of the diode at harmonics can be computed. In the case of the phase spectrum, the phases at a particular harmonic can be found by using Equation 4.5.23. Relative phases of harmonics are found by considering the phase of a particular harmonic with respect to that of the fundamental.

4.6 CONCLUSION

One of the basic aims of the work is to develop a method of measurement of a complete spectrum generated within a nonlinear device at high frequencies. This involved the derivation of mathematical expressions (based on multiple reflections and line resonance) and the establishment of measurement procedures. As the basic equipment employed was a slotted line system with mismatched termination , the procedures involved measurement of the standing waves. There was a need to create standing waves at the harmonics under known conditions and to relate the measurements of a particular frequency component in the spectrum under investigation.

The measurement technique developed is called the Multiple Reflections Resonant Line method. The idea of resonant line comes about because the voltage $|V(x,\ell)|$ along the line reaches a maximum (resonance) and a minimum value (anti-resonance) for particular lengths of the transmission line, i.e. 'ℓ_{max}' and 'ℓ_{min}', respectively. In order to arrive at these conditions of resonance or anti-resonance, an expression for the voltage $|V(x,\ell)|$, based on the multiple reflections was derived. Multiple reflections were achieved when the ends of the transmission line were mismatched.

A deliberate mismatch of the driving source end leads to a new type of measurement of the diode impedances at the harmonic frequencies. Making the load impedance at the harmonics resistive contributes towards a major simplification in the expression for the voltage $|V(x,\ell)|$, given by eqn.4.5.5. This impedance was kept at a known (resistive) value throughout the measurement, thereby making the standing waves at the harmonics identical. This was possible because the standing wave pattern of any reflection is decided only by the load impedance.

In addition to the derivation of the expression for the voltage $|V(x,\ell)|$, an expression for that of the current $|I(x,\ell)|$ was similarly obtained. Thus,

the ratio of the two gives the input impedance $|Z(x,\ell)|$. Under the conditions of resonance (ℓ_{max}) and anti-resonance (ℓ_{min}), the resultant equations for the voltage $|V(x,\ell)|$ and the input impedance $|Z(x,\ell)|$ now may be compared. This was discussed in section 4.5.4. It was shown that under resonant conditions and at a point along the transmission line where the voltage is maximum, the input impedance is also maximum. On the other hand, under the condition of anti-resonance, at a point along the line when the voltage is minimum, the input impedance is minimum. These observations are explained in terms of the resonant equivalent circuits. The parallel and series resonant circuits are referred to the former and the latter cases, respectively.

The method is initially involved with the measurement of the complex reflection coefficient of the nonlinear diode at the n^{th} harmonic. This requires the setting of both the resonant and anti-resonant conditions from which the following quantities may be measured, i.e. $|V_n(x_{max},\ell_{max})|$, $|V_n(x_{max},\ell_{min})|$, $|V_n(x_{min},\ell_{max})|$, $|V_n(x_{min},\ell_{min})|$, ℓ_{max} and ℓ_{min}. From these, the diode impedance Z_n, open circuit voltage $|V_n|$ and phase angle ϕ_n at the n^{th} harmonic may be calculated. Hence the amplitude and the relative phase spectra at different drive levels can now be plotted. In addition, from the approximate equivalent circuit and the impedance of the diode at a particular harmonic, the nature of the parasitics involved may be established and values estimated.

CHAPTER 5

MEASUREMENTS AND EXPERIMENTAL PROCEDURES

5.1 INTRODUCTION

Basically, the measurement technique and the experimental procedures were connected with the Multiple Reflections Resonant Line method. In addition, any test or evaluation of a microwave diode by any technique must also include the measurements of the static characteristics as reference. It provides an initial assessment of the diode and its rectification properties. For example, the values of the reverse saturation current I_s and the series resistance r_s obtained are considered to be important diode parameters. The experimental arrangements and the initial calibrations necessary in any measurement are first discussed. Next, discussions of the diode static characteristics and the spectrum measurements are made. Finally, a general assessment is made of the measurement methods.

5.2 EQUIPMENT AND INITIAL CALIBRATIONS

5.2.1 General Arrangements

The circuit for the d.c. measurements of the diodes is shown in Fig. 5.1. It comprised the d.c. supply source and the potentiometer of 1K Ω . The diode in series with a known resistor of 50 Ω was connected across the potentiometer and the 1M Ω resistor. The 50 Ω resistor was introduced in order to measure the current through the diode while that of 1M Ω to reduce the current drain on the voltage source. The d.c. valve voltmeter was used in the measurements of voltages as shown in Fig.5.1.

The experimental arrangement for the spectrum measurements is shown in the block diagram of Fig.5.2. It comprised four parts, (a) the excitation end, (b) the slotted-line system, (c) the load end and (d) the spectrum

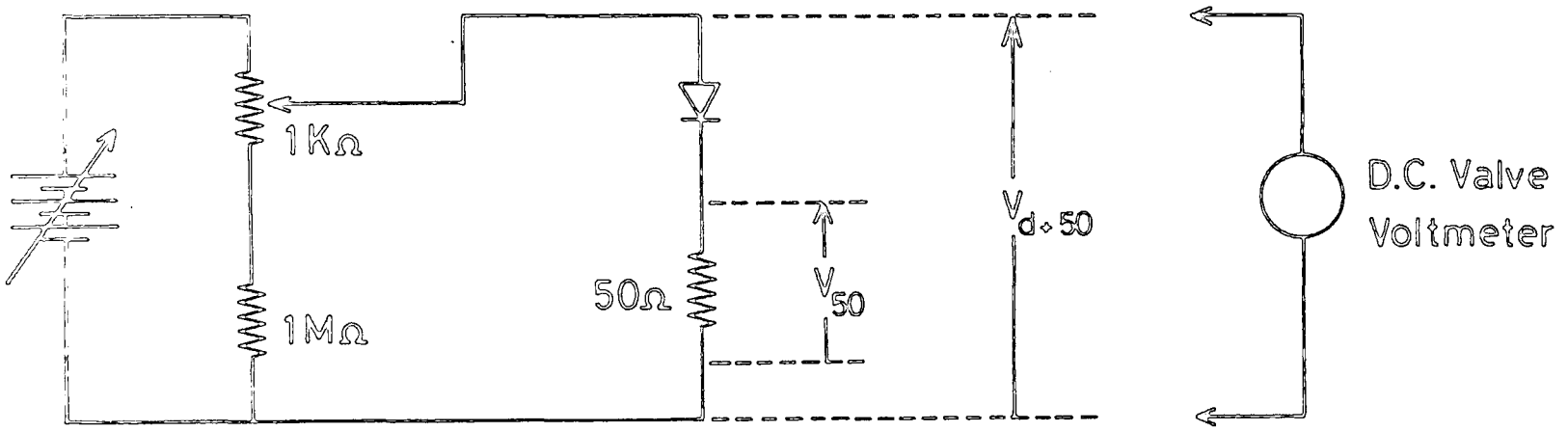

FIG. 5·1 CIRCUIT FOR THE D.C. CHARACTERISATION

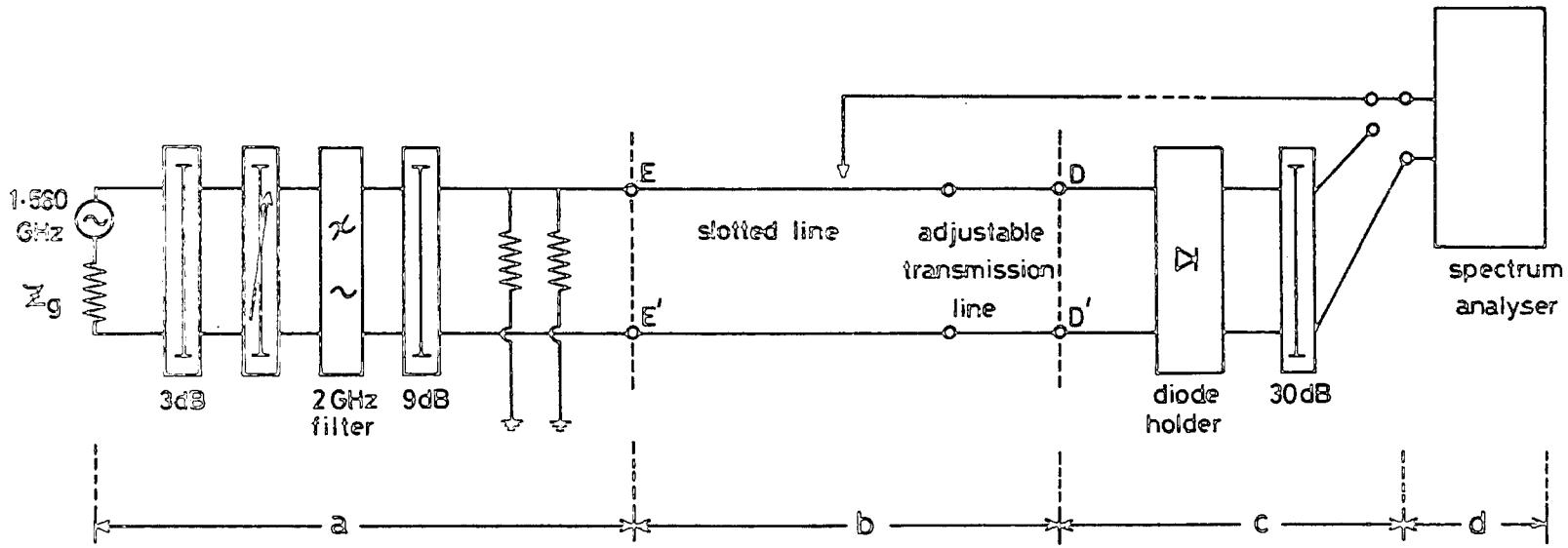

FIG. 5·2 BLOCK DIAGRAM FOR THE COMPLETE COAXIAL LINE SYSTEM

analyser. The excitation end lay to the left of the terminals EE' as shown in Fig.5.2. It consisted of the signal generator followed by a fixed attenuator, variable attenuator, low pass filter and another fixed attenuator. The fixed attenuator was used to reduce the level in order to protect the components that followed in addition to isolating the source from the line. The variable attenuator provided a means of adjusting the input level of the signal. The low pass filter was used to prevent any harmonics and spurious signal from the source reaching the line. Finally, a resistive termination of known impedance was deliberately introduced to provide the mismatch at the excitation end.

The slotted-line was a coaxial type, comprising accessories like the probe and carriage assembly, an adjustable transmission line, a T-junction and a stub tuner. The ends of the line were connected to the generator and the load, respectively. The load end (Fig. 5.2) was on the right-hand side of the terminals DD', and included the diode, placed in the holder. The diode was then terminated with the characteristic impedance, Z_o. The component used for this termination was the precision attenuator, which allowed connections to be made to the spectrum analyser. Finally, the spectrum analyser, an important component in the arrangement, was used to measure, (i) standing waves at the harmonic and fundamental frequencies through the probe and carriage assembly, and (ii) the current at the fundamental frequency through the diode.

5.2.2 Diode Holder

As the project involved the investigation of diode properties, the construction of a proper diode holder was essential. The holder (shown in Fig 5.3) was manufactured in a coaxial form and adapted for use with the General Radio (GR) system having the characteristic impedance of 50 ohm. The main requirement for a properly designed holder was that it should match the line. It had to meet the test that when the diode holder was short-

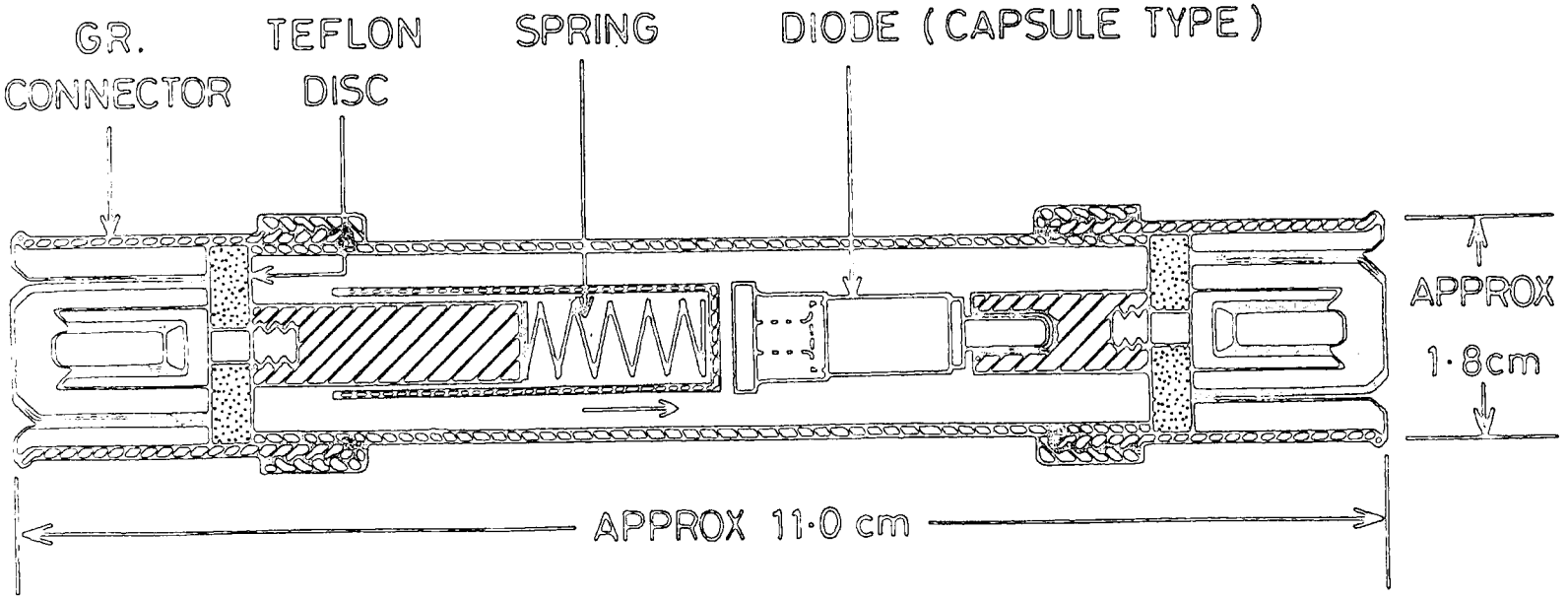

FIG. 5·3 DIODE HOLDER, SHOWING CONSTRUCTION AND APPROXIMATE DIMENSIONS

circuited (with a dummy made of brass, identical in shape to the diode encapsulation) and terminated with the characteristic impedance it produced no standing waves ; under these conditions the dimensions of both the inner and outer conductors of the diode holder would then meet the specifications required for matching purposes. It can be shown that for a coaxial lossless transmission line, the characteristic impedance[32,33,34] at high frequencies is given by

$$Z_o = \frac{1}{2\pi}\sqrt{\frac{\mu}{\epsilon}}\ \ell n\ \frac{a}{b}$$

where μ and ϵ are the permeability and permittivity of the medium, respectively ; 'a' is the internal diameter of the outer conductor and 'b' is the diameter of the inner conductor. The encapsulated diodes used were of the shapes shown in Fig.5.4.

The calibration of the diode holder was made by first placing a dummy in the holder. The whole unit (diode holder) was then used to terminate the transmission line. The unit was in turn connected to a matched termination, Z_o. With the modulated waves incident onto the diode holder, standing waves were measured using a sensitive SWR-meter. In practice, the occurrence of small reflections could be tolerated and the diode holder used had a very satisfactory VSWR of 1.02.

5.2.3 Resistive Multiple Termination

An important element that contributed towards simplification of the measurement method was the introduction of the resistive multiple termination at the energising source end. This was done to create a mismatch with a known value of impedance. The components making up the termination were the precision attenuators ; each was resistive over a wide range of frequencies having the characteristic impedance of R_o.

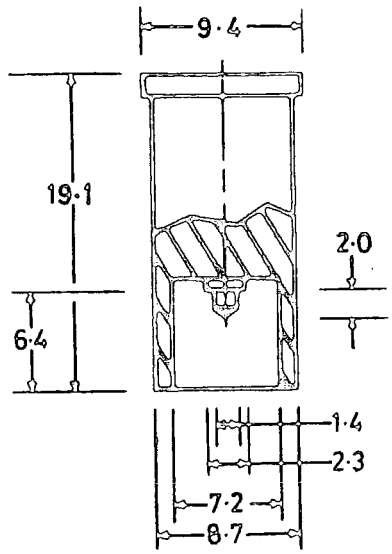

(a)

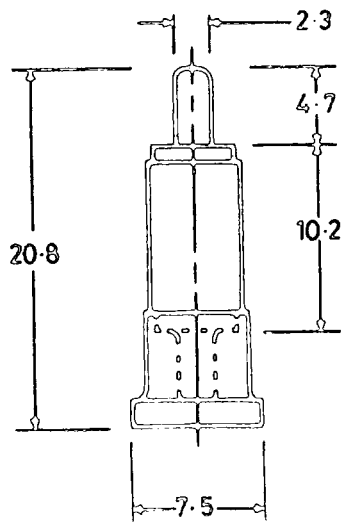

(b)

FIG. 5·4 SHAPES OF (a) COAXIAL AND (b) CAPSULE DIODES SHOWING APPROXIMATE DIMENSIONS (mm)

Thus a parallel connection with two of them constituted a double termination giving an impedance of $R_o/2$. Similarly, three of these components when connected in parallel formed a triple termination having an impedance of $R_o/3$. As these resistive terminations were independent of frequency and level when acting as a load, they always produced the same VSWRs at harmonics although not necessarily of the same magnitudes.

The reflection coefficient of the diode at the n^{th} harmonic $|\rho_n|$, given by eqn. 4.5.10 or 4.5.11, is a function of the reflection coefficient, $|\rho_g|$ at the excitation end. Since therefore, $|\rho_g|$ was required in all the harmonic measurements, its value was made fixed and known by making the impedance at the excitation end, and hence the voltage standing wave ratio (VSWR) on the line, constant.

Tables 5.1a and 5.1b give the results of the line calibrations for the double and triple termination at the fundamental drive frequencies of 1.560 GHz and 450 MHz, respectively. Greater sensitivity in measurement was achieved when the termination with higher VSWR value is chosen. The triple termination was preferred to the double because the resulting VSWR value for the former was higher than that for the latter. For this reason, the triple termination was chosen for the case of the fundamental drive frequency of 1.560 GHz (Table 5.1a). However, this was not the only criterion in deciding which type of termination was preferable in the measurements. Its VSWR values should also be relatively constant over a range of harmonic frequencies. Hence, because of this requirement the double termination was chosen for the fundamental drive of 450 MHz (Table 5.1b).

5.2.4 Coaxial Slotted Line

The coaxial slotted line is a device where normally standing waves are created and measured. The output from the slotted line was obtained via a probe coupled into the field inside the transmission line. As the probe

TABLE 5.1(a): Line Calibrations for the double and triple terminations at f_1 equal to 1.560 GHz

Harmonic n	VSWR double termination		VSWR triple termination	
	dB	ratio	dB	ratio
1	6	2.0	9	2.8
2	6	2.0	9	2.8
3	4	1.6	9	2.8
4	6	2.0	10	3.2
5	6	2.0	11	3.6
6	6	2.0	10	3.2

TABLE 5.1(b): Line Calibrations for the double and triple terminations at f_1 equal to 450 MHz.

Harmonic n	VSWR double termination		VSWR triple termination	
	dB	ratio	dB	ratio
1	6	2.0	7	2.2
2	6	2.0	4	1.6
3	5	1.8	6	2.0
4	6	2.0	8	2.5

coupling was of the capacitive type [21], the voltage induced in the probe circuit was proportional to that existing between the inner and the outer conductors of the line at any probe position. The main advantage of this kind of coupling were the ease and convenience of adjustment of the coupling with only one variable (i.e. the penetration depth of the probe) and the relative insensitivity to small frequency changes.

It was essential that the calibration of the slotted line included the loading effect. This was carried out by determining the coupling coefficient between the line and the probe for different penetration depths of the latter. A large coupling coefficient would eliminate the loading effect ; however, this would reduce the sensitivity of the measurements. The main aim of the calibration was to establish an optimum depth for the probe penetration. This would give a sufficiently high coupling coefficient and an adequate sensitivity in the measurements at different frequencies. Once this depth was found, it was held fixed throughout the entire measurements at the fundamental and harmonic frequencies for different drive levels. Any further variation in the depth would significantly affect the measurements at different harmonics because the properties of the device at different frequencies were inter-related. The measurement of the coupling coefficient for each harmonic was then carried out.

The calibrating procedure was performed by generating the harmonics in the diode from the excitation end with a matched line as the load. The ratio of the level measured at the end of the termination to that on the line gives the coupling coefficient between the line and probe. This calibration was carried out at different harmonic frequencies.

The results of the calibrations of the probe coupling with the slotted line are presented in Tables 5.2a and 5.2b for the fundamental drive frequencies (f_1) of 450 MHz and 1.560 GHz, respectively. It is important to note that

TABLE 5.2(a): Calibration of the Probe Coupling for f_1 equal to 450 MHz

Harmonic n	Voltage measured at the end of the termination (dB)	Voltage measured on the line (dB)	Coupling Coefficient	
			dB	ratio
1	66.0	53.5	13	4.5
2	60.0	42.0	18	7.9
3	56.0	42.0	14	5.0
4	60.0	38.0	22	12.6

Table 5.2(b): Calibration of the Probe Coupling for f_1 equal to 1.560 GHz

Harmonic n	Voltage measured at the end of the termination V(dB)	Voltage measured on the line V'(dB)	Coupling Coefficient	
			dB	ratio
1	56.0	37.0	19	8.9
2	71.0	48.0	23	14.1
3	56.0	38.0	18	7.9
4	54.0	36.0	18	7.9
5	50.0	39.0	11	3.5
6	35.0	29.0	6	2.0

different probe penetrations on the slotted line were used at different fundamental frequencies because of differences in the measured levels. The coupling coefficients at the harmonic frequencies were recorded and used in determining the actual values of the voltages on the line measured with the probe.

5.2.5 Spectrum Analyser

Firstly, the frequency scale was calibrated. This was done by measuring the frequency accurately using the slotted line. The frequency scale was then adjusted to coincide with the correct value. For level measurements, a reference height was established against which all other readings were taken. This was done with all other controls being in calibrated positions. The calibrations of attenuators in the spectrum analyser were compared to the known values of precision attenuators. For proper operation and protection of the spectrum analyser, the input level had to be adequately attenuated. This was because the maximum allowable input level specified was 1 μW.

5.3 MEASUREMENT OF DIODE STATIC CHARACTERISTICS

In the static d.c. characterisation, the diode exponential law[19,35] was assumed to be

$$i = I_s(e^{\alpha V_a - \alpha r_s i} - 1) \qquad (5.1)$$

where i, is the current, I_s, the saturation current, V_a, the applied voltage, r_s, the series resistance and α is defined as,

$$\alpha = \frac{q}{n\,kT}$$

with n the ideality factor. The main purpose of the d.c. measurements was

to determine the above parameters for the practical diodes. The circuit employed was as shown in Fig 5.1.

The forward current I_f was calculated from the voltage across a known load resistance in series with diode. The applied voltage V_a was measured across the diode and the load resistance. For the low current range, the term $\alpha r_s i$ in the exponent of eqn. 5.1 is very small compared to that of αV_a, and hence may be neglected. The eqn. 5.1 may then be written as

$$(I_f + I_s) = I_s\, e^{\alpha V_a}$$

giving

$$\ell n\ (I_f + I_s) = \alpha V_a + \ell n\ I_s \qquad (5.2)$$

However, as the measurable forward current I_f values were generally a few orders of magnitude higher than that for the saturation current I_s, eqn. 5.2 can be written as,

$$\ell n\ (I_f) = \alpha\ V_a + \ell n\ I_s \qquad (5.3)$$

From the graph of ($\ell n\ I_f$) against V_a, the parameters I_s and α can be obtained. The value of α was then used to plot another graph in order to get the parameters r_s and again I_s.

The eqn. 5.1 may be written in the form

$$I_f = I_s\,(e^{\alpha V_a - \alpha R I_f} - 1) \qquad (5.4)$$

where $R = R_L + r_s$

and R_L is the load resistance.

Rearranging the terms gives,

$$(I_f + I_s) = I_s e^{\alpha V_a - \alpha R I_f} \tag{5.5}$$

When working at higher current levels the term $\alpha R I_f$ becomes significant and hence cannot be neglected. However, the saturation current I_s may again be neglected because it is a few orders of magnitude lower than that for the forward current I_f. The eqn. 5.5 can be written as

$$\frac{I_f}{e^{\alpha V_a}} = I_s e^{-\alpha R I_f}$$

giving

$$\ell n \left(\frac{I_f}{e^{\alpha V_a}} \right) = \ell n\, I_s - \alpha R I_f \tag{5.6}$$

Therefore, from the graph of $\ell n \left(\frac{I_f}{e^{\alpha V_a}} \right)$ versus I_f, the parameters R and I_s may be found.

The capacitances of the diodes were measured directly using the 1 MHz capacitance-meter.

5.4 SPECTRUM MEASUREMENTS

5.4.1 Introduction

In general this specially developed technique of spectrum measurements is involved with the standing waves both at the fundamental and harmonic frequencies. The load is a microwave diode. Such a method can also be applied at any suitable frequency for any load. As the standing waves reflect the behaviour of the load, the result of the standing wave measurements can be related to the diode behaviour under its normal operational condition. As an example, a diode working under a certain

drive level will have a different impedance at different frequencies. The expression for the complex impedance of the diode is derived from the basic properties of the standing waves.

As the aim of the work is to assess the harmonic generating properties of a diode, the method of spectral characterisation becomes appropriate. The spectra of interest will be those of the amplitude and relative phases. The quantities that can be determined are, the magnitude of the open circuit voltage, $|V_n|$, and the complex impedance at the n^{th} harmonic. In addition, the diode parasitics may be estimated from the proposed equivalent circuit of the diode.

In developing this new measurement method, one of the first tasks was to design and construct a diode holder suitable for use with the slotted line (discussed in section 5.2.2). Next, the aim was to create standing waves at the harmonic frequency components of the diode spectrum. It is significant to note that even with adequate filtering to prevent harmonics from the source, low level standing waves at the harmonics are still produced due to a slight mismatch at the excitation end. However, this is unimportant, because in order to create standing waves at the harmonics generated within the diode, the excitation generator impedance must be mismatched. From the standing wave measurements diode impedances at different harmonics may be computed.

The above ideas lead to the concept of multiple-reflections along the line when the ends are mismatched, and their characterisation may need nonconventional experimental techniques. From the mathematical formulation for the magnitude of the standing waves at any frequency, the variables involved are the distance from the load end and the total length of the transmission lines as given by eqn. 4.2.15. Variation of the line length contributes towards the idea of resonance along the line.

Manipulation of eqn. 4.5.3 for $|V_n(x,\ell)|$, (to solve for the amplitude of reflection coefficient $|\rho_n|$ at the n^{th} harmonic), shows that it may be computed if the reflection coefficient of the generator ρ_g is known. Furthermore, if ρ_g is real, this contributes towards a major simplification in the expression for $|V_n(x,\ell)|$. Consequently, in order to solve for $|\rho_n|$, ρ_g should be known and real. Fortunately, this can be achieved by introducing 'double' or 'triple' terminations using the characteristic impedances which are resistive ($R_o//R_o$, $R_o//R_o//R_o$) at the energising end.

In conventional slotted line measurements, the waves are modulated normally with an a.f. signal. The standing waves are measured using the VSWR-meter which normally contains a sensitive, narrow-band a.f. amplifier. In this project, however, standing waves at harmonics were measured directly via the probe and carriage assembly using the spectrum analyser. As the spectrum analyser is a high frequency, frequency-selective and very sensitive voltmeter, the harmonic waves need not be modulated. Without the spectrum analyser, other suitable methods of detection would have to be devised.

The proper spectrum measurements were carried out once all the necessary calibrations of the equipments and components were made. Basically, these were concerned with the harmonic components of a spectrum generated within a diode. At each harmonic and for a particular fundamental drive frequency, measurements were carried out over a suitable range of drive levels, after which these were repeated for all the measurable harmonics. At this stage, there was a need to decide on the fundamental drive frequency, the choice of reference drive level and its operational range. The measurement method will then be discussed based on the theory developed in Chapter 4. The spectrum measurements were carried out on six types of diodes (two for each) which were, gallium arsenide and silicon (two types) Schottky barrier, germanium backward and silicon point contact (two types) diodes.

5.4.2 Choice of Reference Drive Level

Generally the characteristics of the diodes are level dependent and therefore the actual drive conditions must be established. This is important because it must form the right basis for reference and comparison. Whatever quantity is selected to fix the drive level, it must be reliably repeatable. This means that any measurements made on the device under similar operating conditions will give identical results. An important parameter is the diode impedance, for it will remain the same for a particular drive level. The quantities that have been considered were power, applied voltage, current at the fundamental and the d.c. rectified current.

Power was not a suitable quantity to monitor the drive level on the diode because the power-meter employed a thermistor which measured only the real part of the complex current. Voltage could not be used either because no voltmeter of sufficiently high impedance was available ; in addition, measurement of voltage poses a problem caused by the uncertainty in the measurement of the applied voltage at the end of the line for it will change on varying the length of the line. The d.c. rectified current[18] was not suitable because of its complex dependence on frequency and the voltage. At low voltage levels the decrease in the d.c. rectified current with increasing frequency was much smaller than at higher voltage levels. It was decided that the true representation of the drive level was the current I_1 at the fundamental frequency measured through the diode. This was justified because the complex impedance of the diode at a particular I_1 level would always be the same. Therefore, as the generated harmonic spectra are critically dependent on the fundamental drive current, the measurements at the harmonics can then be correctly monitored with reference to this level.

5.4.3 Fundamental Drive - Choice of Frequencies and Levels and Calibrations

Firstly, the choice of frequency to drive the diode was made. This depended on the signal generator satisfying the following requirements, viz, that the frequency lay within the operating limits of the slotted line and that simultaneously the generator had adequate output level. There is a need for high outputs so that the devices are driven sufficiently hard to allow measurement of low level higher harmonics. In addition, there was a need to have more attenuation to provide a good termination.

Next, the range of the required fundamental frequency drive levels (I_1) was considered. It was important that the fundamental current drive was properly chosen so that the measurements at all the harmonic frequencies could be carried out. This was to allow for comparison to be made of the diode behaviour at different frequencies for specific drive levels. The upper limit of the drive current, which depends on the maximum output of the signal generator, is restricted by the high attenuation required for a good termination at the excitation source end. Furthermore, as there is a need to change the line length for the conditions of resonance ('ℓ_{max}') and anti-resonance ('ℓ_{min}'), the drive level will vary. This is because at resonance and anti-resonance, the input impedances of the line become maximum and minimum respectively. The highest value of the fundamental drive current under anti-resonant condition will then be its upper limit. The lower limit of the drive was then determined by first obtaining the highest harmonic standing wave under anti-resonant condition after which the level was decreased until the proper measurement at the harmonic could be made. This then gave the lower limit for the fundamental drive. Further reducing the fundamental drive will restrict the measurements to fewer harmonics. It must be emphasised

that throughout this procedure the drive level must not exceed that of the burnout for the device.

The spectrum analyser was next calibrated for the fundamental frequency current. This was done by measuring the r.f. voltage across the characteristic impedance Z_o in series with the diode. The value of the current computed was then related to the reading on the spectrum analyser. Throughout the experiment the spectrum analyser was used to measure the harmonic standing waves along the slotted line and the fundamental frequency current through the diode.

5.4.4 Harmonic Measurement Procedures

The equipment, working at a particular harmonic and drive level is shown in Fig.5.2. The measurement procedure consisted of two parts which were, the setting up of the condition of resonance and the condition of anti-resonance. In both cases (resonant and anti-resonant) the magnitudes of the standing waves at the anti-nodes and the nodes were measured while maintaining the same drive level. The measurements were carried out according to the following steps:

(i) The probe was tuned to the desired harmonic frequency, using a variable matching stub, as indicated by the spectrum analyser. The frequency was also verified by measuring the wavelength along the slotted line.

(ii) The condition of resonance of the line was first obtained. This was done by varying the total length of the line until the standing wave (magnitude) peaked. With this resonant length of the line 'ℓ_{max}' and at any probe position 'x' the magnitude of the standing wave is $|V_n'(x, \ell_{max})|$. The value of 'ℓ_{max}' between the terminals EE' and DD' (Fig.5.2) was then measured and recorded.

(iii) While retaining the line under the resonant condition, the spectrum analyser was reset to measure the fundamental drive current. The drive level was then set to the required value.

(iv) Next, the spectrum analyser was retuned to read the voltage at the n^{th} harmonic (still under the resonant condition). The probe was moved to the anti-node ('x_{max}') and the node ('x_{min}') positions of the standing waves. The corresponding magnitudes of the standing wave

$$|V_n'(x_{max}, \ell_{max})| \quad \text{and} \quad |V_n'(x_{min}, \ell_{max})|$$

were then measured.

(v) The condition of anti-resonance of the line was next obtained. This was done by varying the length of the line until the magnitude of the standing wave reached a minimum. The length of the line 'ℓ_{min}' was then measured.

(vi) Keeping the anti-resonant condition of the line, the spectrum analyser was reset to measure the drive level. This level had to be adjusted to the value set earlier in order to maintain the same drive level under both the conditions of resonance and anti-resonance.

(vii) Finally, the spectrum analyser was retuned to measure the maximum and minimum values of the standing wave under the anti-resonant condition. This was done by moving the probe to the positions of the anti-node('x_{max}') and the node ('x_{min}') of the standing wave. The corresponding magnitudes of the standing wave at these points

$$|V_n'(x_{max}, \ell_{min})| \quad \text{and} \quad |V_n'(x_{min}, \ell_{min})|$$

were then measured.

In summary, the four quantities measured at a particular harmonic frequency and the drive level were the magnitudes of the standing wave at the anti-node and the node under the resonant condition, i.e.

$$|V_n'(x_{max}, \ell_{max})| \quad \text{and} \quad |V_n'(x_{min}, \ell_{max})|$$

and those under the anti-resonant condition, i.e.

$$|V_n'(x_{max}, \ell_{min})| \quad \text{and} \quad |V_n'(x_{min}, \ell_{min})|$$

Other variables involved in the measurements were the line lengths ('ℓ_{max}' and 'ℓ_{min}') and the probe positions ('x_{max}' and 'x_{min}').

Finally, using the measured quantities mentioned above (i.e. voltages, lengths of the transmission line and the probe positions), the following diode parameters

ρ_n - complex reflection coefficient

Z_n - complex impedance

$|V_n|$ - generator voltage

at the n^{th} harmonic and a specific drive level can be determined by the methods shown in the theory. At each harmonic frequency, the process was repeated for different drive levels within the fundamental frequency current range chosen.

5.5 CONCLUSION AND COMMENTS

The theory and the measurement of the diode static characteristics have been outlined. In the measurement it was essential that the bias should not exceed the burn out level. In addition, while taking the measurement, a precaution was taken where the d.c. supply on the diode was for only short time intervals. This was to prevent the diode from getting over heated thereby causing changes in the diode characteristics.

A presentation of the spectrum measurement technique by the Multiple Reflections Resonant Line (MRRL) method was given. This has been specially developed for measurements where the load is a nonlinear diode. Relevant ideas related to the operation and application of the coaxial slotted line have been outlined. In the conventional slotted line measurements, multiple reflections are rarely considered because the source impedance is normally taken to be the characteristic impedance ; hence no reflection of waves would result at the source end. The idea of multiple reflections, leading to that of line resonance, provides another useful application of the slotted line.

With the creation of standing waves at harmonics under well-defined conditions, meaningful measurements at different harmonic frequencies could be made. From the measurement point of view an interesting aspect of this technique is that there are two conditions that have to be satisfied. The first condition is that the VSWR obtained at harmonics should be constant (fixed by the type of termination chosen). The second condition is that the difference in lengths of the transmission line under the conditions of resonance and anti-resonance at a particular harmonic (frequency) should correspond to a quarter wavelength. Checking the extent to which these two conditions are fulfilled helps to confirm whether the measurements taken are reliable.

A discussion on the equipment and the experimental bench was given. One interesting aspect in the experimental arrangement was the key role played by the spectrum analyser. The use of the multiple termination at the energising end represented another unique feature of the method. As the measurements involved the variation in the length of the transmission line, the use of an adjustable line became essential. This line was well lubricated in order that the conditions of resonance and anti-resonance be more precisely established. The connections between the components along the transmission line had to be rigidly made to prevent mismatches. The diode was placed at the end of the line rather than the beginning because of the need for a proper monitoring of the fundamental current drive level If it was placed at the beginning of the line a reliable drive level could not be measured because of variations in the input impedance along the line. A coaxial diode holder was constructed to be compatible with the shapes of the test diodes and the slotted line system. As the nonlinear device behaviour is level dependent, a quantity which measured the level reliably was established, and that was the current at the fundamental frequency. Indications on the procedures adopted in the calibration of various equipments and components were also given. Detailed measurement procedures were finally outlined.

The novelty of the method lies in the fact that a complete spectrum generated within a nonlinear device at high frequencies can be obtained. At the present time only the amplitude spectra can be measured and no high frequency method is available to obtain both the amplitude and the phase spectra. These spectra provide the means of device 'fingerprinting'. From the complex impedance and the equivalent circuit proposed, device characterisation under specific operating conditions can be found. Hence, this might be looked upon as the device characterisation. This technique too provided

a means of comparing the device behaviour under different drive levels. In essence this was device matching at harmonics and it constituted a further application of the method in device assessment. Therefore the technique provided a better way of characterising a device for definite drive levels and frequencies, thus giving a more complete picture of the diodes used as nonlinear elements.

At present, the characterisation of such devices is inadequate because of insufficient information about their capabilities in frequency converting applications. In the data sheet for devices for example, the parameters given are usually vague with no reference to the critical quantities like the drive levels and frequencies. Very often some of these given parameters are based on one point measurements, and others on measurements made at low frequencies. In addition, the quantities obtained are also approximate.

The measurements involved in this high frequency technique are simple once relevant components and instruments are calibrated. In the computation of the device impedance, only relative measurements of the standing waves are required. However, the actual value for the generator voltage of the device at the harmonics can be easily obtained by considering the coupling coefficients between the line and the probe. The sensitivity of measurement may be improved by increasing the precision of the attenuator scale on the spectrum analyser used. The lowest scale available in the spectrum analyser used was 1dB. Another factor is increasing the resulting VSWR value of the multiple termination adapted to the transmission line.

CHAPTER 6

EXPERIMENTAL RESULTS

6.1 INTRODUCTION

The results of the experimental d.c. and the harmonic spectrum measurements carried out on the diodes are presented. In the case of the former, they take the form of the graphs from which the diode parameters were found ; for the latter, the amplitude and phase spectra are given in addition to the diode impedance at different harmonics and the effect of parasitics. The experimental methods and procedures were already discussed in Chapter 5. Two sets of measurements were carried out for each diode. The fundamental drive frequency chosen was 450 MHz for one set and that 1.560 GHz for the other. The first was chosen to suit the measurements for the lower range of frequencies of the slotted line available and the second for the higher range. The 450 MHz source had a maximum available output of 50mW while that for 1.560 GHz source had a constant output of 1.5W.

From the static characteristics and the results of the harmonic spectrum measurements, the six types of diodes (two diodes for each type) were characterised and assessed. The amplitude and phase spectra provided the means for the device 'fingerprinting' and comparison against other devices of the same type. In addition, it provided the required information about the component values of the equivalent circuit.

6.2 STATIC CHARACTERISTICS

Typical results of the d.c. measurements are presented in Figs 6.2.1 and 6.2.2. For each diode, two graphs were drawn, the $\ell n(i_f)$ versus V_a, and $\ell n\left(\frac{i_f}{e^{\alpha Va}}\right)$ versus i_f. The values of the parameters I_s, r_s, α and n, for the static characteristics are summarised in Table 6.1. The actual diode

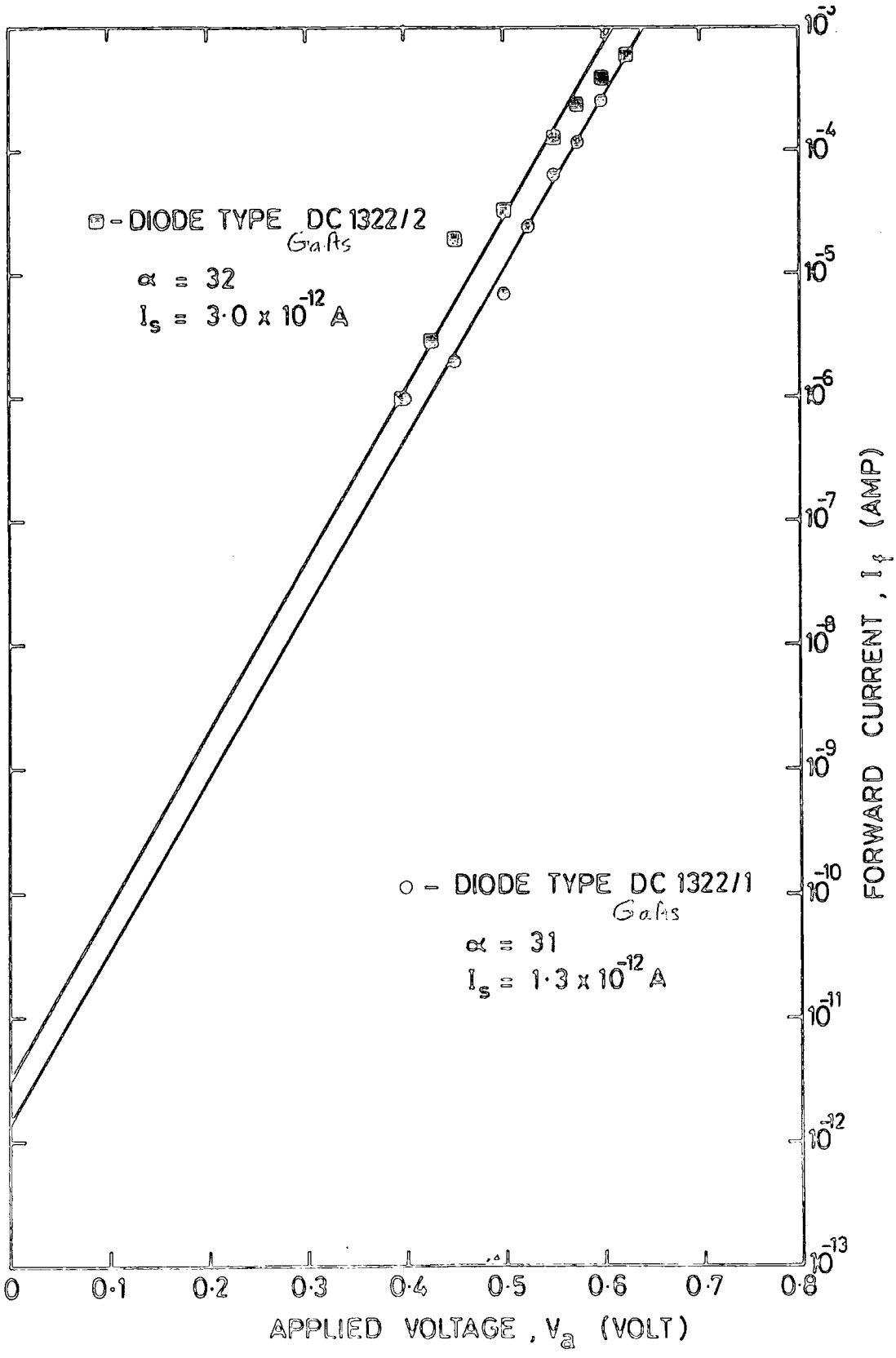

FIG. 6·2·1 DETERMINATION OF α AND I_s

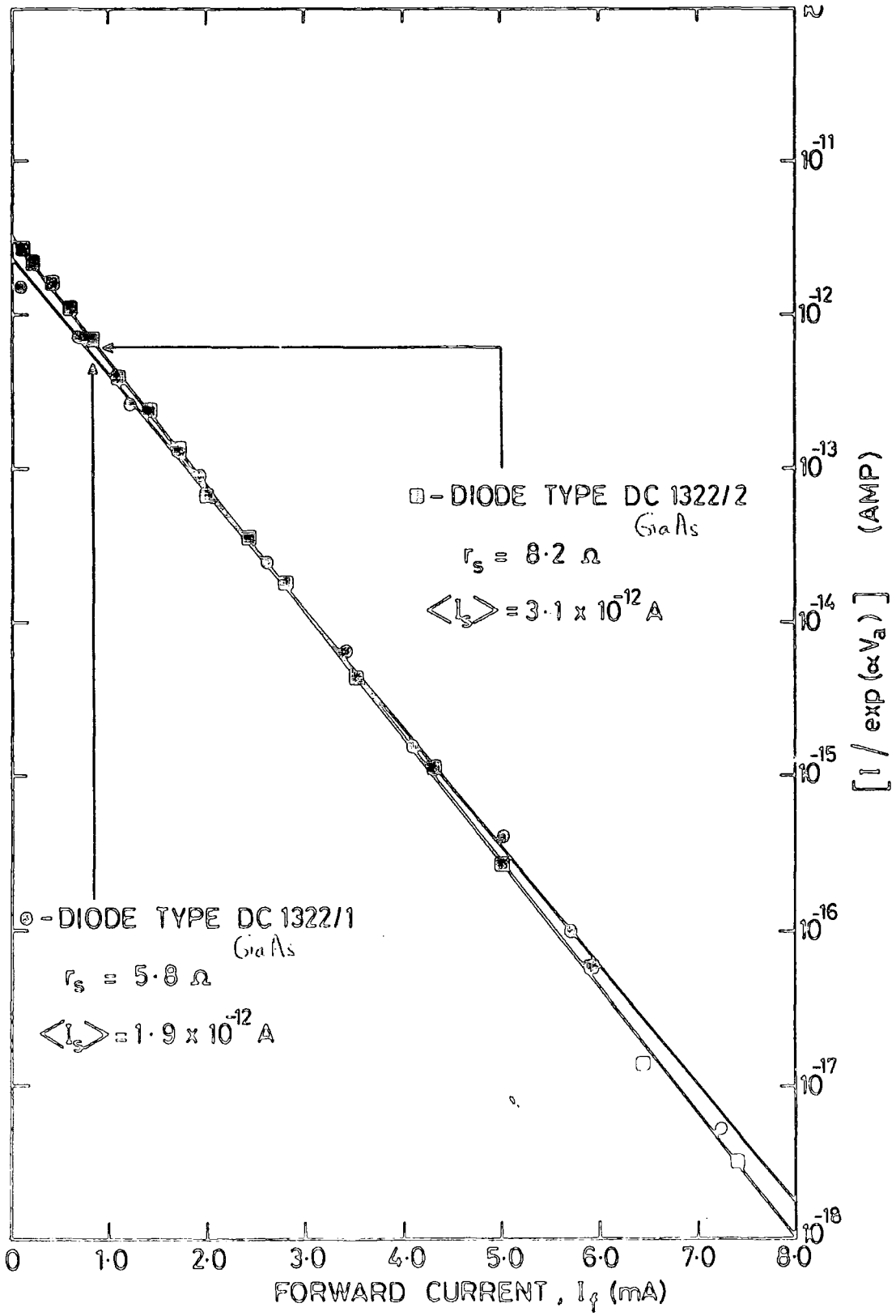

FIG. 6·2·2 DETERMINATION OF r_s AND I_s

parameters given by the manufacturer (on special request) are also included in the table. It was not possible to obtain the parameters of the static characteristics for the germanium backward diode. This may have been due to the fact that they had unacceptable wide variations. In other cases, the measured values of the constant α ($\alpha = \frac{q}{n\ kT}$) were in very good agreement with those supplied by the manufacturer. On examining the measured values of the ideality factor n , those for the silicon Schottky barrier diodes (types DC1504F and DC1515) were about 1.11 and were smaller than those for the gallium arsenide Schottky barrier, silicon point contact and germanium backward diodes. This implied that the I-V characteristics for the silicon diodes were closer to ideal. It is interesting to note that the ideality factor is very close to unity at low dopings and high temperatures. However, it can substantially depart from unity when the doping is increased or the temperature lowered. The value of the ideality factor indicates also the type of mechanism of conduction in devices. In the case of an abrupt p-n junction, when the ideality factor is one, the diffusion current becomes dominant and when the value is two, it is the recombination current that is significant. In general the ideality factor values vary from one to two.

The performance of devices such as rectifiers, mixers and detectors depends greatly on the product of the parasitic components[5,19,36] i.e. series resistance and junction capacitance whose effect should ideally be minimised. There is then a need to minimise the values of this product for the sensitivity property of a diode. From the results in Table 6.1, the series resistance of gallium arsenide Schottky barrier diodes is smaller compared to other diodes, thus may give better detector and mixer performances. The cut-off frequency [19] at zero bias is given by

$$f_{co} = \frac{1}{2\pi r_{so} C_{jo}}$$

(where r_{so} is the series resistance and C_{jo} is the junction capacitance at zero bias). This again shows that the gallium arsenide Schottky barrier diodes will have higher cut-off frequency potential if the junction capacitances of the diodes are of the same order of magnitude. Further, the diode noise temperature ratio depends also on the series resistance.

In the case of the saturation current, no comparison can be made between the measured values and those supplied by the manufacturer because of the differences in the measurement units used. However, in both cases the trends of the values were agreeable. Comparing the values of the saturation current for different diodes, the gallium arsenide Schottky barrier type has the lowest which for the two diodes were 1.9×10^{-12} and 3.1×10^{-12} amperes. The values of the saturation currents for other diodes were, of the order of 1.0×10^{-10} ampere for the silicon Schottky barrier, 1.0×10^{-6} ampere for the silicon point contact and 1.0×10^{-4} ampere for the germanium backward. These results are consistent with the fact that lower saturation is due to larger energy band gap for the semiconductor. For a Schottky barrier diode the saturation current is given by,

$$I_s = aA^* T^2 \exp\left(\frac{-q\, V_B}{kT}\right)$$

where a is the diode area ; A* is the Richardson's constant and V_B is the barrier height. As the saturation current is due mainly to the thermally generated carriers, it has a strong dependence on temperature. So as the saturation current for gallium arsenide Schottky barrier diodes are smaller than those of the silicon type, the former may operate better at high temperatures than that of the latter.

It is hoped that in very many applications that the diodes normally behave as varistors, i.e. pure current dependent resistance. Consequently,

capacitance and the series loss resistance of the p-n junction are the parasitic components. The values of the capacitances measured are given in Table 6.1. The total capacitance for most of the diodes given by the manufacturer was of the order of 0.30 pF. The capacitance measured for the silicon Schottky barrier diode was close to that given by the manufacturer, while that for the gallium arsenide Schottky barrier, the value was 0.60pF (this was twice that given by the manufacturer). However, for the silicon point contact diodes, the values obtained were, 2.00, 1.60, 1.40 and 1.60pF.

6.3 HARMONIC SPECTRA

In presenting the results of the harmonic measurements, the widely employed method of the harmonic discrete spectra[1,2,37] was first considered. Such spectra (amplitude and phase) for the gallium arsenide Schottky barrier diodes a specific fundamental frequency drive level is shown in Figs 6.3.1 and 6.3.2. Each is the 'fingerprint' of the devices at a particular drive level. Unfortunately, this type of representation does not appear to be useful as the number of measurements that may be displayed is limited.

In order to overcome the need for a large number of plots, an alternative method, the continuous amplitude and phase representation of harmonics against the drive level, was introduced. This was done by incorporating the harmonic discrete spectra of a diode at all the drive levels into continuous plots. Each complete display contains therefore the 'fingerprint' at every energised level which can be extracted at will. In addition, the dynamic behaviour of the devices may be compared for different levels at particular harmonics. This was especially suitable because the different types of diodes were tested in pairs.

One of the biggest limitations on the experimental side was lack of sensitivity in the instrument used. Consequently, the sixth and higher harmonics could not be measured. Although the obtained 'fingerprint' of

Diode	$\alpha(V^{-1})$		n		r_s ohm		I_s		C_{total} (pF)	
	measured	manu-facturer	measured	manu-facturer	measured	manu-facturer	measured (amp)	manu-facturer (A/cm^2)	measured	manu-facturer
GaAs Schottky barrier										
DC 1322(1)	32 ± 1	34.8	1.25±0.04	1.15	6 ± 1	6	1.9×10^{-12}	5×10^{-7}	0.30±0.02	0.15
DC 1322(2)	32 ± 1		1.25±0.04		8 ± 1		3.1×10^{-12}		0.31±0.02	
Si Schottky barrier										
DC 1504F(1)	36 ± 1	36.4	1.11±0.03	1.1	34 ± 1	15	9.0×10^{-10}	10^{-4}	1.00±0.02	0.33
DC 1504F(2)	37 ± 1		1.08±0.03		32 ± 1		1.1×10^{-9}		0.36±0.02	
Ge backward										
DC 3021(1)	20 ± 1	-	2.0 ±0.1	-	23 ± 1	-	7.4×10^{-5}	-	-	-
DC 3021(2)	20 ± 1		2.0 ±0.1		10 ± 1		1.0×10^{-4}		-	
Si Schottky barrier										
DC 1515(1)	-	36.4	-	1.1	-	20	-	10^{-4}	-	0.31
DC 151(2)	36 ± 1		1.11±0.03		47 ± 1		8.0×10^{-10}		0.35±0.02	
Si point contact										
CS 12BR(1)	30 ± 1	30.8	1.33±0.04	1.3	12 ± 1	30	2.3×10^{-6}	-	2.00±0.05	0.3
CS 12BR(2)	32 ± 1		1.25±0.04		26 ± 1		1.2×10^{-6}		1.60±0.05	
Si point contact										
CS 9B(1)	29 ± 1	30.8	1.38±0.04	1.3	19 ± 1	30	1.9×10^{-6}	-	1.40±0.05	0.3
CS 9B(2)	32 ± 1		1.25±0.04		12 ± 1		1.6×10^{-6}		1.60±0.05	

TABLE 6.1: The DC Characteristics

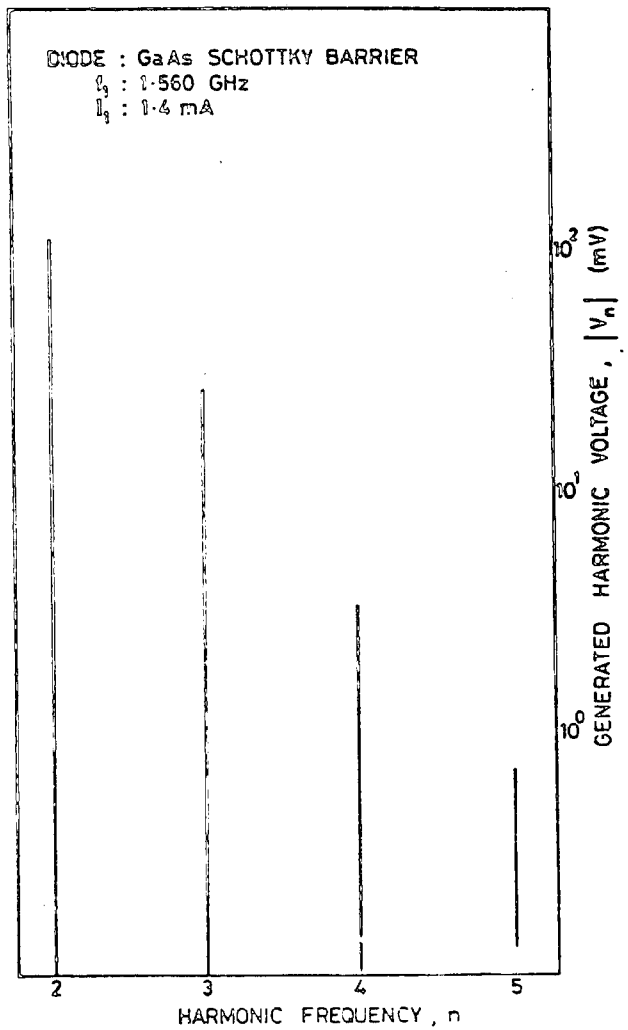

FIG. 6·3·1 AMPLITUDE SPECTRUM

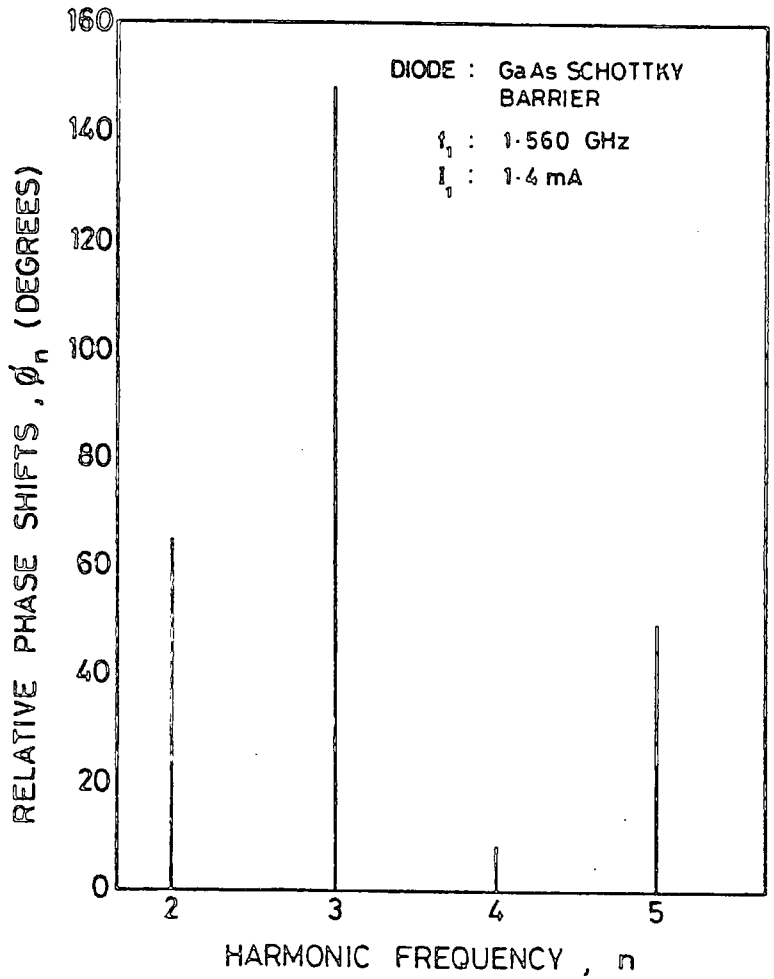

FIG. 6·3·2 PHASE SPECTRUM

the device is still valid, it may not be adequate in some cases.

Presentation of the results on each type of diodes will be made in separate sections (of the Chapter) that follow. Each section comprises two parts and they are the results of measurements at the fundamental frequency of 1.560 GHz and that of 450 MHz. The description of the harmonic spectra and impedances will be made here. However, the explanation and interpretation of different features are to be dealt with in the final Chapter.

6.4 GaAs SCHOTTKY BARRIER DIODE - (X BAND DETECTOR DIODE) - Types DC1322/1 and DC1322/2 - 1.560GHz

Comparing the two amplitude spectra, it can be seen that the second harmonic amplitude for one diode has an unusual drop between 3.5 and 5.0 mA. The pattern for the third, fourth and fifth harmonics appears to be similar for the two devices. It shows that the fourth harmonic is greater than the third above 6.2 mA for one diode and 4.7 mA for the second. There exists also a peak at 1.7 mA for the first diode in Fig 6.4.1(a).

The corresponding phase spectra are shown in Figs 6.4.1(b) and 6.4.2(b). Large variations in phases are observed in all the harmonics for the first diode and that the third and the fifth harmonics for the second diode. On the other hand, the phases for the second and third harmonics of the first diode (for levels above 3.5mA) and that for the second and fourth harmonics of the second diode have relatively small changes. There is a phase discontinuity for the fourth harmonic at 2.5 mA.

The impedance (at different harmonics) plots are given in Figs 6.4.1(c) and 6.4.2(c). The values of the impedance at the second, third and the fourth harmonics of the second diode fall with an increase in the drive level. Similar trends occur for the second, third and the fifth harmonics at levels above 3.5 mA for the first diode. However, the impedance

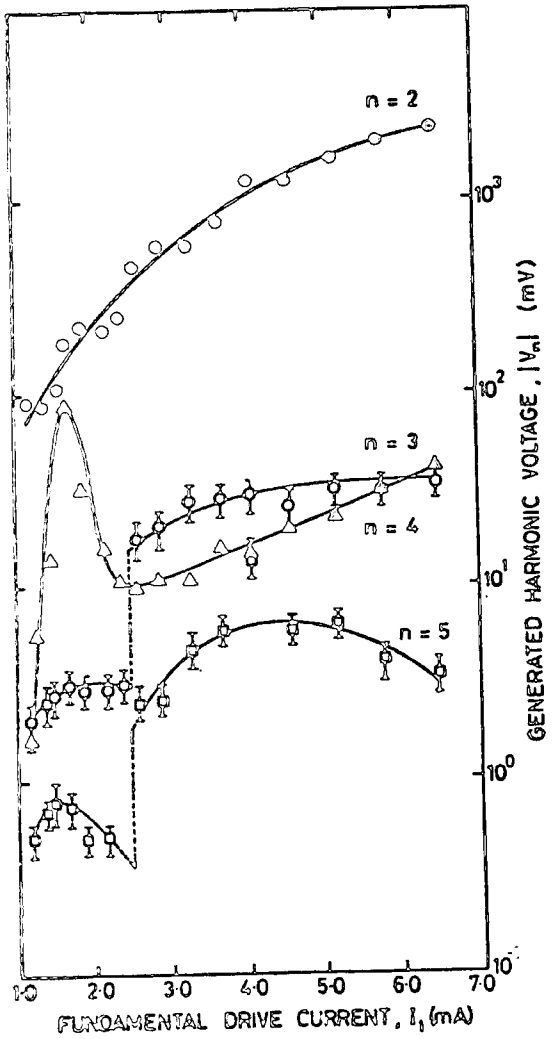

(a) AMPLITUDE

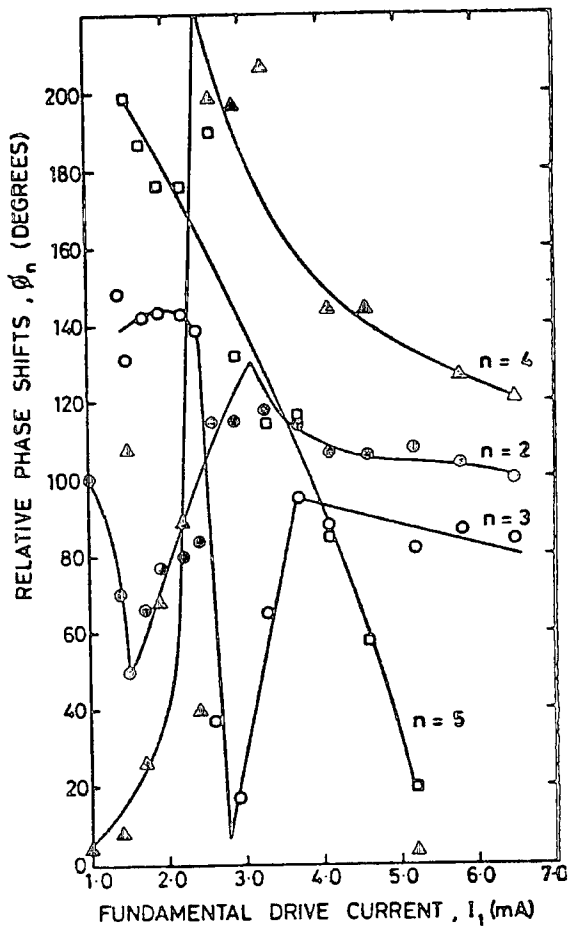

(b) PHASE

Fig 6.4.1: HARMONIC SPECTRA - f_1 = 1.560 GHz

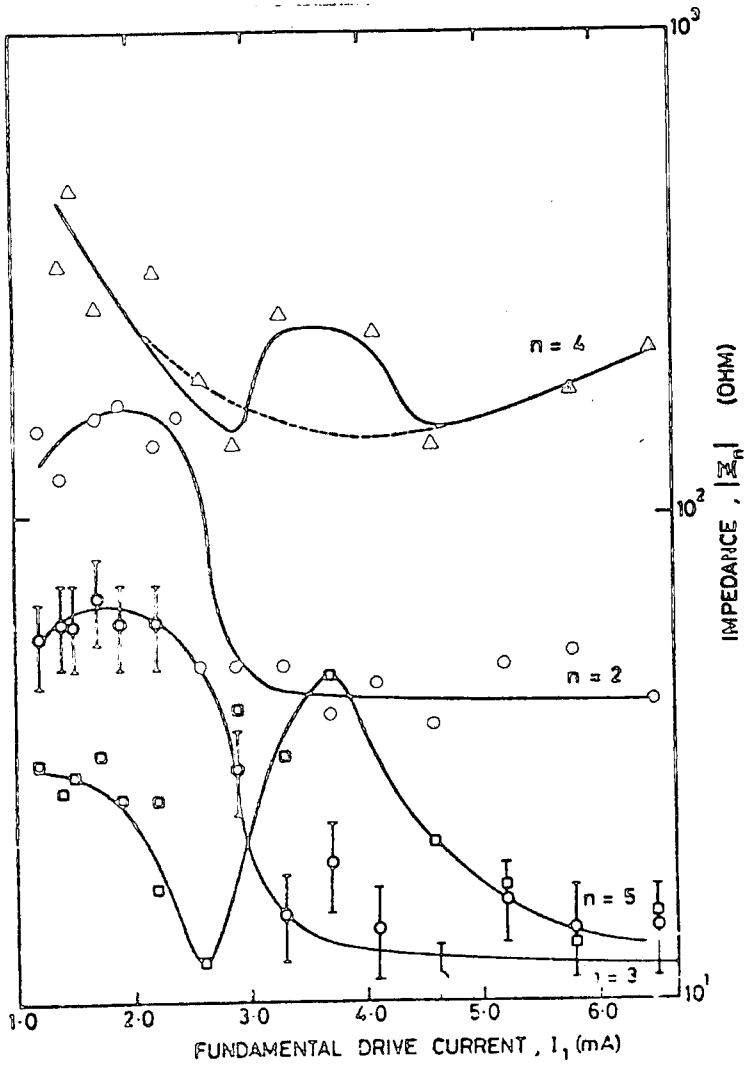

(c) IMPEDANCE

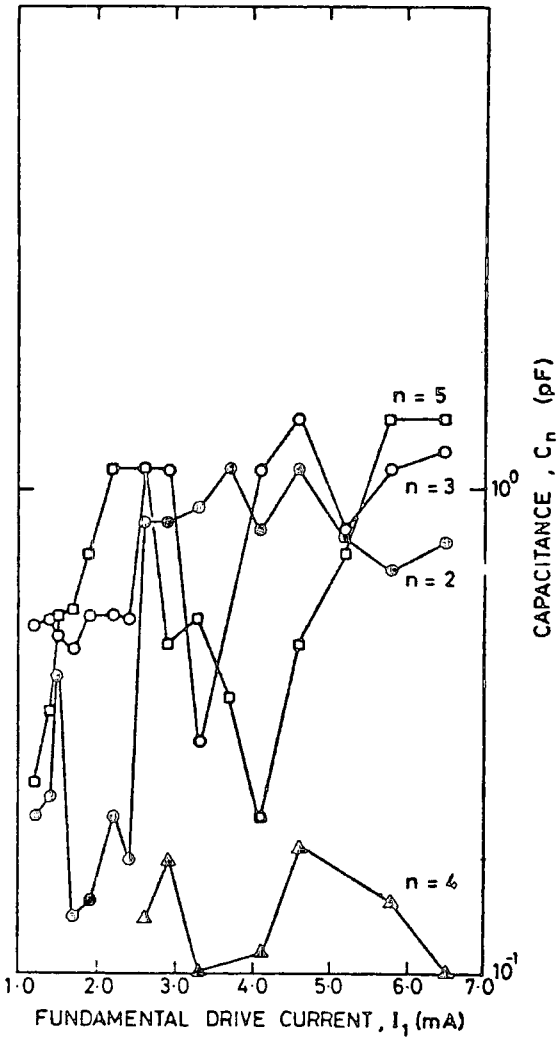

(d) CAPACITANCE

Fig 6.4.1: HARMONIC IMPEDANCE f_1 = 1.560 GHz

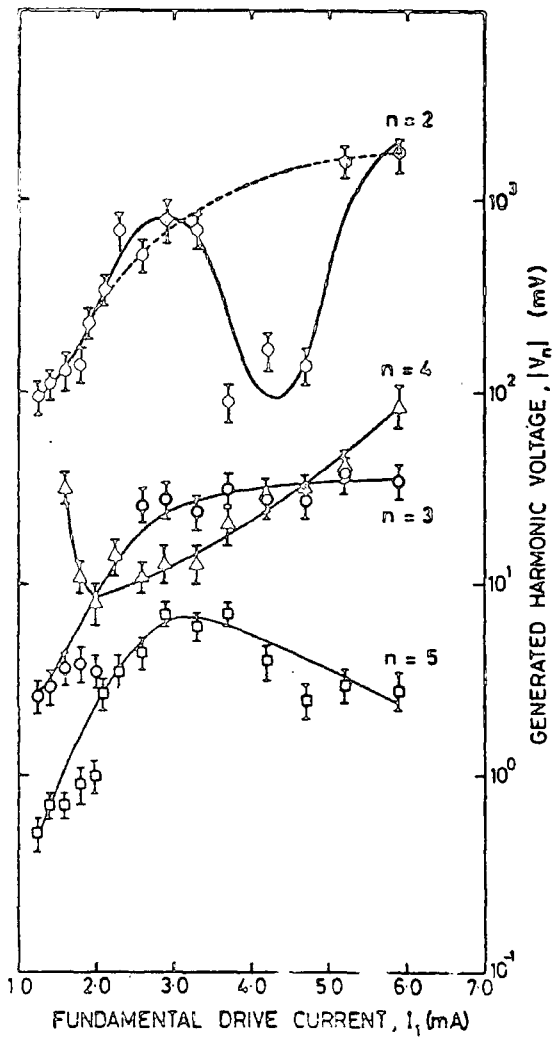

(a) AMPLITUDE

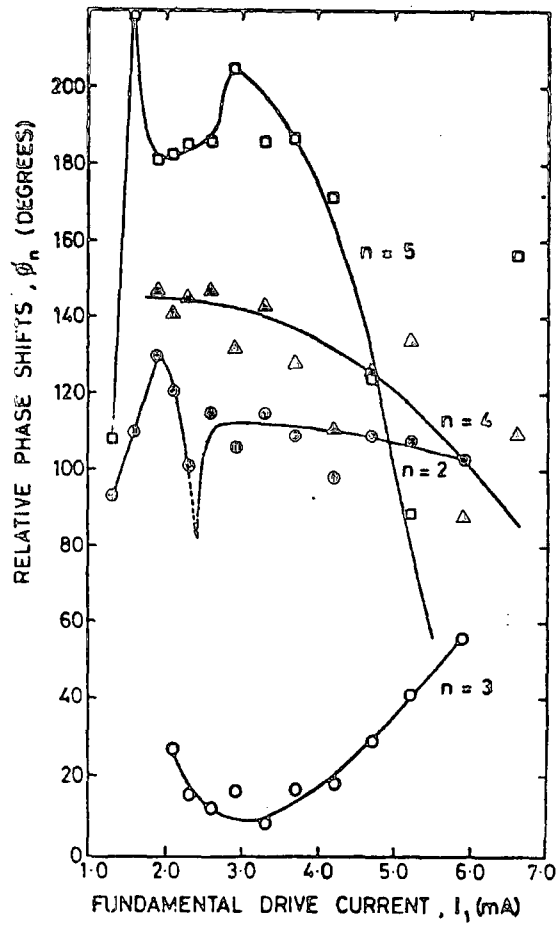

(b) PHASE

Fig. 6.4.2: HARMONIC SPECTRA - f_1 = 1.560 GHz

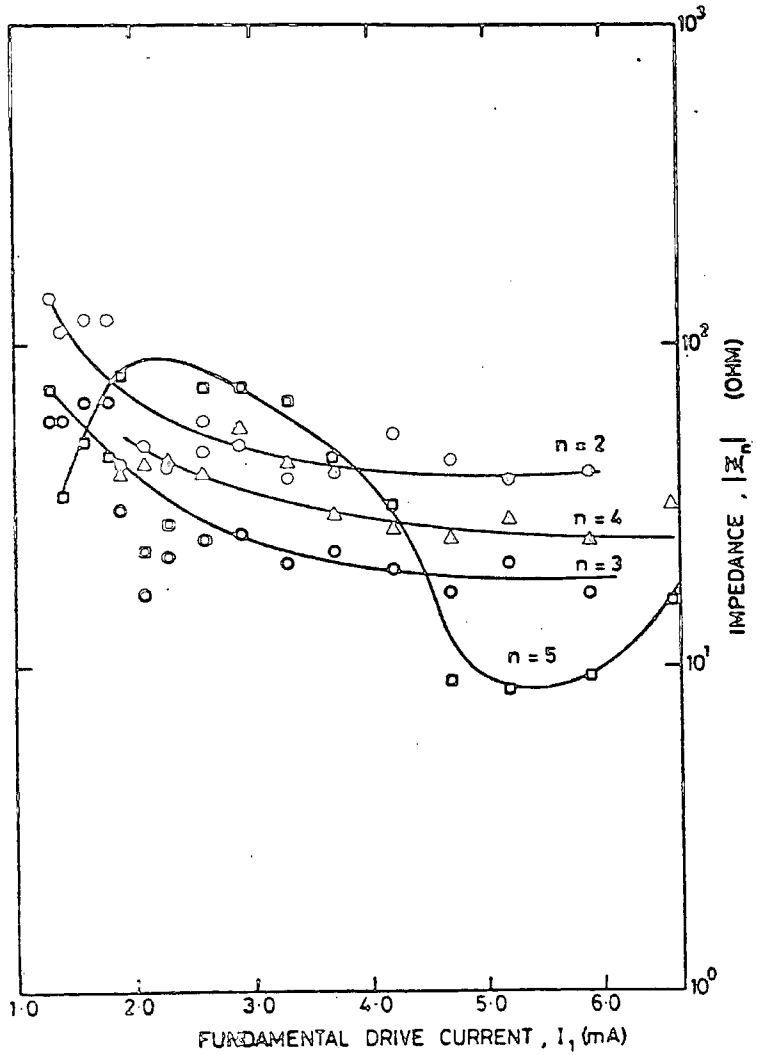

(c) IMPEDANCE

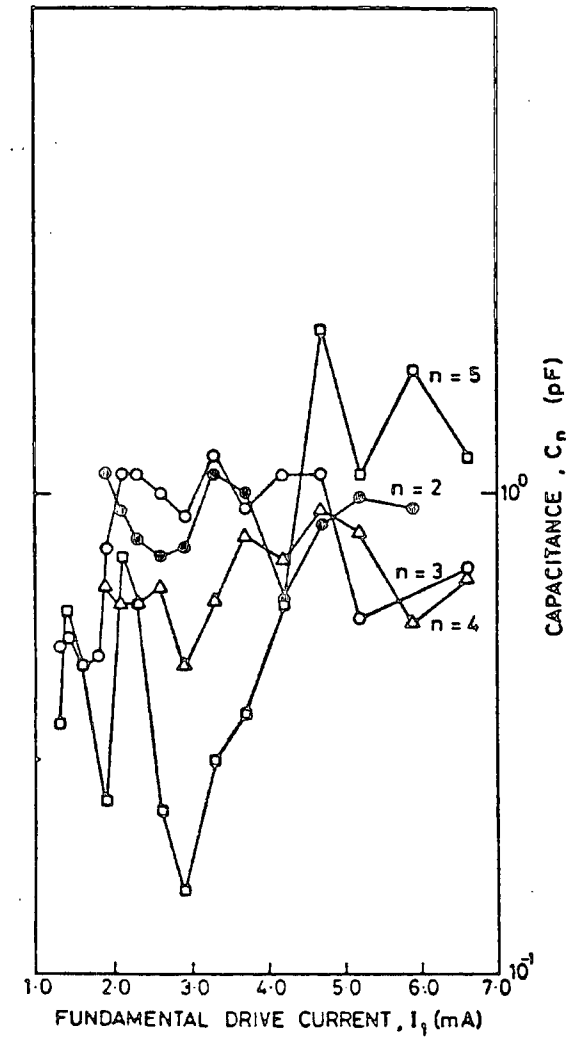

(d) CAPACITANCE

Fig 6.4.2: HARMONIC IMPEDANCE - f_1 = 1.560 GHz

curves at the fifth harmonic for both diodes show large variations.

The plots for the capacitance at the harmonics are shown in Figs 6.4.1(d) and 6.4.2(d). There were less variations in values for the second diode than that for the first. It is apparent in Fig 6.4.2(d) that the average value of the capacitance for all the harmonics lay between 0.6 and 1.0 pF.

There was a trend shown by the first diode to increase the second and fourth harmonic amplitudes with the increase in drive (Fig 6.4.1(a)) and at the same time there was a corresponding decrease in the phases (Fig 6.4.1(b)). Similar behaviour is observed for the fourth harmonic of the second diode. However, the fifth harmonic amplitudes which are generally of low levels (of the second diode) decrease, while that for the corresponding phases increase, with the drive. There exists an inflexion point for each of the impedance curves of the second and third harmonics of the first diode and that of the fifth harmonic for the second diode. At this point there is a corresponding discontinuity in the phases. At a particular drive level, a nonlinear curve between phase and harmonic number is generally obtained. The relative variations in phase and capacitance correspond with those of the impedance. This may be noted in the case of the second harmonic for the first diode (Figs 6.4.1(b), 6.4.1(c) and 6.4.1(d)) where small changes in the impedance contribute towards the similarly small variations in phases and capacitances. All occur at relatively high harmonic amplitudes except in the case of the fifth harmonic.

450 MHz

The amplitude spectra for the pair of diodes are given in Figs 6.4.3(a) and 6.4.4(a). The amplitudes for the second harmonic of both diodes increase with the increase in drive. However, the fourth harmonic amplitude (for the first diode) appears to have a peak and a dip. The third harmonic amplitude for the second diode remains constant when the drive is increased.

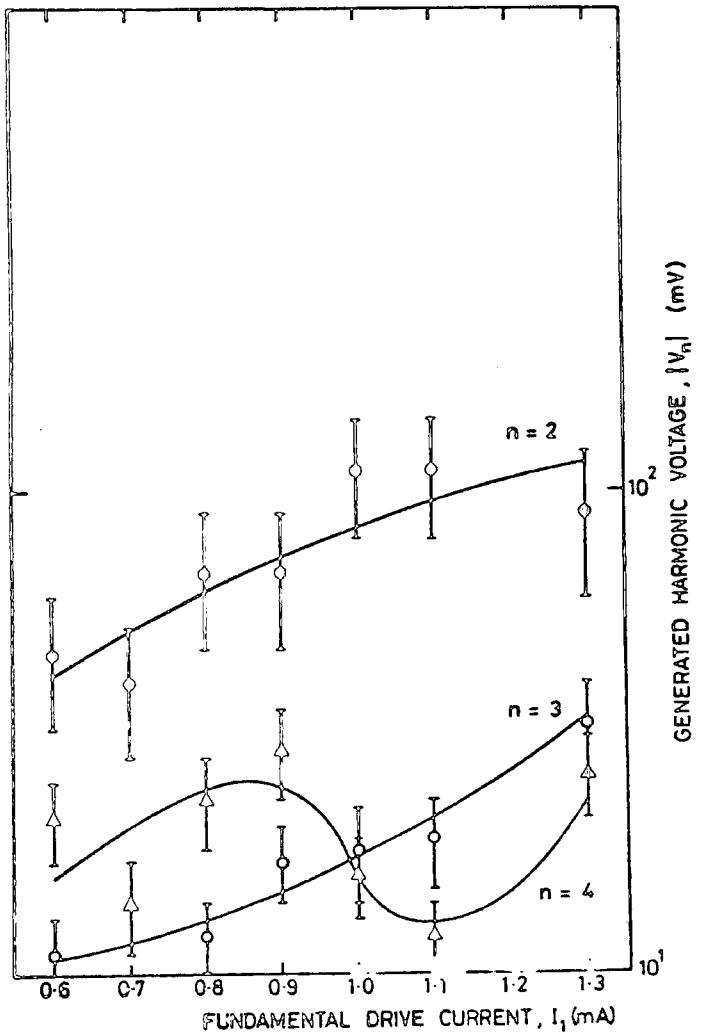

(a) AMPLITUDE

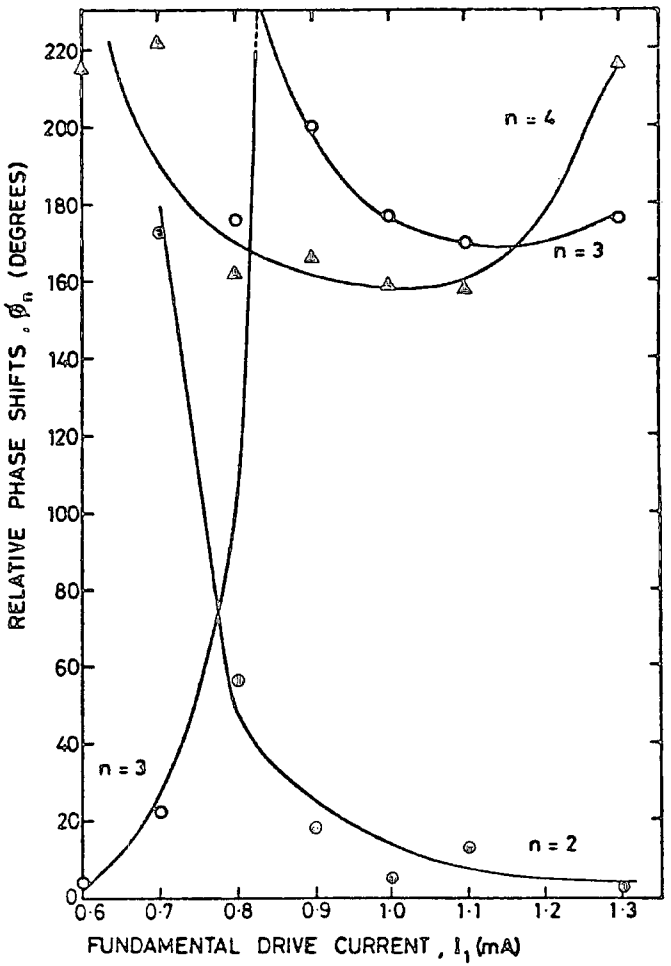

(b) PHASE

Fig 6.4.3: HARMONIC SPECTRA - f_1 = 450 MHz

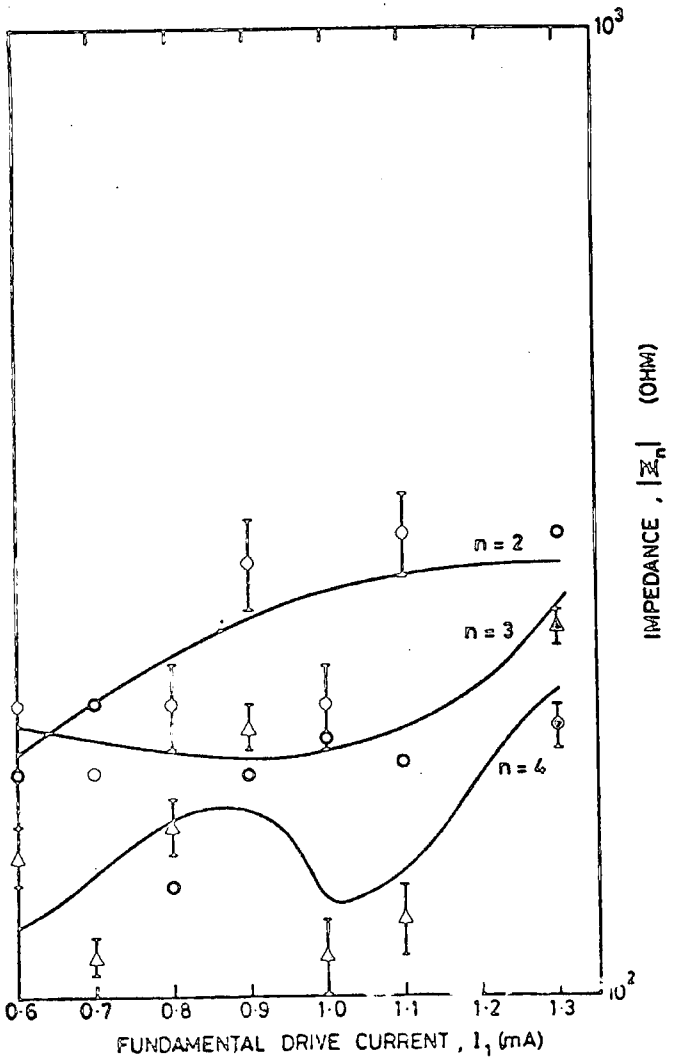

(c) IMPEDANCE

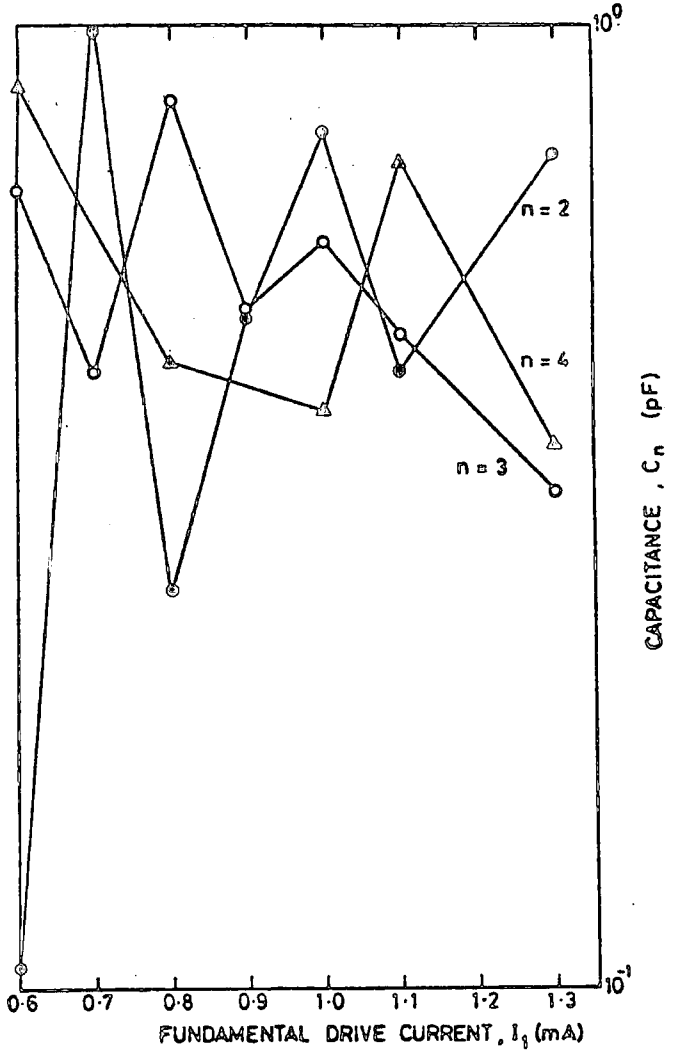

(d) CAPACITANCE

Fig 6.4.3: HARMONIC IMPEDANCE - f_1 = 450 MHz

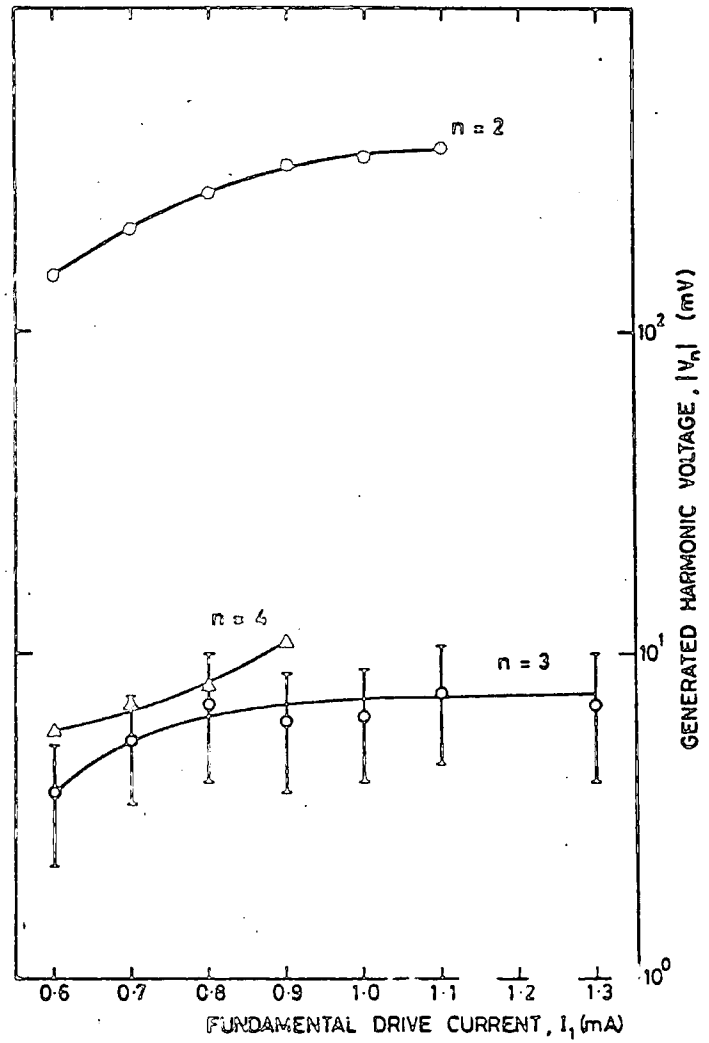

(a) AMPLITUDE

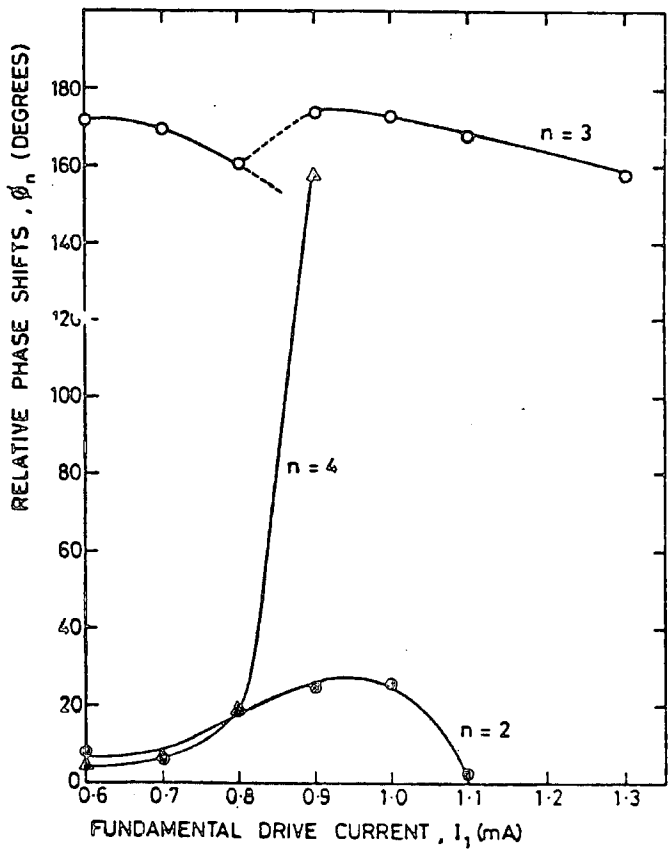

(b) PHASE

Fig 6.4.4: HARMONIC SPECTRA - f_1 = 450 MHz

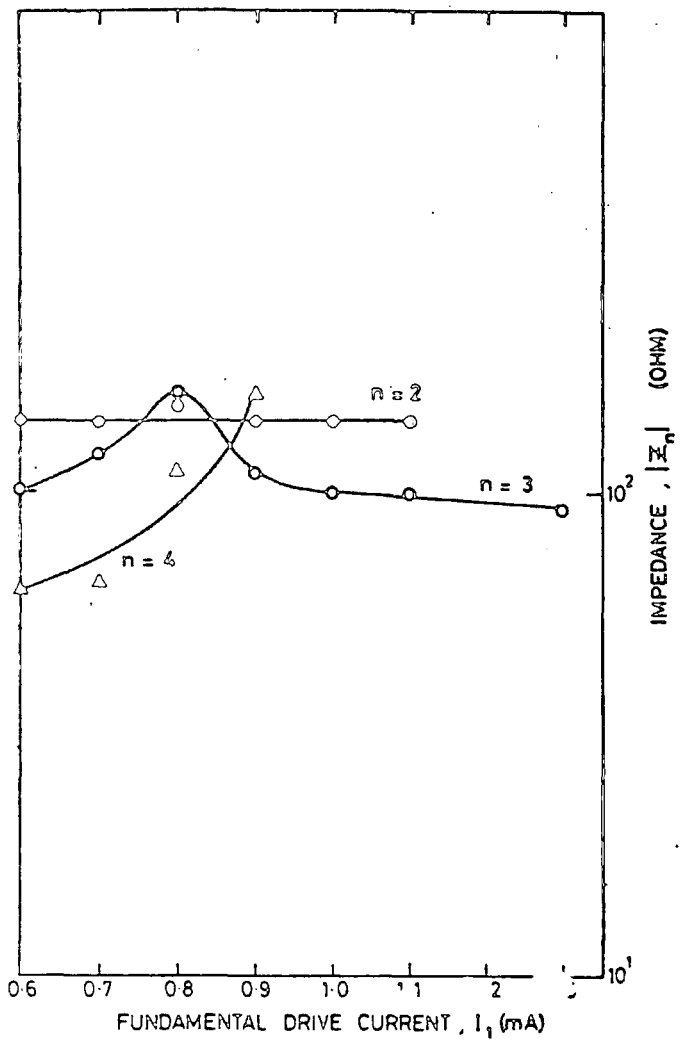

(c) IMPEDANCE

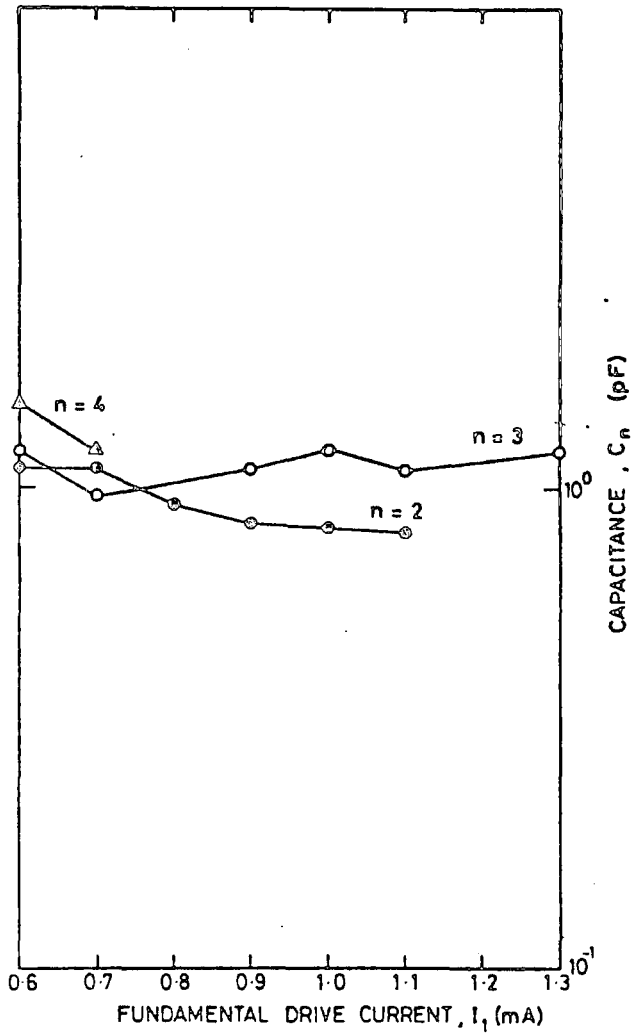

(d) CAPACITANCE

Fig 6.4.4: HARMONIC IMPEDANCE - f_1 = 450 MHz

The phase spectra for the diodes are given in Figs. 6.4.3(b) and 6.4.4(b). The second harmonic phases for the first diode seem to decrease with the increase in the drive level. There are small variations in phases for the second and third harmonics of the second diode. On the other hand, all the other harmonics for both the diodes had big variations in values.

The impedance (at different harmonics) plots are given in Figs. 6.4.3(c) and 6.4.4(c). The values of the impedance at the second harmonic for the first diode seem to increase with the increase in the drive while those for the second diode remain constant. As for the third harmonic the impedance for the first diode tends to increase with drive, however, the reverse is true for the second diode.

Comparing the capacitance plots in Figs 6.4.3(b) and 6.4.4(b), the variations in the values were the same. The average value of the capacitance for the first diode was 0.6 pF and that for the second was 1.0 pF.

In the case of the first diode, the second harmonic phase decreases and the second harmonic voltage, of relatively high value, increases with the increase in the drive. Large changes in the third and fourth harmonic phases correspond to similar variations in the impedance while the harmonic generator voltage is relatively low. The impedance at the second harmonic for the second diode (Fig. 6.4.4(c)) has a constant value over almost a complete range of levels which is also reflected in small variations in the values of the phases and capacitances. In addition, the corresponding harmonic generator voltage, of relatively high value, increases with increase in drive.

6.5 Si SCHOTTKY BARRIER DIODE - (X BAND MIXER DIODE)

(Types DC1504F/1 and DC1504F/2. - 1.560GHz

The behaviour and the order of magnitude of the harmonic amplitudes (Figs 6.5.1(a) and 6.5.2(a)) for both diodes are almost identical except those of the fourth. Generally, the open circuit voltages increase with those of the drive levels. The fourth harmonic amplitudes are higher than those of the third in the case of the first diode. The fifth harmonic amplitudes for both diodes have little variations in values within the given drive range in addition to having low peaks.

The fourth and fifth harmonic phases decrease more with the increae in level, compared against those of the second and third, for the first diode (Figs 6.5.1(b) and 6.5.2(b)). The behaviour of the third and fifth harmonic phases for both diodes is similar. Furthermore, the value of the third harmonic phases are almost constant.

The behaviour of the impedance at the third harmonic for both diodes are almost similar with magnitudes fairly constant (Figs 6.5.1(c) and 6.5.2(c)). There are peaks for the impedance curve for the fifth harmonic at 1.6 mA for the first diode and that of the second harmonic at 1.5 mA for the second diode.

The capacitance at the third harmonic for both diodes is almost constant and of similar values (Figs 6.5.1(d) and 6.5.2(d)). However, the second, fourth and the fifth harmonics of the first diode and those of the fourth and fifth for the second diode have bigger variations in values.

At the drive level corresponding to the peak of the fifth harmonic voltage (for both diodes), there is an inflexion point on the curve of the same harmonic phase. For the first diode, there is a clear case of the

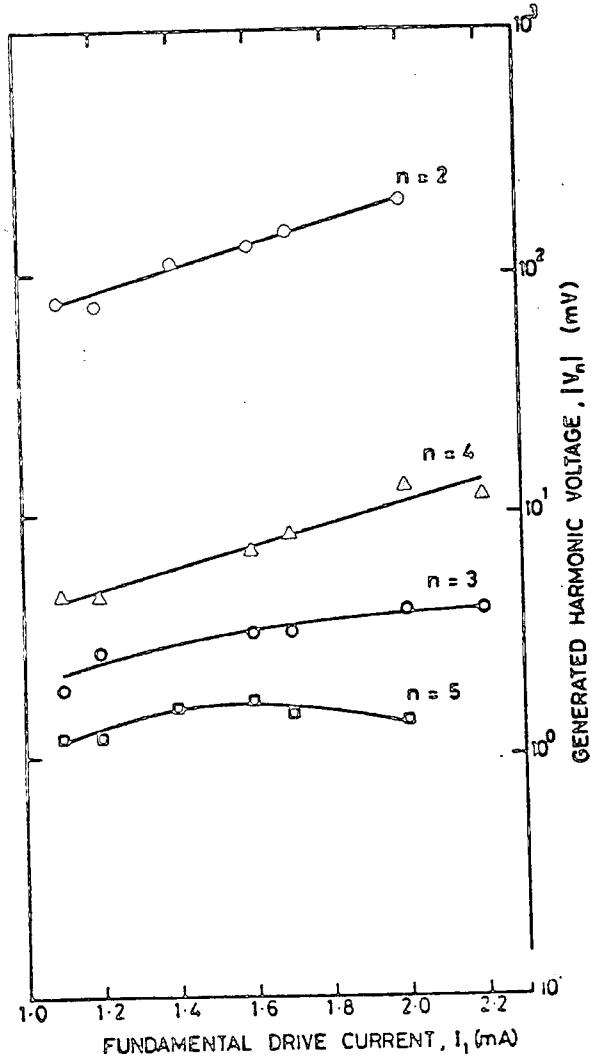

(a) AMPLITUDE

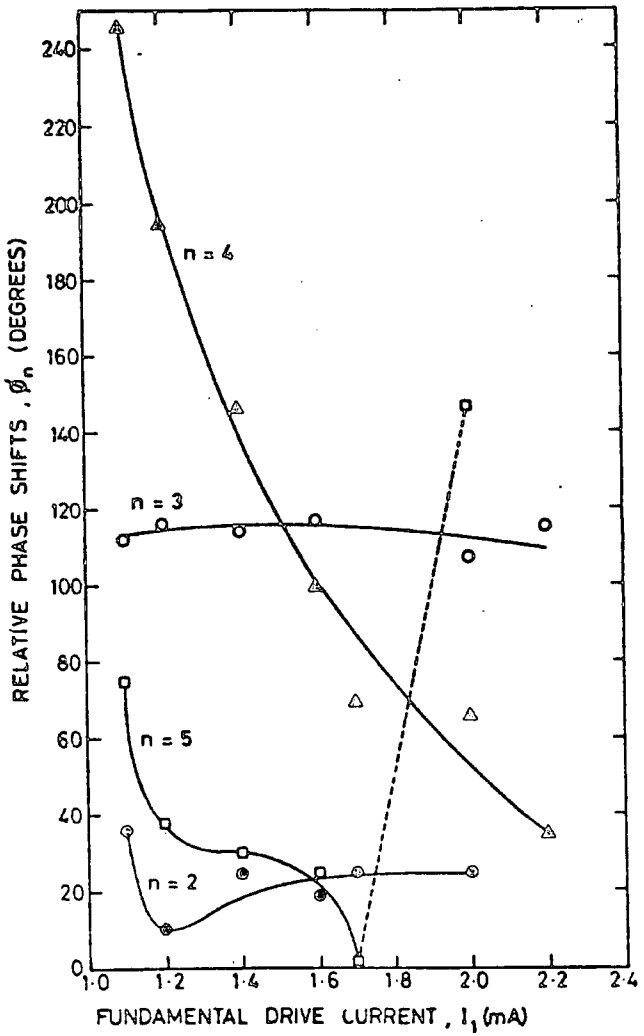

(b) PHASE

Fig 6.5.1: HARMONIC SPECTRA - f_1 = 1.560 GHz

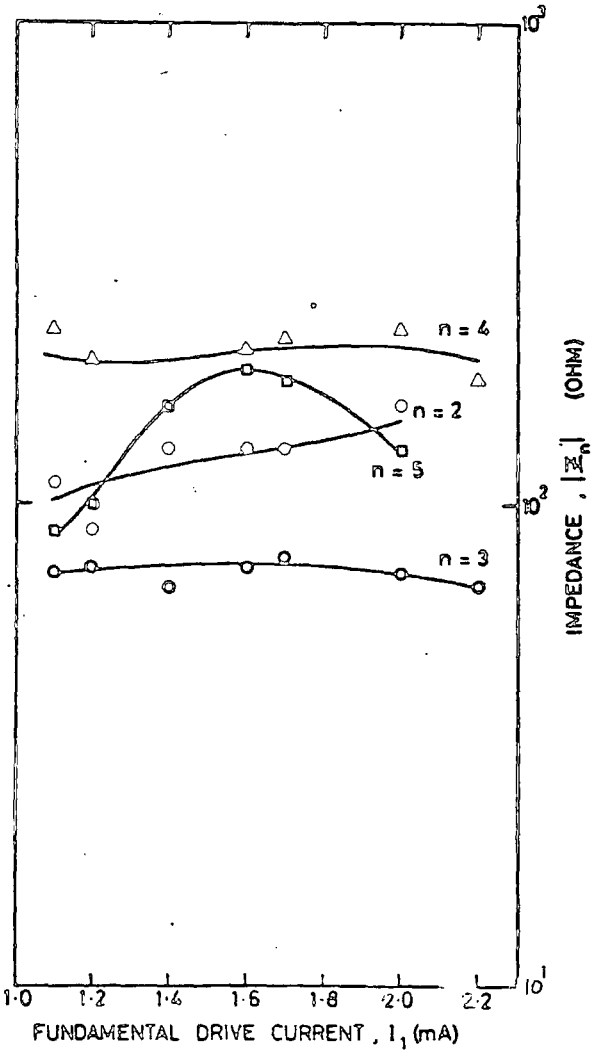

(c) IMPEDANCE

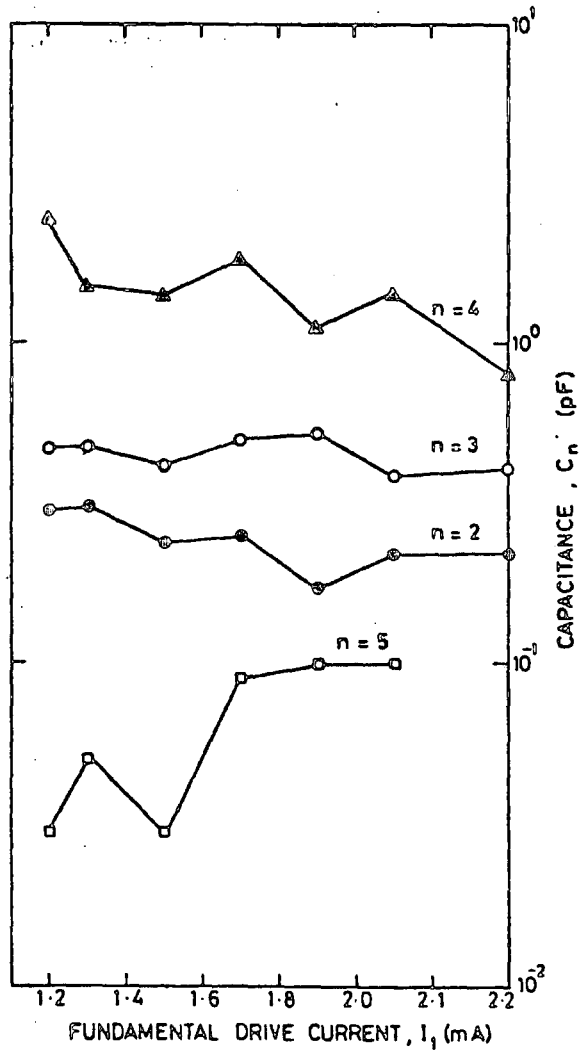

(d) CAPACITANCE

Fig 6.5.1: HARMONIC IMPEDANCE - f_1 = 1.560 GHz

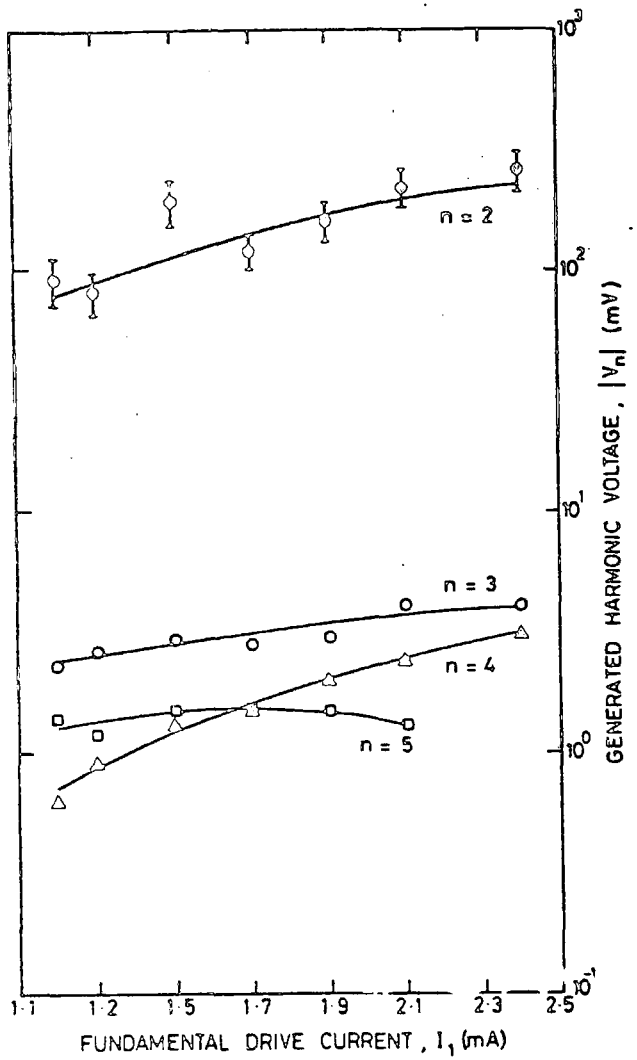

(a) AMPLITUDE

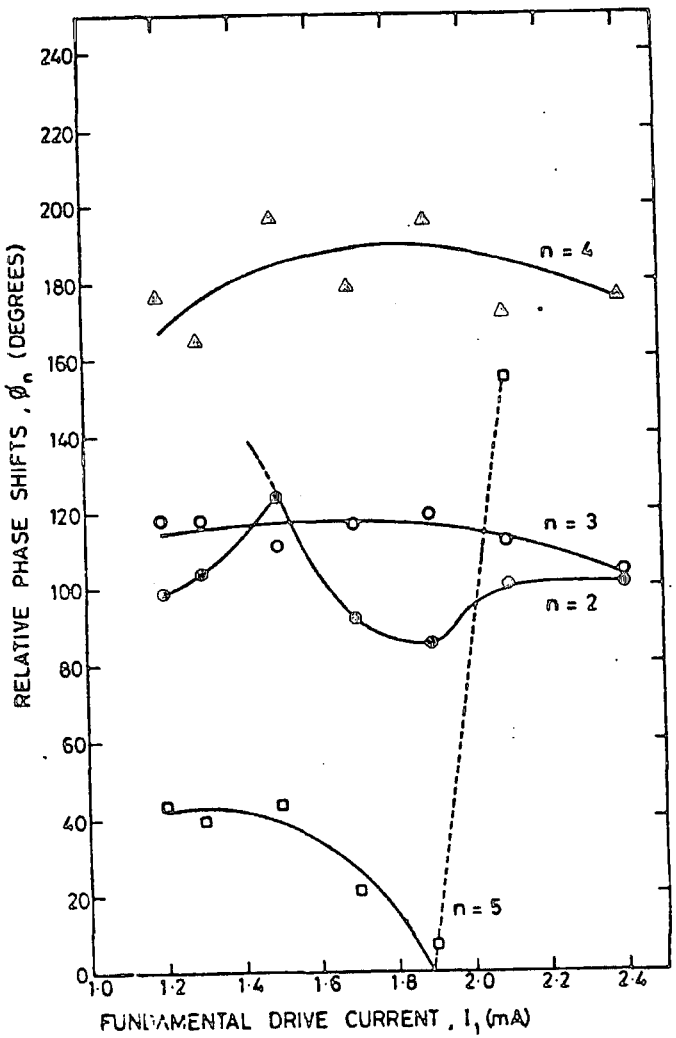

(b) PHASE

Fig 6.5.2: HARMONIC SPECTRA - f_1 = 1.560 GHz

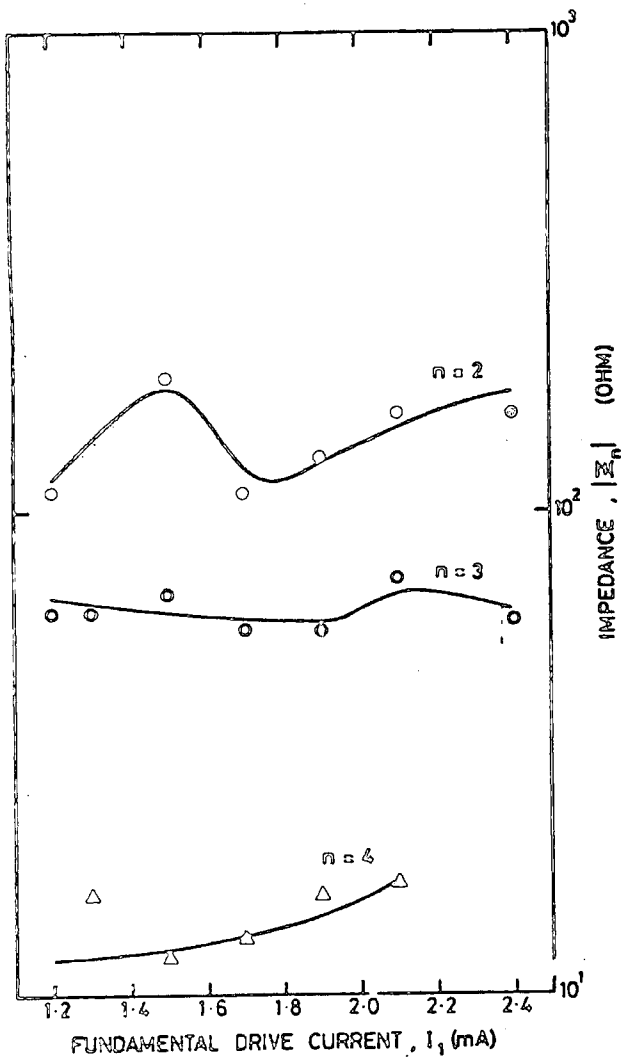

(c) IMPEDANCE

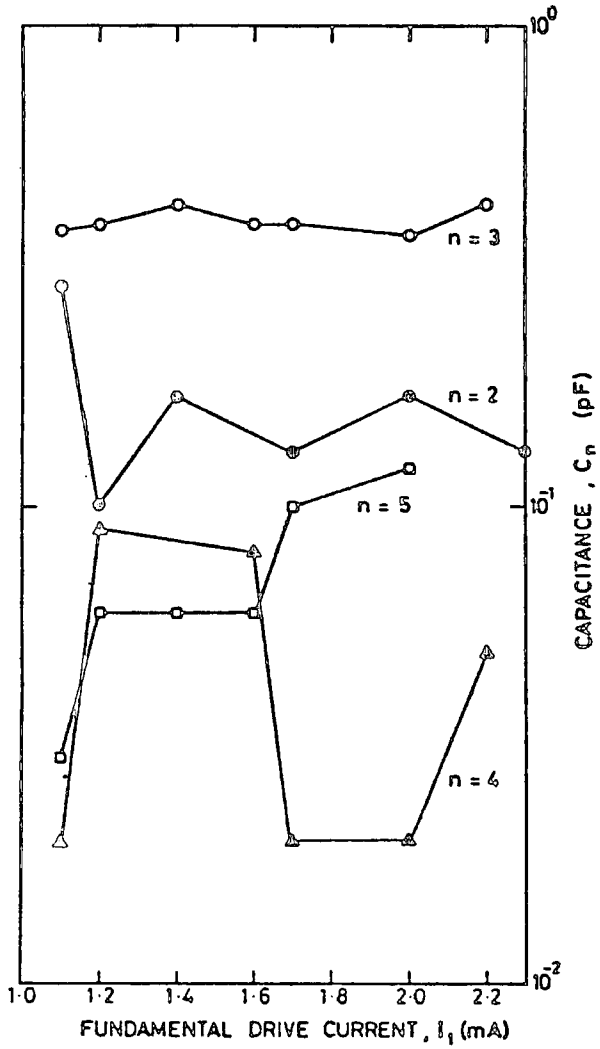

(d) CAPACITANCE

Fig 6.5.2: HARMONIC IMPEDANCE f_1 = 1.560 GHz

decrease in the fourth harmonic phases and an increase in the corresponding amplitude with the increase in the drive level. Another interesting behaviour is that for the third harmonic, values of the amplitude, impedance, phase and the capacitance are fairly constant.

450 MHz

The second and third harmonic voltages of the second diode generally increase with the drive level (Fig 6.5.4(a)). In the case of the first diode, the second harmonic voltage has a peak (Fig 6.5.3(3)) and the curve for the third harmonic is wave-like.

The second harmonic phase of the first diode (Fig 6.5.3(b)) has an abrupt change at 0.9 mA drive. As for the second diode, there are small variations in the values of the second and third harmonic phases (Fig 6.5.4(b)).

The behaviour of the impedance at the second, third and the fourth harmonics of the first diode is wave-like and their values vary substantially (Fig 6.5.3(c)). However, the values of the impedance at the second and third harmonics for the second diode have small variations within the drive level range (Fig 6.5.4(c)).

Similar pattern in the behaviour of the capacitance for the corresponding second and third harmonics for each of the diodes is again observed (Figs 6.5.3(d) and 6.5.4(d)).

There is a distinct difference in the spectral behaviour between the two diodes. In the first diode the harmonic voltages and the impedance at harmonics fluctuate, and consequently showing similar variations for the corresponding phases and capacitances. In contrast to the second diode, there are small variations at each harmonic for the amplitude and impedance and hence the phase and capacitance.

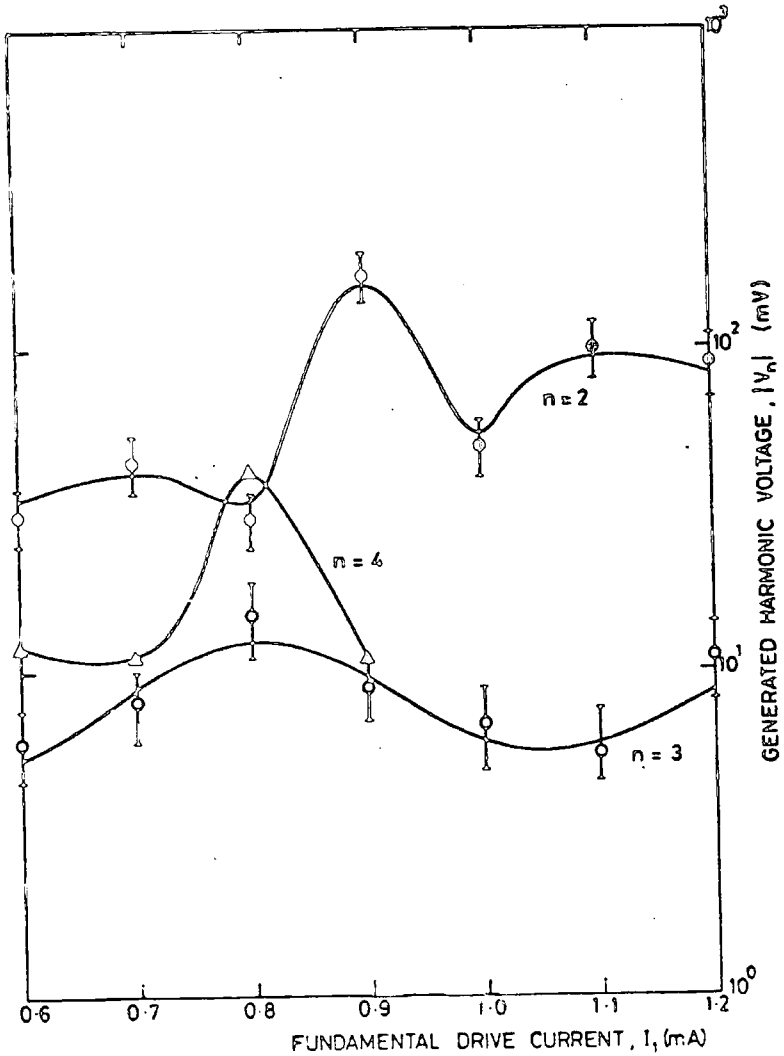

a) AMPLITUDE

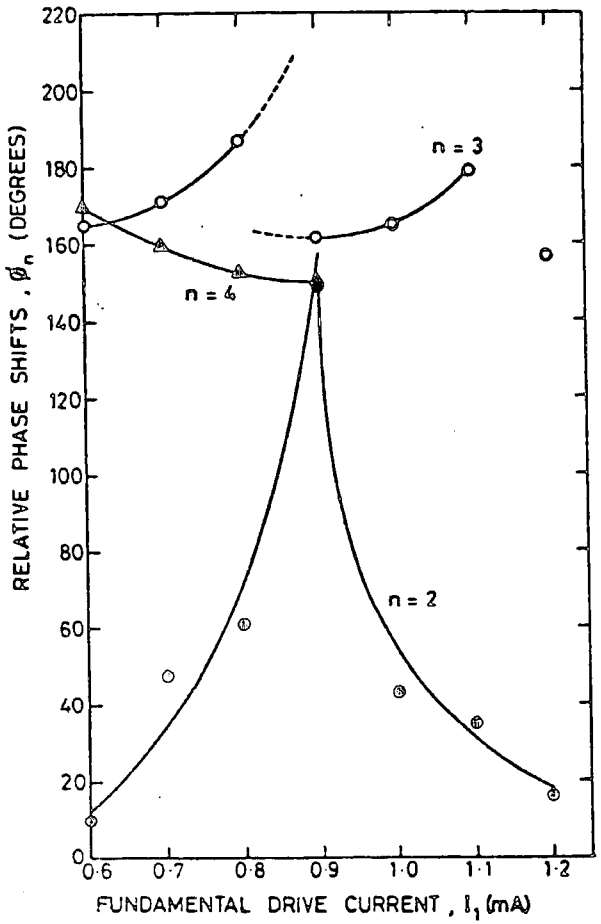

(b) PHASE

Fig 6.5.3: HARMONIC SPECTRA f_1 = 450 MHz

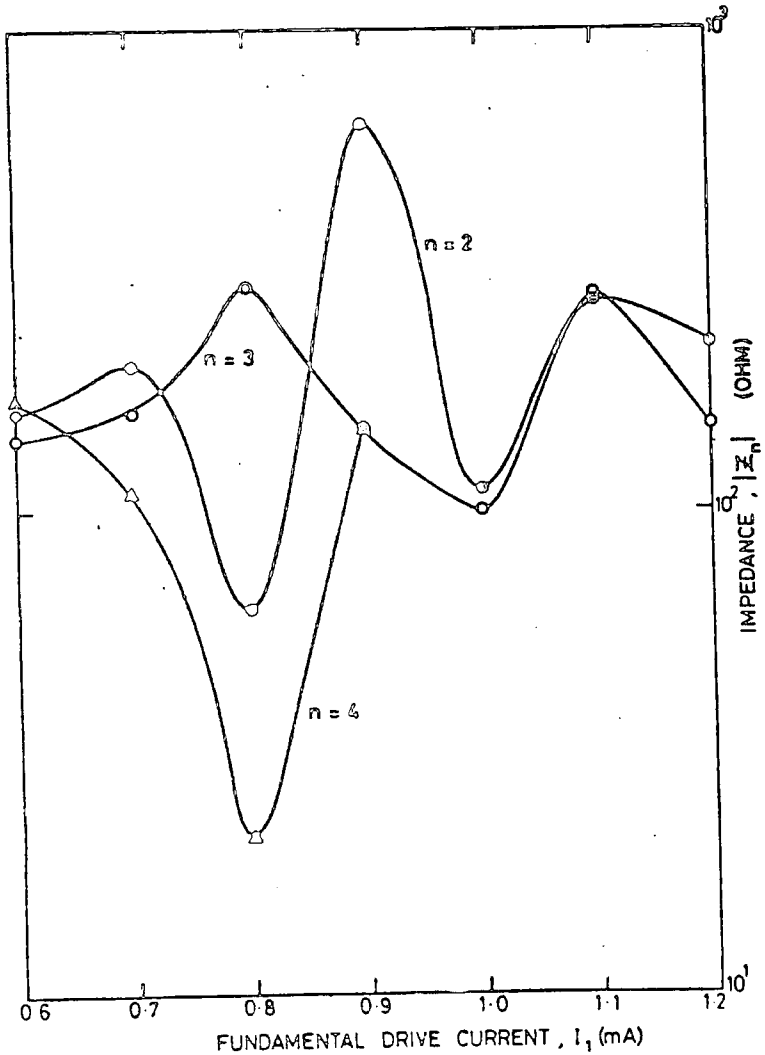

(c) IMPEDANCE

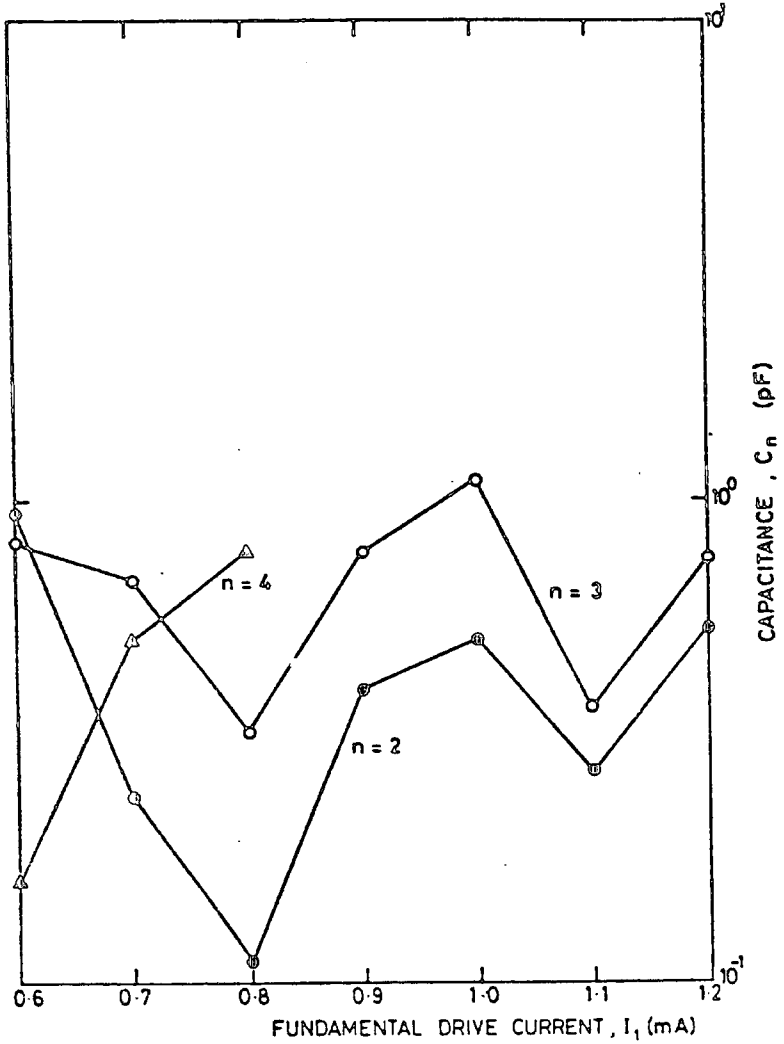

(d) CAPACITANCE

Fig 6.5.3: HARMONIC IMPEDANCE - f_1 = 450 MHz

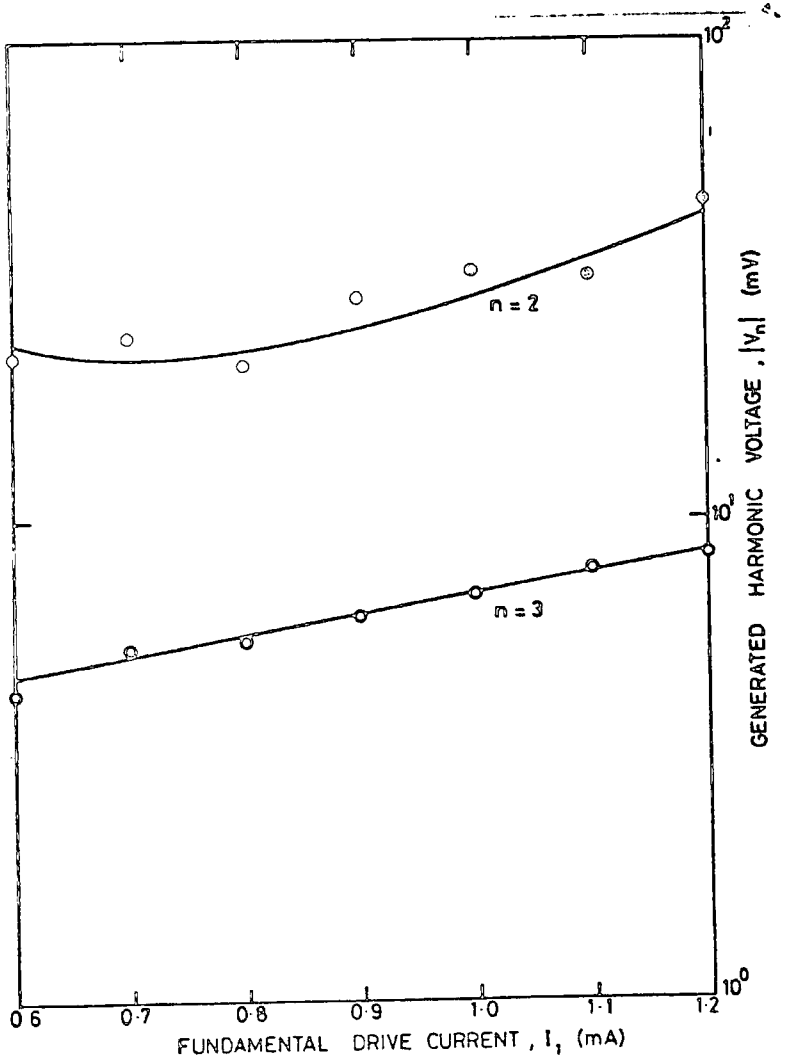

(a) AMPLITUDE

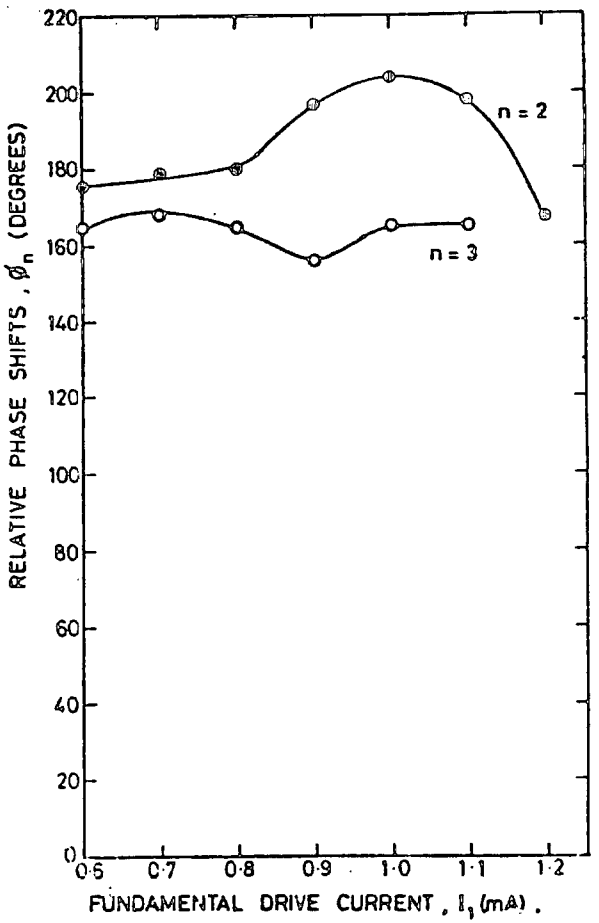

(b) PHASE

Fig 6.5.4: HARMONIC SPECTRA f_1 = 450 MHz

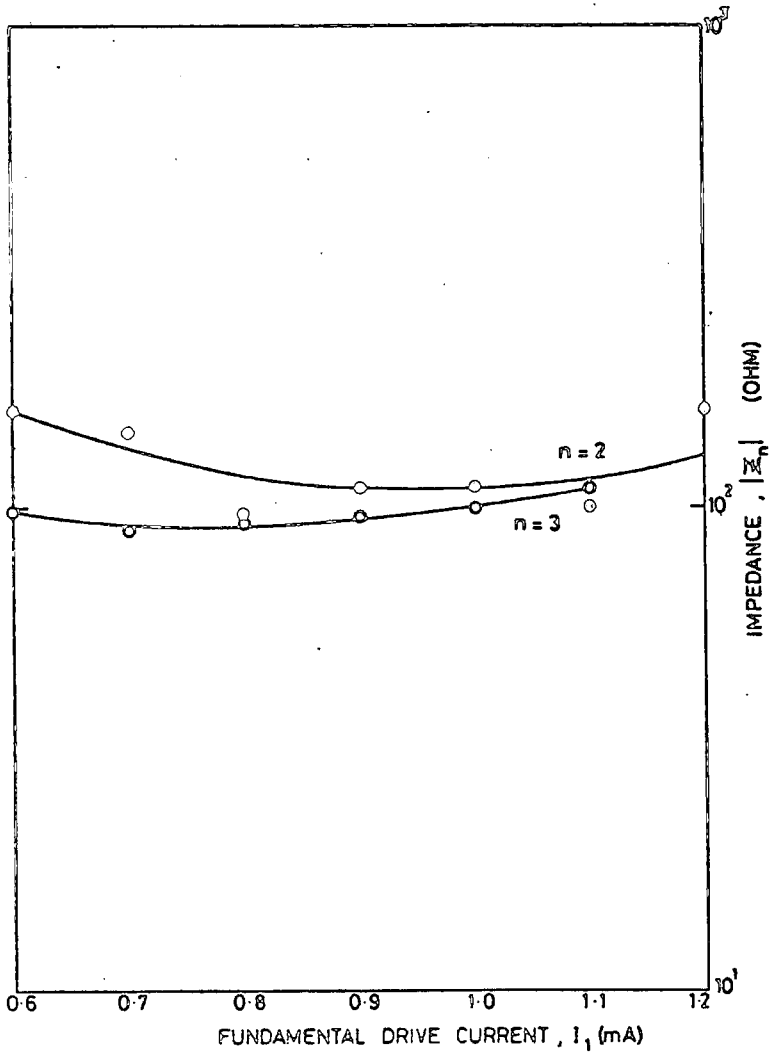

(c) IMPEDANCE

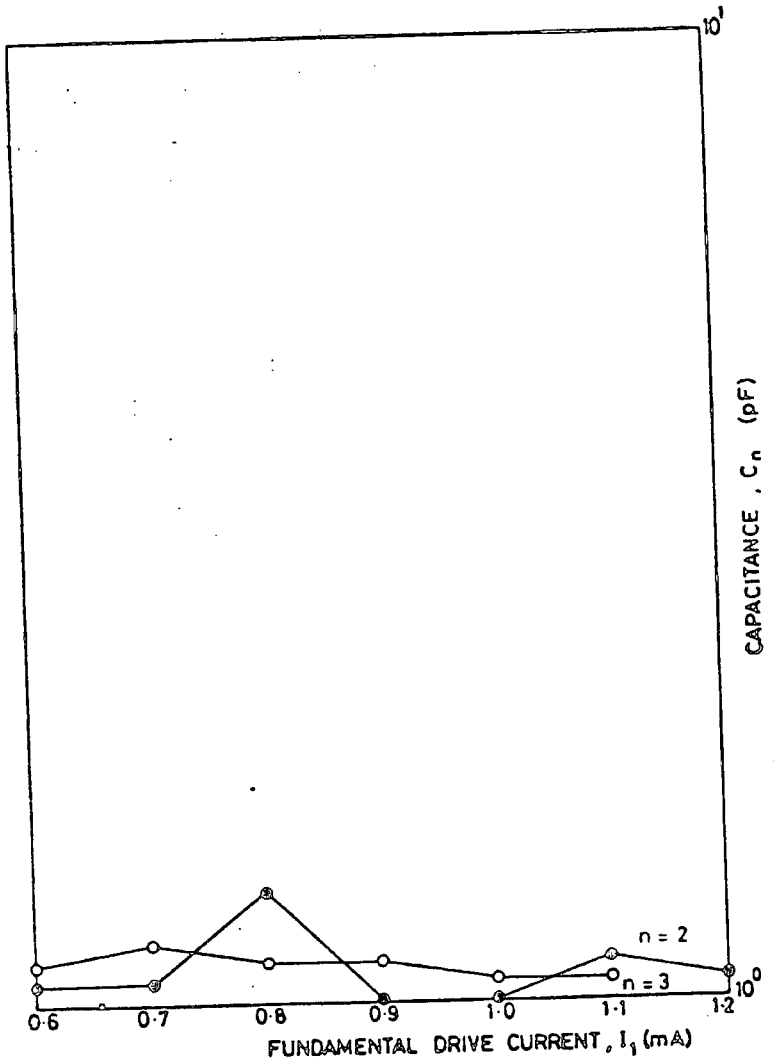

(d) CAPACITANCE

Fig 6.5.4: HARMONIC IMPEDANCE - f = 450 MHz

6.6 Si SCHOTTKY BARRIER DIODE (S BAND DETECTOR DIODE) - Types DC1515/1 and DC1515/2

1.560 GHz

In this section only diode of type DC1515/2 is discussed.

When the drive level is increased above 1.8 mA, the second harmonic amplitudes are constant and those of the third appear to increase (Fig 6.6.1(a)). There is a peak and a dip for the fourth harmonic amplitude and while that for the fifth harmonic the behaviour is wave-like.

The behaviour of the phases for the fourth and fifth harmonics (Fig 6.6.1(b)) is seen to decrease with level whereas that for the third harmonic, there is only a small decrease. Discontinuity in phases appears to occur for the second harmonic when the drive levels are between 1.8 and 2.1 mA. In addition, the discontinuity in the fourth harmonic is at a level of about 1.4 mA.

A peak exists for the impedance curve at the fourth harmonic (Fig 6.6.1(c)) at the drive levels between 1.7 and 2.0 mA. The impedances at the third and fourth harmonics are about constant within the given drive range.

The values of capacitance at the third harmonic are almost constant whose average value is 0.7 pF (Fig 6.6.1(d)). However, there are big variations in values for the second and fifth harmonics.

Taking into account the third harmonic (within the range of the drive level) it is seen that the impedance and capacitance are about constant, while the amplitude increases and the phase decreases with the drive. At the drive level between 1.8 and 2.0 mA, there exists a peak for the values of the impedance at the second harmonic and a discontinuity

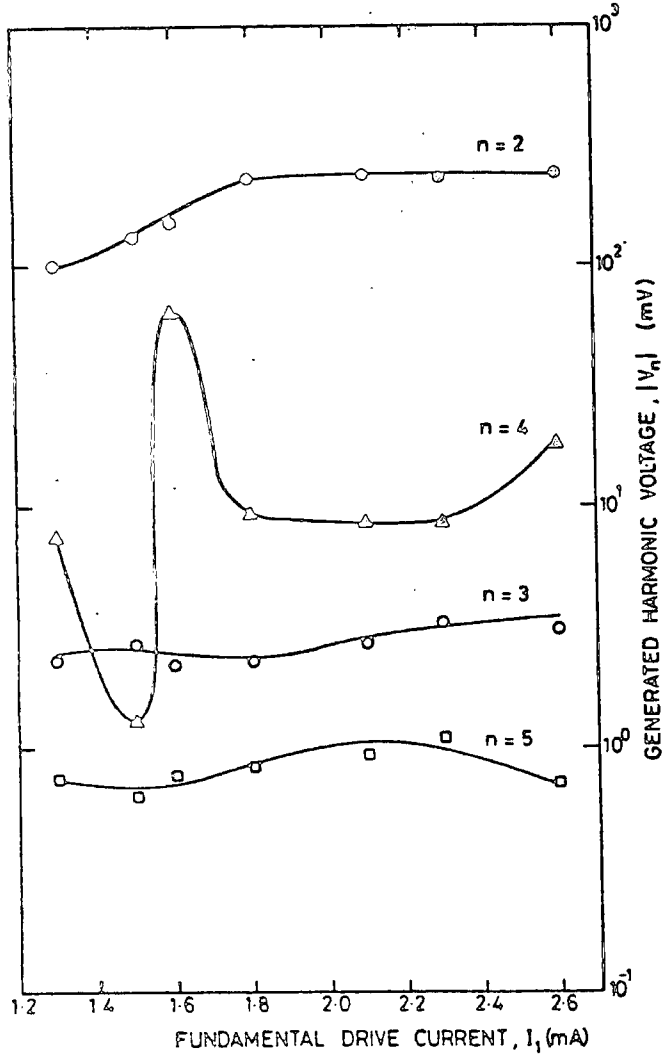

(a) AMPLITUDE

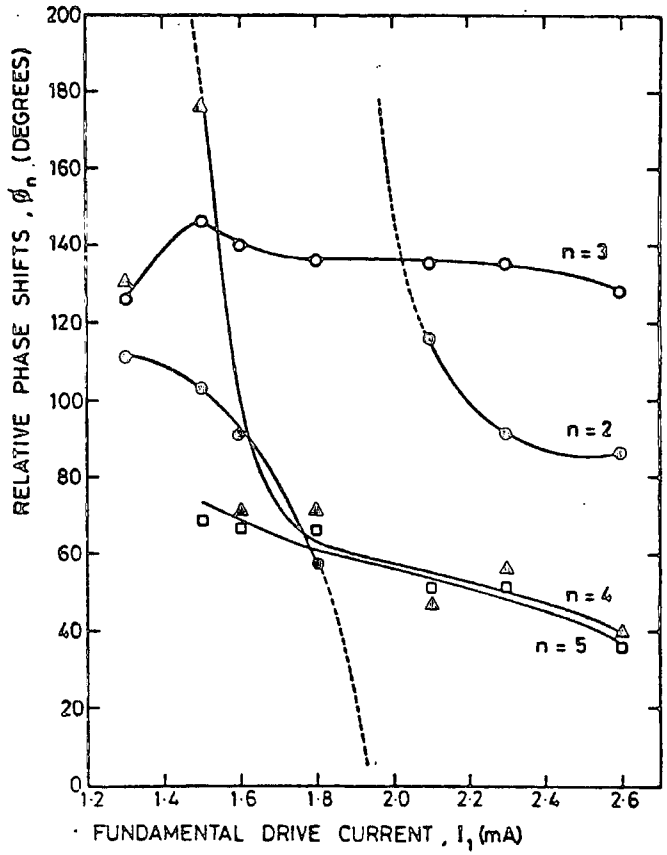

(b) PHASE

Fig 6.6.1: HARMONIC SPECTRA f_1 = 1.560 GHz

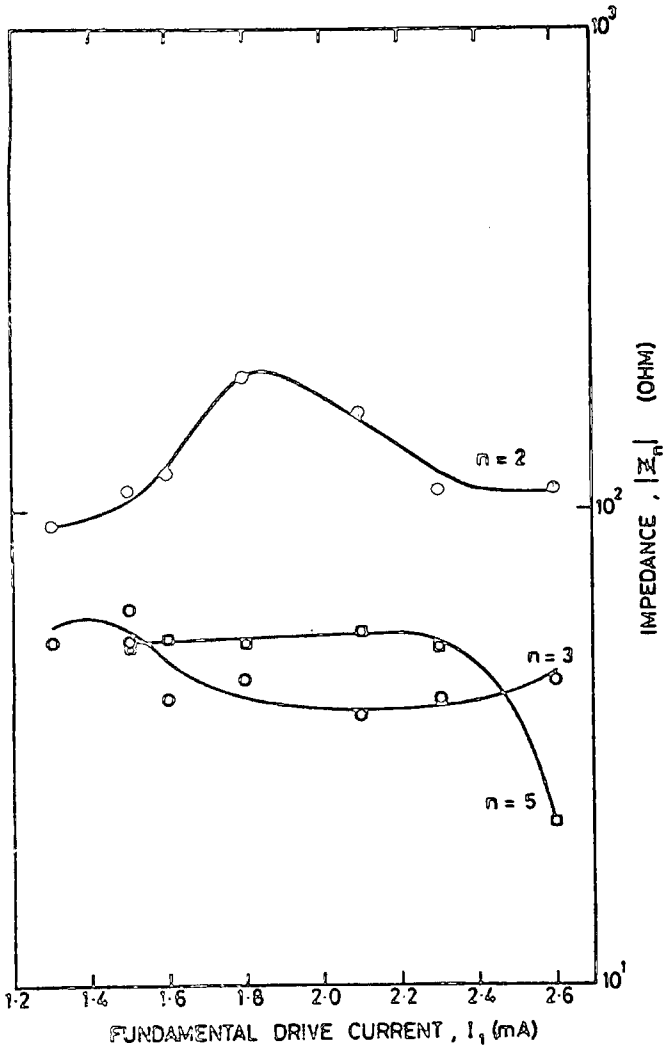

(c) IMPEDANCE

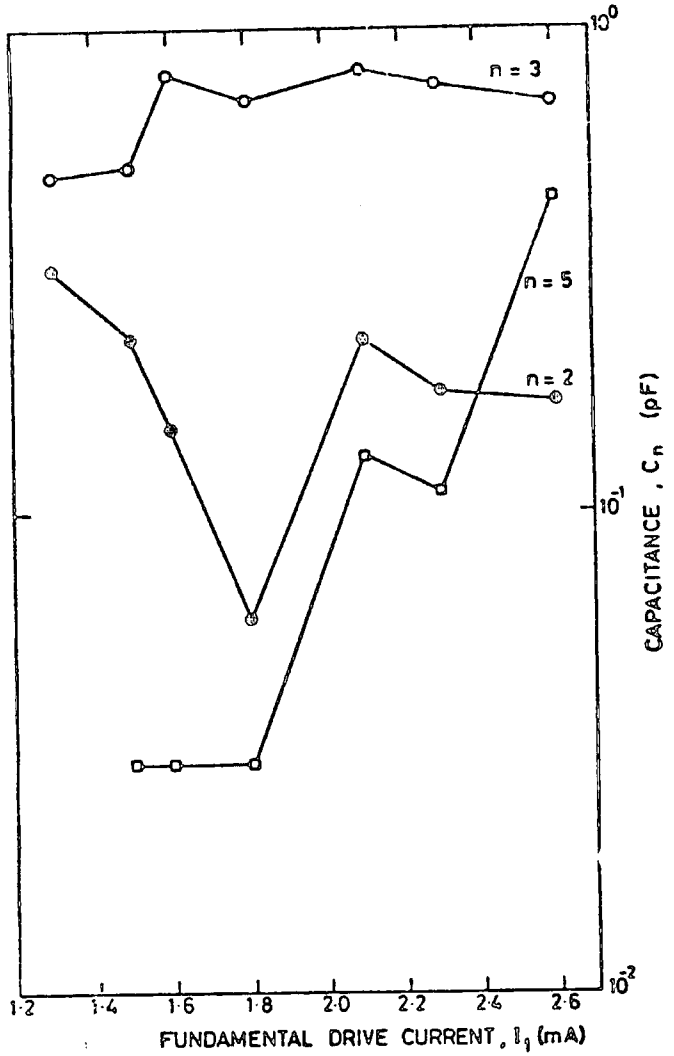

(d) CAPACITANCE

Fig 6.6.1: HARMONIC IMPEDANCE f_1 = 1.560 GHz

in the corresponding harmonic phase.

450 MHz

The second and third harmonic amplitudes increase with the drive level for both diodes (Figs 6.6.2(a) and 6.6.3(a)). In the case of the fourth harmonic voltages the behaviour is wave-like (for both diodes).

As the drive level is increased the phases, of the fourth harmonic for both diodes (Figs 6.6.2(b) and 6.6.3(b)) and those of the third harmonic for the second diode, decrease. In the case of other harmonics, there are moderate variations in the values of the phases for both diodes.

In general, there are fairly small variations in the values of the impedance at harmonics for the second diode within the given drive range. The values of the impedance at the third harmonic is almost constant. However, bigger variations are observed in the case of the first diode (Fig 6.6.2(c)).

The behaviour of the capacitance at harmonics for the two diodes (Figs 6.6.2(d) and 6.6.3(d)) is that, the first has bigger variations with an average value of 0.6 pf. On the other hand the second diode has smaller variations with an average value of 1.2 pF.

In general, the first diode shows bigger variations in the values of the harmonic amplitude and the impedance at harmonics and hence the corresponding capacitance. However, there are small variations in the value of the phases. In the case of the second diode, there are moderate variations in the values of the harmonic amplitude and the impedance at harmonics and hence the corresponding phase and capacitance.

6.7 Ge BACKWARD DIODE (X BAND DETECTOR DIODE) - Types DC3021/1 and DC3021/2

1.560 GHz

The third, fourth and fifth harmonic amplitudes of the first diode (Fig 6.7.1(a)) and those of the fifth for the second diode

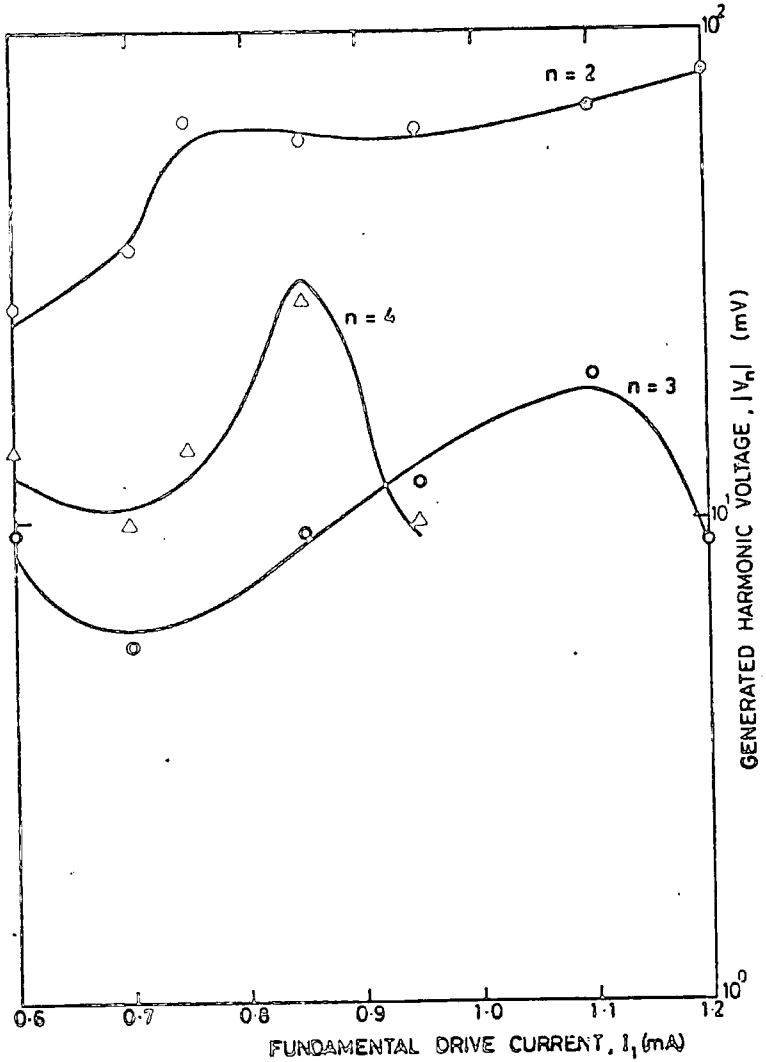

(a) AMPLITUDE

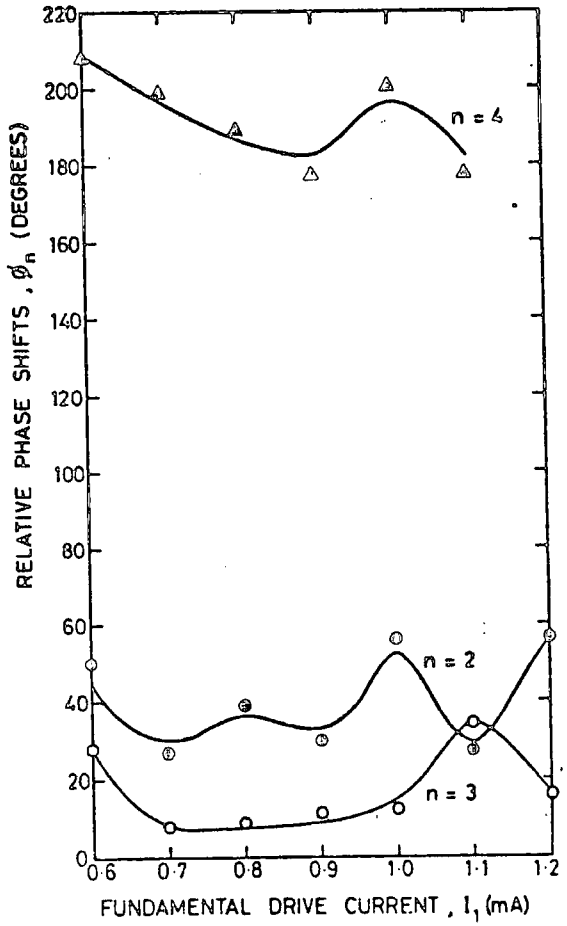

(b) PHASE

Fig 6.6.2: HARMONIC SPECTRA f_1 = 450 MHz

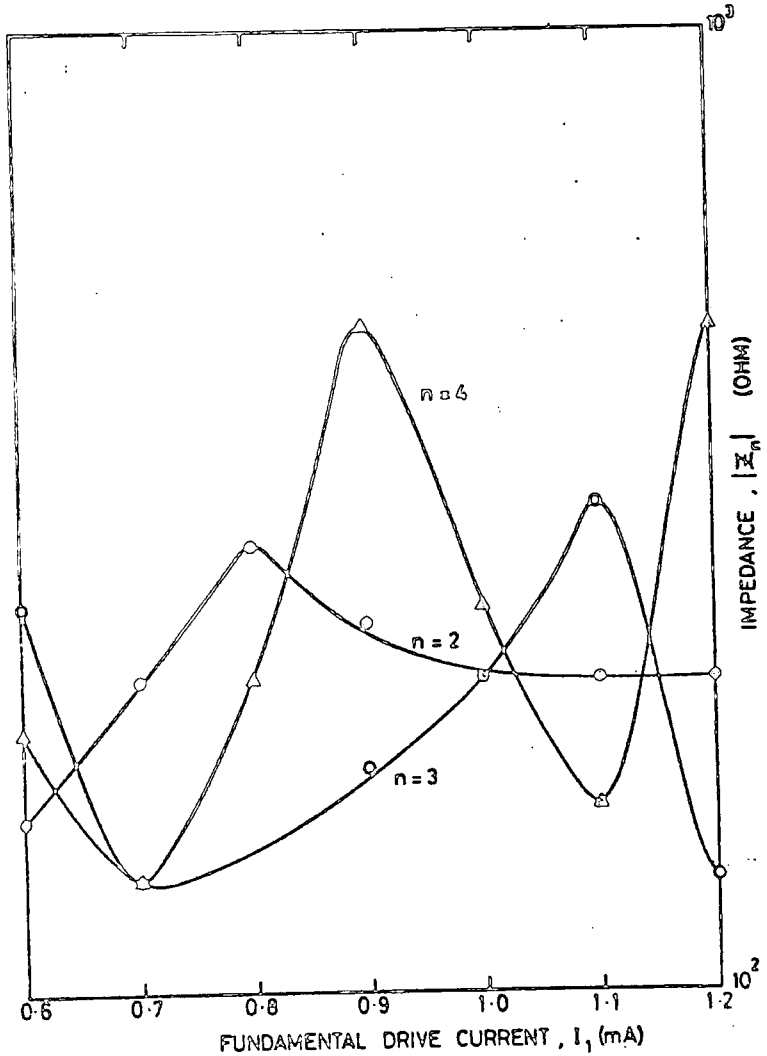

(c) IMPEDANCE

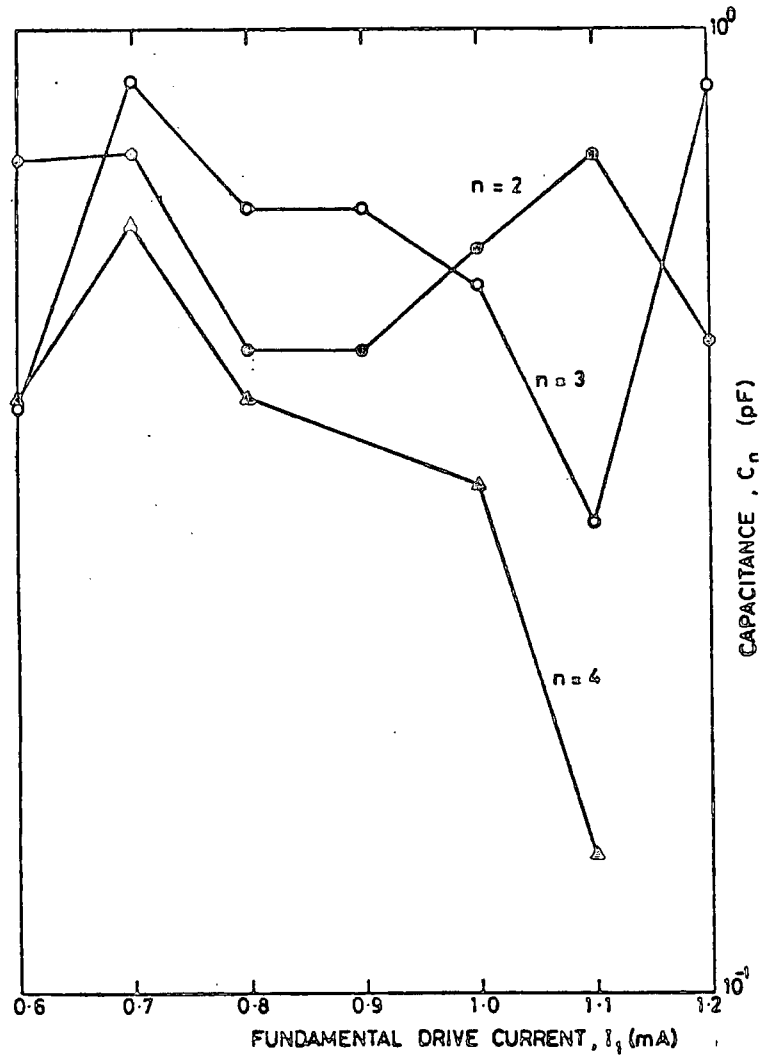

(d) CAPACITANCE

Fig 6.6.2: HARMONIC IMPEDANCE f_1 = 450 MHz

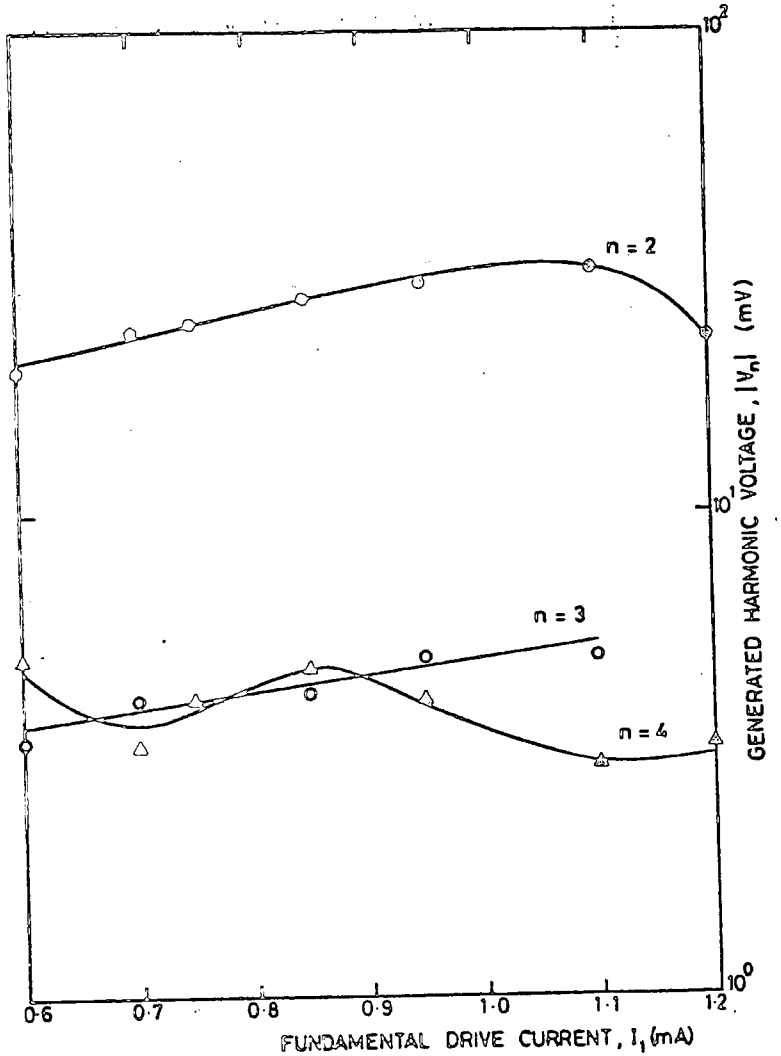

(a) AMPLITUDE

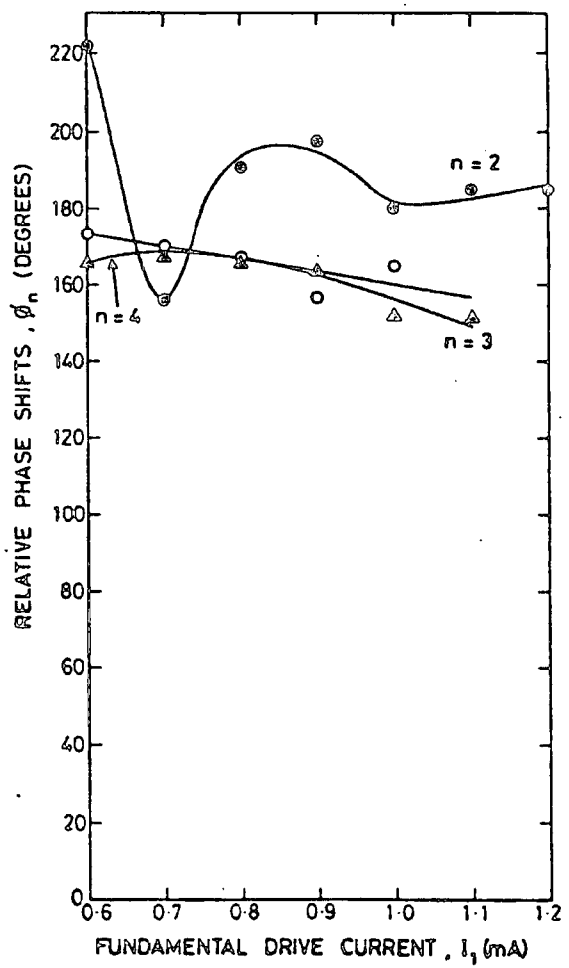

(b) PHASE

Fig 6.6.3: HARMONIC SPECTRA f_1 = 450 MHz

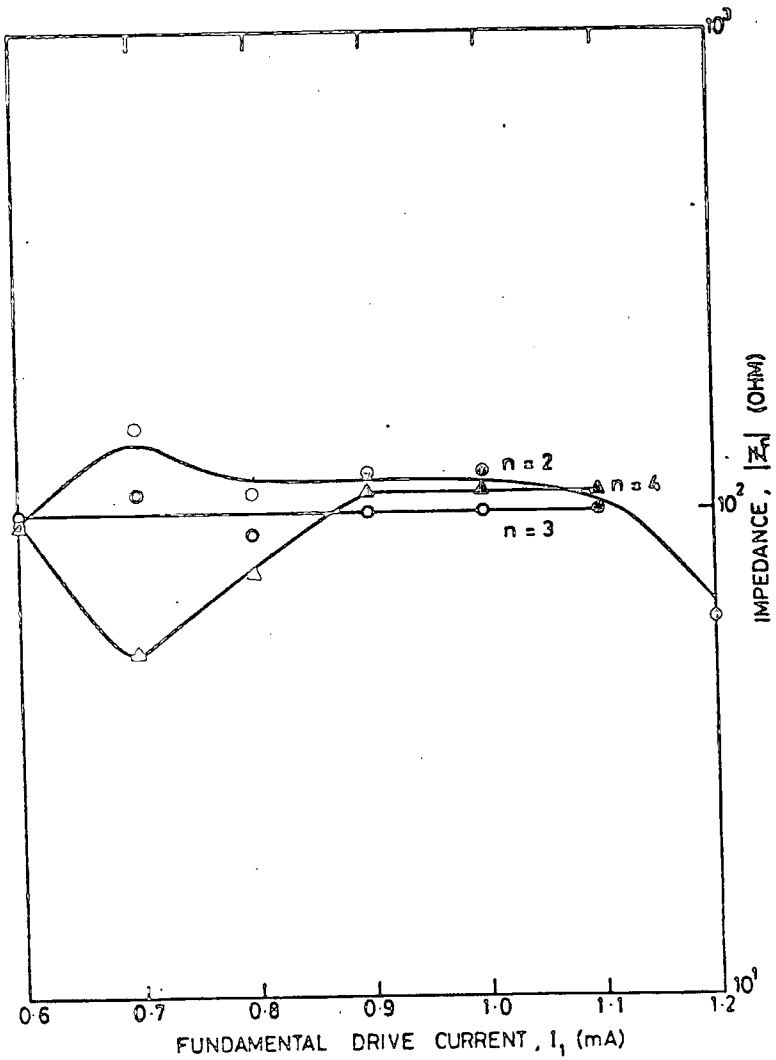

(c) IMPEDANCE

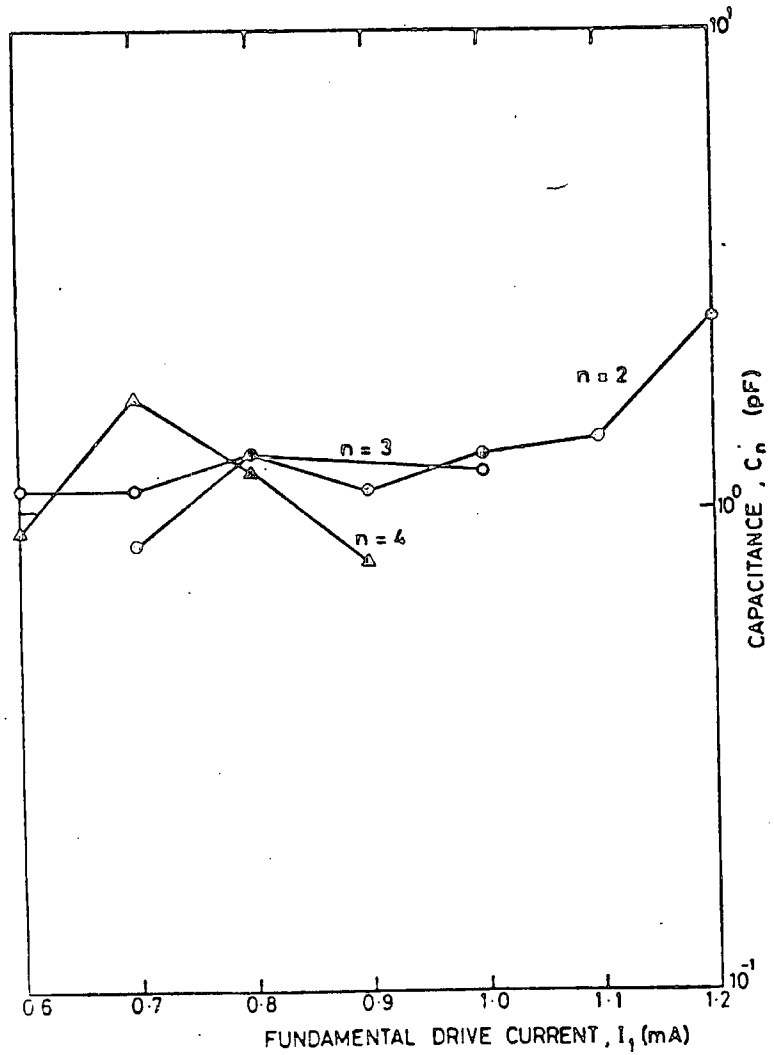

(d) CAPACITANCE

Fig 6.6.3: HARMONIC IMPEDANCE f_1 = 450 MHz

(Fig 6.7.2(a)) increase with the drive level. However, the fourth harmonic voltages of the second diode are fairly constant. The behaviour of the second and fifth harmonic amplitudes for both the diodes is almost similar.

The phases for the third, fourth and the fifth harmonics of the first diode (Fig 6.7.1(b)) and those of the fifth for the second diode (Fig 6.7.2(b)) decrease with the drive level. In contrast, the second harmonic phases of the second diode increase with the drive.

The values of the impedance at the fifth harmonic of the first diode (Fig 6.7.1(c)) decrease with level whereas those of the third and fourth increase. In the case of the second diode (Fig 6.7.2(c)), there are fluctuations in the values of the impedance for the second, fourth and the fifth harmonics within the given drive level range.

The values of the capacitance at the fifth harmonic for the first diode (Fig 6.7.1(d)) are almost constant (within the drive level range), which on the average is 0.4 pF. There are small variations for the second and third harmonics. However, there are big variations in the values of the capacitance at the fourth harmonic for the first diode and those at the second, fourth and the fifth harmonics for the second diode (Fig 6.7.2(d)).

For the first diode, the third, fourth and the fifth harmonic amplitude increase with the drive level and the corresponding harmonic phases decrease. In the case of the fifth harmonic of the first diode, as the level is increased the amplitudes increase, the phases and the impedances decrease and the capacitance remains constant.

450 MHz

Generally, the generated harmonic voltages increase with the drive level for both diodes (Figs 6.7.3(a) and 6.7.4(a)) and the rates of increase are greater for the third and fourth harmonics.

As for the phases, there are small variations with the drive for the

Ge BACKWARD DIODE - DC3021/1

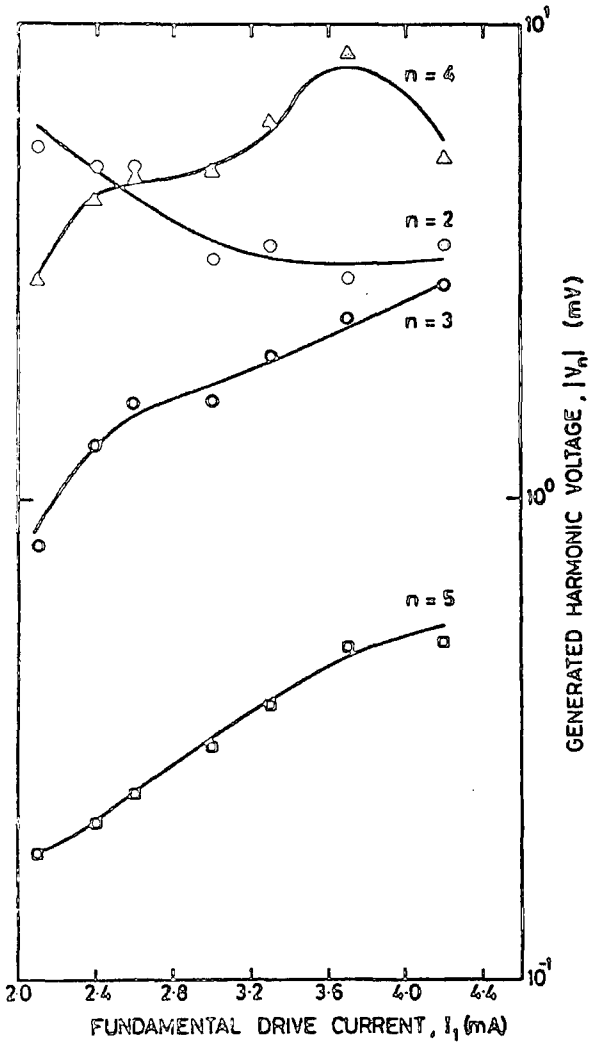

(a) AMPLITUDE

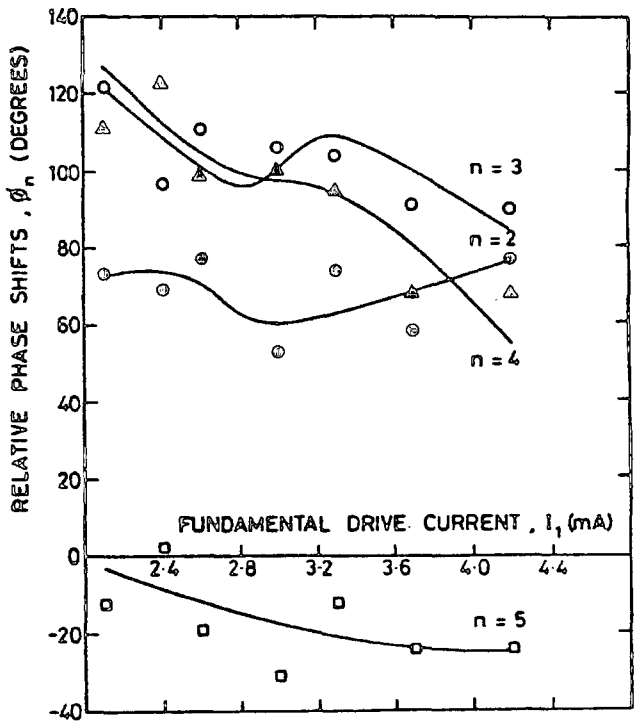

(b) PHASE

Fig 6.7.1: HARMONIC SPECTRA - f_1 = 1.560 GHz

Ge BACKWARD DIODE - DC3021/1

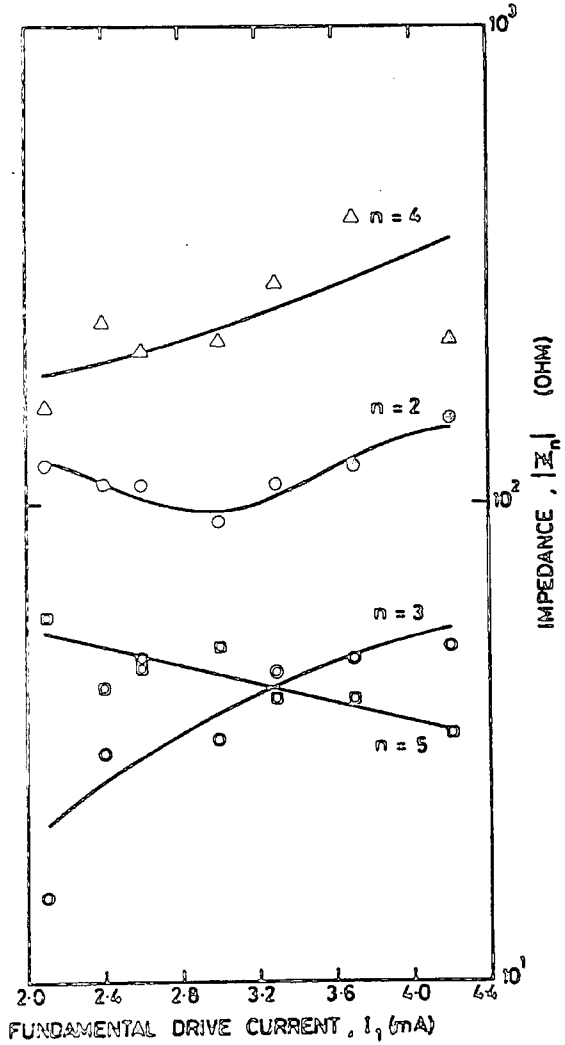

(c) IMPEDANCE

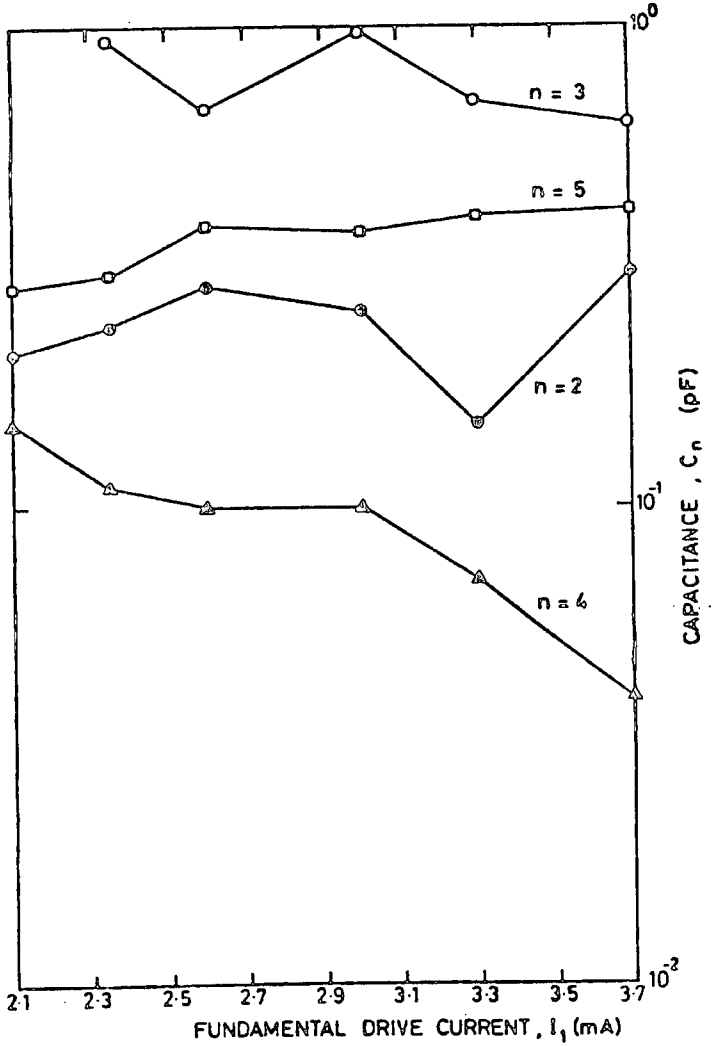

(d)CAPACITANCE

Fig 6.7.1: HARMONIC IMPEDANCE - f_1 = 1.560 GHz

Ge BACKWARD DIODE - DC3021/2

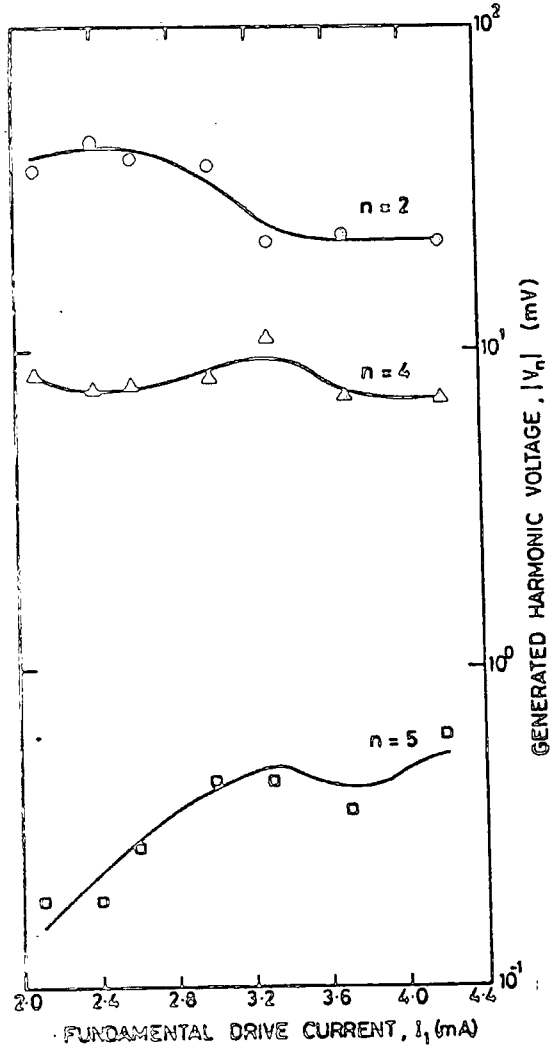

(a) AMPLITUDE

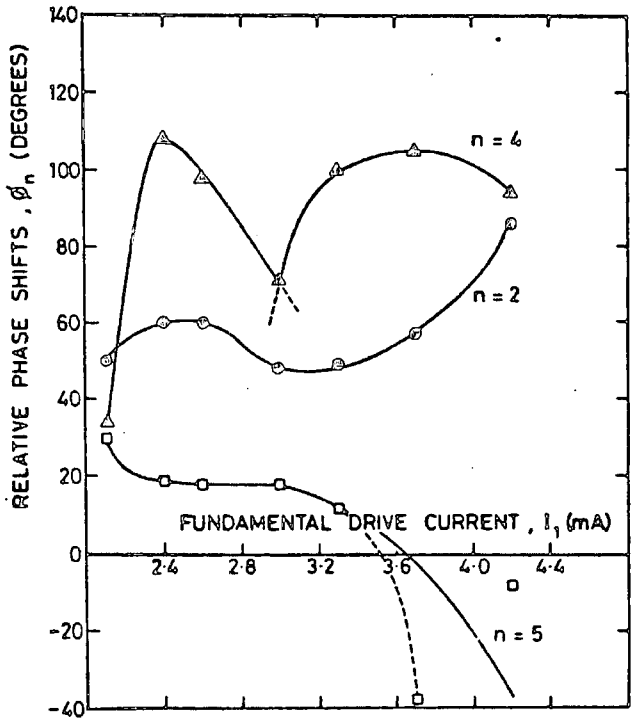

(b) PHASE

Fig 6.7.2: HARMONIC SPECTRA - f_1 = 1.560 GHz

Ge BACKWARD DIODE - DC3021/2

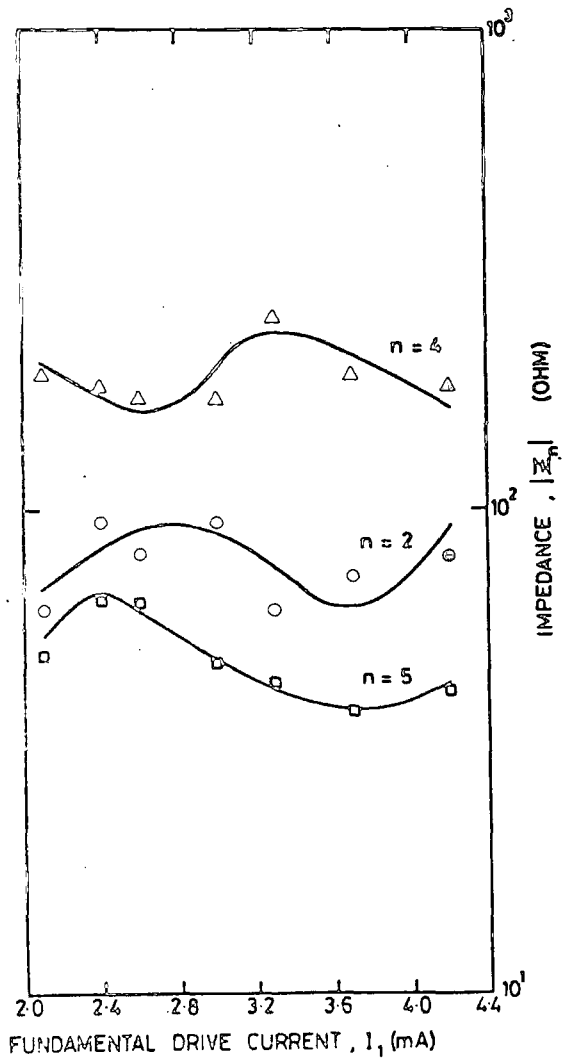

(c) IMPEDANCE

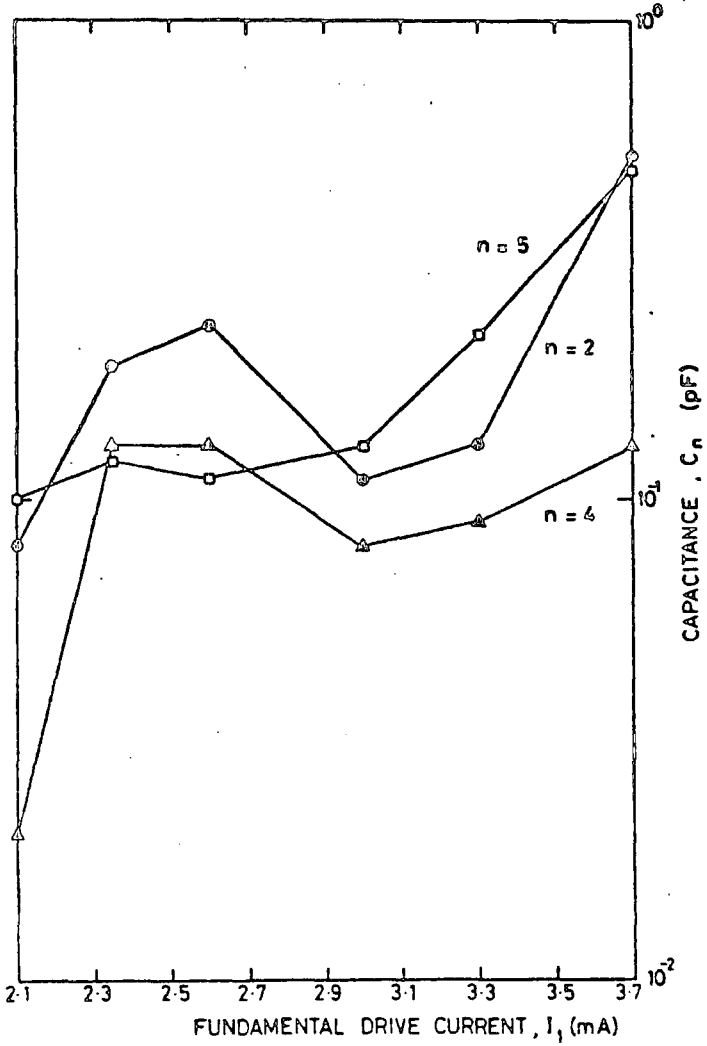

(d) CAPACITANCE

Fig 6.7.2: HARMONIC IMPEDANCE - f_1 = 1.560 GHz

Ge BACKWARD DIODE - DC3021/2

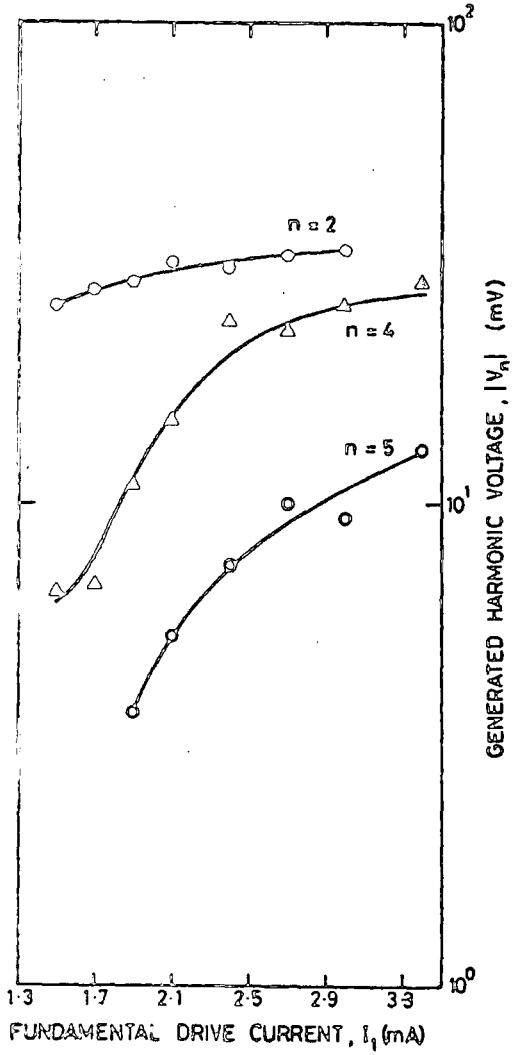

(a) AMPLITUDE

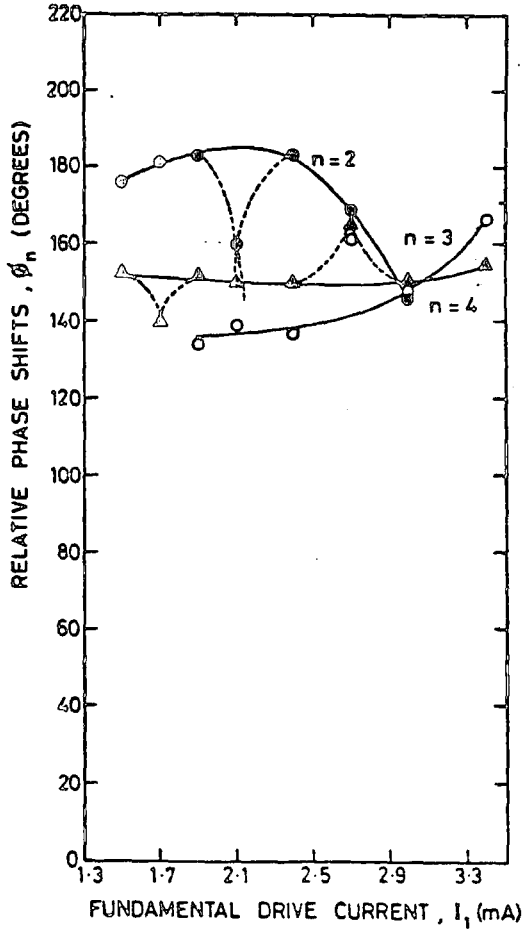

(b) PHASE

Fig 6.7.3: HARMONIC SPECTRA - f_1 = 450 MHz

Ge BACKWARD DIODE - DC3021/1

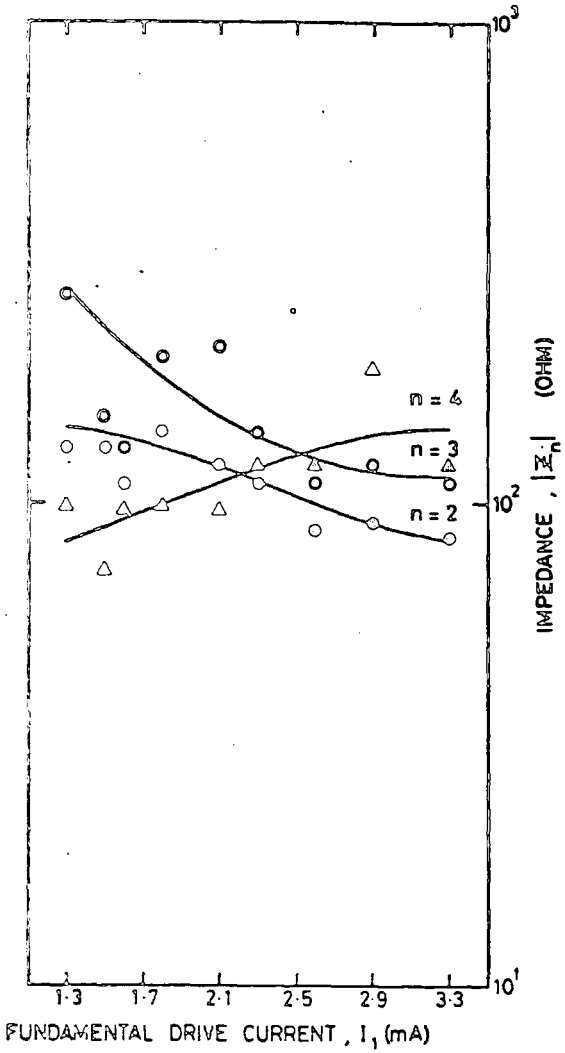

(c) IMPEDANCE

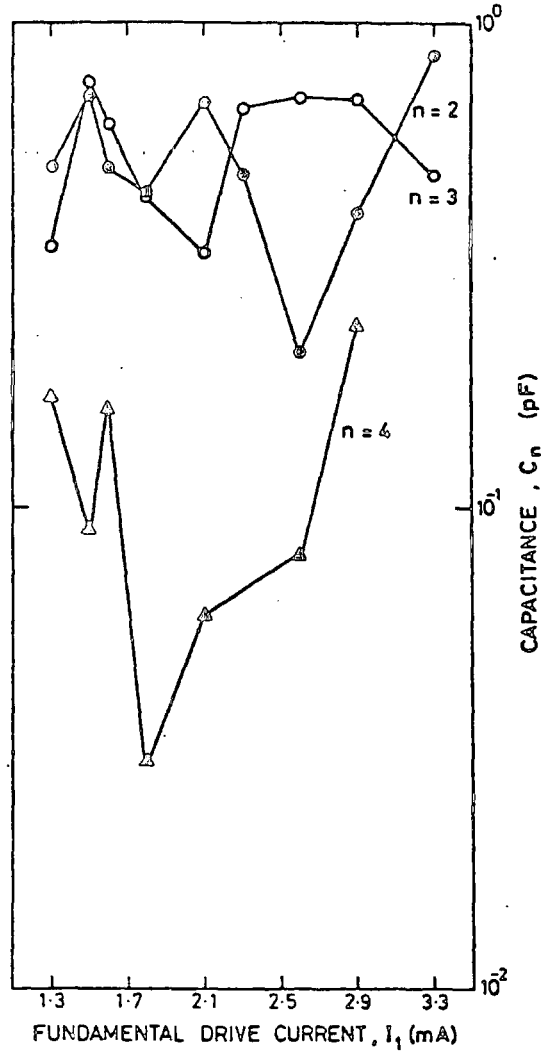

(d) CAPACITANCE

Fig 6.7.3: HARMONIC IMPEDANCE - f_1 = 450 MHz

Ge BACKWARD DIODE - DC3021/1

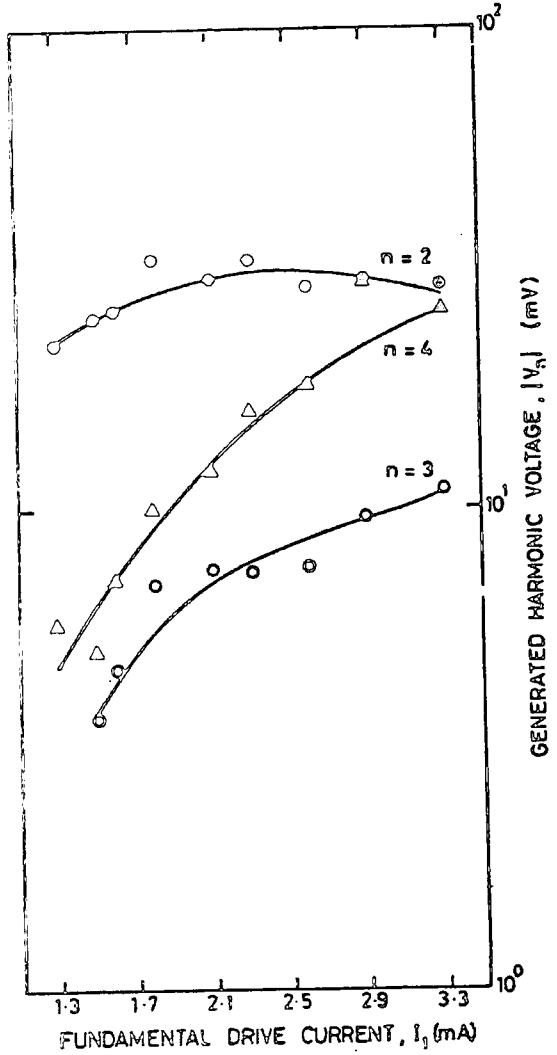

(a) AMPLITUDE

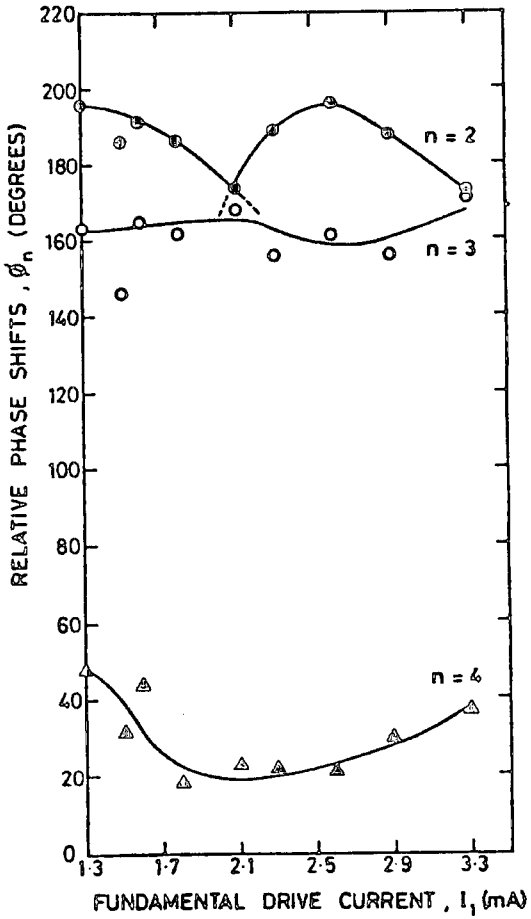

(b) PHASE

Fig 6.7.4: HARMONIC SPECTRA - f_1 = 450 MHz

Ge BACKWARD DIODE DC3021/2

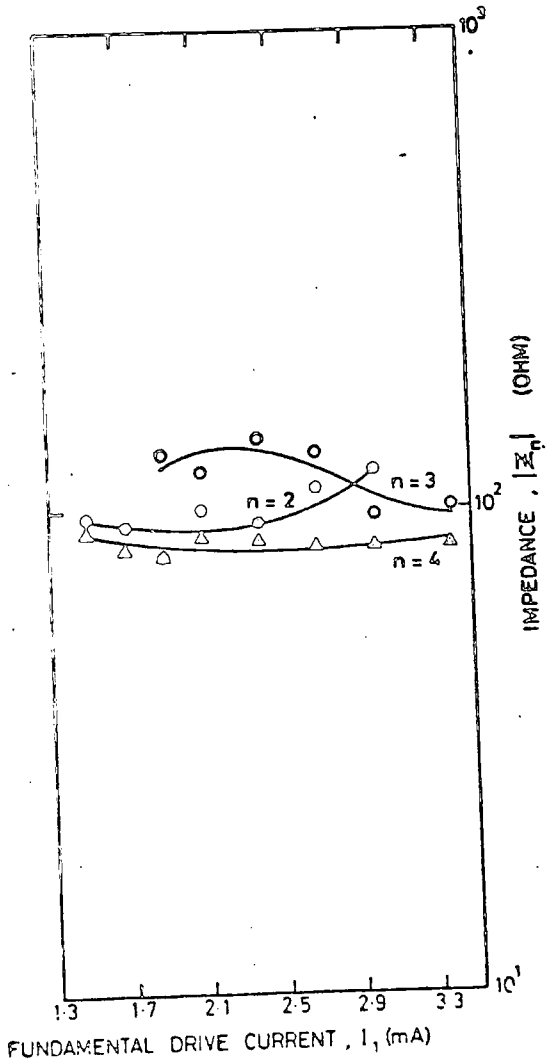

(c) IMPEDANCE

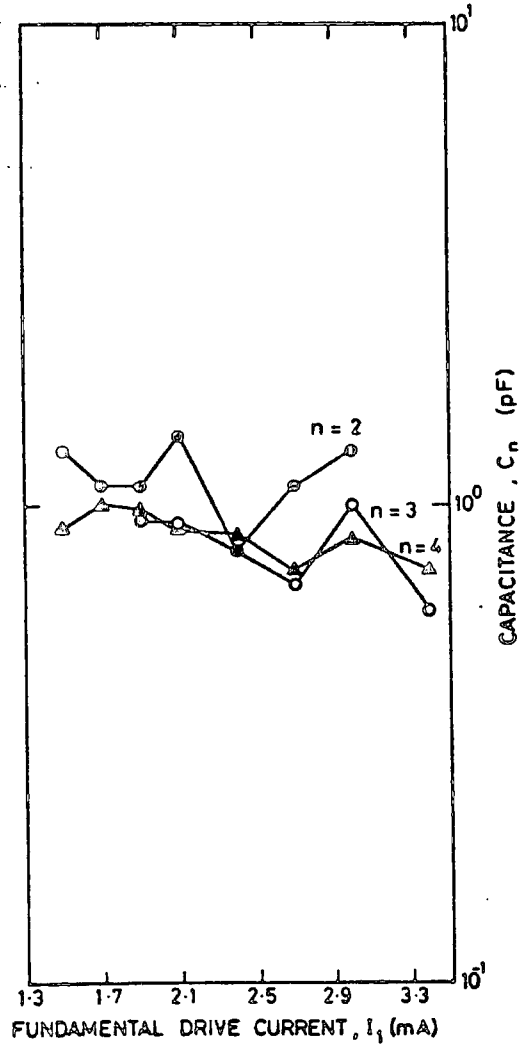

(d) CAPACITANCE

Fig 6.7.4: HARMONIC IMPEDANCE - f_1 = 450 MHz

third harmonic of the first diode (Fig 6.7.3(b)) and those for the fourth of the second diode (Fig 6.7.4(b)). In the case of other harmonics for both diodes, however, there are moderate variations.

The values of the impedance at the second and third harmonics of the first diode (Fig 6.7.3(c)) and those of the third for the second diode (Fig 6.7.4(c)) decrease with the drive level. However, the values of the impedance at the fourth harmonic for the second diode are almost constant. Furthermore, the values of the impedance at the fourth harmonic of the first diode and that of the second harmonic for the second diode, increase slightly with the increase in the drive level.

The values of the capacitance at harmonics for the second diode (Fig 6.7.4(d)) have small variations and range from 0.7 to 1.2pF. In the case of the first diode (Fig 6.7.3(d)), the values of the capacitance at the second and fourth harmonics have bigger variations from 0.03 to about 0.90 pF. Only the values of the capacitance at the third harmonic of the first diode and those of the second for the other diode have moderate variations.

As the drive level is increased (for both diodes) the values of the impedance at the third harmonic decrease and those of the corresponding amplitudes increase. However, in the case of the second diode, the values of the impedance at the fourth harmonic and those of the corresponding capacitance are fairly constant. There is a low peak for the curve of the second harmonic amplitude at 2.1 mA (for the first diode) and at this drive level there is a discontinuity in the corresponding phase.

6.8 Si POINT CONTACT DIODE (S BAND MIXER DIODE) - Types CS12BR/1 and CS12BR/2

1.560 GHz

For both the diodes, the amplitudes for the fourth and fifth harmonics increase with the drive level (Figs 6.8.1(a) and 6.8.2.(a)).

Si POINT CONTACT DIODE CS12BR/1

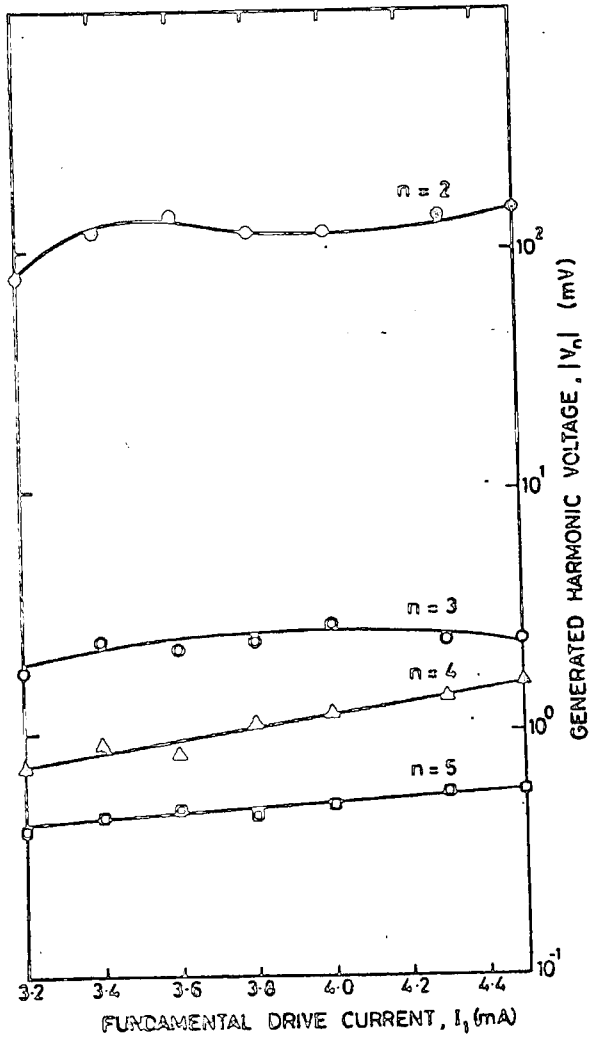

(a) AMPLITUDE

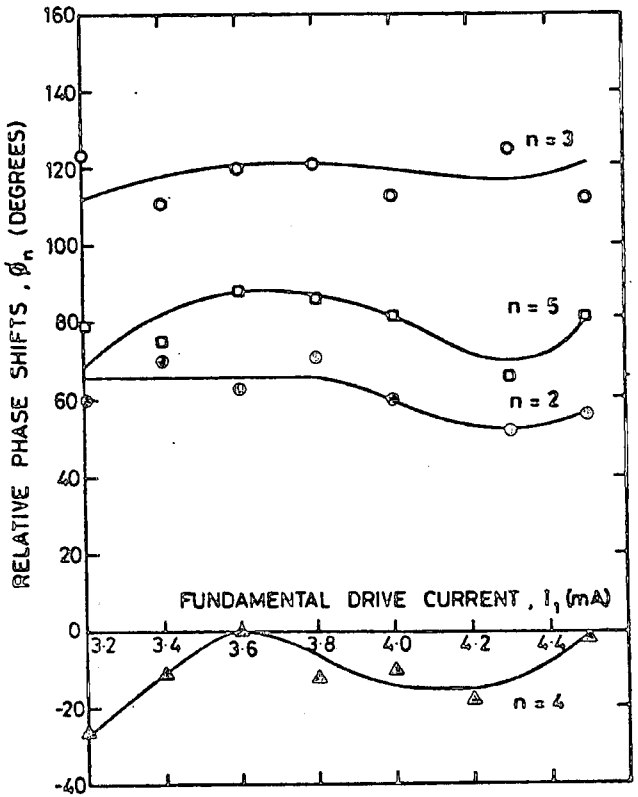

(b) PHASE

Fig 6.8.1: HARMONIC SPECTRA - f_1 = 1.560 GHz

Si POINT CONTACT DIODE - CS12BR/1

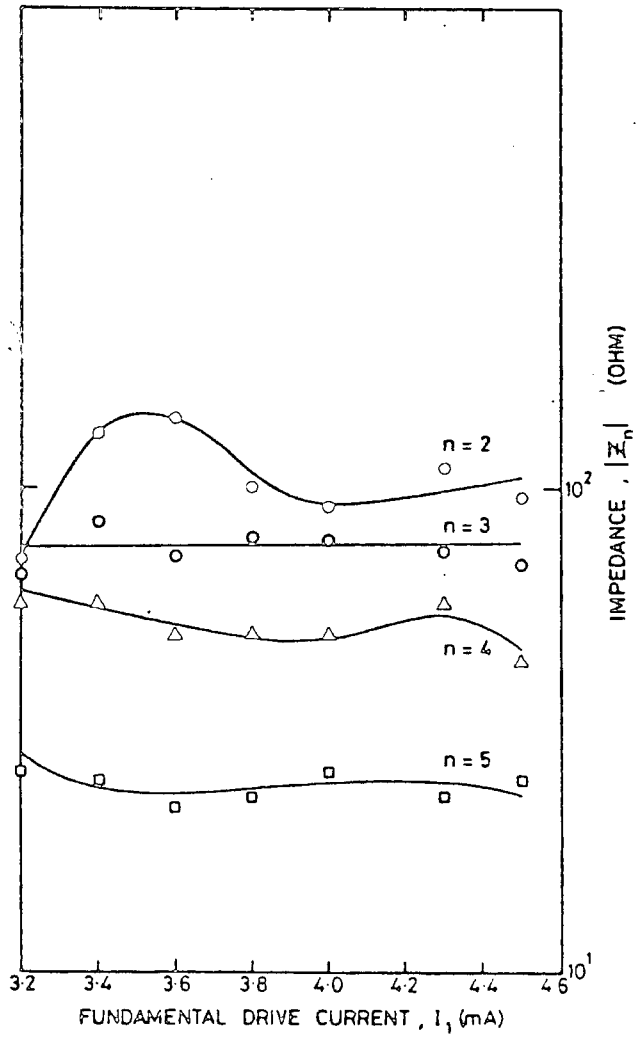

(c) IMPEDANCE

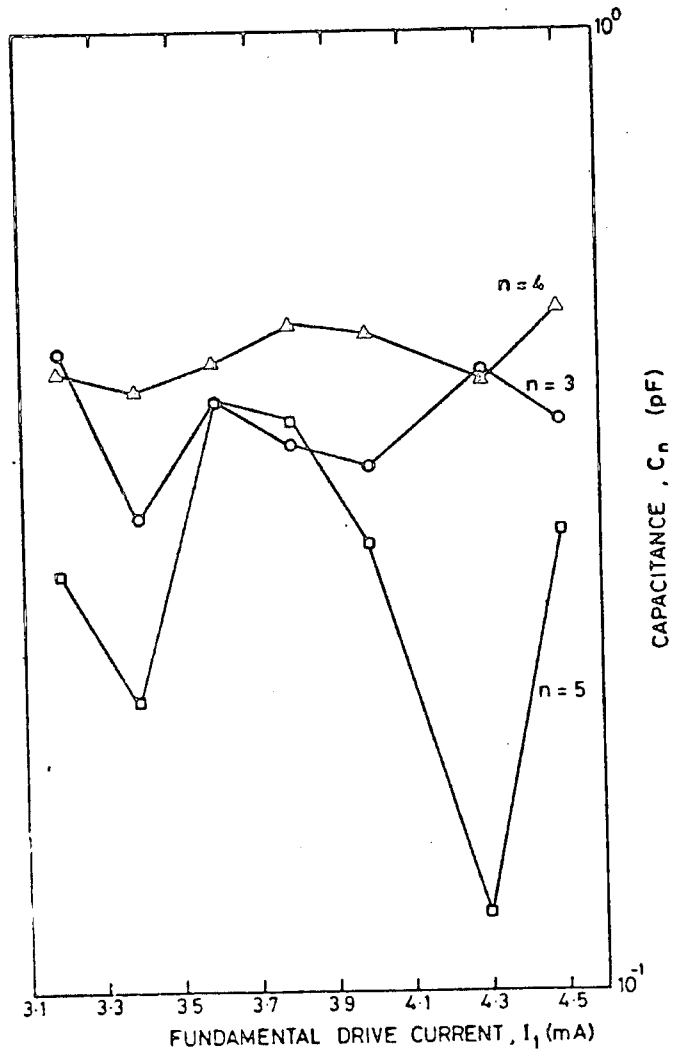

(d) CAPACITANCE

Fig 6.8.1: HARMONIC IMPEDANCE - f_1 = 1.560 GHz

Si POINT CONTACT DIODE - CS12BR/2

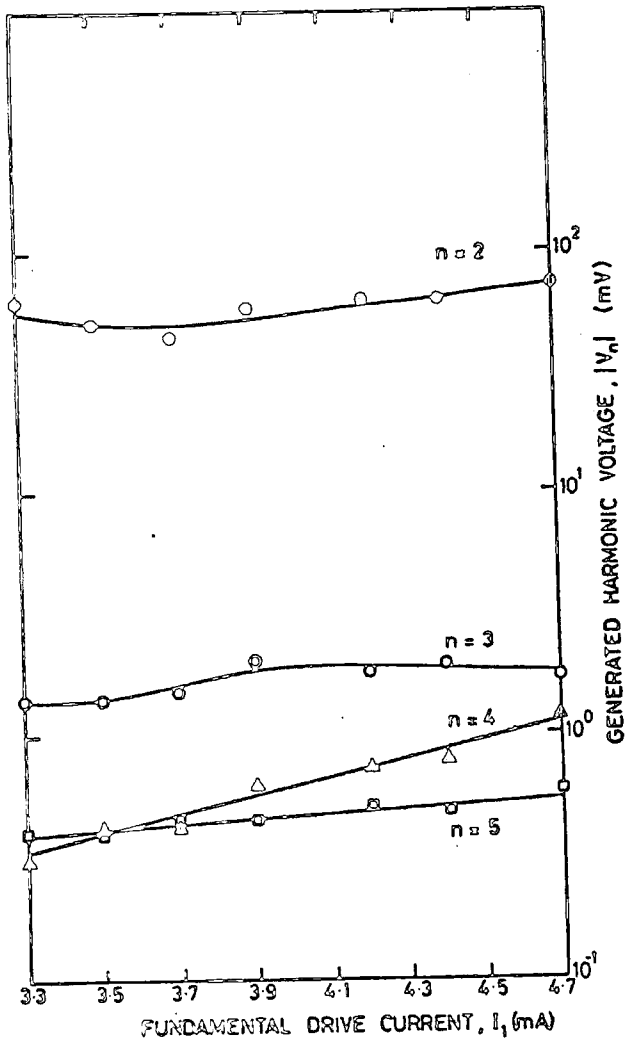

(a) AMPLITUDE

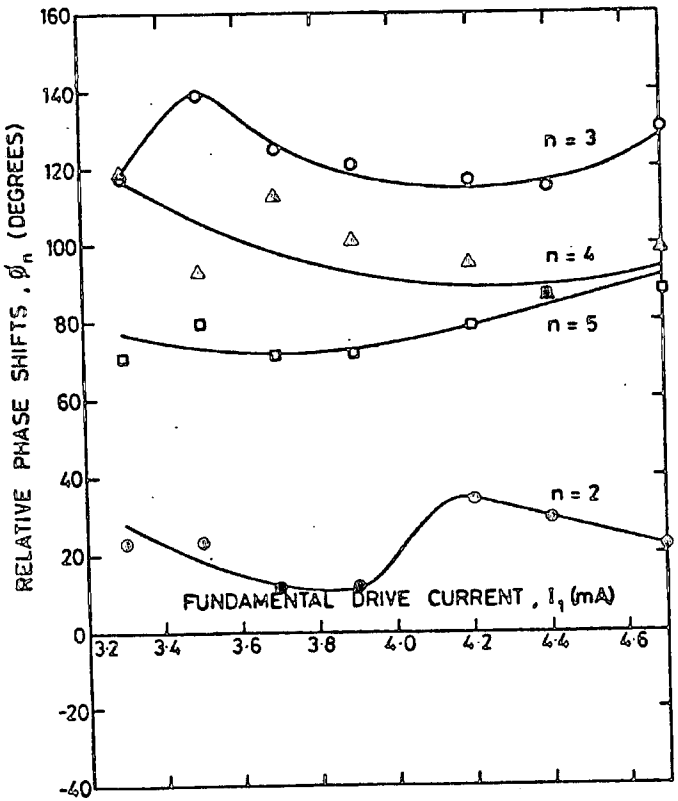

(b) PHASE

Fig 6.8.2: HARMONIC SPECTRA - f_1 = 1.560 GHz

Si POINT CONTACT DIODE - CS12BR/2

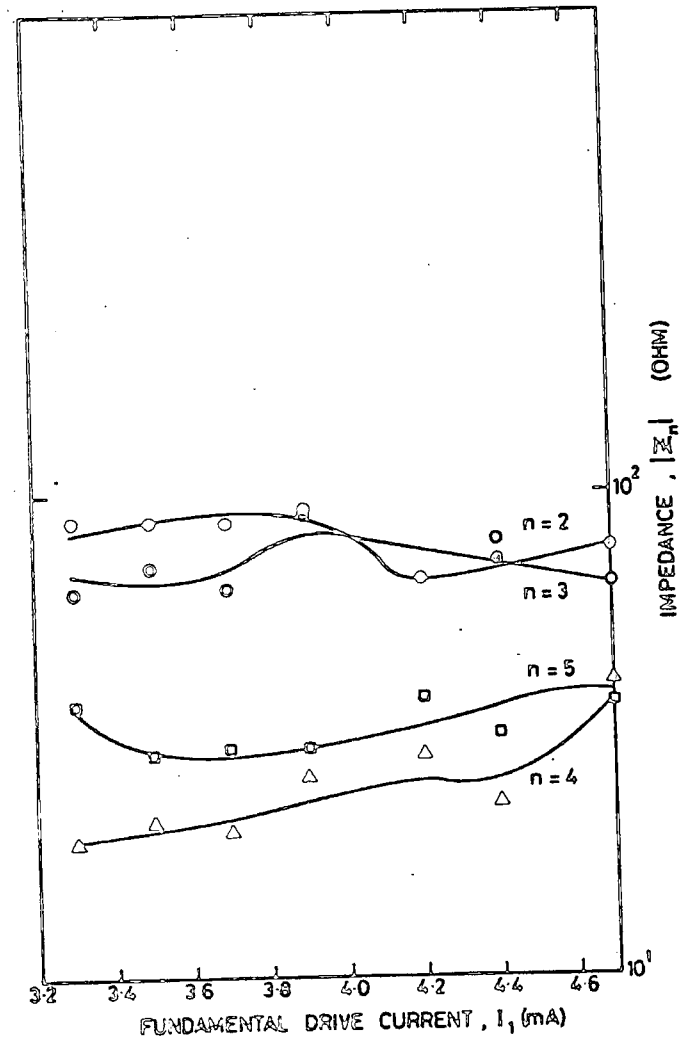

(c) IMPEDANCE

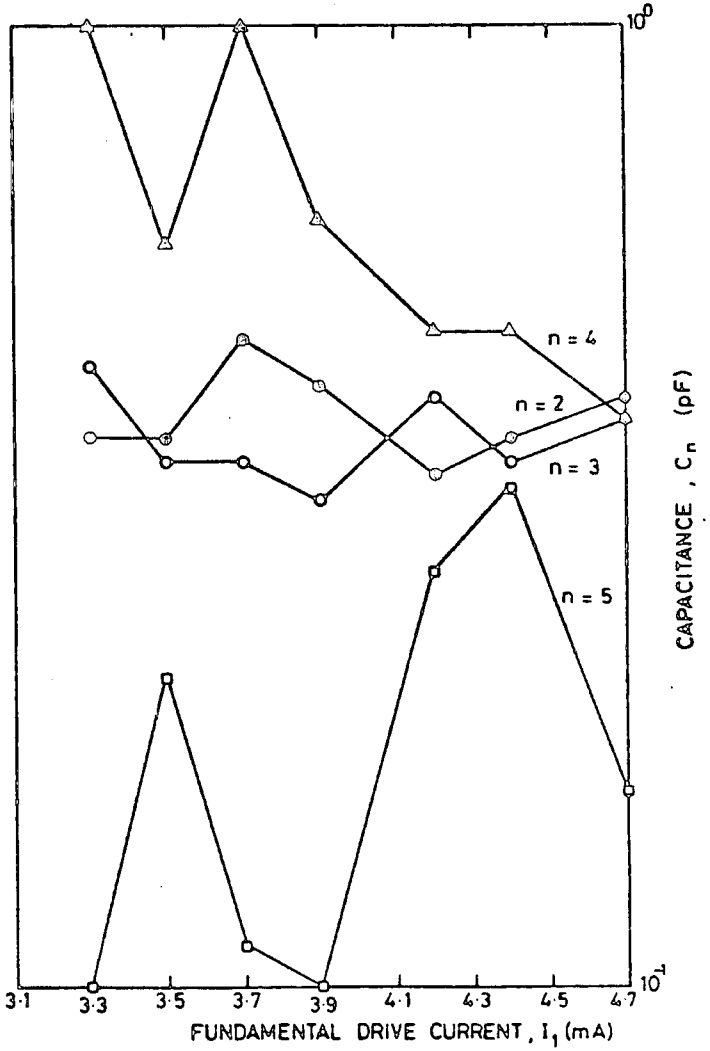

(d) CAPACITANCE

Fig 6.8.2: HARMONIC IMPEDANCE - f_1 = 1.560 GHz

However, the values of the second and third harmonic voltages are almost constant.

The variation in the phases at the harmonics are generally small for both diodes (Figs 6.8.1(a) and 6.8.2(b)). It is seen that there is no apparent trend in teh behaviour of the harmonic phases.

The impedance at the harmonics again have small variations in values for both diodes (Figs 6.8.1(c) and 6.8.2(c)). The impedance at lower harmonics seems to have higher values. In the case of the first diode, the values of the impedance at the third and fifth harmonics are fairly constant.

As for the capacitance, it is seen that the values at the fourth harmonic for the first diode (Fig 6.8.1(d) and those at the second and third harmonics for the second diode (Fig 6.8.2(d)) have small variations. The average value is about 0.4 pF. However, there are bigger variations for cases of the fifth harmonic for the first diode and those of the fourth and fifth harmonics for the second diode.

Generally, there are small variations in the values of the harmonic amplitude and those of impedance at harmonics and hence the corresponding phases. However, for the capacitance at certain harmonics, there are bigger variations in values.

6.9 Si POINT CONTACT DIODE (X BAND MIXER DIODE) - Types CS9B/1 and CS9B/2

1.560 GHz

All the harmonic amplitudes for both diodes (Figs 6.9.1(a) and 6.9.2(a)) increase with the drive level. The values of the second and fifth harmonic voltages are about the same for both diodes. In the case of the third harmonic, the values of the second diode are higher than those of the first.

Si POINT CONTACT DIODE - CS9B/1

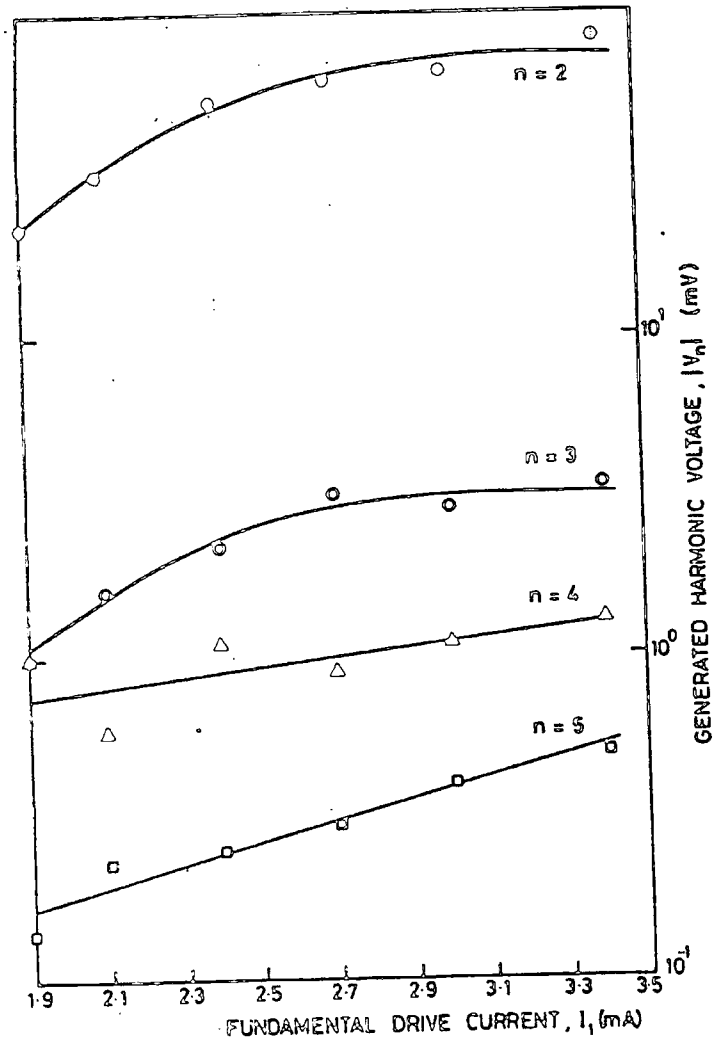

(a) AMPLITUDE

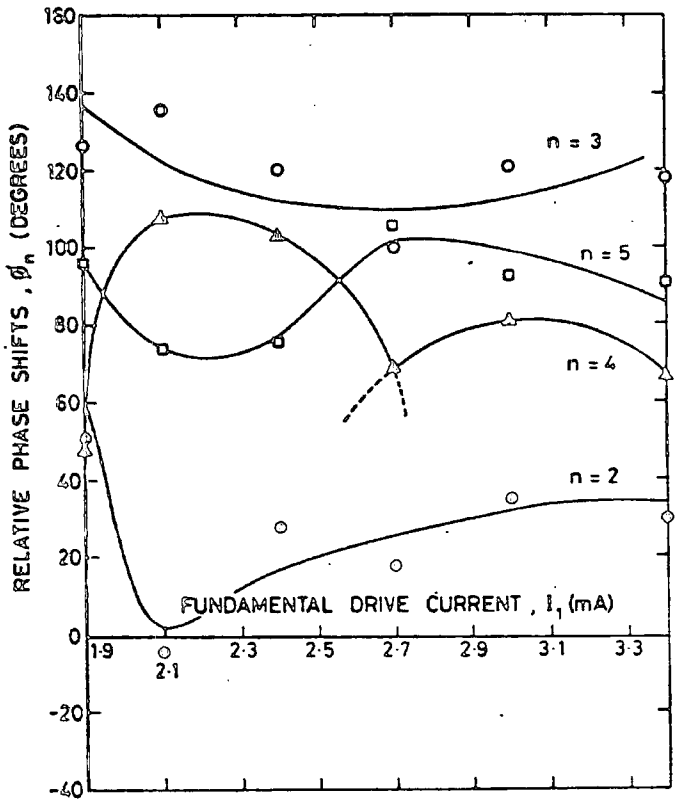

(b) PHASE

Fig 6.9.1: HARMONIC SPECTRA f_1 = 1.560 GHz

Si POINT CONTACT DIODE - CS9B/1

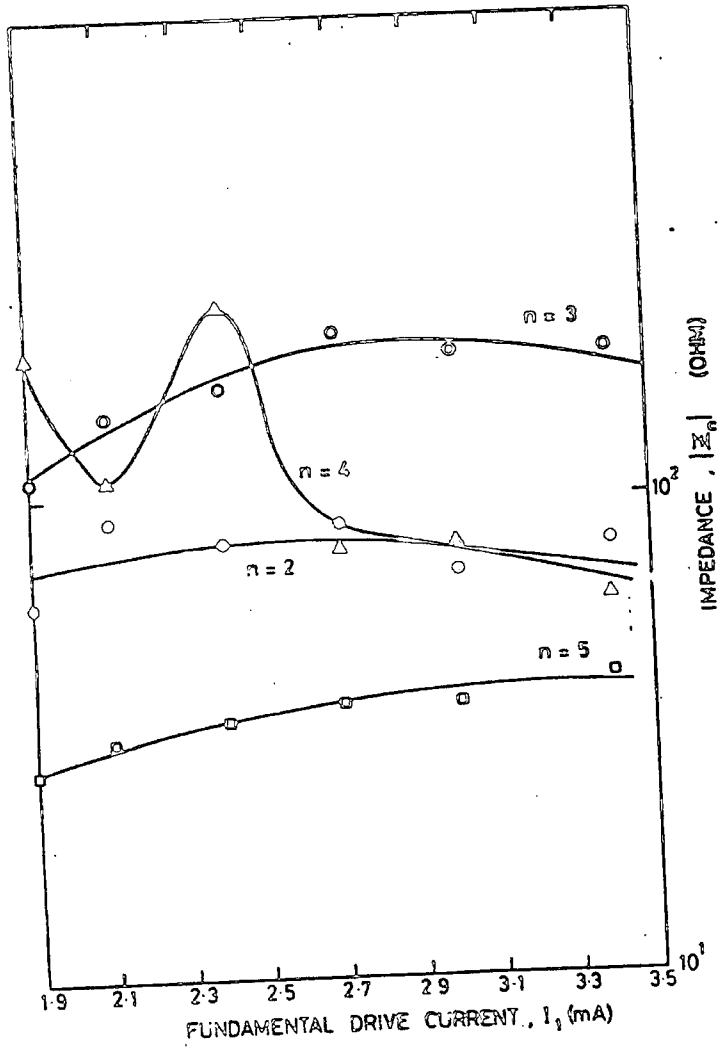

(c) IMPEDANCE

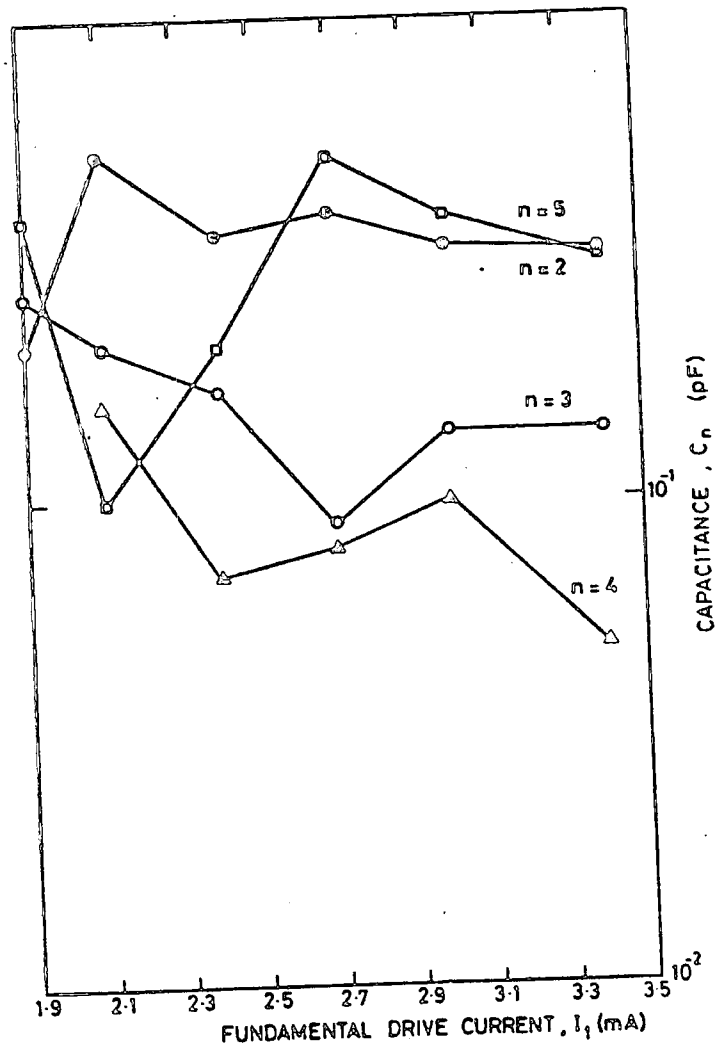

(d) CAPACITANCE

Fig 6.9.1: HARMONIC IMPEDANCE - f_i= 1.560 GHz

Si POINT CONTACT DIODE CS9B/2

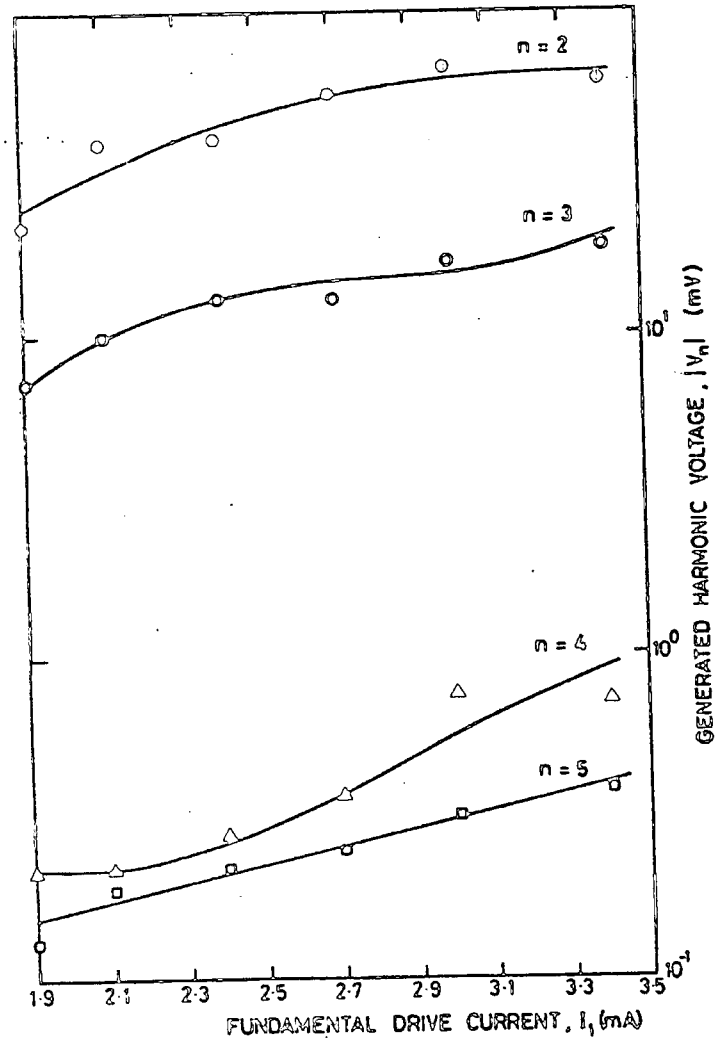

(a) AMPLITUDE

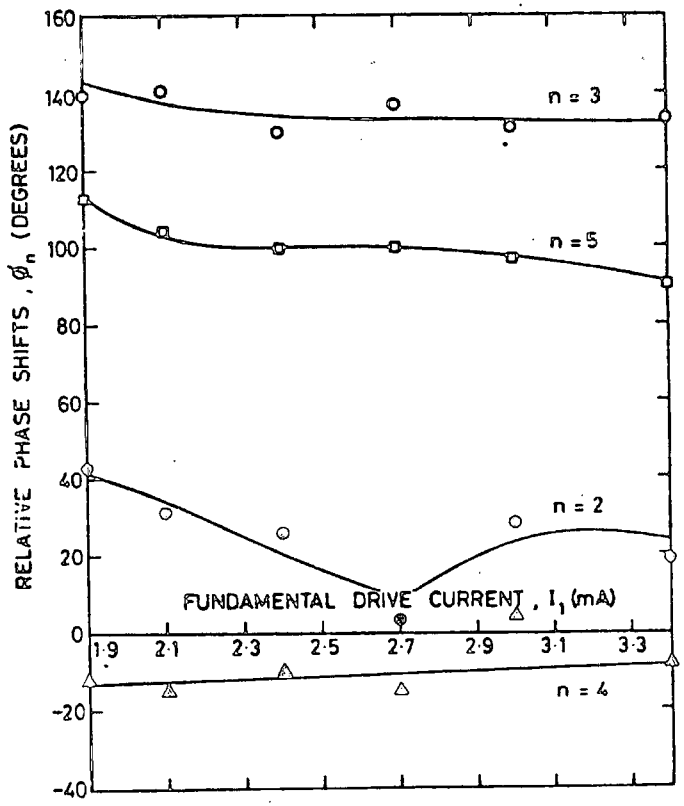

(b) PHASE

Fig 6.9.2: HARMONIC SPECTRA - f_1 = 1.560 GHz

Si POINT CONTACT DIODE CS9B/2

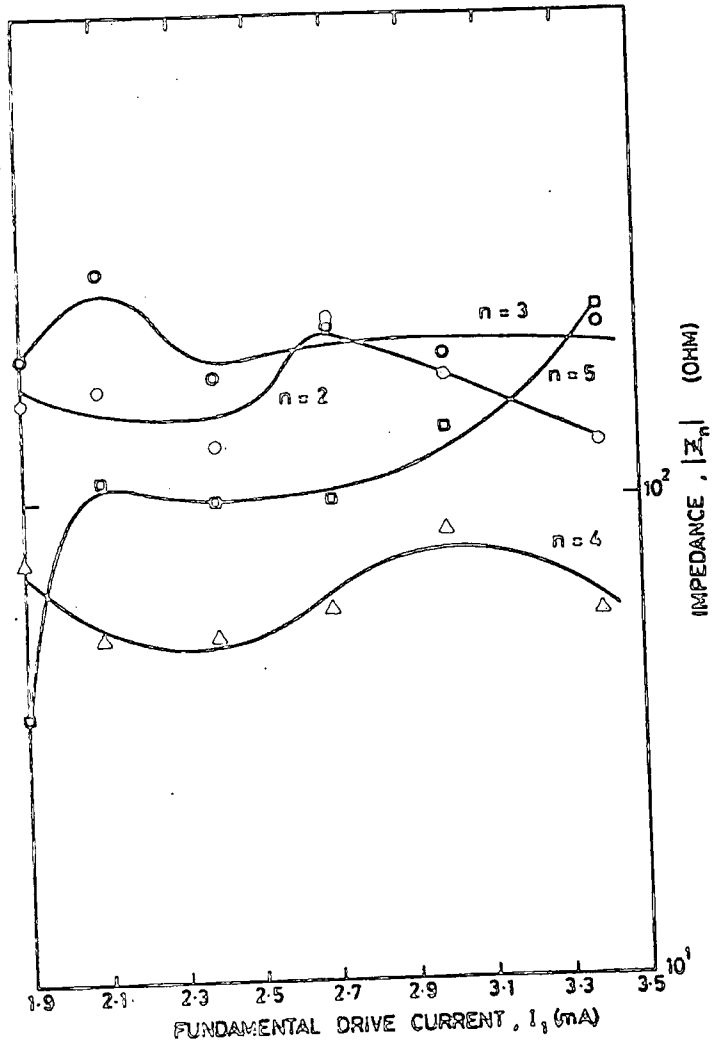

(c) IMPEDANCE

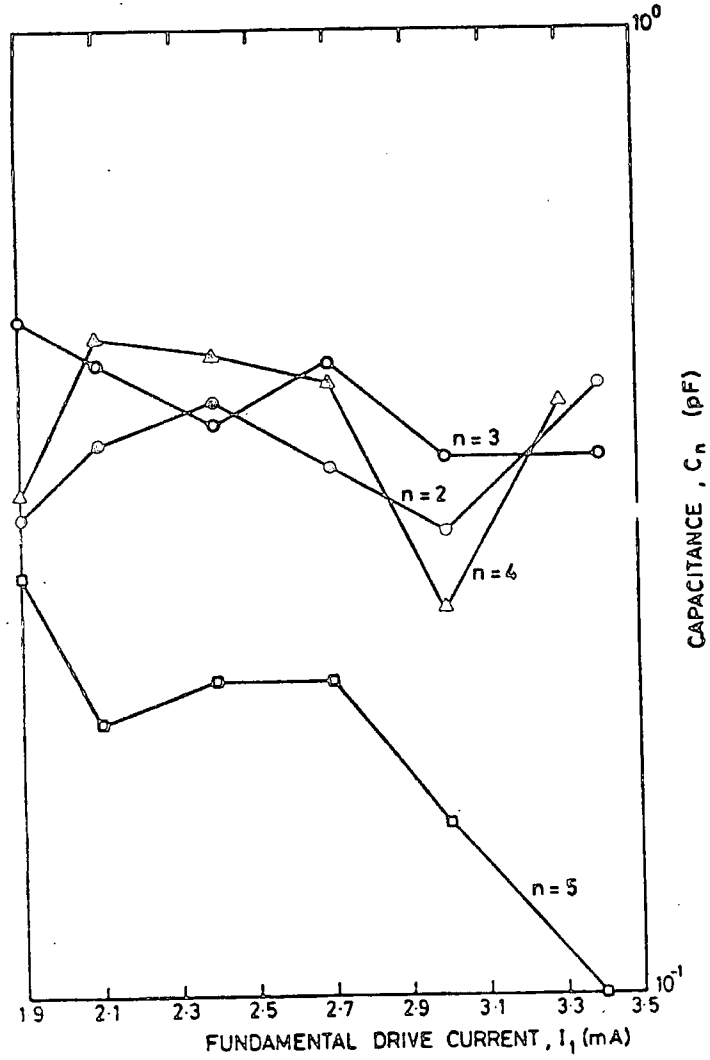

(d) CAPACITANCE

Fig 6.9.2: HARMONIC IMPEDANCE - f_1 = 1.560 GHz

The values of the third and fifth harmonic phases for the second diode (Fig 6.9.2(b)) decrease with levels. However, in the case of the fourth harmonic, the values are almost constant. There is even a dip for the second harmonic phases at the level of 2.7 mA. In the case of the first diode, there is no apparent trend in the behaviour of the harmonic phases (Fig 6.9.1(b)).

For the first diode, the values of the impedance at the fourth harmonic (Fig 6.9.1(c)) decrease with level although there is a peak and a dip. The curve for the impedance at second harmonic has a low peak and the values of those for the third and fifth harmonic increase with levels. The values of the impedance at the fifth harmonic of the second diode increase with the drive, however, there is no apparent trend in the behaviour of that of the second, third and fourth harmonics (Fig 6.9.2(c)).

There are wider variations in the values of the capacitance at harmonics for the first diode than those of the second (Figs 6.9.1(d) and 6.9.2(d)). The values of the capacitance for the first diode range from 0.05 to 0.50 pF whereas those for the second diode were from 0.1 to 0.5 pF.

Generally, for both diodes there are only small variations in the values of the harmonic amplitudes and hence the corresponding phases. It is obvious that the values of the second harmonic amplitude, which are relatively high for both diodes, have small variation over the given range of the drive level. Furthermore, similar behaviour is seen for the impedance and hence phases and capacitances. At an inflexion point for the curve of impedance at the fourth harmonic (first diode), where the drive is 2.7 mA, a discontinuity in the corresponding harmonic phase is observed. In the case of the second diode, at the drive level of 2.7 mA where there is a low peak in the impedance of the second harmonic, there is a dip in the corresponding phase.

6.10 COMMENTS AND DISCUSSION

Basic diode parameters were first obtained from the result of the d.c. measurements. This static characterisation forms an integral part of the harmonic spectrum measurements at high frequencies because it provides an initial assessment of the device.

The results of harmonic spectrum measurements are presented in terms of the parameters amplitude, phase, impedance and capacitance plotted against the drive level. The relationship between these parameters may be established. It is observed that at lower harmonics, generally as the drive level is increased, the harmonic amplitude increases, phase and impedance decrease and the capacitance remains constant. If within the given drive range, there are small variations in the harmonic amplitude and impedance, there will be small variations in the corresponding phase and capacitance. This is associated with the lower harmonics where the amplitude levels are relatively high. On the other hand the reverse is also true.

Within the drive level range and for certain harmonics the diode parameters may be constant, increasing or decreasing ; have a peak, dip, an inflexion point or a discontinuity. Knowing the behaviour of any one of these parameters, it is possible to predict that of others. Moreover, the behaviour of the parameters at different harmonics is useful information, especially in the device application.

CHAPTER 7

COMMENTS, CONCLUSIONS AND FUTURE WORK

7.1 GENERAL

Spectral Analysis (Chapter 2)

The fundamental theory of spectral analysis based on Fourier principles was reviewed in Chapter 2. These were then used in the examination of semiconductor devices, the response of which may be represented by a periodic time function. The theoretical investigations into the analytical relationships between time and frequency domains had produced a number of useful conclusions and provided the foundation for the spectral characterisation of a nonlinear device. Two new forms of sampling procedures, one based on dividing the waveform into vertical pulses and the other approximating the waveform by the pulses of well known shapes were also discussed in this Chapter.

Harmonic Generating Properties (Chapter 3)

The discussion of the harmonic generating properties of nonlinear devices in Chapter 3, began with the emphasis on the need for classification of practical high frequency diodes. Consequently, a brief review of major devices and the scope of their application and significance were included. The high frequency application of these devices is an expanding branch of electronics. The aims in device manufacture have always been to accentuate the nonlinearity and suppress any parasitic components that may affect it. In the investigation into the behaviour of nonlinear devices it is usually difficult to obtain a closed form solution for the response and therefore there is no satisfactory way of characterisation. However, the concept of spectral characterisation should represent a true and unique behaviour of the device, a "fingerprint", under normal working conditions.

The MRRL Method - Theory (Chapter 4)

The theory of the MRRL method of harmonic spectrum measurement was presented in Chapter 4. The application of the basic transmission line theory was extended to deal with the complexity of the standing waves of all the harmonics generated within a nonlinear device. This resulted in the establishment of relationships between the standing wave properties and the device parameters. From the proposed equivalent circuit, a nonlinear device was characterised at a particular harmonic frequency and drive level by the generated harmonic voltage and the complex impedance. This had led to the derivation of expressions for the device parameters.

MRRL - Measurement Method (Chapter 5)

The measurement and experimental procedure were dealt with in Chapter 5. The novelty of this specially developed coaxial slotted line technique lies in the capability of determining the properties of a non-linear device from the measurements carried out on the harmonic standing waves produced under the set conditions. The necessary changes made on the normal slotted line systems were, the addition of an adjustable line, introduction of a known mismatch termination (resistive multiple termination) at the excitation source end and the direct use of the spectrum analyser. The usual precautions, as applied to normal slotted line systems, in addition to those related to the newly adapted components were taken. The design and construction of the diode holder were made compatible with the line and shapes of the diode encapsulations and calibrated accordingly. Finally, the choices of reference drive level, the value of the impedance of the resistive termination, fundamental frequency and the drive level were decided.

Experimental Results (Chapter 6)

In Chapter 6, experimental results were presented. The amplitude and the phase of the generated spectrum and the impedance and capacitance of the equivalent circuit were produced for every diode at each fundamental drive frequency. Discussion of the harmonics produced by each diode was made on the basis of the four spectral "fingerprints" with appropriate cross-references between them. Since there is a relationship between amplitude, phase, impedance and capacitance, some general observations were made. As the measurements were made for two different diodes of the same type, it was convenient to compare their individual properties. The static characteristics of the diodes obtained were the series resistance, saturation current, ideality factor and the low frequency measurements of the capacitance. These were useful items of information about the devices, which however, did not convey anything about their harmonic generating and frequency converting capabilities.

7.2 ASSESSMENT OF THE MRRL METHOD

General

The MRRL technique of harmonic measurement developed is theoretically sound since it was supported by the facts that the harmonic standing waves, under the conditions of resonance (including the corresponding line impedances), could be accounted for and related to the device parameters. Experimentally, the validity of the technique was confirmed from the measurements, at a particular harmonic and drive level, where the difference in the length of the line, under the resonant and anti-resonant conditions, was a quarter of a wavelength. Besides, the VSWR measured could be verified to be equal to that of the value, created by the known resistive multiple termination. An outstanding feature of the experimental technique is that, in the computation of the reflection coefficient ρ_n, only relative measurements were needed.

However, the actual generated harmonic voltage can be determined when the coupling coefficient between the probe and the line is included in the computation. The application covers a wide frequency range from L to X-bands, when the 50-cm slotted line is used. If the levels of the higher harmonics are too low to measure then different fundamental frequency drives may be chosen. Moreover, the highest order of the measurable harmonic is restricted by the "burnout" point of the device. The use of the spectrum analyser was an added advantage because of its versatility where the harmonic standing waves could be measured directly. This was not possible with other detectors like the VSWR-meter where wave modulation was necessary.

Accuracy and Errors

Generally, the errors in the harmonic measurements were lower for cases when the fundamental frequency was 1.560GHz than those of 450MHz. This was because in the latter case the drive levels of available sources were low and the measurements were more affected by the noise level of the spectrum analyser. Typical error estimated for the amplitude, when the fundamental frequency was 1.560GHz, was about 20% and that when the fundamental frequency was 450MHz, it was about 25%, for all the measured harmonics. In the case of the relative phases the error was about 10%. As for the impedance and capacitance the errors were much smaller and of the order of 5%. The basic quantities measured, using the spectrum analyser, were the standing wave voltages, the reflection coefficient of the resistive termination and the fundamental drive current. The accuracy then depended on the precision of the spectrum analyser, where the error in a single measurement was 0.5dB. Other basic quantities measured, from the scale of the slotted line in conjunction with the spectrum analyser, were the total length of the line (at resonance and anti-resonance), the wavelength and the phase angle ψ_n . The error in a single measurement was 0.5mm.

Improvement

In order to improve the accuracy and the range of measurements a number of steps is recommended. As the spectrum analyser played a key role in the measurement so was its effect on the accuracy of the technique. Therefore, it is necessary to improve the precision of this equipment. Further, lowering the impedance of the resistive multiple termination will result in the increase of its VSWR value and hence improve the sensitivity of the standing wave measurements. This is demonstrated in the Appendix C. Other areas of improvement include increasing the measurements to higher harmonics and wider range of drive levels. Consequently, an excitation source of higher output is required. Besides satisfying the above requirements, there is a need to offset the effect of a big coupling loss between the line and the probe. In addition, compensation for the heavy attenuation, required for a good termination, must also be considered.

Significance

This new measurement method offers a means of determining a complete spectrum generated within a nonlinear element over a wide frequency range. The resultant spectra, which are the "fingerprints", represent new forms of device characterisation. The pattern may show a regular trend consistent with the normal behaviour of the device. It may also display an anomalous trend which signifies the peculiarity of the device under certain defined conditions. This provides the information about the harmonic generating and frequency converting properties of the device. Regarding the accuracy, there is no mathematical approximation involved except for the experimental errors. The behaviour of the diodes of the same type may be examined under identical conditions. From the spectra, which can be prominently displayed, the degree of matching between devices at harmonics can be easily detected. Hence, it may be suggested that this method of spectral characterisation be employed in the matching of devices using generated spectra.

In addition, devices may even be graded in terms of the degree of matching.

7.3 DEVICE EVALUATION

General

There are many types of device evaluation[7, 38] depending on its application and the range of operating conditions to be encountered. But testing is time consuming and test equipment is expensive, so manufacturing tests are usually boiled down to a few basic ones and are often performed only on samples. Nevertheless, having the capability for testing diodes is highly valuable for providing feedback to process control and for diagnosing what is wrong with a diode that does not work properly. This work was mainly concerned with performance testing at high frequencies. The method of spectral characterisation introduced provides a number of parameters (amplitude, relative phase, impedance and capacitance) with which a nonlinear device may be evaluated over particular ranges of harmonic frequencies and drive levels. From the behaviour of the frequency spectra of these quantities, it may be possible to ascertain whether the device is working normally or not and to assess its harmonic generating and frequency converting properties. As an example, for the case of the amplitude spectra, it is desirable to have high level harmonics and to know the corresponding drive levels. In addition, probably at a suitable harmonic, the amplitude with constant level is required over a range of drive levels. In some cases, it may be that the levels for a certain harmonic is too low or having a dip or a peak. In the case of the phase spectra much useful information may also be extracted. The extent of variations of the phases for different harmonics over a range of drive levels may give an indication of the behaviour of the complex impedance of the device. Furthermore, any discontinuity in phases may reflect a change in phase. The magnitude of impedance at harmonics will invariably be very important for matching purposes. The value of parasitic capacitance may be deduced from the phase measurements.

The unexpected behaviour of some spectra reflects the peculiarity of the device. This information may be useful in the design, fabrication and application of the device.

Explanation and Interpretation

An attempt will now be made to explain and interpret the behaviour of the harmonic spectra presented in Chapter 6. It is expected that on increasing the drive level, when the generated harmonic voltage increases, there will be a decrease in the corresponding impedance and the relative phase while the capacitance will remain constant. This may be seen for the second and fourth harmonics of the gallium arsenide Schottky barrier diode (type DC1322/1) in Figs 6.4.1(a), 6.4.1(b), 6.4.1(c) and 6.4.1(d). Generally, this was true for the cases of lower harmonics where the associated amplitudes were relatively higher. It is understood that the generated harmonic voltage will increase with the drive level. On increasing the drive level the device impedance decreases and becomes more resistive and hence reducing the phase value. This is because the magnitude of the reactive component will normally fall and that of the resistive component will drop to a constant value, when the drive level approaches the switching condition. The parasitic capacitance however, will be relatively constant if the device is working normally. In principle, if the device behaviour agrees with the observation discussed, then it is working as it should. If however, there is an anomalous trend for particular harmonics, then it reflects the peculiarity of the device or that the measurement of low level higher harmonics may be affected by the noise of the spectrum analyser. This may be shown in Figs 6.4.2(a), 6.4.2(b), 6.4.2 (c), and 6.4.2(d) for gallium arsenide Schottky barrier diode, for the fifth harmonic.

In order to make a general prediction on the behaviour of the device from the spectra further discussion on the experimental results may be useful. The results had shown that over a certain drive level range and at a particular

harmonic, whenever there were drastic variations in the amplitude, there would similarly be big variations in the corresponding phase, impedance and capacitance. This is illustrated, for the case of silicon Schottky barrier diode (type DC1504F/1), in Figs 6.5.3(a), 6.5.3(b), 6.5.3(c) and 6.5.3(d). In the same way, at particular harmonics, whenever the amplitudes were fairly constant or had small variations, again the impedance, phase and capacitance would show similar behaviour. An example is as given, for the case of the third harmonic of the silicon Schottky barrier diode (type DC1515/2), in Figs 6.6.1(a), 6.6.1(b), 6.6.1(c) and 6.6.1(d). An interesting feature was an apparent relationship between the inflexion point on the impedance curve, at a particular drive level, and the corresponding discontinuity in phases. This is illustrated in the case of the second and the third harmonics of the gallium arsenide Schottky barrier diode (type DC1322/1, shown in Figs 6.4.1(b) and 6.4.1(c). Another interesting observation is that at the drive level corresponding to the peak of the fifth harmonic voltage for silicon Schottky barrier diode (types DC1504F/1 and DC1504F/2) shown in Figs.6.5.1(a), 6.5.1(b), 6.5.2(a) and 6.5.2(b) there was an inflexion point on the curve of the same harmonic phase.

The curves of the relative phase against the harmonic frequency, at a particular drive level, were generally found to be nonlinear. From the result of the theoretical investigation discussed in Chapter 2, the nonlinear phase spectral envelope corresponded to the asymmetrical type of the response waveform, due to the device. This implies that the device comprised both the nonlinear resistive component and that of the reactive which could either be linear or nonlinear. The presence of the reactive component suggested a storage capability which will result in an I-V characteristic having an hysteresis. If theoretically, within a lobe, the phase is constant or has a linear variation (when the origin of the waveform

analysed was at the leading edge) then the response waveform is symmetrical, thus implying that the device is purely resistive. Experimentally however, it implied that the device would consist of both the nonlinear resistive and nonlinear reactive components. In addition the components would have identical level dependence.

Recalling the plots in Figs.6.4.1(a) and 6.6.1(a), it is noted that the harmonic generator voltage was higher for the fourth harmonic than for the third. This may be explained in terms of the $\frac{\sin x}{x}$ distribution of the amplitude spectrum, where the fourth harmonic amplitude would appear in the new lobe. A typical example of the distribution is given in Fig.2.5(b). On the other hand, when the amplitudes of the fourth harmonic were lower than those for the third, it was because both appeared in the same lobe.

Classification of Devices

Devices may also be classified from the result of the spectral analysis. Apparently, there are two criteria that can be adopted and they are in terms of the linearity in phases and the value of the second harmonic amplitude. Firstly, from the nature of the variation in the relative phases, whether linear or nonlinear, it is possible to identify the type of symmetry of the response waveform, due to a device. This finally leads to the qualitative deduction on the type and behaviour of the components present in a device. In the case of all the diodes used in the project, the phase spectral envelope were nonlinear, indicating that they (diodes) contained both the nonlinear resistive and reactive components.

Next, there is a need to justify the second criterion. The second harmonic amplitude is directly related to the size of the waveform shown in Figs 2.4(b) and 2.5(b). It was pointed out in Chapter 2 that the bigger the amplitude (implying the corresponding size of the pulse waveform), the smaller would be the range of the phase angle (illustrated in Fig.2.7) and

each lobe would contain lesser number of harmonics (again illustrated in Figs. 2.4(b) and 2.5(b)). A summary of the values of the second harmonic amplitudes, at the drive levels of 2.0 and 3.5mA, and the saturation current for all the diodes is given in the Table in Appendix D. It is apparent that there is a kind of an inverse relationship between the second harmonic amplitude and the saturation current of each diode. However, the general behaviour of the saturation current for all the devices, as indicated in Chapter 6, was explained in terms of the energy band gap of the semiconductors. In the case of the second harmonic amplitude, the trend may be explained in terms of the electron mobility of the semiconductor device. This is because gallium arsenide semiconductor has electron mobility greater than those for germanium and silicon. It can be concluded that a diode whose material has higher electron mobility may have greater value of the second harmonic voltage. Therefore, it is feasible to classify high frequency diodes on the basis of their second harmonic amplitude.

7.4 APPLICATIONS OF "FINGERPRINTING" SPECTRA

In general, one envisages three basic areas of applications of the "fingerprinting" spectrum. Firstly, the "fingerprinting" spectra of non-linear elements, which also include parasitic effects, may be employed in the prediction of performance of devices. The power-handling capability and conversion efficiency of a frequency multiplier[36,39] depend on the magnitude of the harmonic coefficient generated. The efficiency of a rectifier, the current sensitivity of a detector and the conversion loss of a mixer are strongly dependent, in different ways, on the product of the parasitic capacitance and that of the series resistance[7,10,19]. The nature of variations and the value of the parasitic capacitance, at a particular level, may be determined from the graph of capacitance at harmonics against the

drive level. In the case of a mixer, both the R.F. and I.F. impedances, required for matching, may also be found from the spectra.

Secondly, these spectra may be employed in the general evaluation of nonlinear devices. It may be possible to assess and carry out a quality control test on a diode from the obtained spectrum pattern. If the pattern satisfies prescribed conditions it may be inferred that the device would work normally. However, if there is any anomalous trend in the spectrum this could represent a peculiarity of the diode, which may arise from the defects in the material (e.g. nonhomogeneity). This may provide useful feedback information and help in the design and fabrication of devices. The spectral parameters, such as second harmonic amplitude, the relative phase, etc., may provide a basis for the classification of nonlinear devices. The values of impedance at different harmonics can give information regarding the matching conditions whereas those of the capacitance about the noise temperature and conversion loss.

Finally, the "fingerprinting" spectra may be utilised in device physics. The spectrum generated within a device, measured using the high frequency technique, may provide a means of assessing the result of the d.c. or low frequency measurements. It was found that there was an apparent inverse relationship between the reverse saturation current (d.c. measurement), for different diodes, and the generated voltage of the second harmonic (high frequency measurement). The behaviour of each was consistent with the energy band gap of the semiconductor material. In addition, from the relative values of the second harmonic voltage (for different devices), it may be possible to relate them to the comparative magnitude of the mobility of charges and the effective potential barrier. It is known that for a Schottky barrier diode[19,40] made from reasonably high mobility semiconductor, the conduction mechanism should conform to the thermionic emission theory, for

moderate voltages. On examining the linearity of the spectra for the relative phases, it may be possible to predict the nature of the reactive components of a nonlinear device.

7.5 FUTURE WORK

With regard to the future work, there are two areas that can be considered and there are further aspects related to the spectral representation and those concerned with the technique itself. As for the former there is a need to establish this new form of device characterisation on a firmer basis so that a more comprehensive system of device evaluation be achieved. This may be done through extensive tests on more varieties of devices. In addition, the laws derived in the theoretical investigation, in Chapter 2, may further be investigated in order to examine more of the device behaviour in terms of the frequency domain from that of the time and vice-versa.

There are three main proposals, on the future work, related either wholly or partly to the M.R.R.L. technique. The first main part is concerned with the method as a whole where there are two areas of interests. In the first case, it is believed to be feasible to automate the M.R.R.L. method. It is based on the Fourier analysis of the response waveform due to a device. Suitable sweeping mechanism needs to be devised, in order to automatically sample the ordinates of the resultant waveform, to interface with a microprocessor. The ultimate aim of this project will be to display the spectra (amplitude and phase) on the V.D.U. Once this is achieved, the technique will prove to be versatile because the spectra can be readily acquired and displayed for different level and fundamental frequency. The next project is the development of a complete spectrum analyser. This involves the adaptation and incorporation of the M.R.R.L. method in a spectrum analyser. It is hoped that this project will arouse industrial interest because of its additional facility of phase measurement, not available in any spectrum analyser.

Secondly, the work may be aimed at devising means of measuring the harmonic standing waves in place of the high frequency spectrum analyser, which is an expensive piece of equipment. Within this context, two suggestions are put forward. It is proposed to adopt a mixer method where the L.O. is tuned closed to the desired harmonic frequency, so that an I.F. of 30MHz results. Then using the commonly available 30MHz amplifier, the harmonic measurement may be carried out with a wave analyser or a low frequency range spectrum analyser. Another proposal is to measure the harmonic standing waves using a VSWR-meter. As the VSWR-meter is an a.f. detector, the desired high frequency harmonic components must first be modulated. Consequently, the work will deal with an investigation on how the harmonic waves may be modulated.

Another area of investigation is to develop a mixer method of measuring relative phases at harmonics. The L.O. frequency is first set to be equal to that of the desired harmonic frequency. The mixer will then operate as a product detector giving a series of harmonic components including a d.c. term. The resultant d.c. component can be shown to be dependent upon the phase angle between the L.O. frequency and that of the harmonic. Finally a method may then be established where the phase angle may be deduced from a simple d.c. measurement.

REFERENCES

1. STREMLER, F.G. Introduction to Communication System, Addison-Wesley, 1977.
2. SCOTT, R.E. Linear Circuits, Addison-Wesley, 1960.
3. LATHI, B.P. Communication Systems. John Wiley & Sons, 1968.
4. PAPOULIS, A. The Fourier Integral and its Applications, N.Y. McGraw-Hill, 1962.
5. CHERRY, C. Pulses and Transients in Communication Circuits. An Introduction to Network Transient Analysis for Television and Radar Engineers, Chapman and Hall (1949).
6. CHAMPENEY, D.C. Fourier Transforms and their Physical Applications, Academic Press, 1973.
7. WATSON, H.A. (Bell Telephone), Microwave Semiconductor Devices and their Applications, McGraw-Hill Book Co., 1969.
8. HIGGINS, T.J. 'A Resume of the Development and Literature of Nonlinear Control-System Theory'. Instruments and Regulators Division, The American Society of Mechanical Engineers, ASME-AIEE Conference on Nonlinear Control System, Princeton, N.J., March 26-28, 1958.
9. VAN DER POL, B. 'The Nonlinear Theory of Electric Oscillators'. Proc. Inst.Radio Eng., Vol.22, 1934, pp.1051-1086.
10. PIPES, L.A. and HARVILL, L.R. Applied Mathematics for Engineers and Physicists. Third Edition. McGraw-Hill, Kogakusha, Ltd., 1970.
11. BELLMAN, R. Discussion on the Paper of Reference 8.
12. GRAHAM, J.D. Discussion on the Paper of Reference 8.
13. VALLESE, L.M. Discussion on the Paper of Reference 8.
14. MINORSKY, N. Discussion on the Paper of Reference 8.

15. BERGER, M.S. Nonlinearity and Functional Analysis, (Lectures on Nonlinear Problems in Mathematical Analysis) Academic Press, 1977.

16. CHUA, L.O. Introduction to Nonlinear Network Theory. McGraw-Hill Book Company, 1955.

17. CUNNINGHAM, W.J. Introduction to Nonlinear Analysis, McGraw-Hill Book Company, 1955.

18. TORREY, H.C. and WHITMER, C.A. Crystal Rectifiers. McGraw-Hill Book Co. Inc., 1948.

19. HOWES, M.J. and MORGAN, D.V. Variable Impedance Devices. John Wiley & Sons, 1978.

20. SHURMER, H.V. Microwave Semiconductor Devices. Pitman Publishing, 1971.

21. GINZTON, E.L. Microwave Measurements, McGraw-Hill Book Co.Inc,1957.

22. LIAU, S.Y. Microwave Devices and Circuits. Prentice-Hall Inc,1980.

23. DWORSKY, L.N. Modern Transmission Line Theory and Applications, John Wiley and Sons, 1979.

24. Compiled by the Staff of the Radio Research Laboratory, Harvard University, Very High Frequency Techniques. Vols. I & II. McGraw-Hill, 1947.

25. BARLOW, H.M. and CULLEN, A.L. Microwave Measurements. Constable and Company Ltd., 1950.

26. RAMO, S., Whinnery, J.R. and VAN DUZER, T. Fields and Waves in Communication Electronics. John Wiley & Sons Inc. Toppan Company Limited, 1965.

27. SUCHER, M.and FOX, J. Handbook of Microwave Measurements, Vols. I, II and III, Polytechnic Press of the Polytechnic Institute of Brooklyn, 1963.

28. HARVEY, A.F. Microwave Engineering. Academic Press. London & New York, 1963.

29. ROGERS, F.E. The Theory of Networks in Electrical Communication and Other Fields. MacDonald, 1957.

30. CHIPMAN, R.A. Transmission Lines. Schaum Outline Series in Engineering. McGraw-Hill Book Co., 1968.

31. EVERITT, W.L. and ANNER, G.E. Communication Engineering. Third Edition., McGraw-Hill Book Co.Inc., 1956.

32. DAVIDSON, C.W. Transmission Lines for Communication. The MacMilland Press Ltd., 1978.

33. MOOIJWEER, H. Microwave Techniques. MacMillan, 1971.

34. SAAD, T.S., HANSEN, R.C. and WHEELER, G.J. Microwave Engineers Handbook, Vol.I, Artech House Inc.Dedham, Massachusetts, 1971.

35. KAHNG, D. 'Conduction Properties of the Au-n Type Si Schottky Barrier'. Solid State Electronics, 6, (1963).

36. HUNTER, L.P. (Editor). Handbook of Semiconductor Electronics. Third Edition. McGraw-Hill Book Company, 1970.

37. SCHWARTZ, M and SHAW, L. Signal Processing. Discrete Spectral Analysis, Detection and Estimation. McGraw-Hill Kogakusha Ltd,1975.

38. MORGAN, D.V. and HOWES, M.J. Microwave Solid State Devices and Applications, Peter Peregrinus Ltd. 1980.

39. PENFIELD (Jr.), P. and RAFUSE, R.P. Varactor Applications. The MIT Press. Massachusetts Institute of Technology, Cambridge, Massachusetts, 1962.

40. CROWELL, C.R. and BEGUWALA, M.'Recombination Velocity Effects on Current Diffusion and Imref in Schottky Barriers'. Solid-State Electronics. Pergamon Press 1971, Vol.14. pp.1149-1157.

DEPARTMENTAL BIBLIOGRAPHY

1. KATIB, M.K. 'Evaluation of Harmonic Generating Properties of Schottky Barrier Diodes'. Ph.D.Thesis, Durham 1976.

2. KULESZA, B.L.J. and KATIB, M.K. 'Harmonic Generation in Exponential Resistive Diodes'. Departmental Report. July,1977.

3. KULESZA, B.L.J. and MAT HASSAN.Y. 'Spectral Analysis I - Principles of Analytical Methods'. Departmental Report. August 1980.

4. KULESZA, B.L.J. and MAT.HASSAN, Y. 'Spectral Analysis II - Frequency Spectra of Pulse Waveforms'. Departmental Report. Nov. 1981.

5. ARMSTRONG, R. 'Spectral Identification of Nonlinear Devices'. Ph.D.Thesis. Durham, 1983.

APPENDICES

APPENDIX A: SUMMARY OF CONDITIONS GOVERNING THE VALIDITY OF THE USE OF FOURIER ANALYSIS

A.1: Dirichlet Conditions - Convergence Criteria.

There are two Dirichlet conditions that govern the rate of convergence of a Fourier series, namely, the weak and the strong conditions. The weak Dirichlet condition requires that the function f(t) be single valued over a time interval and if periodic the Fourier coefficients a_n and b_n are obtainable. The strong Dirichlet condition specifies the requirements for the Fourier series to be convergent everywhere. The requirements are: the functions f(t) must be finite and must have a finite number of discontinuities. Consequently, under both conditions, the function f(t) may be represented over a complete period and hence from $t = -\infty$ to $t = +\infty$, except at discontinuities, by a series of simple harmonic functions, the frequencies of which are integral multiples of the fundamental frequency.

A.2: Singularities

A point at which a function f(t) ceases to be analytic, i.e. the function does not have a unique derivative, is called a singular point of f(t). At such a point the function is said to have a singularity.

A.3: Uniqueness Condition

A vectorial or a signal representation is said to be unique if it can be specified in space by a given set of co-ordinate axes and each dimension is specified by only one co-ordinate.

A.4: Orthogonality

Two functions whose product integrates to zero are said to be orthogonal over a specific time interval. Many sets of pair-wise orthogonal functions exist and are used for approximating signals.

A.5: Finite Energy Concept of a Signal

An energy signal is a pulse-like signal that usually exists for only a finite interval of time or, even if present for an infinite amount of time, at least has a major portion of its energy concentrated in a finite time interval.

APPENDIX B: THE FOURIER SPECTRUM DUE TO AN APERIODIC SIGNAL

The expression for the frequency spectrum generated by an aperiodic signal can be derived by first taking the case of a periodic signal, whose function is taken as, $f_T(t)$. The Fourier series of such a pulse of period T may be represented in an exponential form as,

$$f_T(t) = \sum_{n=-\infty}^{\infty} F_n e^{jn\omega_o t} \tag{1}$$

where $$F_n = \frac{1}{T} \int_{-\frac{T}{2}}^{\frac{T}{2}} F(t) e^{-jn\omega_o t}\, dt \tag{2}$$

In order that $|F_n|$ is convergent when T is increased, the following conditions must be satisfied, i.e.,

$$\omega_n \simeq n\,\omega_o \tag{3}$$

$$F(\omega_n) \simeq TF_n \tag{4}$$

The eqns.1 and 2 may now be written as,

$$f_T(t) = \sum_{n=-\infty}^{\infty} \frac{1}{T} F(\omega_n) e^{j\omega_n t} \tag{5}$$

and

$$F(\omega_n) = \int_{-\frac{T}{2}}^{\frac{T}{2}} f_T(t) e^{-j\omega_n t}\, dt \tag{6}$$

As the line width in the line spectrum of $f_T(t)$ is given by

$$\Delta\omega = \frac{2\pi}{T} \tag{7}$$

then eqn. 5 becomes,

$$f_T(t) = \sum_{n=-\infty}^{\infty} F(\omega_n) e^{j\omega_n t} \frac{\Delta\omega}{2\pi} \tag{8}$$

When the period T is increased, correspondingly $\Delta\omega$ becomes smaller and hence the line spectrum becomes denser. In the limit as T tends to infinity, the discrete frequency spectrum of $f_T(t)$ becomes continuous. The infinite sum in eqn. 8 may be written as,

$$\lim_{T \to \infty} f_T(t) = \lim_{T \to \infty} \frac{1}{2\pi} \sum_{n=-\infty}^{\infty} F(\omega_n) e^{j\omega_n t} \Delta\omega$$

and therefore becomes the Riemann integral so that

$$f(t) = \frac{1}{2\pi} \int_{-\infty}^{\infty} F(\omega) e^{j\omega t} d\omega \tag{9}$$

Similarly, eqn.6 may be written as,

$$F(\omega) = \int_{-\infty}^{\infty} f(t) e^{-j\omega t} dt \tag{10}$$

and is called the direct Fourier transform, which may be written as,

$$F(\omega) = \mathcal{F}\left[f(t)\right] \tag{11}$$

and that for eqn.9 as the inverse Fourier transform, represented as

$$f(t) = \mathcal{F}^{-1}\left[F(\omega)\right] \tag{12}$$

Both eqns.11 and 12 are known as the Fourier transform pair.

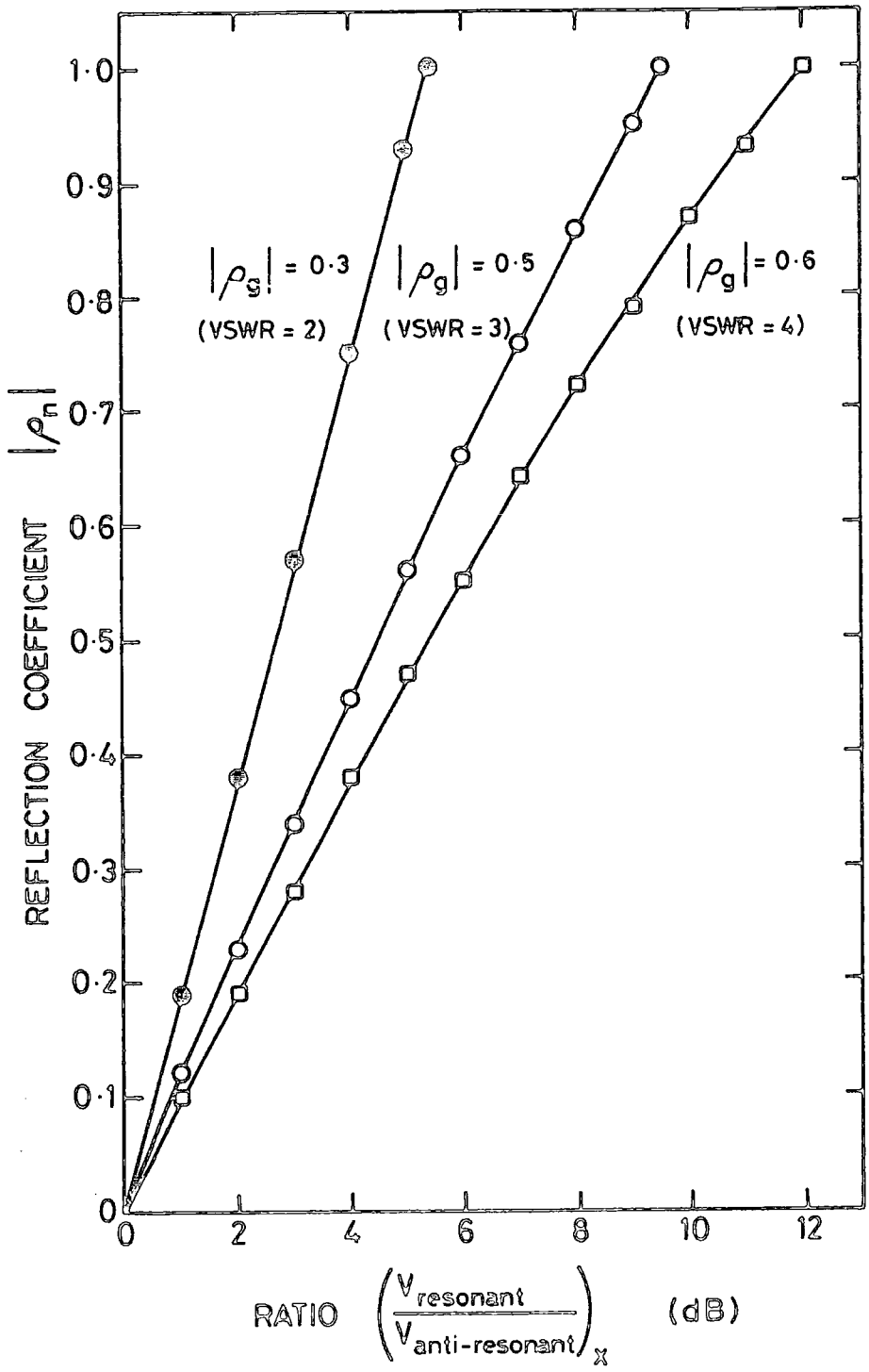

APPENDIX C. SENSITIVITY OF HARMONIC STANDING WAVE MEASUREMENTS

APPENDIX D : THE VALUES OF THE REVERSE SATURATION CURRENT AND THE SECOND HARMONIC AMPLITUDE FOR DIFFERENT TYPES OF DIODES

Diode	I_s measured in Amps	V_2(mV)	
		at I_1= 2.0 mA	at I_1= 3.5 mA
GaAs Schottky barrier			
DC 1322/1	1.9×10^{-12}	2.1×10^{2}	8.0×10^{2}
DC 1322/2	3.1×10^{-12}	2.8×10^{2}	4.6×10^{2}
Si Schottky barrier			
DC 1504F/1	9.0×10^{-10}	2.0×10^{2}	-
DC 1504F/2	1.1×10^{-9}	1.9×10^{2}	-
Ge Backward			
DC 3021/1	7.4×10^{-5}	6.6×10^{0}	3.2×10^{0}
DC 3021/2	1.0×10^{-4}	4.2×10^{1}	2.4×10^{1}
Si Schottky barrier			
DC 1515/1			
DC 1515/2	8.0×10^{-10}	2.5×10^{2}	-
Si point contact			
CS 12BR/1	2.3×10^{-6}	-	1.3×10^{2}
CS 12BR/2	1.2×10^{-6}	-	5.0×10^{1}
Si point contact			
CS 9B/1	1.7×10^{-6}	2.7×10^{1}	7.4×10^{1}
CS 9B/2	1.6×10^{-6}	2.9×10^{1}	6.5×10^{1}